Hydrothermal Carbonisation of Microalgae: Feedstock Characterisation, Model Compound Decomposition, and Assessment of Product Recovery Methods

Sidra Jabeen, MSc Chemical Engineering

This thesis is presented for the degree of

Doctor of Philosophy

Discipline of Engineering and Energy, College of Science, Health, Engineering and Education

July 2020

DECLARATION

To the best of my knowledge and belief, this thesis contains no material previously published by any other person except where due acknowledgment has been made.

This thesis contains no material which has been accepted for the award of any other degree or diploma in any university.

Sidra Jabeen

Date: 29th NOV. 2019

SUPERVISORY STATEMENT

We, the undersigned, attest that Doctorate Degree (Research) candidate, Sidra Jabeen has designed the experimental set-up, conducted the experiments, analysed data, performed computational quantum-mechanical calculations, and has written all papers included in this thesis. Dr Xiangpeng Gao, Professor Bogdan Z. Dlugogorski and Associate Professor Mohammednoor Altarawneh have provided the necessary advice on the experimental design and project direction and assisted with the editing of the papers, consistent with normal supervisors-candidate relations.

.....

Dr Xiangpeng Gao

Date: 29/11/2019

.....

Professor Bogdan Z. Dlugogorski

Date: 30/11/2019

.....

Associate Professor Mohammednoor Altarawneh

Date: 29/11/2019

DEDICATION

This dissertation is dedicated to my beloved parents for their prayers, my dear husband for his support, and my lovely boys for giving me a reason to smile after every thoughtful day spent in this research.

ABSTRACT

Australia presents a reasonable contribution to the World's greenhouse gas emissions because of its heavy reliance on fossil fuels for energy production. Coal is the primary founder of energy in Australia with the secondary sourcing from oil, gas, solar, wind, biomass, and hydro. Bioenergy currently offers only 1 % of the total energy produced in Australia with anticipated uplift to 8 % by 2030 that demands active research on biofuel resources and production processes. Australia lavishes with land, sunlight, and brackish water, necessary for the growth of algal biomass, the unique composition (carbohydrates, lipids, proteins, nucleic acid, and moisture) of which makes it an excellent feedstock for hydrothermal processing. Hydrothermal treatment of algal biomass for the production of biofuels and value-added products is an attractive route towards increasing the bio-energy contribution in Australia to meet the challenges of growing greenhouse gas emissions.

Hydrothermal treatment of algal biomass at high temperatures (280 – 700 °C) to produce energy-dense liquid and gaseous fuels are extensively researched for the last three decades with the exceptional attributes achieved in the field. However, the low temperature (180 – 260 °C) hydrothermal carbonisation (HTC) of algal biomass, which essentially serves as an intermediate stage of intense hydrothermal processing, has received less attention. Hydrothermal carbonisation produces hydrochar as a primary product along with biocrude and aqueous phase as co-products, all of which possess exceptional traits to be employed directly or indirectly as biofuels and/or as advanced carbon materials. Despite the rationale research on hydrothermal carbonisation of algal biomass, there are still significant research gaps in assessing the feasibility of hydrothermal carbonisation process for microalgae in the context of an Algal Biorefinery, including (i) the lack of standardised conditions for the characterisation (e.g., proximate analysis) of algal biomass; (ii) detailed mechanisms for the evolution of

nitrogen-containing species from thermal decomposition of algal biomass; (iii) the product of the impact recovery methods on the yields and properties of hydrochar from HTC of algal biomass; and (iv) detailed characterisation of the biocrude and aqueous phase from HTC of algal biomass.

The present study aims to address the aforementioned research gaps, with the following specific objectives: (1) to validate the applicability of the conventional proximate analysis methods, which are developed for solid biofuels, for algal biomass, using *Spirulina* and *Chlorella* as model algal samples, and then develop an analytical procedure for the proximate analysis of algal biomass; (2) to study the thermo-kinetics of the most plausible reactions encountered during thermal decomposition of 'Leucine' as an algal biomass model compound and establish a robust kinetic model accounting for the emission of nitrogen-containing species; (3) to investigate the impact of the product recovery methods on the yield and properties of hydrochar from HTC of *Chlorella* under the identical reaction conditions; and (4) to characterise the biocrude and aqueous phase from HTC of *Chlorella* and evaluate the impact of reaction temperature and holding time on the recovery of metals in biocrude and aqueous phase, which is essential for recycling and re-use of these products. These research objectives have been successfully fulfilled in this study, with the key findings outlined below.

Firstly, the widely employed ASTM E870–82 designed for woody biomass modified by thermogravimetric analysis (TGA) is found to be inapplicable for the proximate analysis of *Spirulina* and *Chlorella*, as indicated by the presence of unburnt carbon and quaternary nitrogen in the resulting ashes, although it accurately determines the contents of volatile matter. While *Spirulina* can be entirely ashed at 600°C in air, complete oxidation of *Chlorella* requires the aid of hydrogen peroxide (H_2O_2) under a similar condition. An analytical procedure is developed for the proximate analysis of algal biomass, using *Spirulina* and *Chlorella* as a case study. The procedure consists of three steps: (1) application of the TGA–ASTM E870–82 method to algal biomass followed by observing the colour of the ash residue; (2) direct ashing of algal biomass at 600 ºC in the air to get a fully oxidised ash residue and thereby determine ash content; and (3) oxidation of algal biomass in the air at 600 °C for 4 h, with the aid of

H_2O_2. The number of steps required to perform a complete proximate analysis depends on the properties of algal biomass.

Secondly, we map out the potential energy surface for a wide array of unimolecular and self-condensation reactions operating in the thermal decomposition of leucine, which was elected as an algal biomass surrogate compound. Decarboxylation, dehydration, and deamination ensue by eliminating CO_2, –OH, and NH_2, respectively, from α-carbon of leucine. The reaction rate constants indicated comparable branching ratios for decarboxylation and dehydration channels with a minimal contribution from the deamination route. The calculated kinetic parameters served to model a plug-flow reactor that demonstrates species profiles in the gas phase and shows that conversion of leucine attains 100 % in the temperature range 700 – 950 K with a residence time of 10 s. Our kinetics model predicts the formation of isoamylamine ($C_5H_{13}N$), 3-methyl butane-1-imine ($C_5H_{11}N$), 3-methylbutane nitrile (C_5H_9N), CO_2, NH_3, H_2O, C_3H_6, and C_2H_4 as significant products from thermal decomposition of leucine. Kinetic analysis of the plausible channels concluded that the dehydration constitutes the dominant pathway and self-condensation reactions contributed marginally to thermal decomposition of leucine in the gas phase.

Thirdly, the hydrochar produced from HTC of *Chlorella* with 10.0 wt % of solid loading at 180 – 220 °C for holding time of 15 and 60 min was recovered from the batch reactor by two methods that have been commonly employed in the literature. The first method involved direct filtration of the product mixture and subsequent drying of the hydrochar, without the use of solvent, whereas the second method used dichloromethane (DCM) to rinse the reactor contents, which recovered hydrochar from the aqueous phase and biocrude, followed by drying of the hydrochar. These two methods are hereafter termed as “direct filtration” and “DCM-aided filtration”, respectively. We found that direct filtration retains heavy biocrude on the hydrochar surface, which results in high mass and energy yields, high carbon levels, low ash contents, low reactivity, and improved higher heating values (HHVs) of the hydrochars, in comparison with their counterparts from DCM-aided filtration. The adsorption of biocrude on hydrochar surface leads to blockage of the pores and gives higher intensities of functional groups on the hydrochar

surface, both of which strongly influence the retentions of inorganic elements in the hydrochar.

Finally, we performed the detailed characterisation of the biocrude and aqueous phase from HTC of *Chlorella* at 180 – 220 °C for holding time of 15 and 60 min. As the reaction proceeds from mild to severe conditions, mass yield and energy recovery of biocrude increase, and molecular weight distribution of constituent compounds shifts to the smaller size. The highest yield of biocrude was found to be 34.6 wt % on a dry basis of algae at 220 ºC and 60 min with a corresponding heating value of 34.0 MJ/kg. The mass yield of aqueous phase first increases, and then slightly reduces, showing decomposition to biocrude and gaseous products. The relative abundance of N-containing heterocyclic compounds (e.g. 3,6-Diisopropylpiperazin-2,5-dione) in the biocrude increase and oxygenates (such as 1-Hexadecen-3-ol,3,7,11,15-tetramethyl) decrease with an increase of reaction temperature and holding time. The recovery of different metals (Na, K, Mg, Ca, Fe, and Zn) in the biocrude appears to be a strong function of reaction temperature and holding time. For instance, iron in the biocrude decreases from 800.23 to 564.45 mg/kg with an increase in temperature from 180 – 220 °C at 15 min, and a substantial reduction is observed at 60 min (i.e. from 1111.87 to 238.71 mg/kg). The aqueous phase contains most of the essential macronutrients e.g. Na^+, K^+, CH_3COO^-, $H_2PO_4^-$ and NH_4^+, and micronutrients such as Mn, Fe, and Zn, which can be recycled as cultivation media for the growth of algal biomass.

ACKNOWLEDGEMENTS

I am grateful to Murdoch University for the award of Murdoch International Postgraduate Scholarship (MIPS) that provides financial help throughout my studies.

My sincere gratitude goes to my supervisors, Dr Xiangpeng Gao, Professor Bogdan Z. Dlugogorski and Associate Professor Mohammednoor Altarawneh for providing me with the opportunity to undertake this research, and for their proficient advice, patience, guidance, and support throughout this study. Their keen knowledge and expertise have been a great source of learning and motivation for me. I deeply acknowledge Dr Xiangpeng Gao for his quick advice, training, assistance, and understanding.

My immense acknowledgment goes to my beloved parents for bearing my absence for years, and to my husband for his unconditional support and encouragement throughout this PhD study.

I express my earnest appreciation to our research team of the Fire Safety and Combustion Kinetics Research Laboratory, Dr Juita, Dr Ibukun Oluwoye, Dr Zhe Zheng, Dr Sara Mosallanejad, Dr Kamal Siddique, Dr Anam Saeed, Ms Sana Zahid, Dr Nassim Zeinali, Dr Arif Abdullah, Mr Thamsanqa Ncube, Ms Saleha Quadsia, Ms Kanwal Shabbir, Ms Kudzai Angeline Mchibwa, Mr Goruck Soban, and Dr Jakub Skut. With courtesy and assistance from them, I experienced the memorable years of experiments and computation.

I would like to acknowledge Dr Muhammad Usman Rahim, Dr Sui Boon Liaw, and Dr Mingming Zhang for experimental assistance and technical discussions. I am also grateful to the technical staff from Chemistry Labs, Dr Andrew Foreman, Dr Stewart Kelly, Dr Sanda Cricelli, Dr Malgorzata Kowalczyk, Dr Marc Hampton, and Ms Claire Tull for their training on various equipment and prompt help.

LIST OF PUBLICATIONS

Journal Articles:

1. **Jabeen S**, Zeng Z, Altarawneh M, Gao X, Saeed A, Dlugogorski BZ, Thermal Decomposition of Model Compound of Algal Biomass, International Journal of Chemical Kinetics 2019; 51: 696-710, https://doi.org/10.1002/kin.21301
2. **Jabeen S**, Gao X, Altarawneh M, Hayashi J, Zhang M, Dlugogorski BZ, Analytical Procedure for Proximate Analysis of Algal Biomass: Case Study for *Spirulina* and *Chlorella*, Energy and Fuels 2020, 34, 474-482, https://doi.org/10.1021/acs.energyfuels.9b03156
3. **Jabeen S**, Gao X, Altarawneh M, Dlugogorski BZ, 'Effect of Product Recovery Methods on the Yield and Properties of Hydrochar from Hydrothermal Carbonisation of Algal Biomass' (*in progress*)
4. **Jabeen S**, Gao X, Altarawneh M, Hayashi J, Dlugogorski BZ, 'Detailed Characterisation of Biocrude and Aqueous Phase from Hydrothermal Carbonisation of Algal Biomass' (*in progress*)

Conference Presentations:

1. Development of an Analytical Procedure for Proximate Analysis of Algal Biomass: A Case Study for *Spirulina* and *Chlorella*, First Australian Combustion Summer School, Sydney, Australia, 16 – 21st December 2018.
2. Effect of Product Recovery Methods on the Yield and Properties of Hydrochar from Hydrothermal Carbonisation of Microalgae, 27th European Biomass Conference and Exhibition, Lisbon, Portugal, 27 – 30th May 2019.
3. Analytical Procedure for Proximate Analysis of Algal Biomass: Case Study for *Spirulina* and *Chlorella*, 7th Sino-Australian Symposium on Advanced Coal and Biomass Utilisation Technologies, Wuhan, China, 3 – 6th December 2019.

TABLE OF CONTENTS

LIST OF FIGURES

LIST OF TABLES

CHAPTER 1

Introduction

1.1 Research Background and Motivation

Fossil fuels being the primary energy source contribute 94 % of the total energy consumed in Australia, as of 2015.[1] The greenhouse gases mainly CO_2 arising from excessive burning of fossil fuels is a leading cause of global warming that increases the earth's temperature by 0.13 °C per decade. With only 0.3 % of the world's population in Australia, the CO_2 emissions account for 1.04 % of the world's greenhouse gases, which is huge.[2] Coal supports 70 % of electricity production in Australia with the remainder of oil, gas, hydro, solar, wind, and biomass (only 1 %). According to Bioenergy Australia, the biomass contribution is projected to elevate by 1.4 % per year until 2030[3], which draws attention towards exploring the sustainable feedstocks and efficient processes for the production of biofuels that serve as an alternative to fossil fuels in the foreseeable future.

Australia is naturally bestowed with land, sunlight and brackish water suitable for the growth of various algal strains.[4-6] The interest in utilisation of algal biomass as third-generation biofuels has been developing rapidly since the last three decades[7] because of the fast growth rates, high lipid contents and food chain security associated with algal biomass.[8-9] Due to the versatile composition of microalgae (carbohydrates, proteins, lipids, pigments, nucleic acids, antioxidants, and moisture), enormous attention is paid to the hydrothermal processing with envisioning of the algal bio-refinery approach that

focuses not only the biofuels but the likelihood of commercialisation of co-products arising from algae processing with a minimal waste produced.[7, 10-11] For instance, in a joint project of Australian Research Council and industry partners, the hundreds of algal species with high nutrient values, less environmental stress and high lipid contents were targeted to generate biodiesel, protein-rich aqueous culture, cattle feed, and omega-3 fatty acids.[7] Muradel Pty Ltd based in Western Australia grows algae on a larger scale of 6.5 km^2 with a primary focus to optimise the steps in algal biofuel production, from algae harvesting to oil extraction. Over the decade, the interest in the hydrothermal processing of microalgae for biodiesel as an environment-friendly aviation fuel has significantly emerged in Australia.[7, 12-13] Therefore, algal biomass through hydrothermal processing can potentially play an important role in Australia's energy setup due to its significant benefits in overwhelming the challenges of environmental issues and energy crises.

Extensive research has been carried out on the high-temperature hydrothermal processes for algal biomass including liquefaction (280 – 375 °C)[14-20] and gasification (400 – 700 °C)[21-26] to generate the energy-dense liquid and gaseous fuels. Relatively less concern is observed for the mildest hydrothermal carbonisation process (180 – 260 °C) that aims at producing the solid fuel 'hydrochar', along with nutrient-rich aqueous phase and biocrude as co-products.[27-29] The hydrochar experiences high carbon and hydrogen, low oxygen and improved heating values as compared to the raw feedstock that makes it a potential solid fuel analogous to that of coal.[30-31] The exceptional surface functionality, high nitrogen contents, and inorganic matter augments its utilisation as an energy storage carbon material[32-34] and carbon-acid catalyst.[35-37] The temperature and holding time are the most influential reaction parameters affecting the yields and properties of hydrothermal carbonisation (HTC) products.[29, 31, 38-41] The HTC biocrude is essentially the intermediate of hydrothermal liquefaction (HTL) biocrude[42] because the carbonisation temperatures have to be experienced by the algal slurry even if the process is designed for HTL. Mass yields of up to 37 wt % on a dry basis (db) of algae and heating values in the range of 32.2 and 34.9 MJ/kg are reported for HTC-derived biocrude.[43] Moreover, the aqueous phase because of high carbon, nitrogen, and nutrient

levels, got potential for recycling into the cultivation ponds to aid the algal growth[30-31] or anaerobic digesters to produce the bio-gas.[30-31]

Regardless of the rational research on the hydrothermal carbonisation of microalgae, there are still areas in this field, which needs further improvement because of the complex composition of the algal biomass and composite chemistry of the process. For example, there are no standardised conditions to determine the fuel properties of algal species, and the methods developed for other solid fuels are widely employed to algal fuels without any validation. This may affect the accurate quantification of the properties, which govern their transition to high-quality biofuels. The information on the product profiles from thermal processing of high-N containing biomass is scarce, which is an important consideration for the design of thermochemical processes. While the previous research has only focused on the reaction temperature and holding time of HTC, the impact of solid loading and product recovery procedures on the yields and properties of hydrochar is still unclear that substantially affects the field applications of hydrochar. Not least of all, little attention is paid towards the quantification and characterisation of biocrude and aqueous phase from HTC, especially the heavy metal recoveries, the knowledge of which is essential to evaluate the feasibility of the aqueous phase and biocrude for onward applications. Therefore, this study focuses on these fundamental research gaps to improve the understanding of hydrothermal carbonisation for algal biomass and provide essential knowledge for the practical implications of derived products.

1.2 Scope and Objectives

The present study aims to deliver a comprehensive understanding of the hydrothermal carbonisation of microalgae to produce the products in a rationale yields and with the desired properties. The detailed research objectives include to:

1. Evaluate the applicability of the widely used ASTM E870-82 developed for proximate analysis of wood fuels, for the algal biomass using *Spirulina* and

Chlorella as model algal samples. An analytical procedure for the proximate analysis of algal biomass will be proposed.

2. Investigate the thermo-kinetics of the most plausible unimolecular and bimolecular routes encountered in the gas and condensed-phase thermal decomposition of 'Leucine' as an algal biomass model compound.
3. Examine the impact of the product recovery methods on the yield and properties of hydrochar from hydrothermal carbonisation of *Chlorella* under identical reaction conditions.
4. Quantify and characterise the biocrude and aqueous phase from hydrothermal carbonisation of *Chlorella* and evaluate the impact of reaction temperature and holding time on the metal content of the two phases.

1.3 Thesis Outline

To address the above objectives, this dissertation is structured into 7 chapters (excluding this chapter). The thesis outline is schematically shown in **Figure 1-1** and the contribution of each chapter is enlisted as follows:

- Chapter 2 reviews the up-to-date literature on hydrothermal carbonisation of microalgae, highlights the research gaps of the previous studies, and pinpoints the specific research objectives of this study.
- Chapter 3 outlines the samples used, the methodology adopted, and the characterisation techniques employed to achieve the research objectives.
- Chapter 4 examines the applicability of conventional methods of proximate analysis to *Chlorella* and *Spirulina*, followed by the development of analytical procedures for proximate analysis of algal biomass.
- Chapter 5 studies the unimolecular and bimolecular channels governing the thermal decomposition of leucine as a representative model compound for amino acids in algal biomass. This led to building a robust kinetic model that accounts for the emission of nitrogen-containing species from thermal degradation of algal biomass.

- Chapter 6 systematically investigates the impact of the product recovery method on the yield and properties of hydrochar from hydrothermal carbonisation of *Chlorella*. The direct filtration of reaction products (without washing) and subsequent drying versus dilution of reactor contents by dichloromethane followed by phase separation and drying, under the identical reaction conditions of HTC are explored.
- Chapter 7 characterise the biocrude and aqueous phase from hydrothermal carbonisation of *Chlorella* and evaluates the recoveries of the metals in the aqueous phase and biocrude.
- Chapter 8 concludes the present study and recommends future work

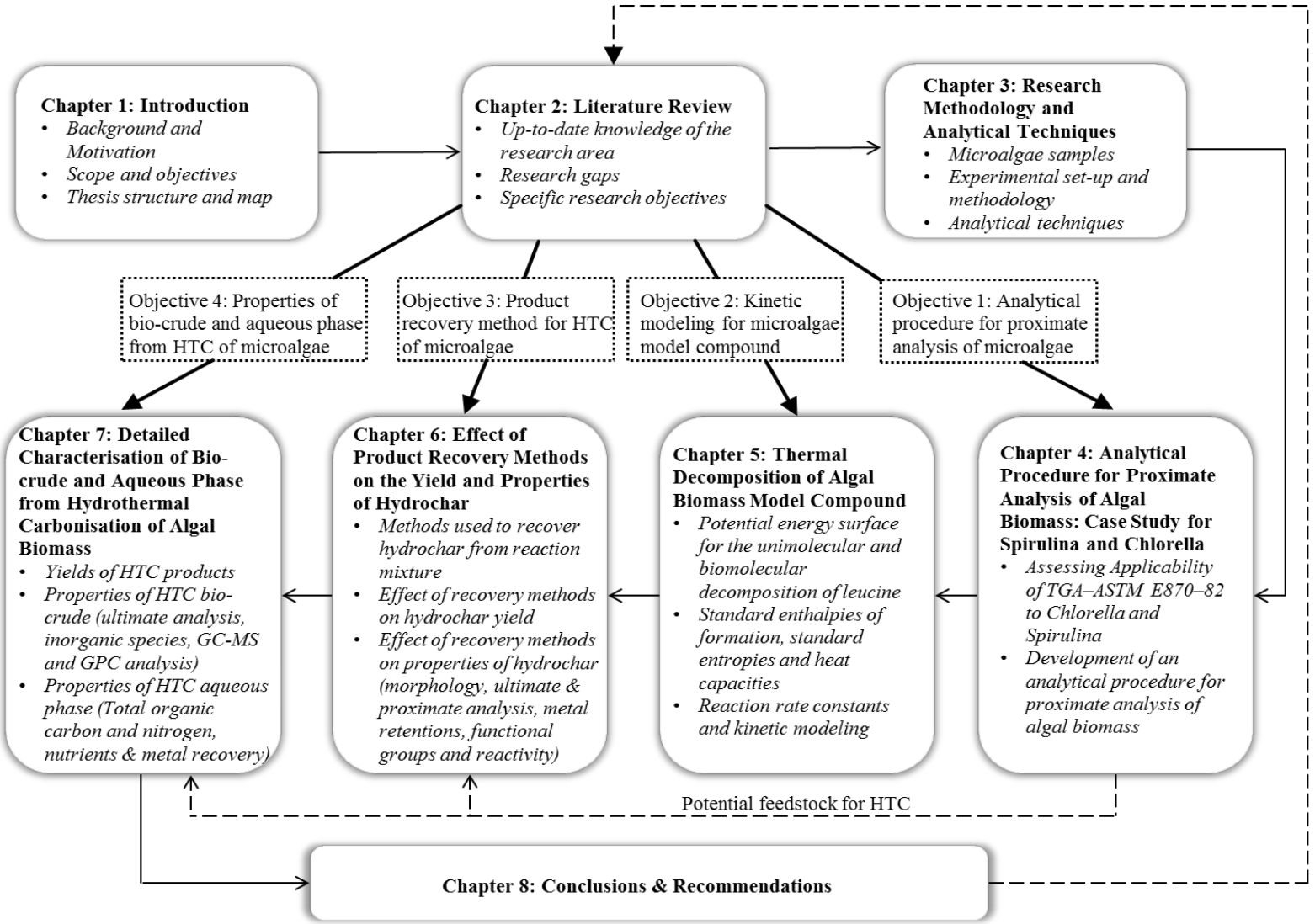

Figure 1-1: Thesis map

CHAPTER 2

Literature Review

2.1 Introduction

Australia's carbon emissions continue to rise because of its heavy reliance on coal as an energy source, which needs to be minimised and/or replaced with environmentally friendly renewable fuels. The third-generation biofuels from fast-growing aquatic biomass enjoy several advantages over biofuels from sugars, vegetable oils[44-45] and lignocellulosic residues.[8-9, 45] Microalgae aids carbon sequestration by absorbing a large amount of atmospheric CO_2 and hold tremendous potential for sustainable production of biofuels.[46-47] Among the various thermochemical processes, hydrothermal treatment is widely deployed for algal biomass[14-20], though the economic and technological challenges of producing in bulk quantities still exist.

This chapter reviews the up-to-date literature on hydrothermal carbonisation of microalgae, identifies the research gaps of the previous studies, and highlight the research objectives of the present study. The review starts with addressing the benefits of hydrothermal processing for algal biomass with the complications that may encounter due to the complex chemical composition of microalgae. Then, the reaction mechanisms and factors affecting the yields and properties of HTC products are elucidated. Furthermore, the potential properties and emergent applications of algal biofuels and the HTC-derived aqueous phase are thoroughly reviewed.

2.1.1 Hydrothermal Processing and Hot Compressed Water as a Reaction Media

Microalgae contain 40 – 80 % of intracellular moisture that has to be removed before lipid extraction and subsequent transesterification to produce biodiesel.[48] Pre-drying of algal biomass is one of the economic drawbacks of processing microalgae for biofuel production, which may consume up to 85 % of the total energy of the process.[49] Hydrothermal treatment (HTT) eliminates the pre-drying phase, by processing algal slurry in hot compressed water over the temperature range 180 – 700 ºC and autogenous pressure of 5 – 40 MPa, aiming to generate an energy densified product.[50-51] Hydrothermal processing falls into three categories, depending upon the properties of hot compressed water and the desired product. Hydrothermal carbonisation (HTC) is the mildest process occurring at 180 – 260 ºC to produce a solid, 'hydrochar' as a major product in addition to biocrude, aqueous phase, and gas as by-products. Hydrothermal liquefaction (HTL) is biomass to the biocrude route at operating temperatures of 280 – 375 ºC, while gasification (HTG) targets at producing synthetic natural gas (syngas) at 400 – 700 ºC in supercritical water. Algal hydrochars are analogous to coal and used as energy storage materials[32-33], while the aqueous phase is recycled for the cultivation of algal biomass[29, 52] and energy recovery via anaerobic digestion.[53-54] The HTL biocrude has calorific values comparable to that of biodiesel and petroleum fuels and can be upgraded to replace the transportation fuel[9], whereas, the syngas from HTG is converted to hydrocarbons by Fisher-Tropsch synthesis.[8]

Hot compressed water has unique properties that make it superior to solvents at room temperature. On increasing the temperature up to the critical point (i.e. 374 ºC), the hydrogen bonding is weakened, which results in the decline of the dielectric constant of water from 80 at 25 ºC to about 14 at 350 ºC, and rise of ionic product from 10^{-14} to 10^{-11} with an increase of temperature to the critical point.[51] The density of liquid water reduces and that of gaseous water increases until they are alike at the critical point, beyond which the density of supercritical water remains unchanged without any further phase transition. This helps water to promote the acid- or base-catalysed reactions, lower the energy of activation, and elevate the miscibility of organic compounds. **Figure 2-1** shows the regions of HTC, HTL, and HTG on the phase

diagram of water. During HTC, the organic compounds are hydrolysed and dissociated in subcritical water, which enhances the degree of carbonisation of feedstock by lowering the oxygen content to produce hydrochar. With further increase in temperature to HTL range, the dielectric constant of water is very close to that of dichloromethane (i.e. 10), which aids the extraction of algal lipids to yield biocrude. At supercritical conditions (> 374 ºC) of HTG, syngas, or gas mixture of H_2, CH_4, CO, CO_2, and light organics is favoured due to thermal degradation of heavier oily fractions and water-soluble organics produced at sub-critical conditions of hydrothermal processing of algal biomass.

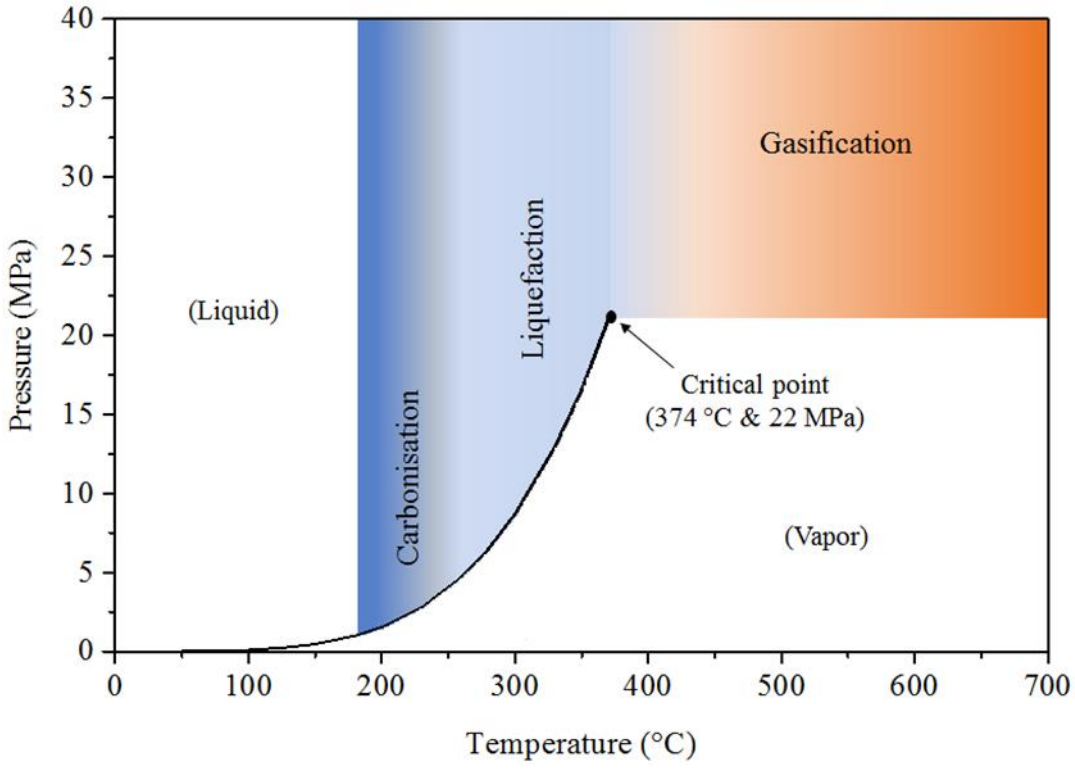

Figure 2-1: The regions of hydrothermal carbonisation, hydrothermal liquefaction and hydrothermal gasification in the sub- to supercritical water

2.1.2 Motivation of 'Hydrothermal Carbonisation of Microalgae'

Hydrothermal carbonisation is the least energy-intensive HTT process to convert microalgae into hydrochar as a key product, with mass yields varying between 16 and 66 wt %[27, 29, 38, 43, 55] depending upon the feedstock composition, reaction conditions, and recovery methods. The distinctive property of algal hydrochars is their high nitrogen content that imparts additional electrons to its graphitic structure

and improves its thermal stability and electrical conductivity.[32] The activation of hydrochars with potassium hydroxide generates highly porous carbon materials suitable for applications as electrodes in the capacitors and lithium-ion batteries.[33] Furthermore, HTC serves as an intermediate stage of extensively researched hydrothermal liquefaction[16-17, 56], the biocrude from which (produced at 280 – 375 ºC) first undergoes the carbonisation conditions (180 – 260 ºC) before being thermally degraded at high temperature. Due to the close linkage between hydrothermal carbonisation and liquefaction, the study of HTC biocrude, in terms of the mass yields and properties, is of fundamental importance towards commercialisation of the algal biocrude. In addition to that, HTC derived aqueous phase is rich in organic carbon, nitrogen, and essential nutrients that can be recycled as a cultivation media to the algal growth systems[29, 52, 57-58], or anaerobically digested to generate methane.[53, 59] Therefore, hydrothermal carbonisation serves as a bottleneck to support the algal bio-refinery, through effective recovery and re-use of products as value-added chemicals.

2.2 Algal Biomass and Hydrothermal Carbonisation

2.2.1 Composition of Algal Biomass

Microalgae are unicellular organisms that uptake sunlight, water, CO_2, and nutrients by photosynthesis and transform them into carbohydrates, proteins, and lipids, the composition of which strongly depends on the strain-specific growth conditions, photosynthetic ability, and cell partitioning mechanism.[60] The biochemical composition of microalgae is widely different from that of lignocellulosic biomass that contains hemicellulose, cellulose, and lignin as principal components.[61-62] Moreover, the complex matrix of nucleic acids, inorganics, carotenoids, chlorophyll, and DNA in the chloroplast[63-65] accounts for the distinctive properties of various algal species that may affect the application of standardised methods from species to species.[66]

In general, carbohydrates form the significant fraction of microalgae (8 – 64 %) existing in the form of both monomers (glucose, fructose, etc.) and polymers (starch, cellulose, hemicellulose).[67] The cell wall is mostly composed of cellulose in the

form of starch as a primary carbohydrate source and a minimal of hemicellulose and lignin.[68] Lipids are non-polar heterogeneous compounds that constitute 4 – 58 % of the dry mass of algal biomass and are mainly composed of triglycerides, glycolipids, phospholipids, and free fatty acids.[69-70] Microalgae can be selectively grown to have high lipid content by reducing the availability of the nutrients and limiting the sunlight intensity.[71] Carbohydrates and lipids play a vital role in raising the heating value of microalgae as well as emissions of carbon dioxide during algal biofuels combustion.[72] Microalgae are capable of producing high protein fractions (28 – 71 %) within their cells[70], which, together with nucleic acids serve to aid the metabolic activity and structural functions during algal biomass growth. Nucleic acids also contain the majority of the cell's phosphorus.[72] Protein and nucleic acids are responsible for the high nitrogen content of the microalgae and its derived fuel. Microalgae accumulate inorganic minerals and salts within their cells, for example, sulphates, chlorides, carbonates and silicates of sodium (Na), potassium (K), magnesium (Mg) and calcium (Ca).[67] Silicates undergo a various transformation and polymerisation reactions during algal biomass growth resulting in the complex inorganic network, which somehow supports the structural rigidity in microalgae, just like the lignin in plant biomass. These inorganic salts account for the high ash content of algal species.

2.2.2 Fuel Properties of Algal Biomass

Algal biomass holds tremendous potential as a biofuel feedstock due to the higher lipid content that can be extracted and converted into biodiesel by transesterification.[73] Microalgae capture 40 % of atmospheric carbon dioxide and convert it into carbohydrates as an outstanding source for biofuel production.[74] The fundamental fuel properties for any feedstock are proximate analysis, ultimate analysis, and higher heating value (HHV), based on which the fuel quality can be assessed. **Table 2-1** enlists the fuel properties of various algal strains used by different hydrothermal carbonisation studies. Carbon and hydrogen are the desirable elements that increase the heating value of biomass as opposed to oxygen and nitrogen that lowers the fuel quality. Likewise, the high volatile matter (VM) and fixed carbon (FC) content indicates the feedstock potential to release energy on combustion, whereas, moisture and ash adversely impact the fuel quality.[75-76]

Therefore, a complete characterisation of the fuel properties of algal biomass is essential to estimate the fuel applications of derived biofuels, but the algal biomass has received less attention in terms of standardised methods of quantification, which developed for lignocellulosic biomass is extensively employed for the algal biomass, without any validation.

Table 2-1 enlists the fuel properties of the algal species used for hydrothermal carbonisation studies in the literature. The widely used freshwater microalgae, *Chlorella* has appreciably high carbon contents (50.4 – 55.5 wt % on a dry and ash-free basis, daf) and hence, calorific values (21.1 – 23.8 MJ/kg), although the nitrogen contents (2.9 – 11.0 wt %, daf) vary from species to species.[30-31, 39, 55, 77-78] *Nannochloropsis* is well known for biofuels production because of their higher contents of polyunsaturated fatty acids that are extracted for subsequent transesterification to yield biodiesel.[40, 79-81] Freshwater species, *Spirulina* contains reasonably high nitrogen levels (11.4 wt %, daf) and is effectively employed to synthesize the N-doped carbon storage materials.[32-33] Macro alga *Laminaria hyperborea*[55], *Scenedesmus*[41], *H. reticulatum*[31], *Laminaria saccharina*[82], *Alaria esculenta*[83], *Laminaria digitata*[83], and *Sargassum horneri*[84] are high in ash content (11.5 – 44.6 wt %, db) and oxygen concentrations (39.7 – 62.8 wt %, daf) that results in their lower calorific values (9.5 – 15.4 MJ/kg). Although hydrothermal carbonisation has the potential to lower the oxygen (by dehydration and decarboxylation reactions) and inorganic content (by dissolution into the aqueous phase) of the resulting hydrochars, the overall fuel value of the hydrochar or biocrude derived from both high oxygen and high ash containing species will be affected. Thus, the choice of the algal species and accurate characterisation of the fuel properties strongly impacts the yields and properties of hydrothermal carbonisation products, which in turn influences the overall energy recovery of the process.

Table 2-1: Basic fuel properties of algal species used for hydrothermal carbonisation in the literature

References	Algal species	Proximate analysis [a]			Ultimate analysis [b]				HHV [e]
		VM [c]	FC [d]	Ash	C	H	O	N	
Heilmann et al.[27]	*C. reinhardtii*	-	-	-	51.6	7.9	-	9.8	18.0
Miao et al.[78]	*Chlorella sorokiana*	-	-	-	50.4	7.8	37.4	2.9	21.6
Falco et al.[32]	*Spirulina platensis*	-	-	-	48.0	7.0	33.7	11.4	-
Broch et al.[85]	*Spirulina maxima*	-	-	5.2	52.7	7.3	27.3	11.9	-
Jena et al.[17]	*Spirulina platensis*	-	-	-	46.8	6.9	34.8	10.7	20.5
Smith et al.[55]	*Chlorella*	-	-	9.2	53.3	7.9	29.8	8.6	21.8
Smith et al.[55]	*Laminaria hyperborea*	-	-	20.6	39.4	6.5	44.5	3.5	11.8
Jazrawi et al.[16]	*Chlorella*	-	-	6.0	53.5	7.4	27.6	11.0	24.3
Ekpo et al.[39]	*Chlorella*	82.7	4.5	9.8	51.8	7.6	29.1	10.7	21.1
Du et al.[38]	*Nannochloropsis*	-	-	24.2	52.7	7.3	31.7	8.2	16.8
Levine et al.[29]	*Nannochloropsis*	-	-	-	49.9	8.0	-	8.5	20.6
Alba et al.[43]	*Desmodesmus sp.*	-	-	-	51.9	7.3	33.8	6.8	23.4
Bach et al.[77]	*Chlorella*	74.6	16.4	9.0	53.0	8.6	35.0	3.3	22.0
Lee et al.[30]	*Chlorella*	80.7	12.6	6.6	50.9	6.9	31.0	10.2	23.1
Liu et al.[41]	*Scenedesmus*	55.3	-	44.6	44.6	6.1	40.8	4.8	9.5
Lu et al.[80-81]	*Nannochloropsis sp.*				46.8	6.6	-	7.3	-
Batista et al.[53]	*Mixed microalgae*	53.6	13.4	32.9	54.6	7.5	28.8	8.3	-
Park et al.[31]	*H. reticulatum*	77.2	9.6	13.3	33.9	5.6	53.8	6.7	15.4
Park et al.[31]	*Chlorella*	85.8	9.6	4.5	55.5	8.7	25.2	10.5	23.8
Yao et al.[86]	*Arthrospira platensis*	-	-	-	45.6	6.8	39.2	6.8	-
Anastasakis et al.[82]	*Laminaria saccharina*	-	-	24.2	48.6	5.7	40.8	3.7	12.0
Smith et al.[83]	*Alaria esculenta*	-	-	22.3	49.2	6.4	39.7	2.9	12.8
Smith et al.[83]	*Laminaria. digitata*	-	-	28.3	46.4	6.5	43.4	2.4	11.4
Xu et al.[84]	*Sargassum horneri*	69.1	19.4	11.5	29.9	4.7	62.8	1.9	-
Zhou et al.[87]	*E. prolifera*	46.0	21.2	32.7	41.1	7.4	46.1	5.2	-

[a] wt % dry basis, [b] wt % dry and ash-free basis, [c] Volatile Matter, [d] Fixed Carbon, [e] MJ/kg

2.2.3 Conversion of Algal Biomass to Hydrochar, Biocrude and Aqueous Phase

Hydrothermal carbonisation initiates from the hydrolysis of algal macromolecules (carbohydrates, proteins, and lipids), as presented in **Figure 2-2**. The increase in temperature intensifies the ionic product of water that hydrolyses the carbohydrates to oligomers and monomers, e.g., glucose and fructose. Concurrently, these monomers undergo dehydration and decarboxylation to yield carboxylic acids (e.g. acetic acid, propionic acid, etc.) that lowers the pH of the reaction media and catalyses the decomposition of carbohydrates.[88] Hydrolysis of carbohydrates and decomposition of oligomers occur in parallel to yield a variety of compounds that includes the straight and branched-chain alkanes, phenols, cyclic ketones, and furfurals, many of them are water-soluble. The peptide bonds (C-N) in protein are hydrolysed under HTC conditions to produce the amino acid, which quickly cyclizes to form the heavier dipeptides, e.g. 2,5-Diketopiperazine or Diisopropylpiperazin-2,5-dion.[89] The yields of amino acids are lower than carboxylic acids for two reasons: first, the nitrogen content of biomass is much smaller than the carbon content, and second, the faster thermal degradation of amino acids to amines, amides, ammonia and light hydrocarbons via deamination reactions.[51] Heterocyclic compounds like pyrroles, pyridines, and indoles emerge from the Maillard reactions between amino acids and sugars.[9] Algal lipids are usually in the form of triglycerides, which break down into glycerol and free fatty acids in HTC media. Glycerol undergoes decarboxylation to produce alcohol and aldehydes, e.g. ethanol, allyl alcohol, 2-Octadecen-1-ol and propionaldehyde.[50] Fatty acids are generally stable in water under hydrothermal carbonisation conditions but may decompose into long-chain alkanes (e.g. hexadecane) at higher temperatures.[89] The high viscosity of biocrude derived from hydrothermal processing of microalgae is attributed to the presence of heavier compounds like long-chain alkanes, fatty acids, and dipeptides in biocrude.

Under HTC conditions, the cell wall of algal biomass ruptures and releases the intracellular molecules into water, thus reducing the yield of solid (hydrochar) and increasing that of biocrude and water-soluble organics. Hydrolysis dominates at low temperatures (< 220 ºC) followed by the onset of depolymerisation and condensation

reactions between different phases at high temperatures.[89] The water-soluble organics are decomposed into biocrude and gases[43], together with the degradation of heavy oil components into light ones that partly goes back to the aqueous phase and gases.[20] These inter-conversions between the hydrothermal phases result in enrichment of heterocyclic oxygen and nitrogen-containing compounds in biocrude.[42, 90] Also, by increasing the reaction temperature, Maillard reaction products (e.g. pyrroles, dipeptides, pyridine) are ending up into the biocrude as indicated by the increase in its nitrogen content.[42] Such nitrogenous species convert into toxic N-bearing compounds, such as NH_3 and HCN[91-94], which serve as a direct precursor for the formation of the harmful gases like NO_x and N_2O during combustion.[95-96] For fuel applications of high-N containing biofuels, the knowledge on the fate of the nitrogen-containing compounds during thermochemical conversions is important to outlook their practicality. Since, hydrothermal media offers a complex reaction network relative to dry feedstock based thermal processes (e.g. pyrolysis), nevertheless; the major reaction pathways (decarboxylation, dehydration and deamination) for thermal degradation of biomass are essentially the same.[51, 97-99] Therefore, a rather simplified approach can be undertaken to model the product profiles of typical nitrogen-containing species, and elaborate on the underlying reaction mechanisms of HTC.

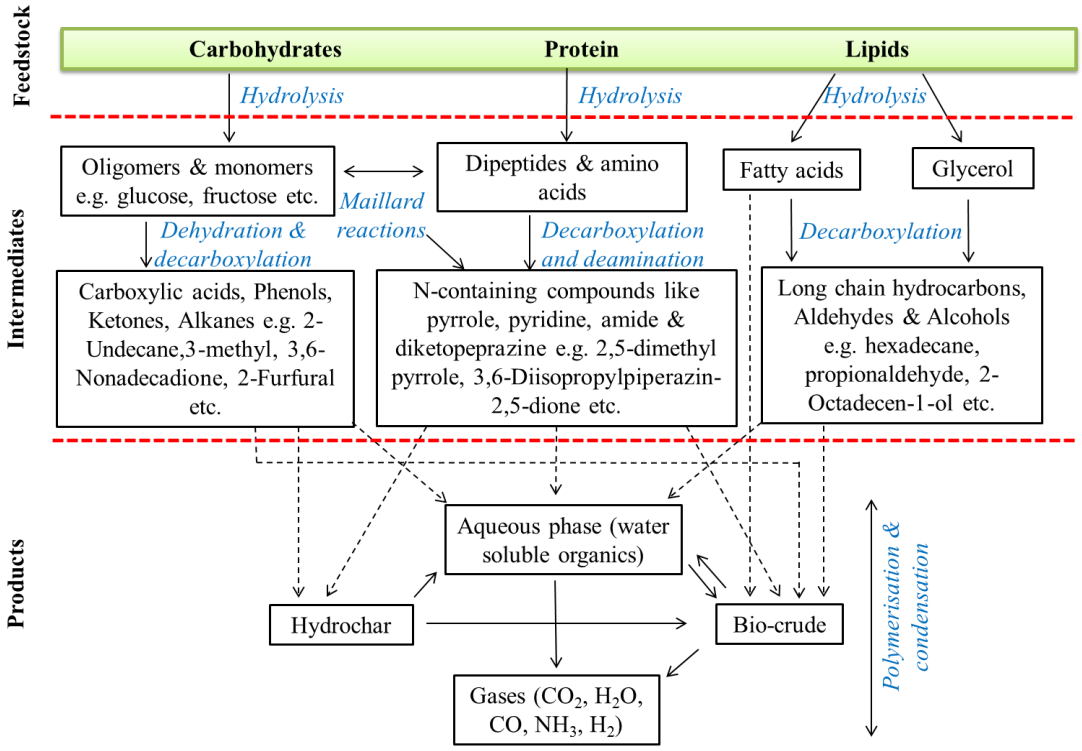

Figure 2-2: Reaction network for hydrothermal carbonisation of carbohydrates, proteins and lipids derived from the studies.[19-20, 50, 89]

2.3 Factors affecting the Yields of HTC Products

2.3.1 Temperature

The hydrochar yield at 170 to 260 ºC for a wide range of retention times (5 – 120 min) from various feedstocks used in the literature are summarised in **Figure 2-3**. The high temperature always results in low hydrochar yield at a given retention time because of an increased rate of hydrolysis and decomposition of intermediates. However, the rate of change differs from species to species, depending upon the feedstock composition, reaction conditions, and product recovery methods etc.

In **Figure 2-3a** at a retention time of 10 min, *Nannochloropsis*[38] shows slightly lower mass yields at 170 – 180 ºC than *Chlorella*.[77] Given the elemental composition (see **Table 2-1**) and solid loading (20.0 %) for both algal species are similar, a high ash content of *Nannochloropsis* (24.2 wt % versus 9.0 wt % for *Chlorella*) catalyses the hydrolysis of carbohydrates, thus reduces the hydrochar

yield. A similar trend is observed for HTC of high ash (44.6 wt %, db) containing *Scenedesmus* at 180 – 260 °C for holding time of 4 h, that displayed higher mass yield after demineralisation with dilute HCl (that reduces the ash content to 14.4 wt %, db.).[41] Levine et al.[29] and Lu et al.[80] studied the HTC of *Nannochloropsis* sourced from different suppliers at similar reaction conditions as illustrated in **Figure 2-3 (b & c)**, the higher hydrochar yield reported by former could be because of the high carbon content of algae, i.e. 49.9 % relative to 46.8 % for the latter, although the ash contents of both species are unknown. *Chlorella sorokiniana* subjected to two-step hydrothermal processing at 220 – 260 °C for 60 min (lower triangles) displays less hydrochar yield than one-step HTT (upper triangles), because of extraction of fatty acids and sugars by the first-step hydrothermal treatment that reduces the availability of water extractives to decompose into hydrochar during the second step HTT.[78]

The hydrochar yield from HTC is not only affected by the feedstock composition and reaction conditions but also the recovery method adopted. In literature, there are mainly two different methods used to recover hydrochar from the reaction product. One is to separate hydrochar directly from the liquid phase by vacuum filtration, followed by water washing and subsequent drying.[27-28, 32, 83] Some other researchers modified this method by omitting water washing.[15, 29, 38, 55, 85] The other method involved dilution of sticky product mixture with an organic solvent such as dichloromethane (DCM), filtration of the diluted mixture to recover hydrochar, and subsequent phase separation to quantify the aqueous phase and biocrude.[39, 43, 82] The use of these different product recovery methods can significantly impact the hydrochar yield and properties. For example, in **Figure 2-3d** (60 min) at 200 and 250 °C, *Laminaria hyperborea*[55] (separated by vacuum filtration without washing with water or solvent) gives much higher mass yield than *Laminaria digitata* and *Alaria esculenta*[83], which were washed with water before drying (that removes inorganics). Hydrochar recovery from *Spirulina* using dichloromethane followed by filtration, phase separation and subsequent drying results in ever lower mass yields at the similar reaction conditions of 200 and 250 °C for 60 min.[17]

Researchers have paid less attention to the quantification of biocrude and the aqueous phase (usually reported as 'water-soluble organics' or 'water extractives')

from HTC, except those who perform HTL at low temperatures (220 – 260 ºC).[17, 43, 78, 82, 87] Generally, the biocrude yield increases with temperature because of increased hydrolysis of lipids to free fatty acids (ends up in biocrude) and extraction of non-polar products (due to reduced dielectric constant of water) formed by the decomposition of sugars and amino acids. It is believed that high lipid-containing algae result in more biocrude yield[90], however, considerable yields are obtained with low lipid algae, e.g. *Desmodesmus sp*. (lipid content 10 – 14 wt %) derived biocrude increase in its yield from 13.5 to 37.0 wt % with the rise in temperature from 170 to 250 ºC, at holding time of 60min.[43] Conversely, *Chlorella sorokiniana,* with high lipid content of 24.0 % gives relatively low biocrude yield of 31.0 wt % at 260 ºC.[78] Other studies report biocrude yield of up to 28.0 wt % from various feedstocks under HTC conditions[17, 82, 87], which largely depends upon the catalyst and solvent used for extraction.

Hydrothermal carbonisation extracts considerable fraction of starting algae into the aqueous phase that ranges between 5 and 55 wt %, based on the dry mass of feedstock.[17, 43, 78, 82, 87] The water-soluble organics continuously increase up to the temperature ~ 240 ºC, followed by a decline due to its decomposition into biocrude and gases, which generally occur in HTL temperature range.[43, 82, 87] The yield of water-soluble organics was greatly reduced from 7.5 to 5.0 % with an increase in temperature from 220 to 260 °C, by two-step hydrothermal processing of *Chlorella sorokiniana*, where low temperature (140 – 200 ºC) treated algae in the first step was further subjected to high-temperature HTT (220 – 300 ºC) in the second step.[78]

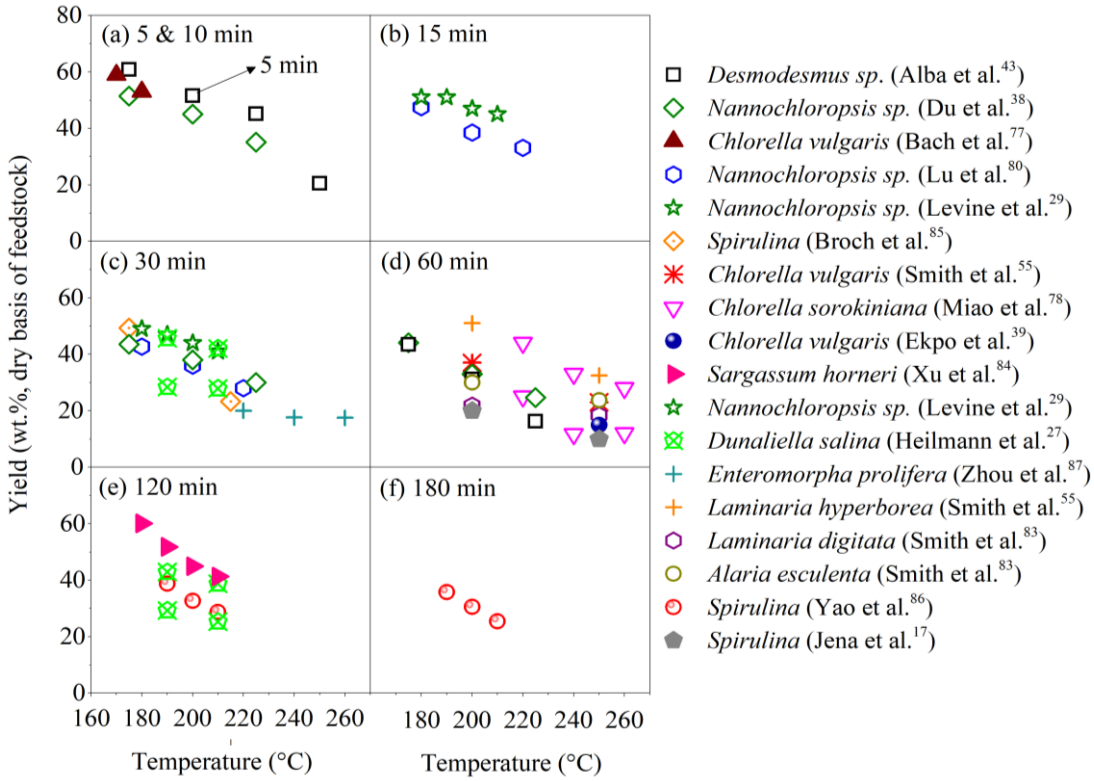

Figure 2-3: Effect of reaction temperature on hydrochar yield at holding times of (a) 5 & 10 min, (b) 15 min, (c) 30 min, (d) 60 min, (e) 120 min and (f) 180 min, for different feedstocks used in the Literature.

2.3.2 Holding Time

Holding time is usually defined as the duration for which the reaction is maintained at the desired temperature, excluding the heating and cooling stages. The impact of holding time is closely linked with reaction temperature and can be collectively termed as reaction severity[80] that drives the hydrolysis of algal macromolecules and decomposition of intermediates to yield different products. For HTC, retention times ranging from 5 min to 24 h have been employed with the most common being 30 – 120 min as presented in **Figure 2-3**. In general, reduced hydrochar yields are observed at longer holding times, as evident for the case of *Desmodesmus sp*[43] and *Nannochloropsis*[29, 38, 80] for an increase in retention time from 5 to 60 min, however, the effect is nullified at longer holding times of 120 and 180 min as observed for *Dunaliella salina*[27] and *Spirulina*.[86] Holding time amplifies the impact of temperature on product distribution of HTT, for instance, the case of *Desmodesmus sp.*[43] With the increase in holding time from 5 to 60 min at 200 ºC, hydrochar yield

reduces from 56.0 to 33.9 wt %, biocrude increases from 10.0 to 23.0 wt % and water-soluble organics rise from 33.1 to 47.2 up to the first 30 min of reaction followed by a decline to 37.4 wt % at 60 min. This dictates that the HTC process can be effectively optimised in terms of reaction temperature and holding time to acquire rationale yields of biocrude and nutrient rich aqueous phase.

2.3.3 Solid Loading

Heilmann et al.[27] were the first to investigate the effect of solid loading (5 and 25 %) on the mass yield and carbon content of the hydrochar derived from *Dunaliella salina* at 190 and 210 ºC for holding time of 30 and 120 min, as presented in **Figure 2-3 (c & e)**. The high solid loading displays superior hydrochar yields and increased carbonisation levels than low, indicating that continuous HTC can be designed with high solid concentrations of algae subjected to low temperatures and reduced holding times to have an acceptable hydrochar yield. Tian et al.[100] processed high-ash (41.6 wt %, dry basis) containing *algal blooms* at 260 ºC with solid loadings of 10, 15, and 20 % together with the increment of holding time from 30 to 90 min. He noticed the increase of hydrochar yield with solid loading and holding time, i.e. from 27.2 wt % (at 10 % solid loading and 30 min) to 33.4 wt % (20 % solid loading and 90 min) on dry and ash-free basis of feedstock. This was associated with a slight rise of biocrude yield from 11.6 wt %, daf (at 10 % solid loading and 30 min) to 15.8 wt %, daf (15 % solid loading and 60 min), and then decline to 11.3 wt %, daf (20 % solid loading and 90 min) for which the reasons are unclear. One explanation for low yield of biocrude could be the heat and mass transfer limitations to the organic matter induced by high concentrations of inorganics during hydrothermal processing.[9] On the other hand, the total nitrogen and total organic carbon of the aqueous phase were significantly enhanced by high solid loading (of 20 %)[100], which show that carbohydrates and proteins are adequately hydrolysed. These contrasted mechanisms and inadequacy of systematic experimental work hamper the complete understanding of underlying chemistry linked with a high solid loading of microalgae for HTC.

2.3.4 Other Factors

There are some specialised HTC conditions, specifically focused on producing carbon materials with high energy storage or catalytic ability. For instance, sulphuric acid and formic acid were employed during HTT (100 – 200 ºC) for holding time of 5 and 15 min, prior to HTL (of treated solids from HTT) with a focus to reduce the nitrogen content of the produced biocrude.[15] It was observed that nitrogen extraction into the aqueous phase was enhanced by the presence of acids at 150 ºC, but then levelled off by increasing retention time to 15 min at 200 ºC, where the acid catalysed hydrolysis was similar to hot compressed water in extracting the nitrogen to the aqueous phase. On the other hand, the addition of glucose to HTC of high protein-containing *Spirulina* at 180–240 °C for 24 h is promising for enhanced mass yields and fixation of nitrogen into hydrochar matrix, for subsequent use as energy storage material.[32-33] The amino acids reacted with monosaccharides via Maillard reactions and produce the stable N-containing heterocyclic compounds, e.g. pyridinic and quaternary nitrogen, that retain on the hydrochar surface. Moreover, in-situ hydrothermal carbonisation of microalgae residue with sulfuric acid at 180 °C for 2 h produces a solid carbon-based acid catalyst with high catalytic activity observed for esterification of oleic acid.[35]

Apart from the above-mentioned aspects, particle size is considered to be the minor factor affecting the hydrochar yield, though carbon recovery is enhanced by the use of smaller particles (150 – 300 μm) of *Sargassum horneri*.[84] Also, the particle size of lesser than 150 μm gives BET surface area of 12.3 m^2/g that marginally rises to 26.0 m^2/g with an increase of particle size to 600 μm. However, the direct relation of particle size with the BET surface area is not fully understood yet. There are some other factors like product recovery methods, reactor pressure, heating rate and cooling rate (of reaction products) that have not been studied for HTC of microalgae.

2.4 Properties of HTC Products

2.4.1 Hydrochar

2.4.1.1 SEM Analysis and BET Surface Area

Although the literature pertinent to SEM analysis and BET surface area analysis of algal hydrochars is scarce, there is a consensus on low porosity and small surface area of algal hydrochars.[101] Heilmann et al.[27] found that algal biomass readily loses its cell morphology under HTC treatment and gives a tortuous appearance as opposed to lignocellulosic biomass that largely retains its original structure. The extent of rupturing of the original cell structure strongly depends upon the cell wall characteristics of algal species. For example, *Desmodesmus sp.* is resilient to cell wall breakage even up to 250 °C[43], contrary to *Chlorella*[16], whose cell wall appears completely distorted at a similar temperature though the effect of this phenomenon on hydrochar porosity is unclear in the literature. Further, the improvement in BET surface area of the algal hydrochar is reported for longer holding times (than 4 h) due to decomposition of hydrolysis products contained within the pores.[84] Also, the BET surface area is influenced by the particle size of feedstock and heating rate of the HTC process[84, 102] that needs a thorough investigation.

2.4.1.2 Functional Groups

Algal hydrochar contains a variety of oxygen-containing functional groups such as O-H stretching vibrations in hydroxyl or carboxyl group, C-O and C=O stretching vibrations in carboxylic acids, ethers, alcohols, and ketones. The other popular functionalities include C-H stretching vibrations of aliphatic, N-H stretching vibrations in amino compounds and C=C for the aromatic ring.[41, 84, 103] The presence of these hydrophilic functional groups on the hydrochar surface imparts unique properties such as cation exchange capacity and water holding. The cation exchange capacity of hydrochars is related to their deprotonation tendency to acquire a negative charge and attract the metal cations from aqueous solution.[104] Water retaining capability of hydrochars could be useful for their soil conditioning applications.[105] The surface functionality of hydrochars declines at prolonged

holding because of excessive depolymerisation reactions, converting oxygen functional groups to stable water-soluble compounds.[88]

2.4.1.3 Proximate Analysis

Figure 2-4 shows the proximate analysis of hydrochars from different algal species. Chemical compositions of the feedstock and product recovery methods are the major factors that should be considered while comparing the proximate analysis of hydrochar from different studies. For instance, the ash content of hydrochars obtained from *mixed microalgae* (at 180, 220 & 240 °C for 60 min)[53], *Scenedesmus* (at 180, 220 & 260 °C for 4 h)[41] and *Chlorella* (at 170 & 250 °C for 60 min)[39] are exceptionally high, ranging between 34.7 and 68.9 wt % on a dry basis of feedstock. The high ash content of raw *mixed microalgae* (32.9 wt %, db) and *Scenedesmus* (44.6 wt %, db) explains the high inorganic yield of the derived hydrochars. For *Chlorella* with relatively low ash content (9.8 wt %, db), the high inorganic yield of the hydrochar (particularly at 250 °C i.e. 50.3 wt % db) can be inferred from the different product recovery method used, which involves rinsing the hydrochar with dichloromethane that might elevate the ash content. It is also evident that reaction temperature has remarkable impact on increasing the ash content of hydrochars due to immobilization of ash forming elements (such as Ca, Mg, and P) into the hydrochar matrix.[55] The increase in ash content of hydrochars with temperature is associated with a decline in its volatile matter as observed for the case of *Chlorella*[30-31, 39], *mixed microalgae*[53], *Scenedesmus*[53] and *H. reticulatum*[31]. For *Sargassum horneri*, the effect of temperature on VM and ash content of hydrochars is not obvious due to washing with water that also results in the removal of inorganics.[84]

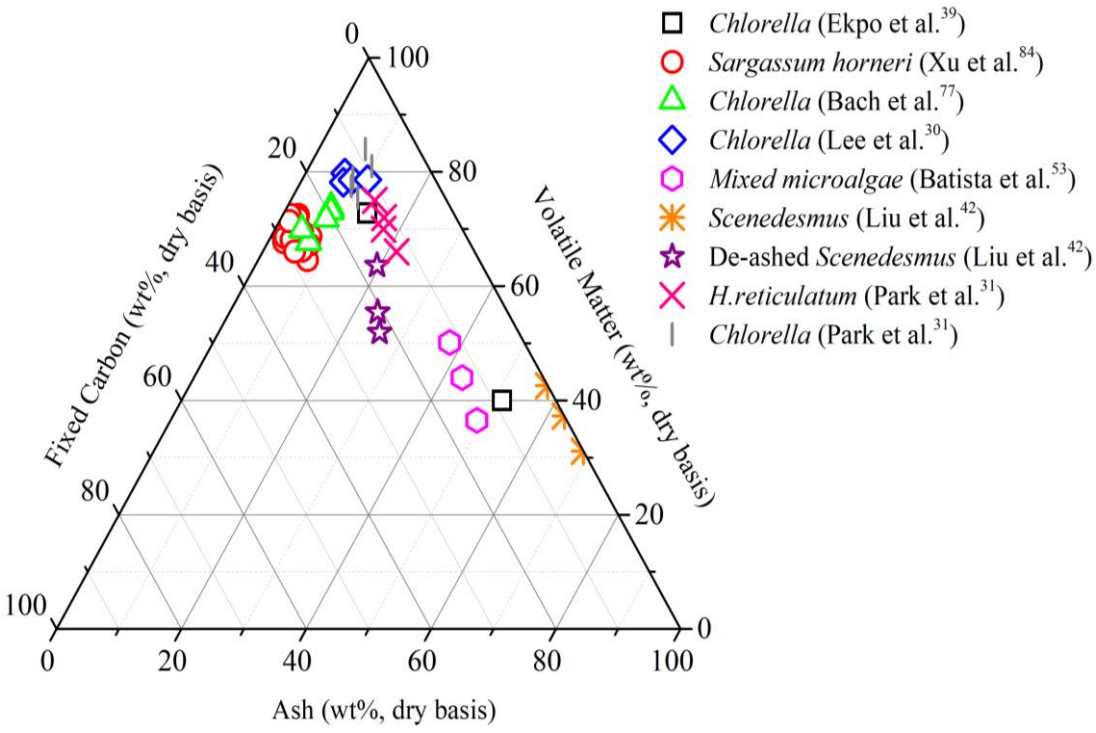

Figure 2-4: Proximate Analysis of Algal hydrochars expressed on wt %, dry basis

2.4.1.4 Ultimate Analysis

Ultimate analysis of hydrochars (on a dry and ash-free basis, daf) derived from various algal species at different reaction conditions is shown as **Figure 2-5**, which demonstrates that carbon contents of hydrochars are higher than the feedstocks. For the selected hydrochars, carbon, hydrogen, oxygen and nitrogen lies in the range 38.1 – 69.1 %, 5.0 – 8.3 %, 18.0 – 54.7 %, and 1.71 – 10.24 %, respectively. Differences in the elemental composition of the feedstock are crucial while comparing the ultimate analysis from different species processed under similar conditions. Such as hydrochar from *Arhrospira platensis* shows carbon content of 68.3 wt % daf, considerably higher than that of 38.1 wt % daf from *Sargassum horneri*, carbonized at a similar reaction temperature of 210 °C, because of entirely different chemical compositions of feedstocks (see **Table 2-1**). Moreover, recovery methods of the hydrochar also affect its elemental composition. For example, *Chlorella* with nearly similar chemical composition, processed at 250 °C and 60 min, with different recovery methods adopted, result in inconsistent trends of carbon and nitrogen in the hydrochars.[39, 55] High carbon (67.8 wt %, daf) and low nitrogen (5.24 wt %, daf) is reported by Smith et al.[55] on separating the hydrochars by solely

by filtration (without contacting with solvent), as opposed to low carbon (61.7 wt %, daf) and high nitrogen (8.45 wt %, daf) presented by Ekpo et al.[39] on rinsing the hydrochars with dichloromethane. Moreover, the hydrochars derived from macroalgae (e.g. *Alaria esculenta*, *Laminaria digitata*, and *Sargassum horneri*) are typically low in nitrogen contents (1.71 – 3.40 wt %, daf) as compared to microalgae (5.52 to 10.24 wt %, daf). Nitrogen content is the distinguishing property of algal hydrochars that negatively impacts its application for energy production, whereas, augments its utilisation as an energy storage carbon material.

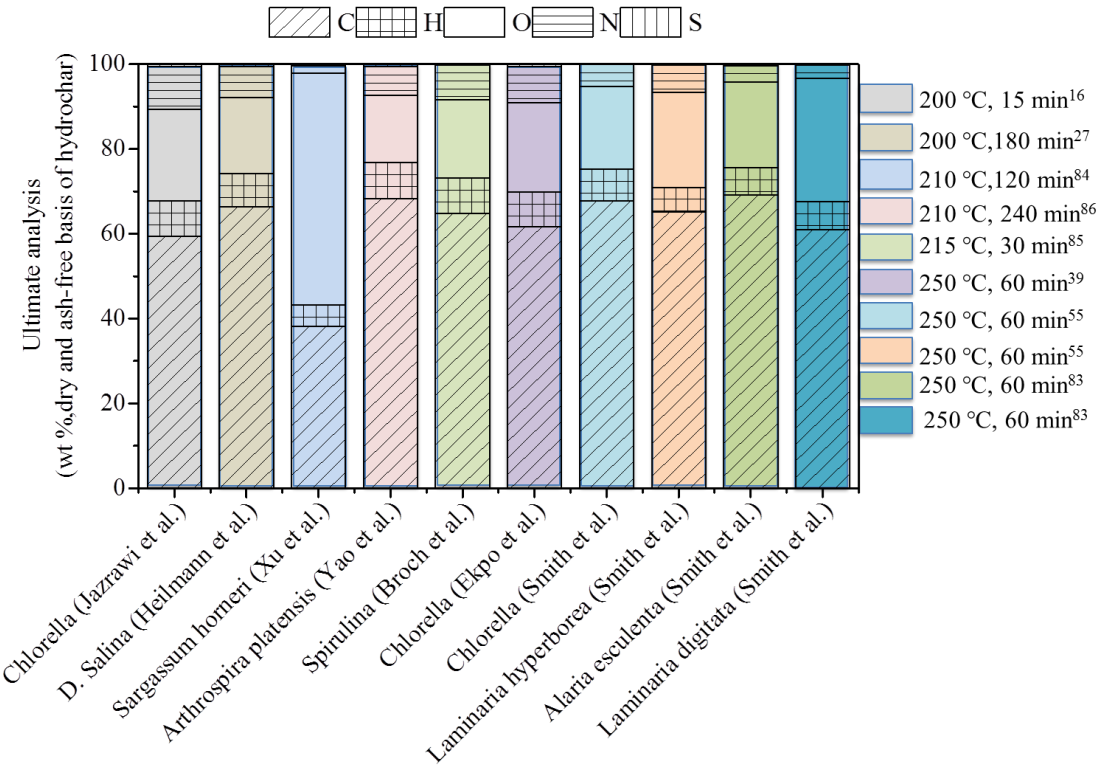

Figure 2-5: Ultimate analysis of hydrochars expressed on a dry and ash-free (daf) basis, from different algal species processed at various reaction conditions

Van-Krevelen diagram plotted for algal hydrochars as **Figure 2-6** depicts that O/C atomic ratio of most of the hydrochars lie between 0.05 (for Bituminous Coal) and 0.40 (for Lignite), while H/C atomic ratios (1.12 – 1.90) are generally higher than that of Coal (0.75) and Lignite (1.04). The fuels with smaller O/C and H/C atomic ratios cause fewer energy losses during combustion in terms of carbon emissions and steam formation. Dehydration and decarboxylation are the prevailing mechanisms during HTC of algal biomass, the extent of which increases with reaction

temperature and holding time. Hydrochars from macroalgae such as *H. reticulatum*[31], *Sargassum horneri*[84] and *Laminaria hyperborea*[55] exhibits much higher oxygen contents than those derived from microalgae. *Scenedesmus* (ash content 44.6 wt %, db) after de-ashing shows reduction in O/C ratios of the hydrochars indicating that inorganic matter influences the hydrothermal reaction chemistry.[41] *Chlorella* processed by Park et al.[31] shows high H/C ratios compared with other *Chlorella* species[30, 39, 55], carbonised at similar reaction conditions (180 – 270 °C for 60 min), because of the high hydrogen content of former compared with others (i.e. 8.7 versus 7.4 – 7.9 wt %, daf, respectively).

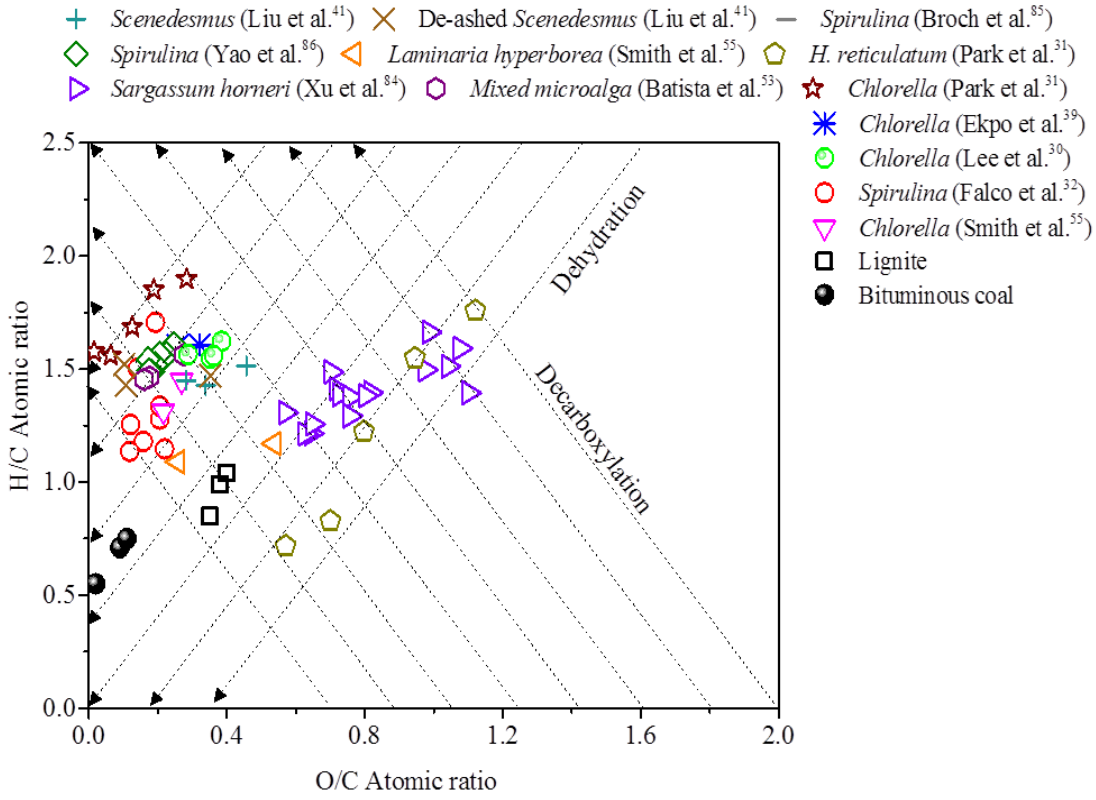

Figure 2-6: Van-Krevelen diagram for algal hydrochars derived from HTC of various species at different experimental conditions

2.4.1.5 Higher Heating Values

The higher heating values (HHV) of hydrochar are directly related to their elemental composition and ash content. High carbon and hydrogen concentration give superior heating value, while high oxygen and ash content negatively affects the HHV of hydrochar. This is evidenced in **Figure 2-7** that summarises the HHV of hydrochars

(on a dry basis) derived from different algal species at various experimental conditions. The highest HHV in the range of 32.5 – 33.0 MJ/kg is observed by *Arthrospira platensis* (at 210 °C for 4 h)[86], *Nannochloropsis* (at 225 °C for 60 min)[38] and *Chlorella* (at 240 °C for 60 min)[31], under the similar product recovery procedure (no use of solvent). Provided the carbon and hydrogen content of raw *Arthrospira platensis* is reasonably lower than *Nannochloropsis* and *Chlorella* (see **Table 2-1**), equivalent heating value is achieved at the cost of longer holding time (4 h), which shows that HTC process parameters can be optimised to obtain the desired hydrochar properties. The hydrochars with high ash contents such as *mixed microalgae*[53], *Scenedesmus*[41], *Chlorella*[39], *H. reticulum*[31] and with high oxygen levels, e.g. *Sargassum horneri*[84], *Laminaria hyperborea*[55], *Laminaria digitata*[83] and *Alaria esculenta*[83] depicts HHV in the low to medium range (15 – 28 MJ/kg).

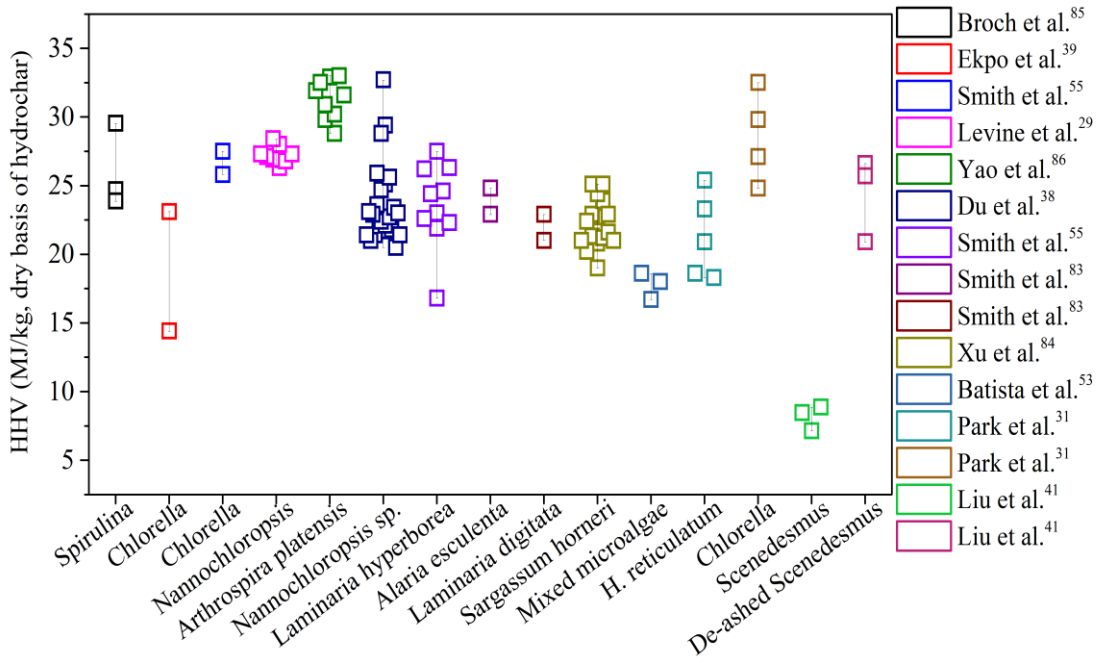

Figure 2-7: Higher Heating Values, expressed on a dry basis of hydrochar from HTC of different algal species processed at various experimental conditions

2.4.1.6 Concentrations of Key Inorganic Elements and their Retentions

Most of the algal species show an abundance of alkali and alkaline earth metals (Na, P, Mg, Ca) in addition to phosphorus that usually comes from the cultivation media. These elements show solubility in HTC aqueous media (e.g. Na and K) or are

extracted into hydrochar (e.g. Mg, Ca and P). Only a few studies are focusing on the retention of such elements in algal hydrochars. Smith et al.[55] and Ekpo et al.[39] with different product recovery methods (no washing for former and solvent washing for later), investigated the effect of reaction temperature at a fixed holding time (60 min) on concentrations and retentions of Na, K, Mg, Ca and P in hydrochars using *Chlorella* as a feedstock. Hydrochars obtained at 250 °C and washed with DCM contains 9.31 wt % P, 0.17 wt % K, 9.82 wt % Ca, 3.38 wt % Mg and 0.53 wt % Na on a dry basis, which was much higher than the concentrations of these elements at 170 °C (i.e. 2.12 wt % P, 0.02 wt % K, 2.60 wt % Ca, 0.76 wt %, Mg and 0.36 wt % Na).[39] In the other study, the contradictory trend is observed for Na and K i.e. it decreases in concentrations by rising temperatures from 200 to 250 °C.[55] Such differences may arise from different recovery methods used in these studies[39, 55], whose effects on metal concentrations of the hydrochars are unknown in the literature. The retentions of Na, K, Mg, Ca and P in hydrochars at reaction conditions of 250 °C and 60 min are plotted as **Figure 2-8**, which shows that washing of hydrochar with DCM always results in higher extraction of metals as compared to direct filtration (or no washing) method. This effect is more pronounced for Ca, Mg and P due to cross-linking of these metals with carbon matrix in the hydrochar.[55]

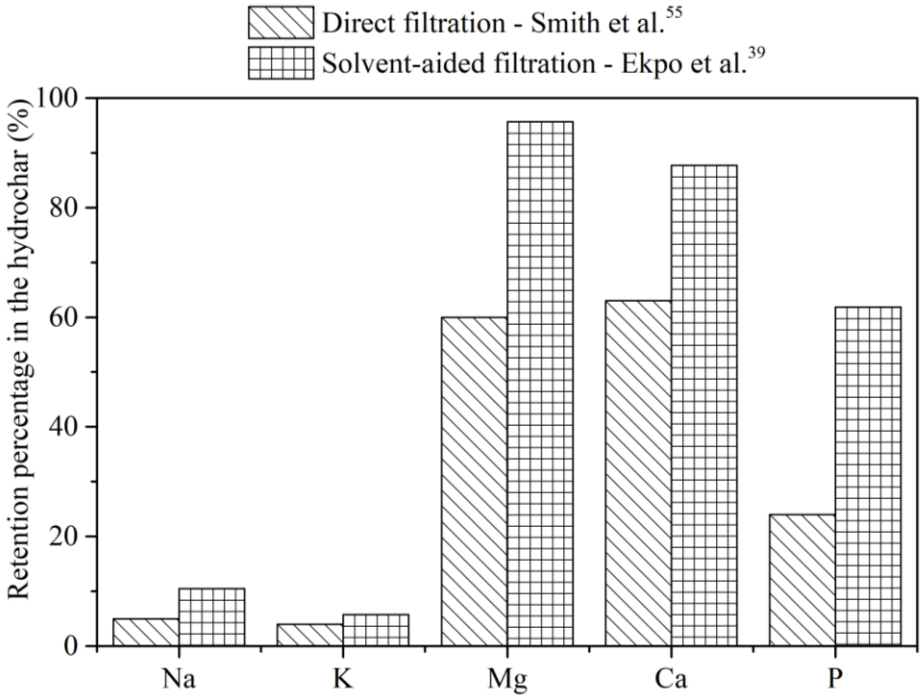

Figure 2-8: Retentions of Na, K, Mg, Ca and P in hydrochar, recovered by different recovery methods from HTC of *Chlorella* at 250 °C and 60 min

2.4.2 Biocrude

2.4.2.1 Elemental Composition and Higher Heating Values

Alba et al.[43] studied the elemental composition of biocrude from *Desmodesmus sp*. at 175 – 450 °C for holding time of 5 and 60 min, and reported the carbon and hydrogen content of up to 72.8 and 9.6 wt %, respectively, under HTC conditions (175 – 250 °C for 60 min), which is very close to carbon (75.8 wt %) and hydrogen (9.1 wt %) of the biocrude at 350 °C and 60 min.[43] Nevertheless, HTC biocrude is relatively high in oxygen (12.4 – 21.7 wt %) and low in nitrogen (1 – 5.9 wt %) than the biocrude at 350 °C and 60 min (i.e. 9.1 wt % oxygen and 6.0 wt % nitrogen). Equivalent carbon contents of biocrude, i.e. 74.7 wt % from *Chlorella*[15], 68.3 wt % from *Spirulina*[17] and 76.6 wt % from *Laminaria saccharina*[82] at 250 °C exist in the Literature. The high carbon concentrations of the HTC biocrude drive attention towards its re-use as upgraded fuel, which further requires the detailed characterisation (e.g. molecular weight, viscosity, type of compounds present and metal analysis) of the biocrude that have never been done in the literature.

The Van-Krevelen diagram for HTC biocrudes compared with Bituminous coal, bio-diesel and HTL biocrudes (at 350 °C and 60 min) from *Desmodesmus*[43] and *Chlorella*[18] is presented as **Figure 2-9**. The O/C and H/C atomic ratios of HTC biocrudes are close to the Bituminous coal, bio-diesel, and HTL biocrude. High temperature has a substantial impact on reduction of O/C and H/C atomic ratios of biocrude as demonstrated in the case of *Desmodesmus sp.*[43] and *Spirulina.*[17] *Laminaria saccharina* shows the lowest O/C (0.10) and H/C (1.19) atomic ratios among all species, which corresponds to the low carbon and hydrogen levels of raw algae.[82]

Higher heating values for HTC biocrude ranges between 25.2 and 33.16 MJ/kg from *Spirulina*[17] and between 32.3 and 34.9 MJ/kg from *Desmodesmus sp.*[43] that are close to HHV of HTL biocrude (i.e. 34.5 – 39.0 MJ/kg)[17, 43, 90, 106], but lower than HHV of 42.7 MJ/kg for crude petroleum.[82]

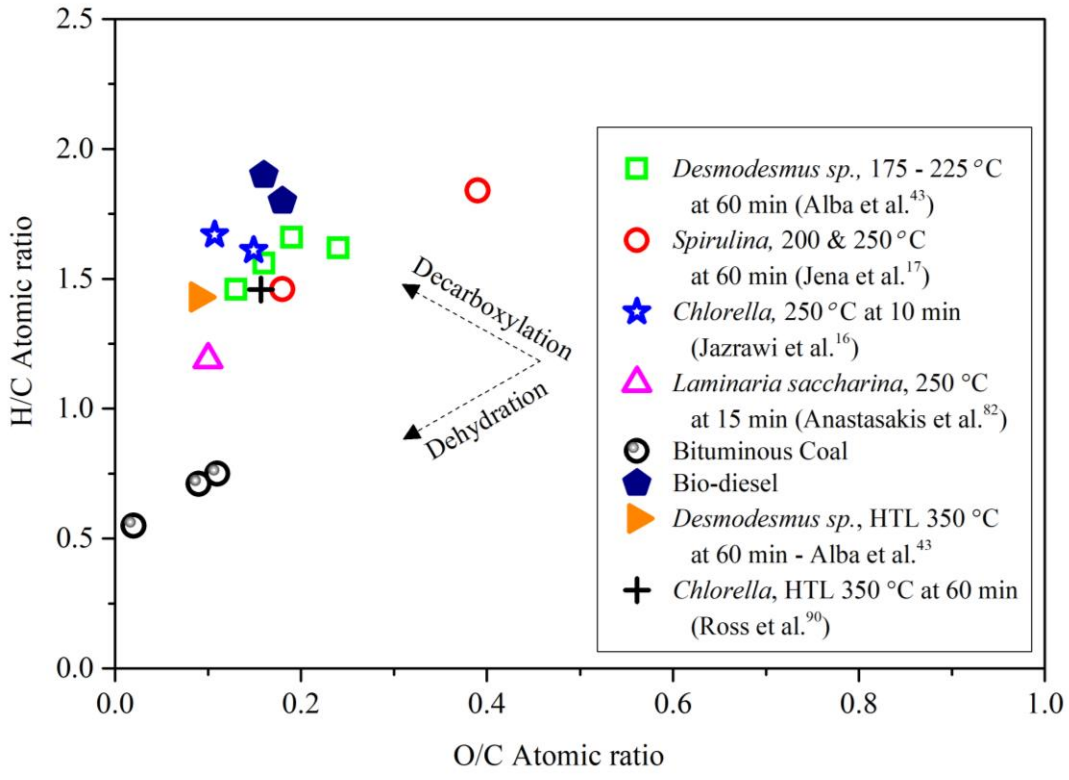

Figure 2-9: Van-Krevelen diagram for HTC biocrudes from various algal species

2.4.2.2 Identification of Compounds

The biocrude from HTC can be regarded as an intermediate product for HTL biocrude because temperatures of HTC reactions have to be experienced by algal slurry even the process is designed for hydrothermal liquefaction. There is limited research on compounds identification in HTC biocrude and their molecular weight distribution, which is vital for the understanding of the hydrothermal reaction mechanisms. Alba et al.[42] employed pyrolysis coupled to gas chromatography-mass spectrometer (Py-GC-MS) analysis for biocrudes from *Desmodesmus sp.* at 200 – 375 °C for 5 and 60 min, and showed the qualitative linkage between HTC and HTL biocrudes. The hydrolysis of carbohydrates, proteins and lipids steadily start at 200 °C, with the formation of a large fraction of algaenans (alkane containing polymers), cyclic dipeptides (from depolymerisation of proteins), linear alkanes (e.g. $C_{15}H_{36}$ and $C_{15}H_{32}$), and fatty acids under HTC conditions (200 – 250 °C). Temperature higher than 250 °C becomes more favourable to yield biocrude because of thermal fragmentation of algaenans with dipeptides through Maillard reactions producing hydrophobic compounds that end up in HTL biocrude.

2.4.3 Aqueous Phase

2.4.3.1 pH, Total Organic Carbon and Total Nitrogen

The aqueous phase from HTC of algal biomass is usually acidic due to the formation of fatty acids during the hydrolysis of lipids and carbohydrates. *Spirulina* after hydrothermal treatment of 215 °C for 30 min[85], *Nannochloropsis Oculata* at 200 °C for 15 min[29], and *mixed microalgae* at 180 – 240 °C for 60 min[53] show pH of 5 – 7 in the aqueous phase. Comparatively high pH (7 – 9) in aqueous phase from *Laminaria saccharina* at 250 – 375 °C[82] could be because of the release of alkali metals and formation of basic NH_4^+ ions with an increase in temperature.[39]

Total organic carbon in aqueous phase widely varies between 4.5 and 27.6 wt % for different species carbonised under various experimental conditions.[29, 39, 52, 83, 85] The aqueous phase from HTC retains much higher organic carbon than that of HTL (0.9 - 1.5 wt %)[57-58] due to the extraction of carbon (using solvent) by the biocrude in later. This shows that recovery methods used to recover hydrochar from reaction mixture

not only affects the hydrochar yield and properties but also the carbon content and composition of the aqueous phase. The organic content of the HTC aqueous phase comprises fatty acids, sugars, and N-containing heterocyclic compounds such as pyrroles and indoles.[82-83, 85]

Due to the high nitrogen content of the algal biomass, aqueous phase retains a significant proportion of organic nitrogen in the form of amino acids and dipeptides and inorganic nitrogen as NH_4^+, NO_3^-, and NO_2^- ions (next Section). Kruse et al.[107] studied the fate of nitrogen during HTC of *Chlorella* at 190 – 250 °C for holding time of 2 – 12 h.[107] Organic nitrogen in the aqueous phase at 220 °C for holding time of 2 h is 1.1 wt %, which steadily declines to 0.75 wt % with an increase in holding time to 12 h. Equivalent nitrogen content of 0.96 wt % has been observed in the aqueous phase from *Nannochloropsis* (with a nitrogen content of 6.2 wt %) at 200 °C for 40 min[52], contrary to reasonably high TN of 3.9 wt % for aqueous phase from *Nannochloropsis Oculata* (nitrogen content 8.5 wt %) processed at similar reaction conditions.[29] Overall, the algal species with high nitrogen content results in more nitrogen ending up in aqueous phase.

2.4.3.2 Macronutrients and Micronutrients

Smith et al.[83] investigated the macronutrients in the aqueous phase from HTC of *Laminaria digitata, Laminaria hyperborea* and *Laminaria esculenta* at 200 and 250 °C for 60 min, that includes sodium (Na^+) and potassium (K^+) ions (at higher concentrations) in addition to chlorine (Cl^-) indicating the possible presence of water-soluble alkali salts. The divalent magnesium (Mg^{+2}) and calcium (Ca^{+2}) ions are present to a lesser extent, e.g. there is 3.71 wt % Na, 4.08 wt % K, 0.65 wt % Mg^{+2} and 0.60 wt % Ca^{+2} in aqueous phase from *Laminaria digitata* at 200 °C and 60 min[83]. Some other authors also reveal the existence of alkali metals in the HTC aqueous phase.[39, 52]

Phosphorus is typically present in the form of phospholipids and phosphate monoesters in algal biomass that readily dissociate into the aqueous phase or immobilise with hydrochar matrix. *Nannochloropsis* at 200 °C[29] and *Chlorella* at 250 °C[39] yields 0.53 and 0.83 wt % of total phosphorus, respectively, in the aqueous phase. Phosphorus in the aqueous phase exists as either phosphate ions (PO_4^{-3} or

$H_2PO_4^-$) or organic phosphorus (bonded with lipids). Ekpo et al.[39] reported 65 % of total phosphorus existing as PO_4^{-3} ions, which is also the major nutrient (ranging between 1.1 and 7.5 wt %) in aqueous phase from different macroalgae species.[83] Phosphorus in the form of dihydrogen phosphate ($H_2PO_4^-$) has been detected in the aqueous phase from HTC of *Chlamydomonas reinhardtii* at 200 ºC.[28]

Among nitrogen-containing nutrients, NH_4^+, NO_3^-, and NO_2^- ions are commonly found in the aqueous phase, with a greater concentration of NH_4^+ ions than NO_3^- and NO_2^- ions.[39, 107] For *Chlorella* (9.9 wt % raw nitrogen), NH_4^+ ions increases from 0.40 to 0.66 wt % with an increase in holding time from 2 to 12 h at 220 °C, whereas NO_3^- and NO_2^- levels varies negligibly (around 0.15 and 0.00025 wt %, respectively) under similar experimental conditions.[107] A similar trend is observed for the aqueous phase from *Nannochloropsis*.[52] For macroalgae with much low nitrogen content (1.7 – 2.4 wt %), the concentrations of NH_4^+ (0.00 to 0.60 wt %), NO_3^- (0.10 to 0.25 wt %) and NO_2^- (0.00 to 0.05 wt %) are comparable to those from high N-containing species.[83] Overall, the content of organic nitrogen (amino acids) in the aqueous phase is much higher than that of inorganics (NH_4^+, NO_3^-, and NO_2^-).

There is very little attention being paid to heavy metals in the aqueous phase that acts as micronutrients for the cultivation of algal biomass[108-109] and inhibiting agents for energy recovery by anaerobic digestion.[110-111] Du et al.[52] revealed the presence of 0.01 ppm manganese, 3.08 ppm iron, 1.85 ppm boron, 0.005 ppm nickel and 0.11 ppm chromium in the aqueous phase from *Nannochloropsis* at 200 °C and 40 min, though the effect of HTC reaction temperature on recoveries of these heavy metals in the aqueous phase is unknown. For recycling of HTC aqueous phase to algal growth systems or anaerobic digesters, detailed knowledge on extractions of heavy metals in the aqueous phase under HTC conditions is necessary.

2.5 Applications of HTC products

2.5.1 Hydrochar

Algal hydrochars are different from those derived from lignocellulosic biomass, in terms of their high nitrogen content, high lipid retention, low porosity, low surface area, and high inorganic matter. These unique properties (e.g. high nitrogen and

inorganic matter) of hydrochar affect its direct use for energy production nevertheless indirect applications of HTC of algal biomass through coupling with other processes offers some benefits. For example, Du et al.[38] reported that less nitrogenous compounds were produced in biocrude produced from pyrolysis of hydrochar than the raw algae because of removal of nitrogen by the HTC aqueous phase. Lipids retained in algal hydrochars produced by HTC were converted into fatty acid ethyl esters (the highest yield of 79 – 98 %) by reacting with ethanol via in situ supercritical transesterification[40] and Triflate-catalyzed in situ esterification.[79] Conversely, hydrochars after extracting lipids (using ethanol) were subjected to supercritical water gasification, which results in overall 75 % of energy recovery (in the form of flue gases) and almost complete extraction of nitrogen as ammonium in the aqueous phase.[81] Such applications of HTC of algal biomass stimulate its potential for algal bio-refinery. Furthermore, high nitrogen content and inorganic matter of the hydrochar is beneficial for its utilisation in energy storage, carbon capture and as a catalyst. The recent advances in potential applications of algal hydrochars are summarised here.

2.5.1.1 Energy Storage Carbon Material

Falco et al.[32] investigated the HTC of high N-containing *Spirulina* in the presence of glucose. This yields hydrochar with a high nitrogen content, which typically enhances the electron availability on carbon surface (nitrogen-doped carbon material) and makes it beneficial for use in energy storage and carbon capture. Later, activation of the hydrochar using potassium hydroxide results in large surface area (2200 m^2/g) and pore volume (0.94 cm^3/g) that shows excellent electrical conductivity when tested as a supercapacitor in lithium chloride electrolyte.[33] Even higher BET surface area of 2502 m^2/g and pore volume of 1.43 cm^3/g, was exhibited by KOH activation of hydrochar obtained from *Carrageenan*, a polysaccharide of red seaweeds.[34]

2.5.1.2 Carbon-based Acid Catalyst

A carbon-based solid acid catalyst with amorphous structure and enrichment of active catalytic sites in the form of O=S=O and $–SO_3^{-2}$ stretching modes was

prepared by in situ carbonisation and sulfonation of microalgae residue in concentrated sulphuric acid.[35] Further, ex-situ preparation of catalyst was explored by HTC at optimised conditions of 217 °C and 4.6 h, followed by sulfonation at 108.5 °C for 2 h.[37] These HTC-based carbon materials exhibited excellent catalytic activity during esterification of oleic acid and transesterification of triolein with methanol. Furthermore, hydrochar derived from *Cladophora glomerata* via hydrothermal gasification (460 °C for 20 min) was directly used as a catalyst (without activation) for supercritical water gasification (SCWG) of almond shells.[36] The catalytic use of hydrochar (carbon and ash content 44.2 and 36.2 wt %, respectively) during SCWG increased the hydrogen yield of the process by 1.48 %, which draws attention towards direct use of high ash containing algal hydrochars from HTC, as a catalyst in other hydrothermal processes.

2.5.1.3 Carbon Sequestration and Soil Conditioner

The use of algal hydrochar for carbon sequestration and as a soil conditioner is still on its underway. *Enteromorpha prolifera* after HTC (at 180 °C for 24 h) and activation with KOH were washed with hydrofluoric acid (HF) which results in BET surface area of 418 m^2/g and pore volume of 0.37 cm^3/g.[103] Washing with HF removes the inorganic metals and leaves voids on the carbon matrix that aids carbon capture as demonstrated by the highest CO_2 sorption capacity of 105 mg/g (at 0 °C), and 61.4 mg/g (at 25 °C). Further, the raw microalgae (*Chlorella* and *Spirulina*) versus their HTC-derived hydrochars (pelletised and activated with CO_2) were investigated for carbon dioxide sorption capacity.[112] None of them demonstrated a tendency towards carbon capture, however, the pellet density was improved after hydrothermal treatment. The utilisation of hydrochar for plant growth shows positive effects only for delipidified hydrochars (using hexane) obtained from HTC of *Phaeodactylum tricornutum* (210 °C for 2h in 0.1 M citric acid). The toxic impacts of lipids on root hair growth of seedlings were observed for non-delipidified hydrochar.[113]

2.5.2 Biocrude

The HTC biocrude has received minor attention from the researchers. As demonstrated in Section 2.3.1 and 2.4.2.1, the theoretical yields and elemental

composition of HTC biocrude are very close to the biocrude produced via hydrothermal liquefaction though the viscosity could be much higher. The raw form of HTC biocrude may be useful as asphalt, boiler fuel and for briquetting of biomass for energy densification. The identification of a large number of oxygenated and nitrogenous compounds (Section 2.4.2.2) in HTC biocrude drives attention towards the extraction of valuable compounds, e.g. diketopiperazines are well-known for their biological activity and applications in medicine.[114] Due to the high nitrogen and oxygen content, HTC biocrudes cannot be directly applied as a transportation fuel and has to undergo the upgrading processes e.g. catalytic cracking, hydrotreatment, and denitrogenation.

2.5.3 Aqueous phase

2.5.3.1 Cultivation of Algal Biomass

The aqueous phase from HTC of *Nannochloropsis* (at 200 °C and 40 min) at dilutions of 50, 100, and 200 times, were used for cultivation of *Chlorella* in shaker flasks incubated under continuous illumination for five days. *Chlorella* grew faster (0.79 g/L in 4 days) in the aqueous phase than the standard growth media (BG-11) and retained 18.9 % higher carbon, 7.8 % lower nitrogen, and 59.0 % more lipid contents as compared to that in BG-11.[52] Large scale cultivation of marine bi-culture consisting *Nannochloris* and *Synechocystis*, in the aqueous phase produced from its own hydrothermal carbonisation (180 – 210 °C for 15 – 30 min) using a two-stage production process was demonstrated by Levine at al.[80] In the first stage, synthetic media (from urea and sodium phosphate) using brackish water was prepared. Most of this media served as a culture in bubble column reactors used in the second stage, while a fraction remains in the first stage to produce algae for the subsequent HTC batch. The reactors were filled with an aqueous phase generated from HTC and recycled media from the preceding harvest. With this two-stage approach, high lipid productivities were achieved relative to the algae grown on conventional growth media containing only inorganic components. In another study, the aqueous phase generated from HTC (190 – 210 °C for 2 – 4 h) of *Arthrospira platensis* was recycled for the cultivation of the same microalgae in Erlenmeyer flasks for 5 – 6 days. The results showed a higher yield of harvested algae with improved quality in

terms of high carbohydrate content, and overall savings of 60 % of nitrogen from conventional cultivation media.[86]

2.5.3.2 Anaerobic Digestion

Nuchdang et al.[59] proposed that the recycling of HTC aqueous phase into digester followed by hydrothermal treatment of resulting digestate (in a closed loop) may lead to improved overall energy recovery as compared to conventional single-stage anaerobic digestion (AD). The post hydrothermal carbonisation (120 – 200 °C for 60 min) resulted in 4-fold improvement of the digestate biodegradability for the case of *Scenedesmus*, with the production of about 200 L STP of methane/kg of volatile solids, based on the organic content of the untreated algae. Likewise, the increase in overall energy recovery by 3.5 times is reported by recycling HTC aqueous phase for anaerobic digestion compared to the AD of fresh microalgae.[53] Aqueous phase generated from mixed microalgae (at 180 – 220 °C) was anaerobically digested in sealed serum vials, held at 35 °C for 35 days. The methane yield elevated exponentially because of consumption of volatile fatty acids by methogenic bacteria. The highest methane yield of 356 mL STP/g of volatile solids (in aqueous phase) was exhibited by the aqueous phase obtained after HTC at 180 °C.

2.6 Conclusions and Research Gaps

By thorough review of the literature, the major findings are drawn as follows:

1. Microalgae are the potentially viable feedstock for the hydrothermal carbonisation process.
2. Microalgae have a complex chemical composition that varies widely from species to species. This may influence the applicability of commonly used standardised methods developed for other solid fuels to the different algal species.
3. Hydrothermal carbonisation is the mildest HTT technique capable of producing the valued products: hydrochar used as an energy storage material or as a catalyst, biocrude with appreciable mass yields and carbon contents,

and aqueous phase suitable for recycling in algae cultivation ponds and anaerobic digesters.

4. The reaction mechanisms underlying hydrothermal carbonisation of microalgae are multiplex and should be considered for understanding the release mechanisms of nitrogen-containing products from algae-derived biofuels.
5. The reaction temperature and holding time have been of central interest, and the most influential factors affecting the HTC product yields, i.e. hydrochar yield decrease, biocrude increase, and that of aqueous phase first rise and then decline with an increase of reaction temperature and holding time. Besides, solid loading and product recovery methods are crucial while comparing the hydrochar yield and properties from various researches.
6. For different microalgae used in the literature, the yields of hydrochar, biocrude, and aqueous phase lie in the range 15 – 66 wt %, 9 – 37 wt %, and 5 – 55 wt %, respectively, on a dry basis of feedstock, though biocrude and aqueous phase have received much less attention than the hydrochar.
7. Hydrochar has more carbon and hydrogen concentrations, and high heating value, while less nitrogen, oxygen, and ash contents than the raw algae. Among the major elements (Na, K, Mg, Ca & P), hydrochar retains more Ca, Mg and P than Na and K, and from minor metals (Fe, Al, Ni, Si, and S), Fe and Al are concentrated in hydrochar.
8. Biocrude contains higher levels of carbon and hydrogen than the hydrochar, along with enrichment of nitrogenous and oxygenated heterocyclic compounds. There has been no quantitative analysis of the major and minor elements in the HTC biocrude.
9. The aqueous phase of HTC of algal biomass is rich in total organic carbon, nitrogen, and nutrients (Na^+, K^+, NH_4^+, PO_4^{-3}, $H_2PO_4^-$). Nothing is known about the recoveries of heavy metals in the aqueous phase.

Based on the above concluding remarks on the preceding studies focused on hydrothermal carbonisation of algal biomass, **firstly**, it is evident that algal species have a widely different chemical composition from lignocellulosic biomass and coal, so care must be taken while applying the conventional methods derived for later to the former. **Secondly**, the reaction chemistry of the thermal processes used for the

conversion of algal biomass is primarily important to estimate the product profiles, which is essential for the design of thermochemical routes. However, there has been paid inadequate attention to reaction mechanisms of high-N containing biomass in the literature. **Thirdly**, most of the research to date has tended to focus on the reaction temperature and holding time as major parameters affecting product yields rather than the impact of solid loading on product distribution of HTC. **Fourthly**, the generalised way of comparing the hydrochar yield and properties in the literature excludes considering of the method used to separate hydrochar from other reaction products because of an absence of studies depicting the hydrochar yield and properties from different recovery methods under similar reaction conditions. **Fifthly**, the suitability of hydrothermal carbonisation for algal bio-refinery cannot be justified by solely characterising the hydrochar, unless the HTC aqueous phase and biocrude are equally treated, in which the literature is mostly lacking.

All-inclusive, hydrothermal carbonisation of microalgae requires further research and development to generate products in rationale yield, and with desired properties, in the following areas:

1. Investigation of applicability of conventional methods of quantification developed for coal, wood, and lignocellulosic biomass to the algal biomass. This study will address one of the common problems faced during the characterisation of algal biomass due to unavailability of standardised methods in the literature.
2. Exploring the reaction mechanisms for thermal decomposition of high-nitrogen containing compounds such as amino acids, with an overall focus to determine the contribution of N-containing species in product profiles of thermal processes. The outcome of this study will be a ‘one-step forward’ in the field of reaction kinetics, which still needs a lot of research.
3. Impact of solid loading of algal biomass on the yields and properties of HTC products with a particular focus on using the high-ash versus low-ash containing algae, to demonstrate the impact of inorganic matter in terms of both catalysis and limiting

mass and heat transfer tendencies towards thermal degradation of organic matter. Such a study should be useful to evaluate the feasibility of HTC as a continuous process, which has never been researched.

4. Role of product recovery methods on the yield and properties of hydrochar under identical reaction conditions. This typically involves comparing the washing versus non-washing of the hydrochar before drying. This work is required to demonstrate that hydrochar yield and properties from different studies should be cautiously compared.
5. Effect of HTC reaction conditions on the surface properties of algal hydrochars (such as porosity and BET surface area etc.) needs further study. The reaction conditions include the particle size of feedstock, holding time, heating rate, cooling rate (of products), and pressure. This is particularly important to investigate the utilisation of hydrochar for carbon sequestration, soil conditioning, and activated carbon.
6. Potential of hydrothermal carbonisation of algal biomass for algal bio-refinery, by detailed characterisation of the aqueous phase and biocrude with emphasis on transformations of key inorganic species (such as Na, K, Mg and Ca etc.) and heavy metals (e.g. Al, Fe, Cu, Ni, Co, Cr, Mn, Zn etc.), which have never been focused in the literature. The evaluation of inorganic recoveries in the biocrude and aqueous phase is required to assess their suitability for potential applications.

2.7 Research Objectives of the Present Study

As demonstrated by the literature review, there are many research gaps in the field of hydrothermal carbonisation of algal biomass. However, in a short duration of 3.5 years for PhD study, it's not possible to research all these gaps. Therefore, this study will focus only on the following research objectives:

1. To evaluate the applicability of the widely used ASTM E870-82 developed for proximate analysis of solid biofuels, for the algal biomass using *Spirulina* and *Chlorella* as model algal samples. An analytical procedure for the proximate analysis of algal biomass will be proposed.

2. To study the thermo-kinetics of the most plausible unimolecular and bimolecular routes encountered in the gas and condensed-phase thermal decomposition of 'Leucine' as an amino acid model compound.

3. To investigate the impact of the product recovery methods on the yield and properties of hydrochar. We compared the direct filtration of reaction products and subsequent drying versus dilution of reactor contents by dichloromethane followed by filtration, phase separation and drying of hydrochar, under the identical reaction conditions of HTC using *Chlorella* as a feedstock.

4. To characterise the biocrude and aqueous phase from HTC of *Chlorella* and evaluate the impact of reaction temperature and holding time on metal contents and recoveries of the biocrude and aqueous phase.

CHAPTER 3

Research Methodology and Analytical Techniques

This chapter explains the microalgae samples, experimental processes, research methodologies and analytical techniques adopted for the comprehensive experimental work and detailed characterisations (of raw microalgae and HTC products) required for accomplishing the research objectives outlined in Section 2.7.

3.1 Microalgae Samples

The microalgae used in this study are *Chlorella Vulgaris* and *Spirulina Platensis* (shortly expressed as *Chlorella* and *Spirulina*, respectively), purchased from Synergy Natural (Sydney). Briefly, the algal species are grown in freshwater ponds, spray dried and stored in tight containers flushed with nitrogen. We homogenised the samples and used them as-received for the experimental work. **Table 3-1** shows the proximate analysis, ultimate analysis, and metal composition of the two species, expressed on a dry basis of the feedstock. The moisture content of the as-received *Chlorella* and *Spirulina* is 4.6 and 5.4 wt %, respectively. The proximate analysis shows the ash content of *Spirulina* is slightly higher than that of *Chlorella* (i.e. 7.3 wt % versus 5.3%). The two species show quite similar concentrations of carbon, hydrogen, nitrogen, sulphur and oxygen as determined by the ultimate analysis. Among the metal concentrations, *Chlorella* shows an abundance of K and Mg, whose concentrations are comparatively low in *Spirulina.* The contents of Na and Ca are higher in *Spirulina*. The methods used to determine these chemical and elemental compositions of algal species are detailed in Section 3.4.

Table 3-1: Properties of the microalgae species used in this study

	Chlorella	*Spirulina*
Proximate analysis [b] (wt %, dry basis)		
Moisture [a]	4.6 ± 0.4	5.4 ± 0.3
Volatile matter	84.3 ± 0.2	82.3 ± 0.4
Fixed carbon	10.4 ± 0.2	10.4 ± 0.4
Ash	5.3 ± 0.3	7.3 ± 0.2
Ultimate analysis [b] (wt %, dry basis)		
Carbon	49.7 ± 0.6	47.6 ± 0.6
Hydrogen	6.2 ± 0.4	6.6 ± 0.4
Nitrogen	9.53 ± 0.12	10.05 ± 0.12
Sulphur	0.50 ± 0.01	0.53 ± 0.01
Oxygen	29.5 ± 0.3	28.9 ± 0.3
Metal concentration [b] (mg/kg, dry basis)		
Na	347.0 ± 1.8	1972.3 ± 32.5
K	25532.3 ± 71.3	12109.3 ± 81.7
Mg	3500.3 ± 9.8	2122.5 ± 13.5
Ca	558.2 ± 1.5	1939.6 ± 26.9

[a] Expressed on an as-received basis, [b] Methods for determination of properties are highlighted in Section 3.4

3.2 Experimental Processes

The microalgae samples were subjected to a series of experiments and analytical measurements, performed in duplicates or triplicates to ensure the repeatability of our results. Majorly, two experimental processes and/or rigs were employed for the study as explained below.

3.2.1 Tubular Reactor for Ashing of *Chlorella* using Gaseous H_2O_2

To determine the ash content, *Chlorella* was oxidised at 600°C in the air with the aid of hydrogen peroxide (H_2O_2) in a tubular reactor shown in **Figure 3-1**. The reactor consists of a fused quartz tube (600 × 50 mm) heated by an electric furnace (OTF-

1200 X, MTI Corporation), and equipped with a syringe pump (with a 100 mL stainless steel syringe), and a mass flow controller (for air). Ashing was done in three steps:

- In step 1, *Chlorella* was pre-ashed by loading ~ 3 g (dry mass) sample into a porcelain crucible, which was then placed in the isothermal zone of the reactor and heated from room temperature to 250 °C (with a stream of air, 2.0 L/min), held for 30 min to remove light volatiles, and then heated to 600 ºC at a heating rate of 10 °C/min and further held for 30 min.
- In step 2, the pre-ashed residue was cooled down to room temperature (with the air continuously flowing through the reactor), weighed, and homogenised in a mortar and pestle.
- In step 3, a thin layer (~ 60 mg) of homogenised and pre-ashed residue was evenly spread in the crucible and heated to 600 ºC at 10 °C/min in the air (2.0 L/min) in the reactor. Once the ashing temperature was achieved, H_2O_2 was introduced into the reactor via the syringe pump (loaded with 34 wt % H_2O_2 solution) for 1 – 5 h.

The flow rates of H_2O_2 solution and air were adjusted to acquire an oxidative atmosphere of 9.2 % H_2O_2, 34.5 % H_2O, 11.8 % O_2, and 44.5 % N_2, on a volumetric basis. Before the completion of ashing, the syringe pump was stopped, while the reactor was kept at 600 ºC for 30 min, with the airflow passing through, to decompose metal hydroxides formed (if any) and thereby avoid distortion to the ash content. The ash content was calculated based on the dry mass of *Chlorella* fed for step 1.

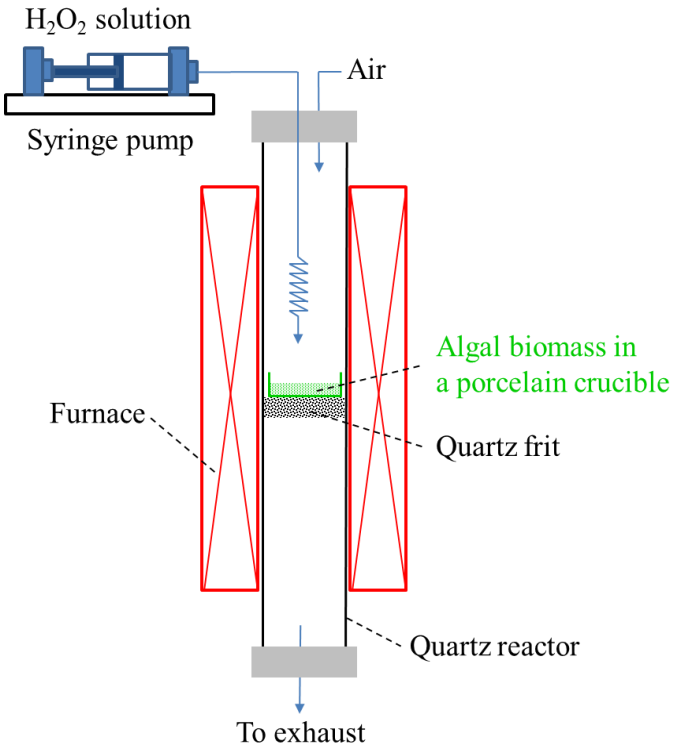

Figure 3-1: Schematic diagram of the reactor used for ashing *Chlorella* with the aid of H_2O_2.

3.2.2 Batch Reactor for Hydrothermal Carbonisation Experiments

Chlorella was hydrothermally carbonised in 1 L of the batch reactor (PARR Instruments Company) equipped with a pressure booster schematically shown in **Figure 3-2**. In each experiment, the vessel was first loaded with 300 g (10.0 wt % solid loading) of well-mixed algal slurry, sealed, and purged with helium gas for 15 min to get rid of oxygen. During purging, the helium passes through the dip tube and exhausts via the gas outlet valve. Then, the gas outlet valve was closed and the vessel was pressurized to 1.5 – 3.0 MPa, slightly higher than the vapour pressure of water at a given HTC peak temperature. Afterwards, the vessel contents were heated to the desired temperature (180, 200 and 220 °C) at a heating rate of approx. 5 °C/min. Once the vessel reached the set point temperature, it was considered as time '0 min' at which the contents were held for 15 min or 60 min. On completion of the reaction time, the vessel was cooled down to 40 ºC with the help of cooling water that flows through the internal coils. The contents were continuously stirred at 600 rpm during the heating, holding, and cooling periods. Once cooled, the vessel was

de-pressurized by opening the gas outlet valve and then unsealed. The hydrochar was recovered from the reactor vessel using the two different methods, which will be explained in Section 3.3.3.

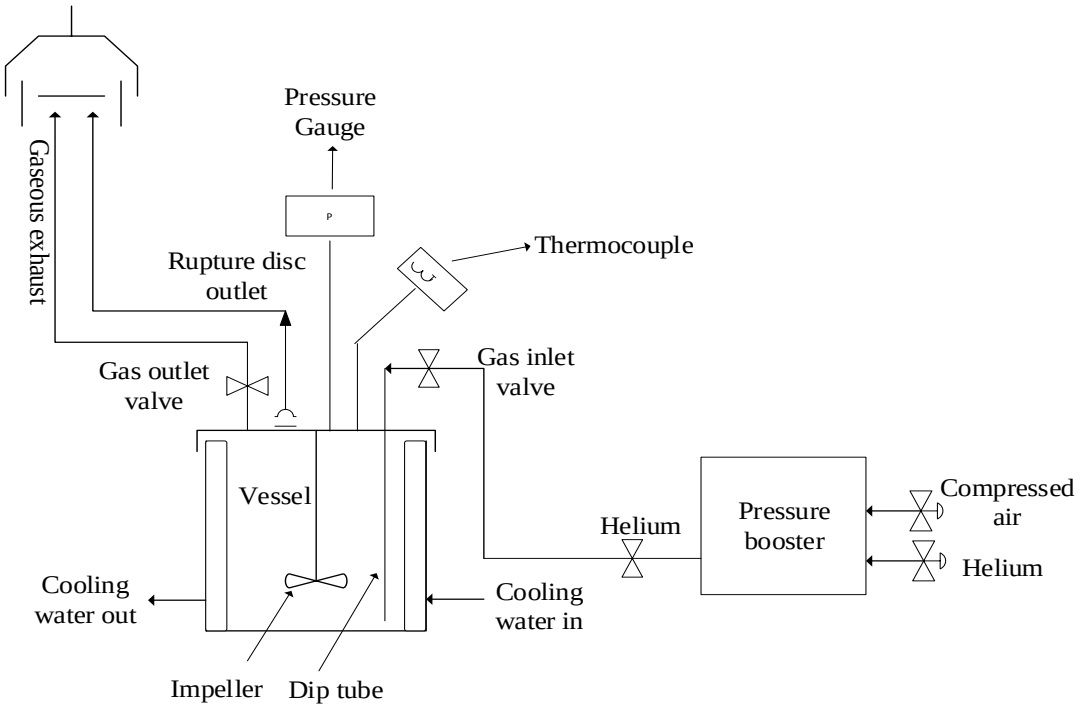

Figure 3-2: Schematic diagram of the batch reactor used for hydrothermal carbonisation experiments

3.3 Research Methodology

The methodology adopted for each of the research objectives is explained below:

3.3.1 Analytical Procedure for Proximate Analysis of Algal Biomass: Case Study for *Spirulina* and *Chlorella*

As discussed in Section 2.7, the applicability of widely used ASTM E870–82 developed for wood fuels, for the algal biomass needs to be investigated because of the unavailability of standardised methods of proximate analysis for the latter, which determines the important fuel properties. The research objective was accomplished using *Chlorella* and *Spirulina* as model algal species, by three major experimental tasks. F**irstly**, the algae were subjected to a series of thermogravimetric analysis (TGA) designed to do proximate analysis in a single-run or multiple-runs (will be

discussed in Section 3.4.1). **Secondly**, the preliminary experiments suggested that it was difficult to ash *Chlorella* completely in the TGA, which was then oxidized with the aid of gaseous hydrogen peroxide (H_2O_2) in a tubular reactor (as explained in Section 3.2.1). **Thirdly**, the produced ash residues from *Chlorella* and *Spirulina* were analysed for functional groups, unburnt carbon and nitrogen, X-ray powder diffraction and metal concentrations (see Section 3.4) based on the results of which the analytical procedure for proximate analysis of algal biomass is proposed in Chapter 4.

3.3.2 Thermal Decomposition of Algal Biomass Model Compound

To achieve the research objective 2 as elaborated in Section 2.7, the amino acid 'Leucine' was elected as a surrogate compound because of its abundance in various algal strains (4 to 20 wt % of the total amino acids).[115-117] Thermal decomposition of leucine in the gas and condensed-phase pyrolysis was investigated by the computational and quantum chemistry calculations carried out in three steps:

(1) Determination of the potential energy surfaces for all the unimolecular and bimolecular channels: The geometric optimisation and energy computation for all reactants, intermediates, and products were performed at the accurate chemistry composite method of CBS-QB3 as implemented in the Gaussian 09[118] suite of programs. The CBS-QB3 approach optimised geometries at the B3LYP/CBSB7 level of theory and performed single-point calculations at CCSD(T)/6-31+G(d') and MP4SDQ/CBSB4 levels. Additionally, CBS-QB3 accommodated spin contamination correction factor open-shell species.[119] It has been demonstrated that CBS-QB3 provides accurate thermo-kinetics parameters for general applications in organic chemistry.[120-122] For bimolecular reactions, structural optimisations and energy calculations were executed by the M06-2X level of theory in combination with a basis set of 6-31+G(d,p). The meta hybrid density theory functional (DFT) method of M06-2X exhibited the satisfactory performance in computing reaction kinetics, especially for hydrogen transfer reactions.[123-125]

(2) Computing the thermodynamic properties of all the products and intermediates: The standard enthalpy of formation ($\Delta_f H°_{298.15}$) of leucine was calculated by the isodesmic reactions scheme. To validate our adapted methodology for thermodynamics, we computed $\Delta_f H°_{298.15}$ for selected reference compounds (Acetamide, glycine, alanine, morpholine, and proline) using the CBS-QB3 method shown in the Appendix. We contrasted our computed values with the analogous experimental $\Delta_f H°_{298.15}$ estimates, which dictated that our calculated $\Delta_f H°_{298.15}$ values of leucine and reference compounds were in a reasonable agreement with the experimental $\Delta_f H°_{298.15}$ values. The calculated $\Delta_f H°_{298.15}$ values minimally departed from analogous experimental values in the range of 0.3 to 2.2 %. The standard entropy and heat capacity of the products and intermediates was computed by ChemRate Code.[126]

(3) Calculation of reaction rate constants and building of a robust kinetic model: We employed the kinetic and statistical thermodynamic (KiSThelP) program[127] to compute reaction rate constants for all unimolecular and biomolecular reactions. The reaction rate constants were calculated based on transition state theory (TST) using one-dimensional Eckart functional to account for tunnelling effects. For kinetics validation, our previous CBS-QB3-based calculations on N-containing compounds[128-131] yielded reaction rate constants that were in accord with analogous experimental observations. ChemRate Code[126] served to drive the NASA polynomials (enlisted in Appendix) via the Lennard-Jones parameters for leucine (σ = 5.950 Å and ε = 740.8 K) computed based on its critical temperature = 743.19 K, critical pressure = 40.2 atm, and acentric factor (proline) = 1.213.[132] Then a kinetic model was built for gas-phase pyrolysis of leucine in the temperature range of 500 – 1200 K and 1 atm using the ChemKin-Pro code.[133] Temperatures profiles of products for thermal decomposition of leucine in an inert atmosphere of nitrogen were obtained based on plug flow reactor (diameter = 1 cm and axial length 30 cm) with a residence time of 10.0 s.

The outcomes of the kinetic model for the thermal decomposition of leucine are presented in Chapter 5 of the thesis.

3.3.3 Effect of Product Recovery Methods on the Yield and Properties of Hydrochar from Hydrothermal Carbonisation of Algal Biomass

To investigate the effect of product recovery methods on the yield and properties of hydrochar (research objective 3), we carried out the hydrothermal carbonisation experiments using *Chlorella* with a solid loading of 10.0 wt % at 180, 200 and 220 °C for holding time of 15 min and 60 min in a batch reactor (as explained in Section 3.2.2). On cooling down the reactor, the product in the vessel was the three-phase mixture of hydrochar, biocrude and aqueous phase. Hydrochar was recovered from the reactor using two different methods commonly employed in literature[15, 29, 38-39, 43, 55, 82, 85], as displayed in **Figure 3-3**. The produced hydrochar samples were compared for their properties, for instance, morphological structure, ultimate analysis, proximate analysis, concentrations of alkali and alkaline earth metals (AAEM), functional groups, and reactivity (see Section 3.4). The results of the comparative analysis of the product recovery method in terms of both the mass yields and properties of hydrochar are discussed in Chapter 6.

As **Figure 3-3** shows, the first method includes filtering the reactor contents directly via vacuum filtration (using glass microfiber filter, Whatman GF/B, 1 μm pore size) for separating hydrochar from an aqueous phase. The emptied vessel was thoroughly washed with acetone first and then with ultra-pure water to remove any residue hydrochar particles from the reactor walls. Both washings were collected in separate beakers for accurate quantification of hydrochar yield. The method is hereafter referred to as "direct filtration". The second method employed dichloromethane (DCM) as a dilution/extraction media. Specifically, we put ~300 mL of DCM into the reactor product and stirred the mixture at 800 rpm for 20 min. Afterwards, the product (diluted with DCM) was collected in a beaker, and the vessel was rinsed with DCM twice to remove any residual char particles and biocrude from the reactor walls. The rinsing was taken in the same beaker (with the product) and set aside for further separation. The emptied vessel was first rinsed with acetone and then with ultra-pure water, which was collected in the separate beakers, as done for the first method. The reactor contents collected in the beaker were filtrated under vacuum, and the filter paper containing hydrochar cake was repeatedly washed with DCM to remove the biocrude completely from hydrochar

particles. The filtrate was subjected to phase separation in a separatory funnel. We optimized the separation between the two phases by adding more DCM (several times) until the organic phase becomes as colourless as the pure DCM. The bottom layer (biocrude + DCM) was transferred to the rotary evaporator to concentrate biocrude and recover DCM, the latter was then reused in the process. Further, biocrude was flushed with N_2 gas for 24 h to allow residual DCM (if any) to escape. This method is hereafter termed as "DCM-aided filtration". For both recovery methods, the hydrochar samples obtained after filtration were dried at 65 ºC for 24 h. The mass yield of HTC products was computed as the ratio of the dried mass of hydrochar, biocrude and aqueous phase to the dried mass of *Chlorella* multiplied by 100. The dried hydrochar samples were homogenised in a small blender and saved in air-tight containers.

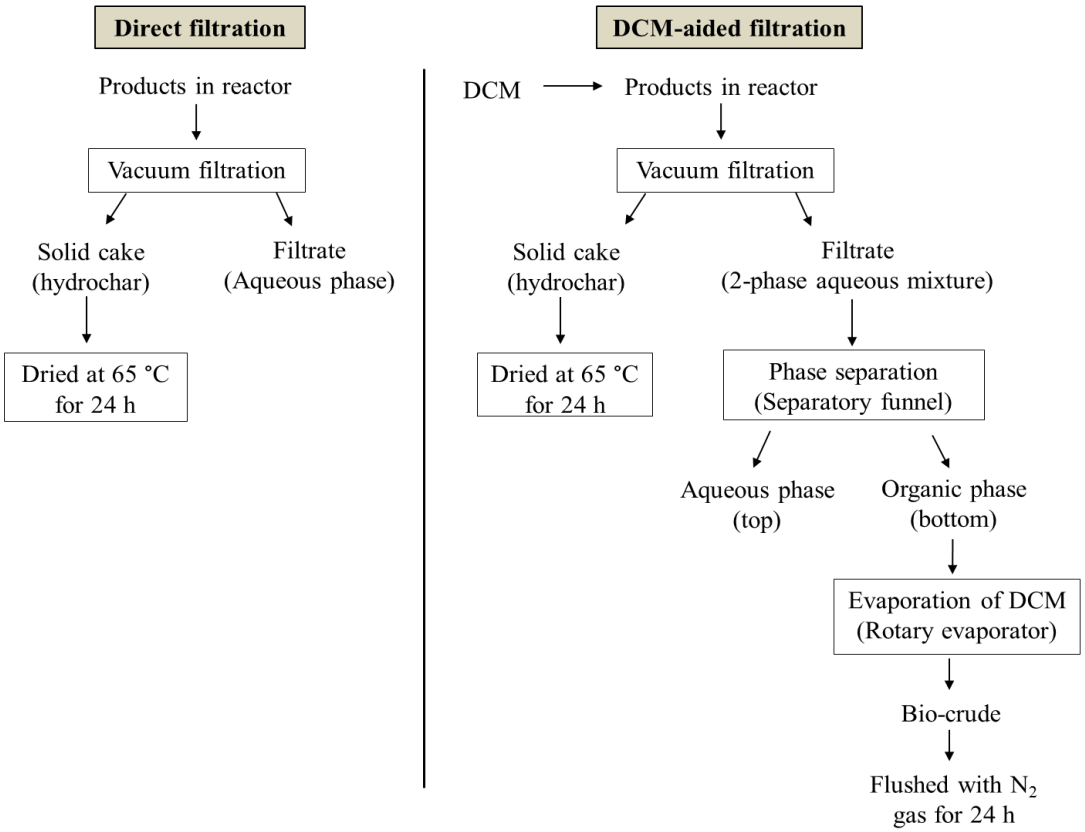

Figure 3-3: Methods used for recovery of hydrochar from the reactor

3.3.4 Detailed Characterisation of Biocrude and Aqueous Phase from Hydrothermal Carbonisation of Algal Biomass

To accomplish the objective 4 of the study (Section 2.7), the biocrude and aqueous phase samples derived from DCM-aided filtration (see **Figure 3-3**) were characterised in detail. The aqueous phase was dried at 70 ºC for 24 h for quantitative and qualitative analysis. The mass yield of the biocrude and aqueous phase are computed based on the dried mass of the two products and the raw *Chlorella*. For the biocrude, the gas chromatography-mass spectrometer (GC-MS) and gel permeation chromatography (GPC) detected the compounds present and their molecular weight distribution, respectively. Besides, the biocrude samples were subjected to elemental analysis, ion chromatography (IC) and inductively coupled plasma mass spectrometry (ICP-MS) for the determination of elemental and metal composition. For the aqueous phase samples, ultimate analysis, pH, total organic carbon, nutrients (anions and cations) and composition of AAEM and heavy metals were studied. The details of the analytical techniques and instruments are given in Section 3.4, and the results of the research are presented in Chapter 7 of the thesis.

3.4 Instruments and Analytical Techniques

3.4.1 Proximate Analysis

For the proximate analysis, the two algae were analysed via three batches of TGA with a Netzsch STA 449 *F3* instrument. We imposed the heating ramp of 10 °C/min and flowed argon or air at a rate of 50 mL/min in all the batches that are explained below:

- In the first batch, a temperature program based on ASTM E870–82 (termed as "TGA–ASTM E870–82" hereafter) shown in **Figure 3-4** was employed for the proximate analysis of both algal species. Specifically, ~20 mg of algal biomass was heated to 105 °C in the atmospheric flow of argon and held for 20 min (weight loss as moisture content), followed by heating to 950 °C and holding for 30 min (weight loss as volatile matter), and cooling down to 600 °C, where the gas flow was switched from argon to air and kept for 60

min to burn off fixed carbon (mass percentage of solid residue as ash content).

- In the second batch, the *Spirulina* (~20 mg) was heated to 105 °C, held for 20 min to remove moisture, and then heated to desired devolatilisation temperatures (600, 650, 700, 750, 800, 850, 900 and 950 °C) and then kept for 4 h in argon to measure contents of volatile matter.
- In the third batch, *Spirulina* (~20 mg) of algal biomass was ashed in the air at temperatures 600, 650, 700, 750 and 800 °C, and held for 2 h to determine the ash contents.

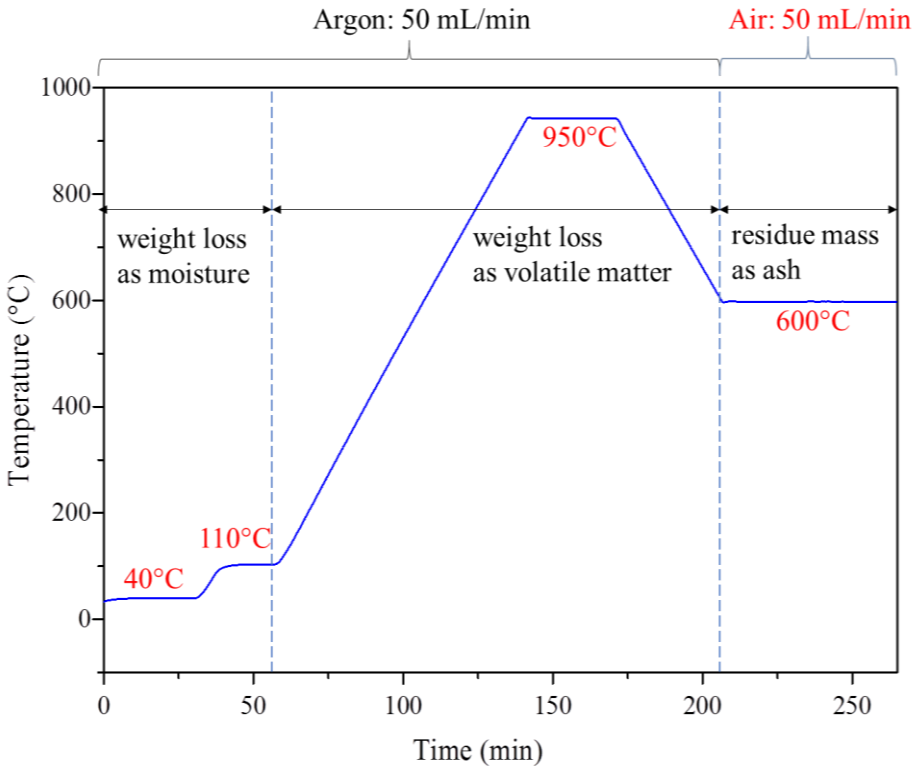

Figure 3-4: TGA-ASTM E870–82 method used for the proximate analysis of *Spirulina* and *Chlorella*.

We measured the ash content of *Chlorella* (and hydrochars produced from HTC treatment of 180 °C and 15 min) by heating roughly 0.50 g of the sample in a continuous flow of air (2.0 L/min) in a tubular reactor (**Figure 3-1**) to 600 ºC holding for 2 – 4 h, with aid of hydrogen peroxide[134], as discussed in Section 3.2.1. *Spirulina* and remaining hydrochar samples were analysed for moisture content, ash content, and volatile matter by the TGA analysis as mentioned above. For the

aqueous phase and biocrude samples, water and DCM were evaporated at 70 and 40 ºC, respectively, overnight and the dried mass of the sample was recorded before ashing. Fixed carbon (FC) is calculated as 100 – (VM + ash), all on a dry basis.

3.4.2 Ultimate Analysis and Higher Heating Values

The ultimate analysis was conducted using an elemental analyser (Thermofischer Flash HT Plus) that measures oxygen directly by pyrolysis of the sample that reduces oxygen to CO, subsequently separated in a GC column and measured by the mass spectrometer. Before analysis, the microalgae and hydrochar samples were dried at 105 ºC, while biocrude and aqueous phase at 40 and 65 °C, respectively, for overnight and stored in a desiccator.

Higher heating values (HHV) of raw algae and hydrochar samples were measured by oxidizing 0.5 g of sample in a bomb calorimeter (Cal 3K-U), and values are reported on a dry basis. For biocrude, HHV is calculated either using a unified correlation of 0.3491C + 1.1783H + 0.1005S – 0.1034O – 0.0151N – 0.0151A from Channiwala and Parikh[135] or from Boie's formula (0:3516C + 1.16225H – 0.1109O + 0.0628N)[43], depending upon the nitrogen content of the biocrude.

3.4.3 Unburnt Carbon in *Chlorella* Ashes

A two-step method modified from Komada et al.[136] were used to measure the content of unburnt carbon in ash residues. In the first step, ~10 – 15 mg of ash sample was weighed and reacted with 1 N of hydrochloric (HCl) acid solution in a crucible at room temperature. The residue was dried in the oven at 40 ºC for 30 min to evaporate excess HCl. This procedure of acidification and drying was repeated thrice to ensure the complete release of inorganic carbon in the form of carbonates. The acid-treated residue was then dried at 50 ºC overnight and weighed. In the second step, the Thermofischer Flash HT Plus elemental analyser served to determine the carbon and nitrogen content of the acid-treated ash samples. Unburnt carbon was quantified based on the original mass of ash taken for acid treatment.

3.4.4 Quantification of AAEM Species and Other Metals

The samples were firstly ashed in a Platinum crucible at 600 °C for holding of 2 h at the peak temperature in air (2.0 L/min) in a tubular furnace. On cooling down, the ash residue (roughly 2 – 4 mg) together with crucible was digested with 4 mL of HF and HNO_3 (1:1) at 80 ºC for 16 h in 15 mL Teflon vials, followed by the evaporation of the surplus acids at 120 °C. Alkali and alkaline earth metals (AAEM i.e. Na, K, Mg and Ca) were quantified by dissolving the digested ash residue in 30 mM of Methasulphonic acid (MSA) and analysed by Dionex ICS-5000 Ion Chromatograph (IC) using Dionex CS16 column.

For heavy metals (Fe, Ni, Co, Cr, Mn, and Zn), the digested ash residue was dissolved in 2.0 % HNO_3 and subjected to inductively coupled plasma-mass spectrometry (ICP-MS) from Thermo Scientific, iCAP Q. The instruments were calibrated using a range of standards for different elements.

3.4.5 Reactivity Measurements

Hydrochar were subjected to isothermal reactivity measurement using the same STA as mentioned in Section 3.4.1. Firstly, 3 mg (approx.) of the sample was heated to 105 ºC (argon, 50 mL/min) and held for 20 min to get a dry mass. Then, the temperature was raised to 400 ºC, where argon was switched with air (50 mL/min) and held for 4 h. Ash content was calculated by further heating the sample to 600 ºC and holding for 1 h. Reactivity (R) of hydrochar at any given time was computed from the DTG data (dW/dt) of the isothermal regime as:

$$R = \frac{-1}{W} \times \frac{dW}{dt}$$

Where W is the weight (dry and ash-free basis) of the hydrochar at any given time t.

3.4.6 X-ray Powder Diffraction, Fourier Transform Infrared Spectroscopy, and Scanning Electron Microscope

The diffraction patterns the ash residues were recorded using X-ray Powder Diffraction (XRD) technique on GBC eMMA instrument. The method operated at scanning angle of 2θ, in the range 10º to 70º with a speed 1º min^{-1} and a step size of

0.010º. The instrument used Ni filtered Cu Kα1 radiation (λ = 1.5406 Å) with voltage and current settings of 35 mV and 28 mA respectively.

The functional groups were analysed using Fourier transform infrared (FTIR) spectroscopy (Agilent Cary 670) equipped with the attenuated total reflectance (ATR, Pike Technologies) accessory. The spectra were recorded at the resolution of 4 cm^{-1} in the wavelength range of 4000 to 400 cm^{-1} using 64 scans per spectrum.

The morphological structure of the raw algae and hydrochar samples was studied using a JEOL JCM-6000 scanning electron microscope. The samples were coated using a gold sputter before the image analysis.

3.4.7 pH, Total Organic Carbon and Anions Analysis

The pH of the aqueous samples was measured by the portable Hanna Instruments kit provided with buffer solutions (3 – 10 pH) for calibration. Total organic carbon (TOC) in the aqueous phase was quantified with a TOC analyser (Shimadzu TOC-V_{CPH}). Anions were analysed with a Shimadzu LC-20 prominence liquid chromatography system equipped with a conductivity detector (CDD-10A_{VP}) and a Shim-pack IC-A3 column, with 1.5 mL/min of a mixed solution of 8 mM p-hydroxybenzoic acid, 3.2 mM bis-tris and 50 mM boric acid as mobile phase.

3.4.8 Gas Chromatography Mass Spectrometer and Gel Permeation Chromatography

GC-MS (QP 2010S) with an SGE BPX5 column (30 m length, 0.25 mm diameter and 0.25 μm film thickness) was used for the qualitative analysis of the biocrude samples. The injection and interface temperatures were maintained at 250 ºC, while the ion source at 200 ºC. The column temperature was ramped from 100 to 200 at 5 ºC/min and held at 200 ºC for 5 min, then increased from 200 – 280 ºC at 5 ºC/min and kept at 280 ºC for 3 min. The spectrum was recorded at a split ratio of 1:20, and the compounds were identified using the NIST database.

Molecular weight distribution of the biocrude samples was obtained via Gel Permeation Chromatography (GPC) analysis. It uses a Shimadzu LC-20 prominence liquid chromatography system equipped with a refractive index detector (at a

wavelength of 254 nm) and three polystyrene gel packed columns in series (Tosoh TSK-gel G1000HXL, G2000HXL, and G3000HXL), with 1.0 mL/min of tetrahydrofuran as mobile phase.

3.5 Summary

Overall, the two microalgae sample *Chlorella* and *Spirulina* were investigated to propose the analytical procedures for proximate analysis of algal biomass that principally includes the development of the novel procedure using gaseous hydrogen peroxide for the oxidation of complex algal species. *Chlorella* is further studied to elaborate on the impact of product recovery methods on the yield and properties of hydrochar produced via hydrothermal carbonisation. The raw microalgae and HTC-derived products were extensively characterised by different analytical techniques. Moreover, the computational methodology for studying the reaction mechanism of 'leucine' as microalgae model compound is presented that accounts for the emission of nitrogen-containing species from thermal degradation of algal biomass.

CHAPTER 4

Analytical Procedure for Proximate Analysis of Algal Biomass: Case Study for *Spirulina* and *Chlorella*

4.1 Introduction

Design of the conversion techniques requires systematic characterisation of the fuel properties of the feedstock. One basic but the important property is proximate analysis, which determines the contents of moisture, volatile matter (VM), fixed carbon (FC), and ash. Various standard methods for the proximate analysis were initially developed for coal and lignocellulosic biomass, and have been used extensively for algal biomass in the literature (see **Table 4-1**). These methods use drying ovens and muffle furnaces, employing devolatilisation temperature of 900 or 950 °C and a wide range of ashing temperatures (550 – 950 °C). Also, methods based on thermogravimetric analysis (TGA) have often been adopted in the proximate analysis of the algal biomass because the instrument is readily available and these methods are less time-consuming.[76] As summarized in **Table 4-2**, various temperatures over a range of 550 – 1000 °C for devolatilisation and 500 – 950 ºC for ashing have been applied to algal biomass, without any standardised conditions.

Table 4-1: Standard methods that have been used for proximate analysis of algal biomass

Sample [a]	Method	Measurement temperature (°C)			Ref [b]
		Moisture	Volatile matter	Ash	
Coal	GB/T212-2008[c] [137]	105 – 110	900 ± 10	815 ± 10	138-139
	ASTM D 3172-13[c] [19]	104 - 110	950	700 – 950	140-142
	ASTM D 3173 / D3173 – 17[d] [143], ASTM D 3175 - 17[e] [144], ASTM D 3174 – 12[f] [145]	104 - 110	950	700 – 950	142, 146-147
Particulate wood fuels	ASTM E871 – 82(2013)[d] [148] ASTM E872 – 82(2013)[e] [149], ASTM D1102 – 84(2013)[f] [150]	103 ± 1	950	580 – 600	76, 151-156
	ASTM E870 – 82(2019)[c] [157]	103 ± 1	950 ± 20	580 – 600	158-159
Solid biofuels	ISO 18134-2:2015[d] [160], ISO 18123:2015[e] [89] ISO 18122:2015[f] [161]	105 ± 2	900 ± 10	550 ± 10	162-163
Lignocellulosic Biomass	ASTM E 1756 – 08(2015)[d] [164] ASTM E1755 – 01(2015)[f] [165]	105 ± 3	-	575 ± 25	76, 151, 154-155
Microalgae	NREL Determination of total solids and ash in algal biomass (LAP)[d, f] [166]	105	-	575 ± 25	66

[a] 'Sample' means the fuels/biomass which these methods are developed for. [b] References that employed these methods for algal biomass. Standard test method for [c] proximate analysis [d] moisture, [e] volatile matter, and [f] ash

Table 4-2: Key temperatures used for proximate analysis of algal biomass by TGA

Sample	Measurement temperature (°C)			References
	M	VM	Ash	
Spirulina[85, 167a], *D. communis*[167], *Hapalosiphon.* & *B. braunii*[168a], *E.prolifera*[140], *S. acutus*[169], *D.tertiolecta*[170]	110	950	700 – 950	ASTM D7582-15[99]
C.reinhardti & *Chlorella* [171b]	110	950	950	ASTM E1131-08 (2014)[47]
Nannochloropsis & *Chlorella*	105	-	550	Rizzo et al.[172]
Chlorella vulgaris	104 – 110	950 ± 20	750	Wang et al.[93, 173]
Scenedesmus	104 – 110	950 ± 20	750	Kim et al.[174]
Chlorella vulgaris	140	800	650	Babich et al.[175]
F.vesiculosus, Chorda filum, L.digitata, F. serratus, L. hyperborea,& M. pyrifera	110	550	550	Ross et al.[176]
Reclaimed nutrient algae	110	850	850	Roberts et al.[177]
L. hyperborea, F. vesticulosus & *M. pyrifera*	110	800	800	Anastasakis et al.[178]
S.obliquus,P. ellipsoidea, C. fritschii, Chlorella & *Spirulina*	105	-	550	Biller et al.[179]
Nannochloropsis oculata & *Tetraselmis sp.*	110	1000	500	Ceylan et al.[180]
Chlorella sorokiniana	110	900	950	Zakariah et al.[181]
Chlorella sorokiniana & *Chlorella vulgaris*	105	800	800	Mwangi et al.[182]
Lyngbya sp. & *Cladophora sp.*	-	575	-	Maddi et al.[183]
Chlorella pyrenoidosa & *Spirulina platensis*	-	800	-	Gai et al.[184]

[a] References [85] and [168] measure volatile matter at 700 and 800 °C respectively.

[b] Reference [171] measures ash at 575 °C.

There are at least two issues associated with the direct application of those standards/methods, which have been developed for other solid fuels, to the algal biomass. One is the difficulty in comparing results of proximate analysis reported in different studies due to the application of diverse methods that employ dissimilar temperatures for devolatilisation and ashing. For example, the extensively used ASTM E870 – 82(2019)[157] and ASTM D7582-15[99] for algal biomass (see **Table 4-1** and **Table 4-2**) measures ash at entirely different temperatures i.e. 580 – 600 ºC and 700 – 950 ºC respectively, which could result in uncertainties. The other issue is the applicability of the existing methods, even those designed for lignocellulosic biomass, to the algal biomass, which have significantly different compositions of organic components (hemicellulose, cellulose and lignin for the former[61-62], and carbohydrates, proteins, and lipids for the latter[178, 185]). In particular, the complex chemical matrix of lipids and proteins with inorganics in the chloroplast of algal biomass[64] hinders its complete oxidation under normal conditions, unless aided by oxidising agents.

Therefore, the validity of the widely used ASTM E870–82 for the algal biomass is questionable. Hence, the objective of Chapter 4 is to use *Spirulina* and *Chlorella* as model algal samples to carry out the systematic proximate analysis as outlined in Section 3.4.1 for investigating the applicability of TGA-ASTM E870–82 to algal biomass. The preliminary experiments in TGA suggested that *Chlorella* could not be oxidised completely at 600 °C in air, for which the tubular reactor-based hydrogen peroxide ashing method was designed as explained in Section 3.2.1. Following that, a three-step analytical procedure is proposed for proximate analysis of algal biomass, corresponding to the first research objective as defined in Section 2.7.

4.2 Assessing Applicability of TGA–ASTM E870–82 to *Chlorella* and *Spirulina*

As summarised in **Table 4-1**, the ASTM E870–82 initially designed for woody biomass, has been commonly employed for the proximate analysis of algae without any validation. To assess its applicability to algal biomass, the TGA–ASTM E870–

82 was employed for the proximate analysis of *Spirulina* and *Chlorella*, the results of which are illustrated in **Figure 4-1**. Whereas the contents of VM for *Spirulina* and *Chlorella* were accurately determined as 82.3 and 84.3 wt % (dry basis, db), respectively, at a devolatilisation temperature of 950 °C, ash contents of 7.4 and 7.8 wt % (db), determined at 600 °C, were considerably overestimated due to the presence of unburnt carbon, as demonstrated by the black colour of the ash residues. This indicates the inapplicability of the ASTM E870–82 to the investigated algal biomass.

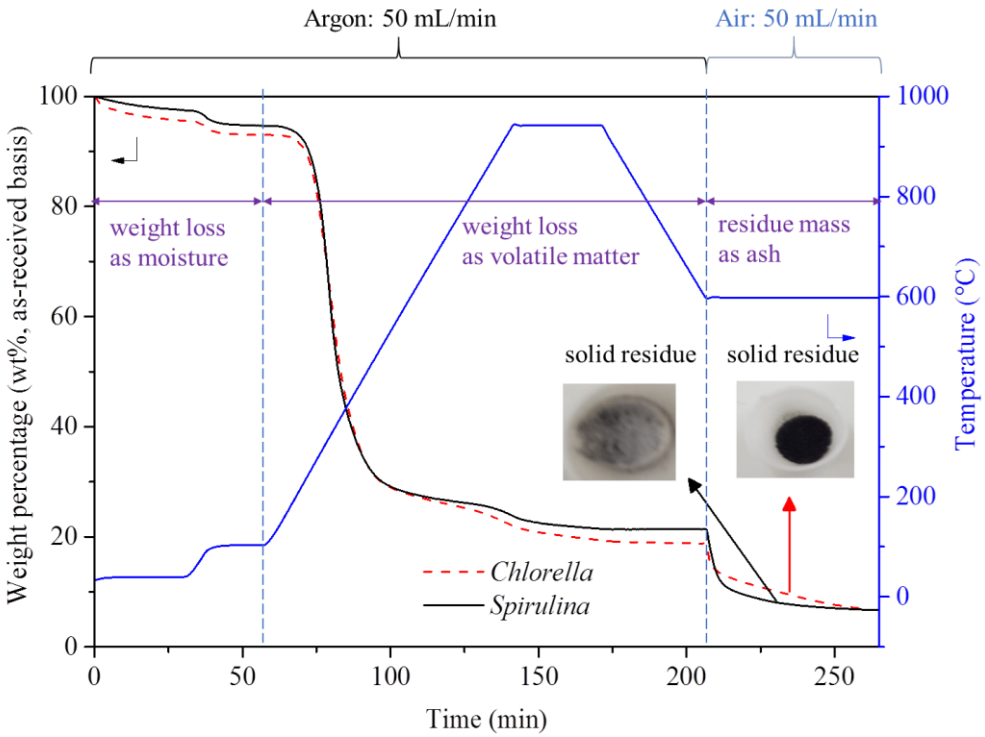

Figure 4-1: Application of the TGA-ASTM E870–82 for the proximate analysis of *Spirulina* and *Chlorella*.

The functional groups in these ash residues were analysed by FTIR and are presented in **Figure 4-2**. The peaks at 1020–1120 and 885 – 900 cm^{-1} are assigned to C – N stretching vibrations, the intensities of which are higher for *Chlorella* than *Spirulina*. This indicates the possible presence of a pyrrole ring and 4-substituted pyridine N-oxides.[186] Under severe pyrolysis condition of 950 °C, pyridine-N further undergoes ring condensation reactions to form thermally stable quaternary nitrogen[101], which cannot be entirely oxidized at 600 °C in the air.[187] The presence of nitrogen in the

ash residues is confirmed by elemental analysis, the contents of which are 3.5 wt % for *Chlorella* and 2.3 wt % for *Spirulina*, based on dry ash residue. The C – C skeletal vibrations in the range 715 – 760 and 460 – 570 cm^{-1} manifest themselves particularly intense for the case of *Chlorella* that displays completely black ash residue.

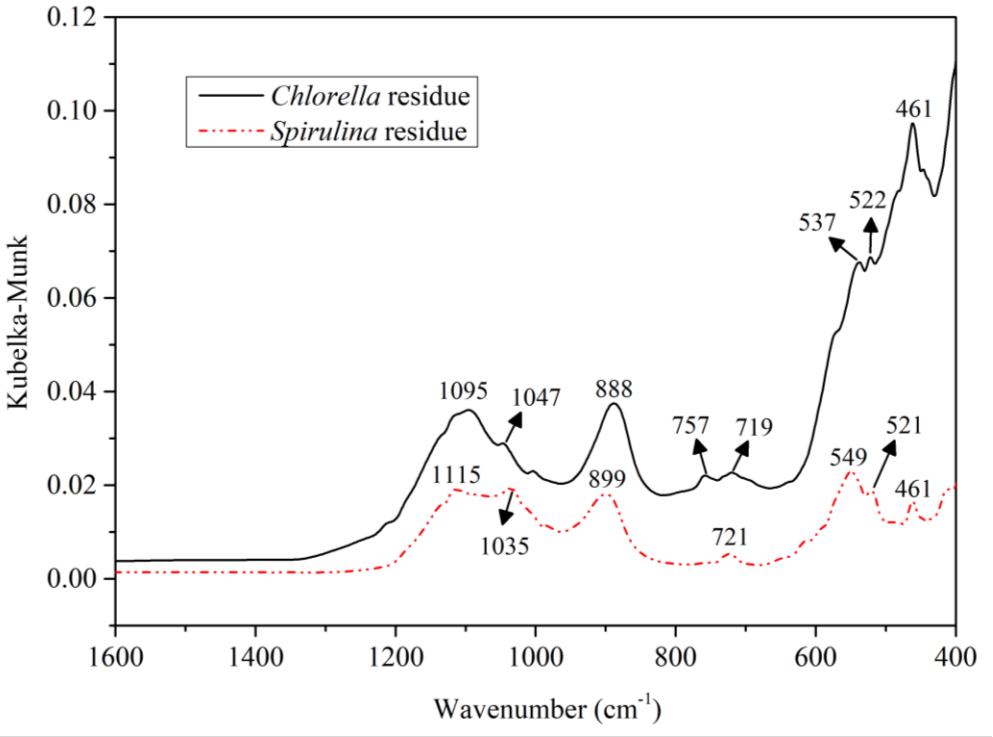

Figure 4-2: FTIR Spectra for the ash residues from *Chlorella* and *Spirulina* by TGA–ASTM E870−82.

4.3 Attempts to accomplish Proximate Analysis of Algal Biomass in a Single TGA Run

The char produced at 950 °C is very refractory to the oxidation at 600 ºC as depicted in **Figure 4-1**. To accomplish the proximate analysis of the algal biomass in a single TGA run, two efforts were made. One is to lower the devolatilisation temperature, aiming to avoid or reduce the formation of stable quaternary nitrogen formed at 950 °C without distorting the VM contents. As illustrated in **Figure 4-3**, decreasing the devolatilisation temperature from 950 to 900 °C leads to a reduction of VM content for *Spirulina* by 3.6%, from 82.3 to 79.3 wt % (db). An opposite trend is observed

for the contents of FC + ash. Since 950 °C is a generally-accepted devolatilisation temperature to determine the contents of VM in solid fuels (see **Table 4-1** and **Table 4-2**), such a considerable reduction in the VM content of *Spirulina* clearly indicates that lowering devolatilisation temperature is not necessarily a feasible option. Details of pyrolytic behaviour of *Spirulina* are given in **Figure 4-4**, where Stage I (40 – 110 ºC) corresponds to water removal. The devolatilisation of organic matter mainly occurs in the temperature range from 110 to 600 ºC, which is referred to as Stage II. The peak devolatilisation temperature is 314 – 319 ºC for all the tested conditions. The Stage III (600 – 950 ºC) accounts for the slow decomposition of carbonaceous material and, possibly, part of mineral matter.

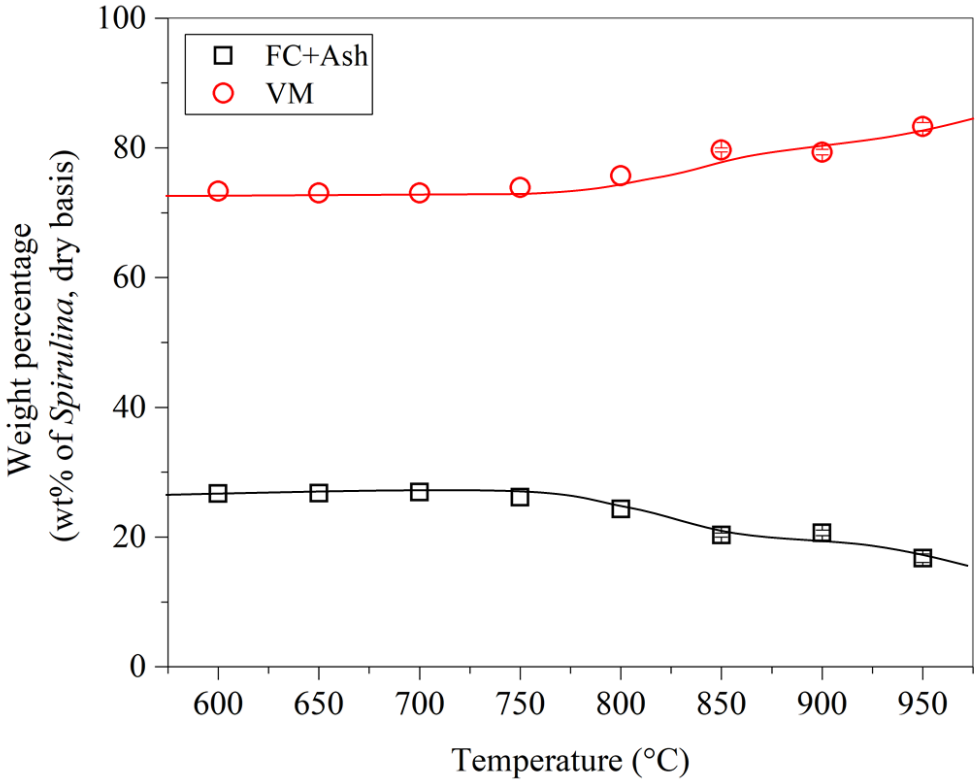

Figure 4-3: Effect of devolatilisation temperature on the contents of volatile matter (VM) and the sum of fixed carbon (FC) and ash in *Spirulina*.

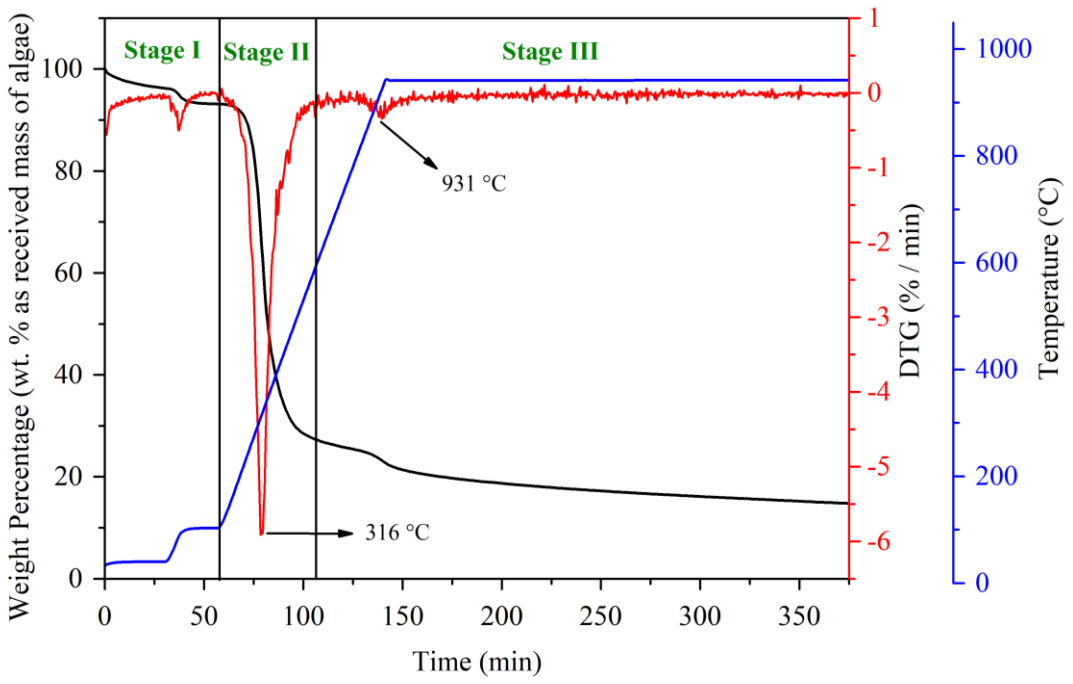

Figure 4-4: Stages in the thermal decomposition of *Spirulina*.

The other attempt is therefore to explore the possibility of employing an oxidation temperature higher than 600 °C (the so-called "safe ashing temperature"), at which carbonaceous material can be completely oxidised without lowering its ash content. If such a temperature exists, it can then be employed to modify the TGA–ASTM E870–82 method. **Figure 4-5** depicts the contents of ash in *Spirulina* and *Chlorella* determined via ashing the algal biomass in the air at 600–800 °C, in comparison with those determined from the TGA–ASTM E870–82 method (**Figure 4-1**). For *Spirulina*, increasing ashing temperature from 600 to 800 ºC results in a slight but continuous decrease of the ash content by up to 2 %. Such reduction in the ash content is consistent with the trend observed for the concentrations of volatile Na and K determined at temperatures 600 – 800 ºC (see **Figure 4-6**). A similar phenomenon on the reduction of ash contents as a result of increasing ashing temperatures from 600 to 800 or 815 °C has also been reported for algae[188] and lignocellulosic biomass.[189] Due to the absence of unburned carbon in the ash residues over the entire temperature range of 600 – 800 °C, although the reduction of ash content is minor, it is recommended to determine the ash content for *Spirulina* (7.3 wt %, db) via direct ashing the algal biomass at 600 ºC in air, to eliminate the volatilisation of alkali metals at a higher temperature.

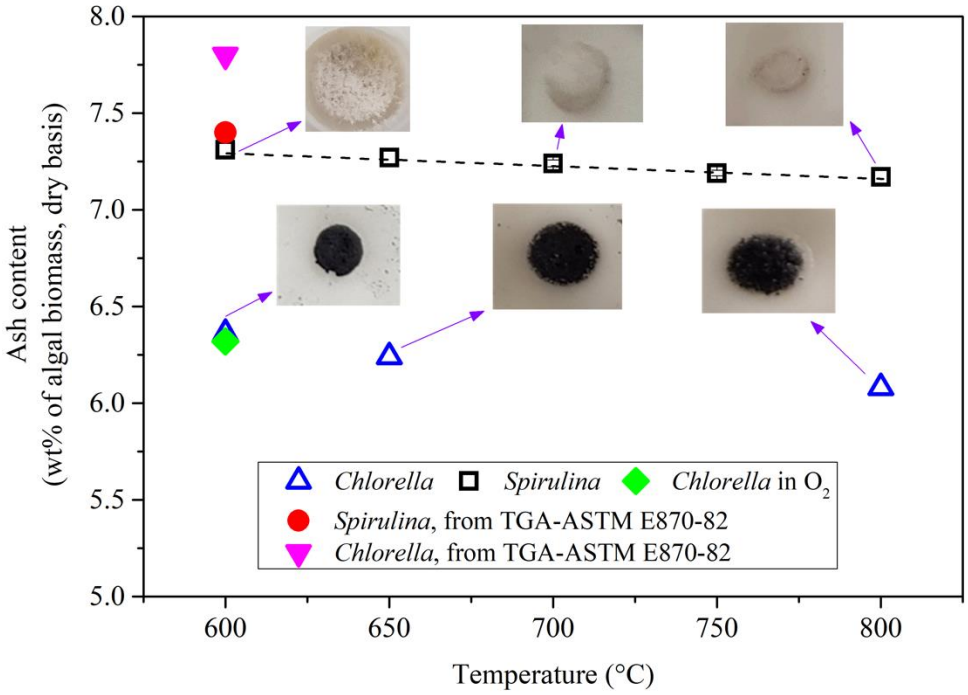

Figure 4-5: Contents of ash in *Spirulina* and *Chlorella* determined from direct ashing of algal biomass in the air using the TGA, in comparison with those measured via the TGA method modified from ASTM E870-82.

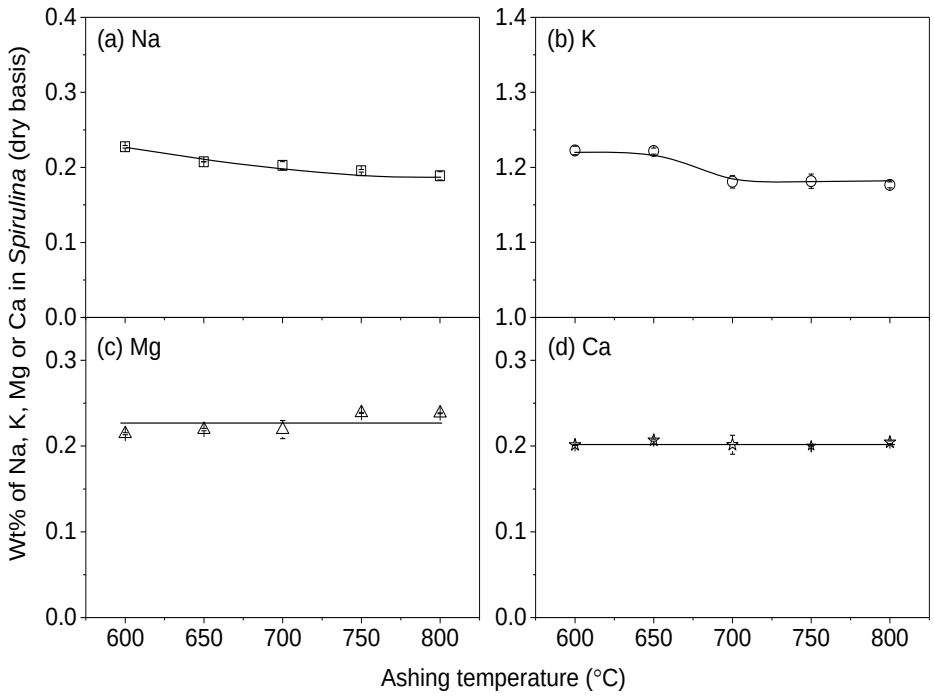

Figure 4-6: Concentrations of (a) Na, (b) K, (c) Mg, and (d) Ca in *Spirulina* as a function of ashing temperature.

It is further observed from **Figure 4-5** that the appearance of ash residues changes from porous to shrink with increasing ashing temperature. Such change is attributed to the melting of alkali metals or salts, in the temperature range of 680 – 800 ºC as shown by melting peaks in the DSC curves presented as **Figure 4-7**. The melting peaks at ~ 690 and 780 ºC correspond to that of eutectic mixture of KCl with K_2SO_4 + $CaSO_4$ and $CaCO_3$, respectively.[190-191] This is confirmed by the XRD analysis of the ashes depicted in **Figure 4-8**, which shows the presence of KCl, K_2SO_4, $CaCO_3$, and $CaSO_4$.

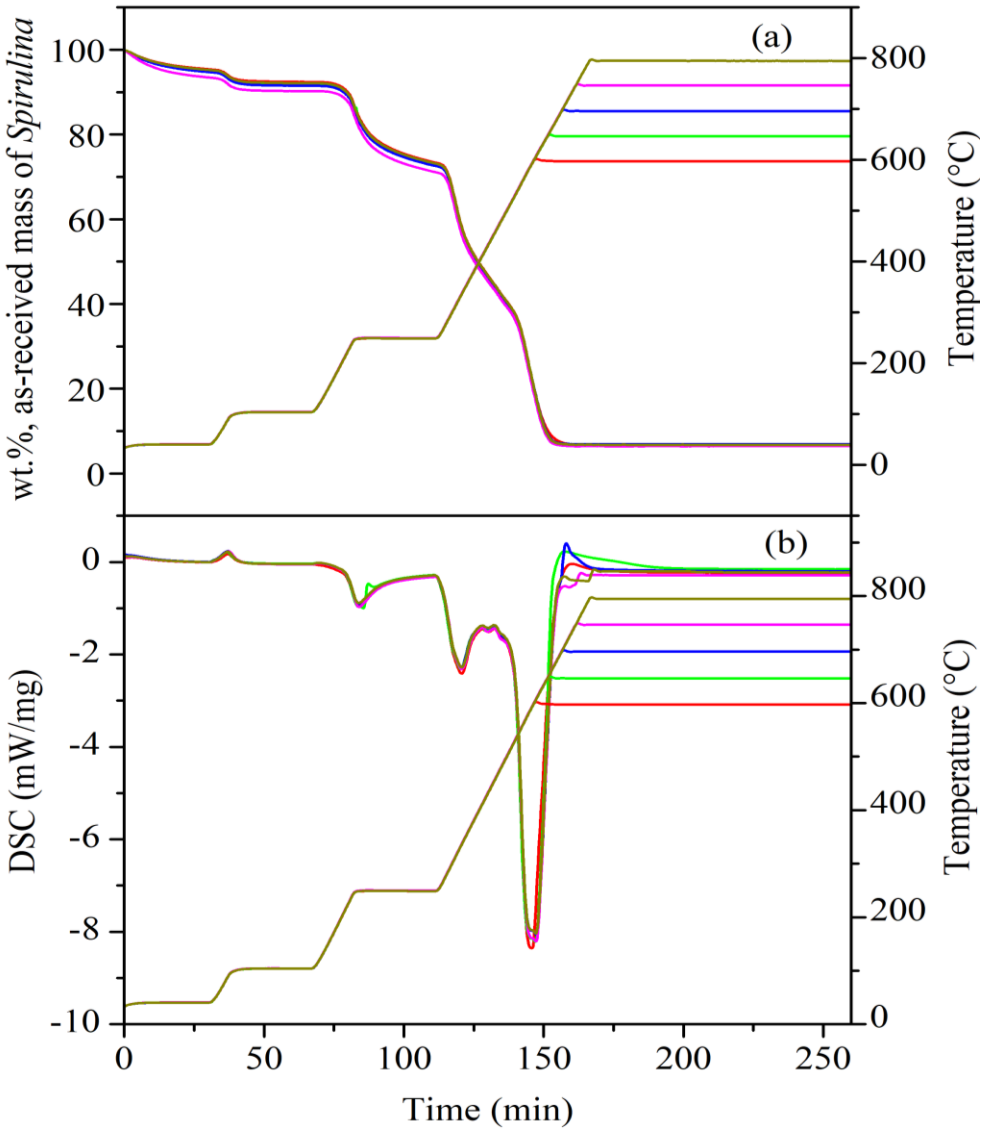

Figure 4-7: (a) TGA and (b) DSC curves for ashing of *Spirulina* at temperatures 600 – 800 °C.

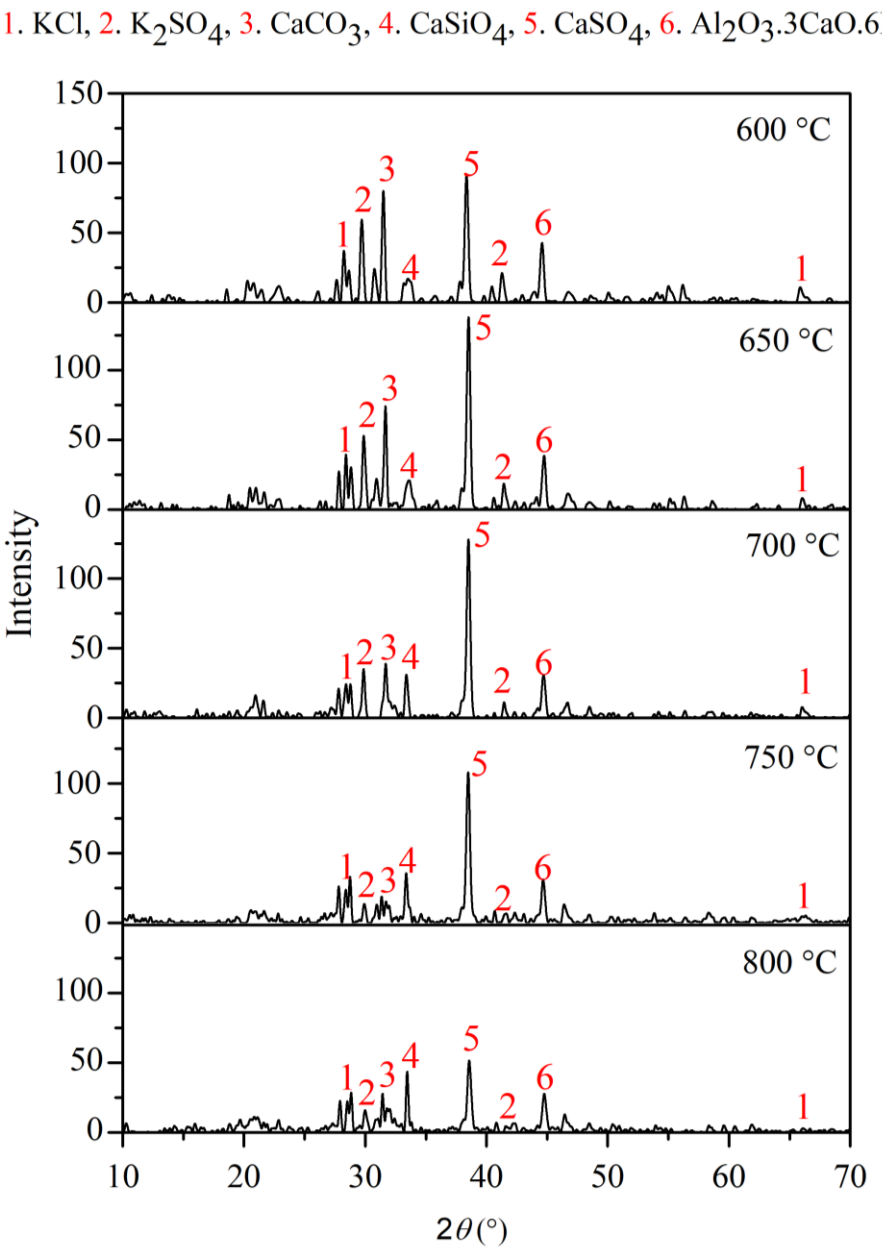

Figure 4-8: XRD analysis of *Spirulina* ashes resulted from ashing temperatures of 600 – 800 °C.

4.4 Oxidation of *Chlorella* with the Aid of H_2O_2

Unlike *Spirulina*, complete oxidation of *Chlorella* is challenging. As shown in **Figure 4-5**, although direct ashing of algal biomass at 600 °C considerably reduces its ash content to 6.4 wt % (db), as compared to that (7.8 wt %, db) determined from the TGA–ASTM E870–82 method, the ash residue is still black coloured, indicating the presence of unburnt carbon and thereby overestimation of the ash content.

Neither switching air into pure oxygen at 600 °C nor increasing ashing temperature to 800 °C achieves complete oxidation of *Chlorella*, as demonstrated by the black colour of the ash residues. The incomplete oxidation of *Chlorella* is attributed to stable quaternary nitrogen in char[101], elimination of which would require a temperature above 927 °C.[192] Indeed, further increasing ashing temperature to 1000 °C enables to burn off the entire portion of the carbonaceous material, only leaving a transparent melt layer on the base of the TGA crucible as shown in **Figure 4-9**. This temperature is, however, too high for accurate determination of ash content due to the volatilisation of alkali metals.

Figure 4-9: Appearance of *Chlorella* ash in TGA crucible after ashing at 1000 °C in air.

To oxidise *Chlorella* completely at the safe ashing temperature of 600 °C, H_2O_2 vapour was introduced into the ashing reactor as explained in Section 3.2.1. Hydrogen peroxide is a well-known oxidizing agent that catalyses the oxidation of solid and liquid fuels in the combustion systems.[193-195] In the gaseous atmosphere of air, H_2O_2 is decomposed into hydroxyl radicals[134, 196], which reacts with the parent H_2O_2 molecule to generate H_2O and O_2.[197] The formation of both hydroxyl radicals and water vapour in the gaseous mixture exhibits the catalytic effect on the oxidation of carbon[134] and helps to oxidize the quaternary nitrogen compounds in the char formed during thermal decomposition.

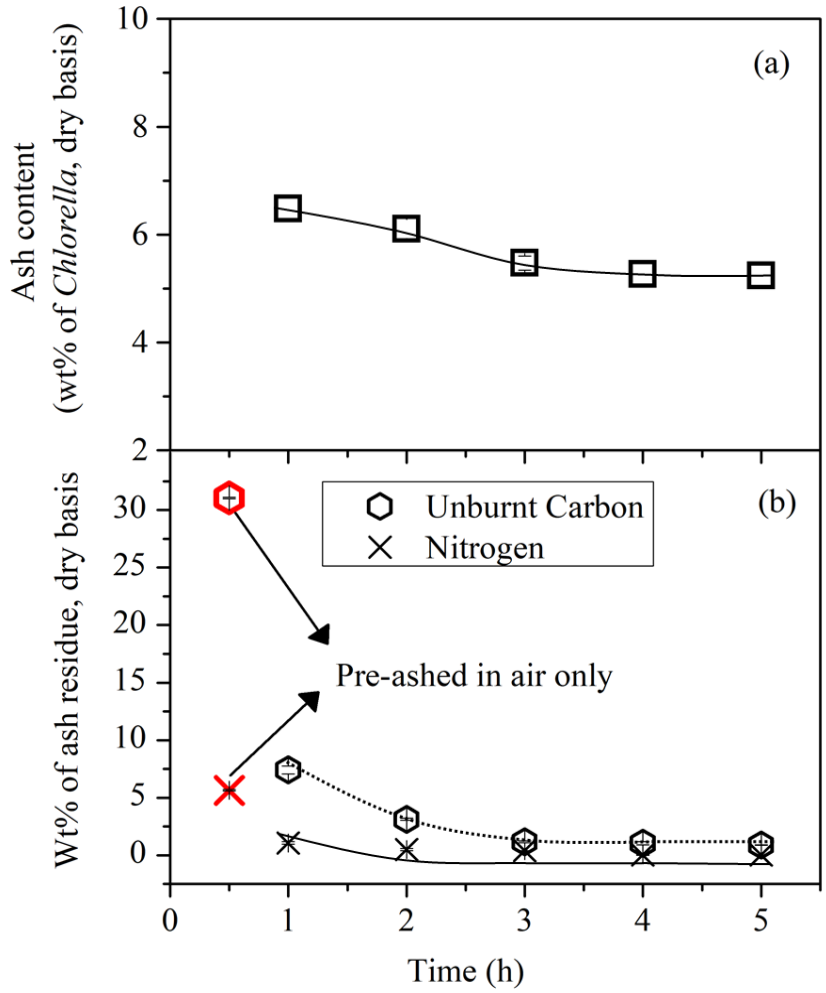

Figure 4-10: The contents of (a) ash in *Chlorella* and (b) unburned carbon and nitrogen in the ash residues measured from ashing at 600 ºC in air with the aid of H_2O_2 as a function of holding time. The ashing atmosphere contains 9.2 % H_2O_2, 34.5 % H_2O (steam), 11.8 % O_2 and 44.5 % N_2, on a volumetric basis.

Figure 4-10 shows the content of ash in *Chlorella* determined at 600 °C in the air with the aid of H_2O_2 and that of unburnt carbon and nitrogen in the ash residues as a function of holding time (1–5 h). The apparent ash content of *Chlorella* rapidly decreases from 6.4 wt % (db) at 1 h to 5.3 wt % (db) at 4 h and then levels off with further increasing the holding time to 5 h. Pre-ashing of *Chlorella* in the air (step 1) gives a high content of unburnt carbon and nitrogen (31.0 and 5.6 wt % of the dry ash residue, respectively), as measured by the ultimate analysis detailed in Section 3.4.3. Exposure of 1 h to an oxidative atmosphere of H_2O_2 and air results in a sharp decline of carbon and nitrogen content to 7.4 and 1.1 wt % (of the dry basis of residue) respectively. The unburnt carbon in ash residue at 4 h is as low as 1.0 wt %

of dry ash residue revealing the decomposition of quaternary nitrogenous compounds. This is also confirmed by the FTIR analysis of the residues shown in **Figure 4-11**. The pre-ashed residue (with air only) displays strong intensities of C-N stretching and C-C skeletal vibrations at the peaks 1089 and 888 and 707 cm^{-1}, respectively. Low intensities of these peaks in H_2O_2 ashed residues (for 1 – 3 h) are direct evidence of cleavage of C – N bonds. Besides, the ashing reactor was kept at 600 °C for 30 min with air continuously flowing through after terminating H_2O_2. This is to promote the decomposition of hydroxides of Na, K, Mg, Ca and other metals (if any), the decomposition temperatures of which are well below 600°C.[198-201] Indeed, elemental analysis of the resulting ash residues indicates the absence of hydrogen (not presented here) and thus the distortion to ash content is avoided. Therefore, the recommended holding time for ashing *Chlorella* in H_2O_2/water/air atmosphere is 4 h, with a corresponding ash content of 5.3 wt % (db).

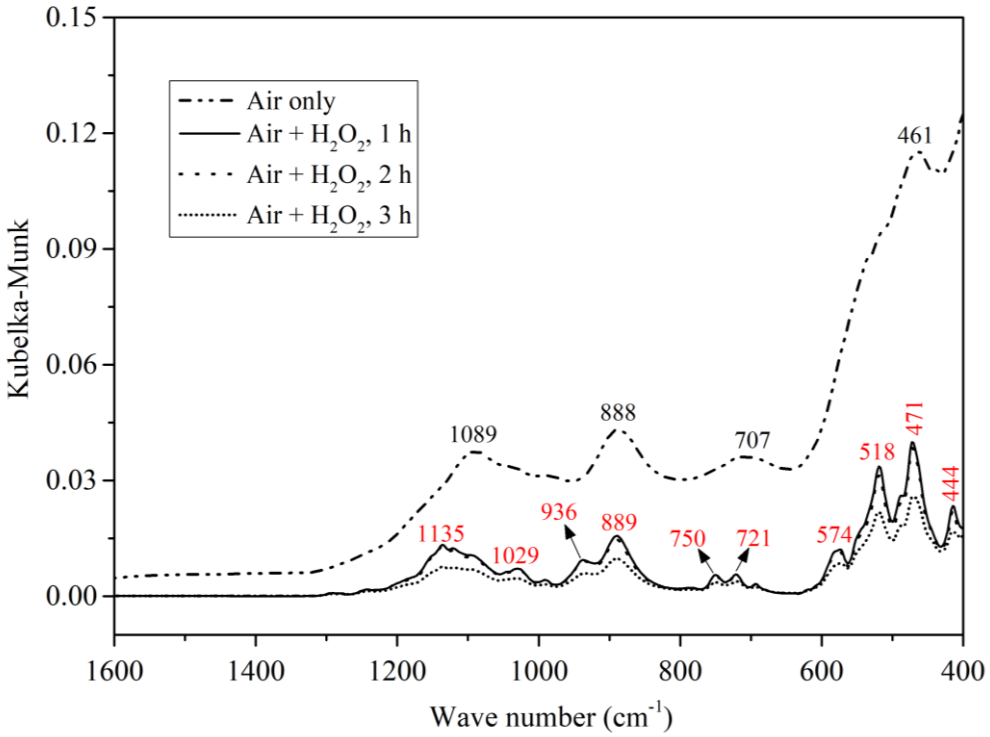

Figure 4-11: FTIR of the ash residues of *Chlorella* from ashing in air and oxidative atmosphere of 9.2 % H_2O_2, 34.5 % H_2O (steam), 11.8 % O_2 and 44.5 % N_2, on a volumetric basis, at holding times of 1 – 3 h.

4.5 Summary of the Analytical Procedure for Proximate Analysis of Algal Biomass

Based on the practices above, an analytical procedure is proposed for the proximate analysis of algal biomass, as illustrated in **Figure 4-12**. The procedure consists of three steps, the number of which required to accomplish proximate analysis depends on the properties of algal biomass. In the first step, the TGA–ASTM E870–82 method is applied, followed by visual observation of the ash residue. If the colour of the ash is light grey, the method applies to the algal biomass, and its proximate analysis is completed. If the ash residue is black coloured, it indicates the presence of unburned carbon and thereby the overestimation of ash content, although VM content is accurately measured. In this case, the second step is required, which involves direct ashing of algal biomass (rather than char produced after devolatilisation) at 600 °C in the air in a TGA. This is to avoid or minimize the effect of stable quaternary nitrogen formed during pyrolysis at 950 °C in the first step. If the ash residue is light grey, the ash content determined in this step is accurate, and the proximate analysis is accomplished. Otherwise, the third step is necessary, in which H_2O_2 is introduced to the ashing reactor for 4 h to facilitate the complete oxidation of algal biomass at 600 °C in air, for accurately measuring the ash content. Following this procedure, the results for the proximate analysis of *Spirulina* and *Chlorella* are presented in **Figure 4-12**.

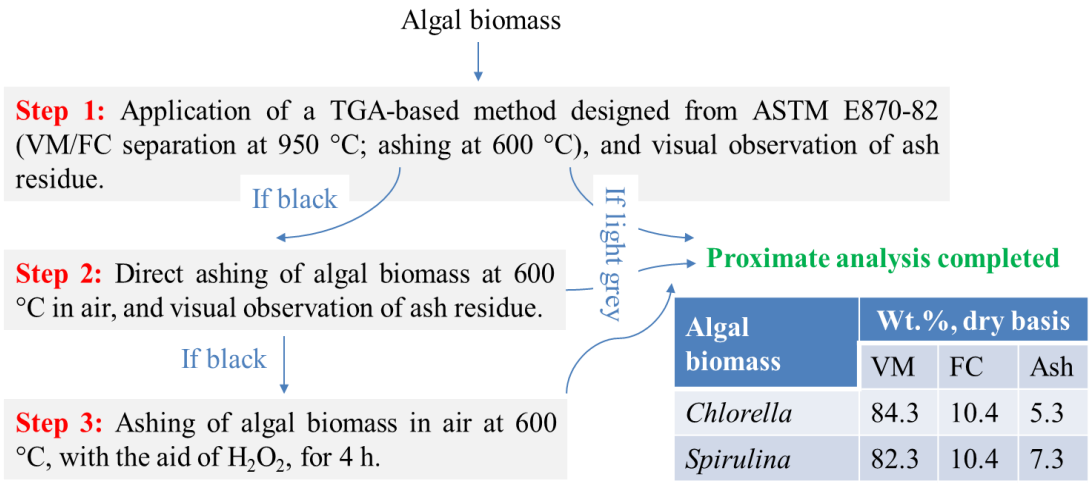

Algal biomass	Wt.%, dry basis		
	VM	FC	Ash
Chlorella	84.3	10.4	5.3
Spirulina	82.3	10.4	7.3

Figure 4-12: Summary of the proposed analytical procedures for proximate analysis of algal biomass, using *Spirulina* and *Chlorella* as a case study.

4.6 Investigating the Contributor(s) to the Incomplete Oxidation of *Chlorella*

To identify the contributor(s) to the incomplete oxidation of *Chlorella* under normal experimental conditions of TGA, two efforts were made. First, we extracted lipids from *Chlorella* with a mixture of methanol, chloroform, and water, following the Bligh and Dryer method. The resulting lipid-extracted *Chlorella* was subjected to oxidation at 600 ºC in TGA in the presence of air (50 mL/min). It gives ash content of 3.6 wt %, which is reasonably lower than 5.3 wt % for that of raw *Chlorella*, because of removal of inorganics (particularly Na and K) during the lipid extraction procedure. However, the residue is still black (see **Figure 4-13**), indicating that removal of lipids does not lead to easy oxidation of the lipid-extracted *Chlorella*. Further, a whey powder containing 73.3 wt % of protein (sourced from a local food store) was ashed under the conditions identical to those for lipid-extracted *Chlorella*. We found the ash residue to be light grey as shown in **Figure 4-14**, representing nearly complete oxidation of the carbon. Although direct contributor(s) to the incomplete oxidation of *Chlorella* is not identified, it is clearly demonstrated that lipid or protein alone is not directly responsible for such incomplete oxidation. Most likely, lipid and protein may indirectly influence the oxidation of *Chlorella* when combined with a complex matrix of inorganics, carotenoids, chlorophyll, and DNA in the Chloroplast.[63-65]

Figure 4-13: Residue from oxidation of lipid-extracted *Chlorella* in TGA at 600 ºC in presence of air.

Figure 4-14: Residue from oxidation of whey protein in TGA at 600 ºC in presence of air.

4.7 Conclusions

In this chapter, we concluded that ASTM E870–82 designed for woody biomass is not applicable for the proximate analysis of *Spirulina* and *Chlorella*, as indicated by the presence of unburnt carbon in the resulting ashes, although it accurately determines the contents of volatile matter. While *Spirulina* can be entirely ashed at 600 °C in air, complete oxidation of *Chlorella* requires the aid of H_2O_2 under a similar condition. An analytical procedure is developed for the proximate analysis of algal biomass, using *Spirulina* and *Chlorella* as a case study. The procedure consists of three steps: (1) application of the TGA–ASTM E870–82 method; (2) direct ashing of algal biomass at 600 ºC in the air; and (3) oxidation of algal biomass

with the aid of hydrogen peroxide (H_2O_2). The number of steps required to perform a complete proximate analysis depends on the properties of algal biomass. Based on the proposed analytical procedure, the contents of volatile matter, fixed carbon, and ash are 82.3, 10.4 and 7.3 wt % for *Spirulina*, and 84.3, 10.4 and 5.3 wt % for *Chlorella* expressed on a dry basis.

CHAPTER 5

Thermal Decomposition of Model Compound of Algal Biomass

5.1 Introduction

The inhomogeneous composition of algal biomass[91, 94, 202] hinders thorough understanding of its thermal decomposition mechanism and contributes significantly to the complex temperature-species profiles. In particular, amino acids (proteins) and other nitrogenous species convert into toxic N-bearing compounds, such as NH_3 and HCN[91-94], which serves as a direct precursor for the formation of NO_x and N_2O.[95-96] Literature reports the mechanisms and pyrolytic products of thermal decomposition of several N-model compounds, including proline[203], morpholine[204-205], pyrrole[206], pyridine[207], and nitromethane.[208] However, literature pertinent to the thermal decomposition of surrogates of amino acid is somewhat limited and confined to providing mechanistic pathways without a rigorous comparison with experimental observations via detailed kinetic modelling. This has generally hampered complete understanding of the decomposition kinetics of N-rich algal biomass.

Leucine represents one of the primary amino acids found in the algal biomass, ranging from 4 to 20 wt % of the total amino acids present in various strains.[116-117, 209] It is an α-amino acid that consists of an α-amino group, α-carboxylic acid group and a side chain of isobutyl group. Several experimental studies have focused on different aspects of leucine pyrolysis. Simmonds et al.[210] employed gas chromatography-mass spectrometry (GC-MS) technique to identify major products from pyrolysis of several amino acids and developed an integrated reaction scheme

to suggest plausible thermal dissociation pathways. Three principle reactions may prevail in the thermal decomposition of amino acids, namely decarboxylation, deamination, and dehydration. This is evidenced from relatively high concentrations of corresponding amides, CO_2, NH_3, H_2O and N-alkyl aldimines in pyrolysate.[211] The appearance of N-alkyl aldimines reveals the likelihood of bimolecular reactions between primary amines and intermediate imines. The double dehydration self-reaction of leucine forms dipeptides and diketopeprazine (DKP), which may then decompose to yield N-alkyl aldimines.[212]

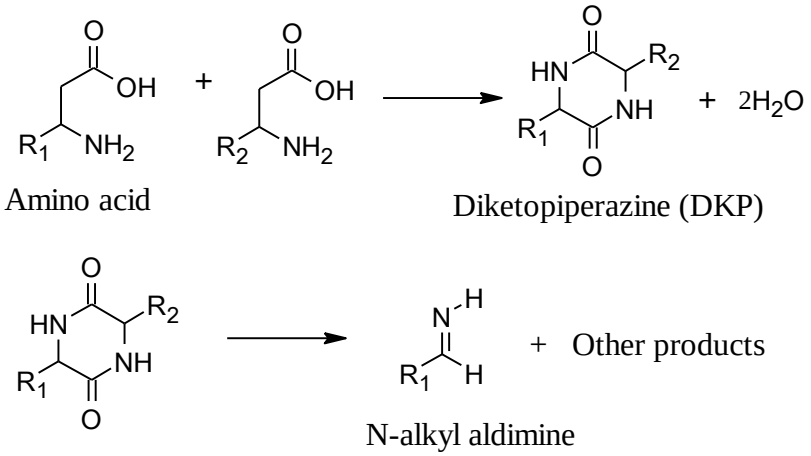

Scheme 1: Formation of N-alkyl aldimine from the amino acid

Detection of piperazine-2,5-diones (PD) by GC-FTIR evidences the occurrence of self-condensation reactions during pyrolysis.[211] Lien et al.[211] and Chiavari et al.[213] postulated the thermal decomposition routes for major pyrolysis products via unimolecular channels and biomolecular interactions among secondary products. These reaction routes generally accord with the mechanistic model of Simmonds et al.[210] However, none of these proposed reaction schemes is validated against the results of accurate quantum-chemical calculations.

Therefore, the key objective of Chapter 5 is a detailed theoretical thermo-kinetic analysis illustrating plausible unimolecular and bimolecular routes encountered in the gas and condensed-phase pyrolysis of Leucine, which addresses the research objective 2 as mentioned in Section 2.7. Calculation of the energetic requirements of these reactions are carried out systematically in three steps: (1) determination of the reaction rate constants for all ensuing unimolecular and bimolecular channels; (2)

computation of the thermodynamic properties of all the products and intermediates; and (3) building a robust kinetic model, as explained in Section 3.3.2. Such calculations facilitate the evaluation of the relative occurrence of competing reaction routes as demonstrated in the following sections.

5.2 Stationary Point Determinations

In the initial stages of pyrolysis prior to the establishment of a radical pool, the thermal degradation of leucine occurs via unimolecular pathways. These routes comprise direct bond scissions producing two radical species, and degradation pathways that generate two stable molecules. Starting with the first category, **Figure 5-1** illustrates the homolyses of C-C, N-H, C-N, C-H, C-O and O-H bonds in a leucine molecule along with their bond dissociation enthalpies (at 298.15 K). These bond fission reactions proceed without encountering intrinsic reaction barriers. The lowest enthalpy of 323.1 kJ/mol accompanies the formation of the M6 radical through fission of H from α-carbon of leucine. Enthalpies for the breakage of other C-H bonds are significantly higher and lie in the range of 414.3 – 428.2 kJ/mol. These results agree with the corresponding dissociation enthalpies of C-H bonds in proline.[203] The scission of the C-N bond, to produce the M3 and NH_2 radicals, represents a potentially feasible pathway characterised by the enthalpy of dissociation of 338.9 kJ/mol. ß-C-C scission produces the M1 and M10 adducts entailing the endothermicity of 374.7 and 371.7 kJ/mol, respectively. These values are comparable to the enthalpic requirement of 372.4 kJ/mol for the fission of the C-C bond in a propane molecule.[214] Homolysis of N-H bond in leucine displays a substantial endothermicity of 432.1 kJ/mol, which falls close to the dissociation energy of the N-H bond of 422.5 kJ/mole in tert-butylamine[215], calculated at the same level of theory. Likewise, cleavage of the C-O bond demands 468.6 kJ/mol, as the dissociation energy that exceeds slightly the experimentally-determined dissociation enthalpy of 451.8 ± 2.9 kJ/mol for the C-O bond in acetic acid.[216] Hence, the formation of the M3 and M6 radicals represents the most thermodynamically feasible channels among the direct bond fission reactions. However, as will be shown in the next section, degradation pathways featured by decarboxylation, deamination and dehydration require lower energies.

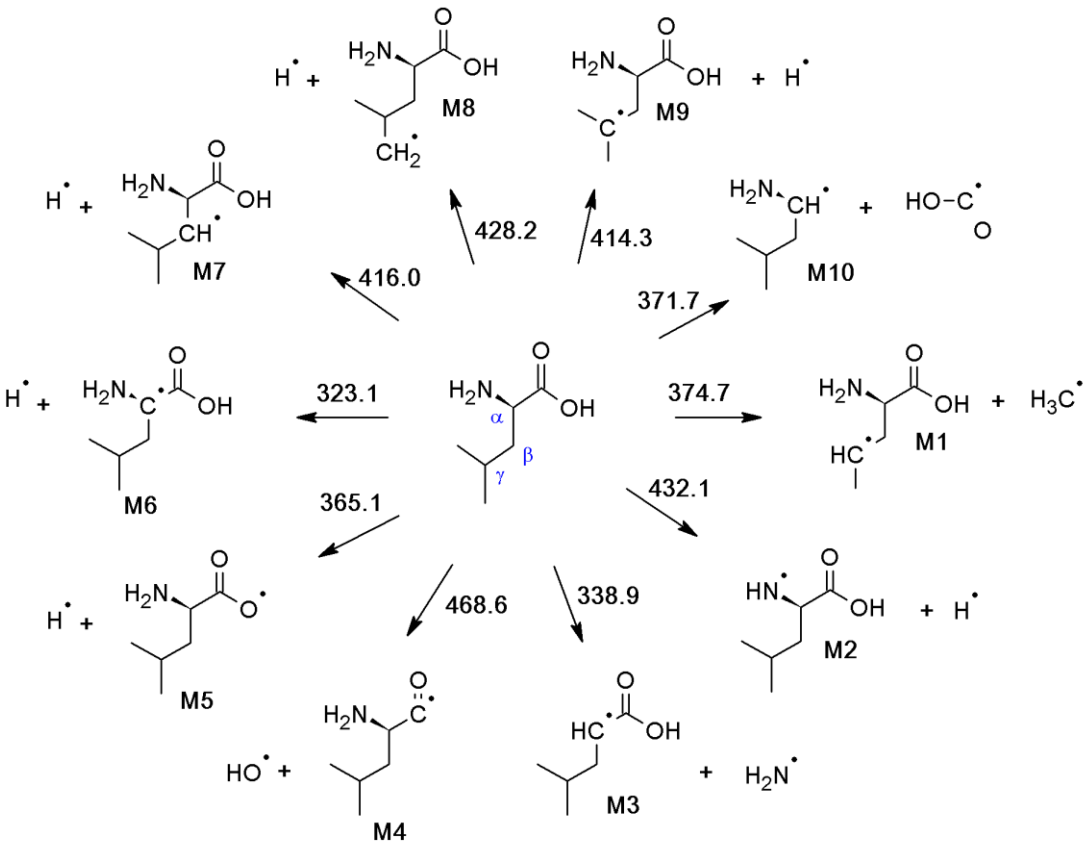

Figure 5-1: Bond dissociation enthalpies for the homolysis of C-C, N-H, C-N, C-O, O-H and C-H bonds in a leucine molecule. All values are in kJ/mol at 298.15 K.

5.3 Potential Energy Surface for the Unimolecular Decomposition of Leucine

Here, we investigate the thermal decomposition pathways for leucine in accordance with the model for amino acids proposed by Simmonds et al.[210] The model consists of unimolecular decomposition pathways, initiated mainly by the scission of α-C-H, N-H and C-O bonds in amino acids. Decarboxylation prevails if an acid exists in a zwitterion form[212], however, due to a weak dipole moment of leucine in the gas phase (5.73 D), the zwitterion form displays less stability compared to that in solution (dipole moment 7.37 D).[217] In addition to the intramolecular pathways of Simmonds et al.[210], we also consider the free-radical chain reactions. **Figure 5-2** displays the unimolecular decomposition pathways for decarboxylation, deamination, and dehydration of leucine, with the optimised geometries of leucine and transition states presented in **Figure 5-3**.

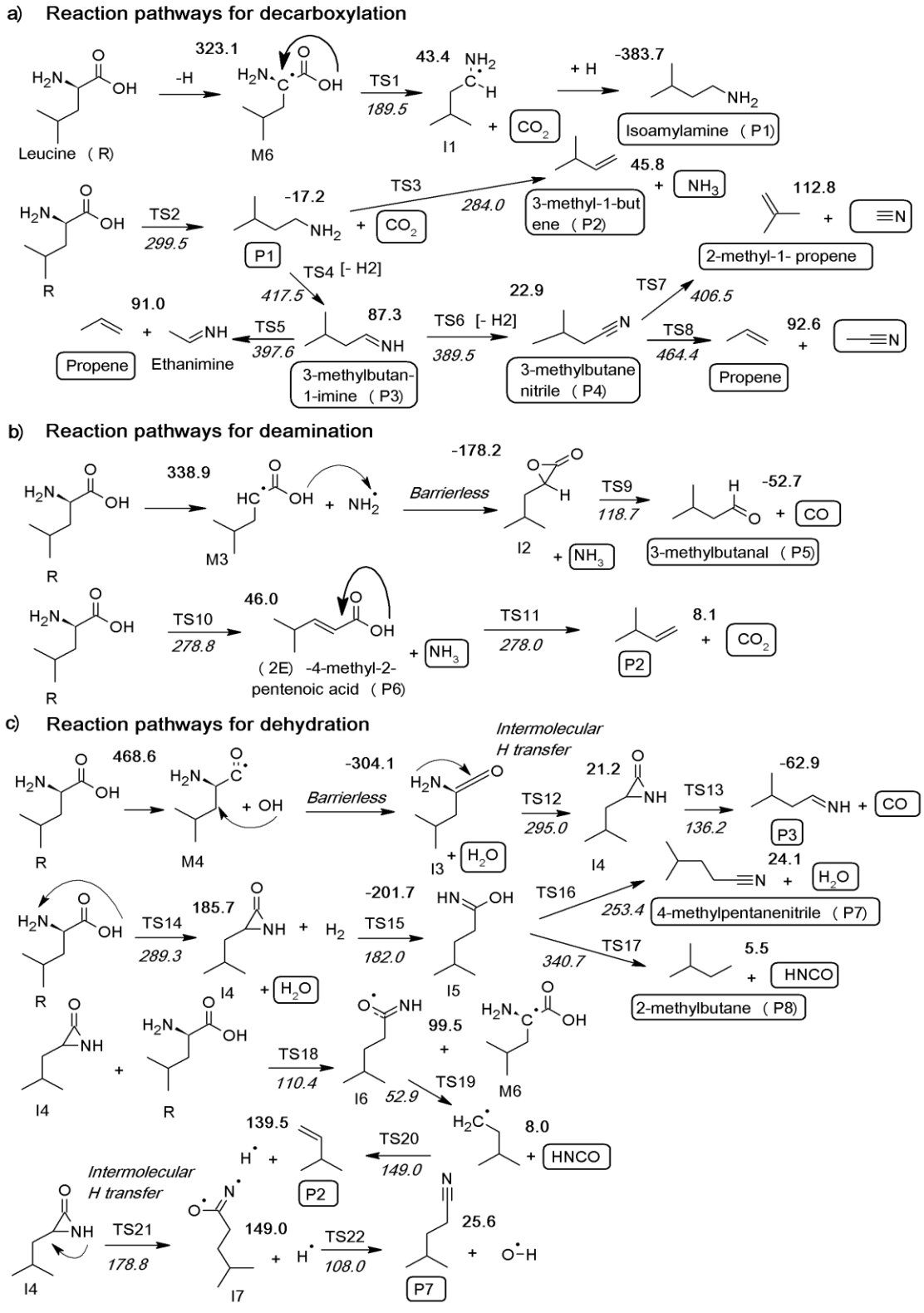

Figure 5-2: Reaction pathways for (a) decarboxylation, (b) deamination and (c) dehydration of leucine. Values in bold are reaction enthalpies and values in italic signify activation enthalpies. All values (in kJ/mol) are calculated at 298.15 K. The products detected experimentally are enclosed in boxes.

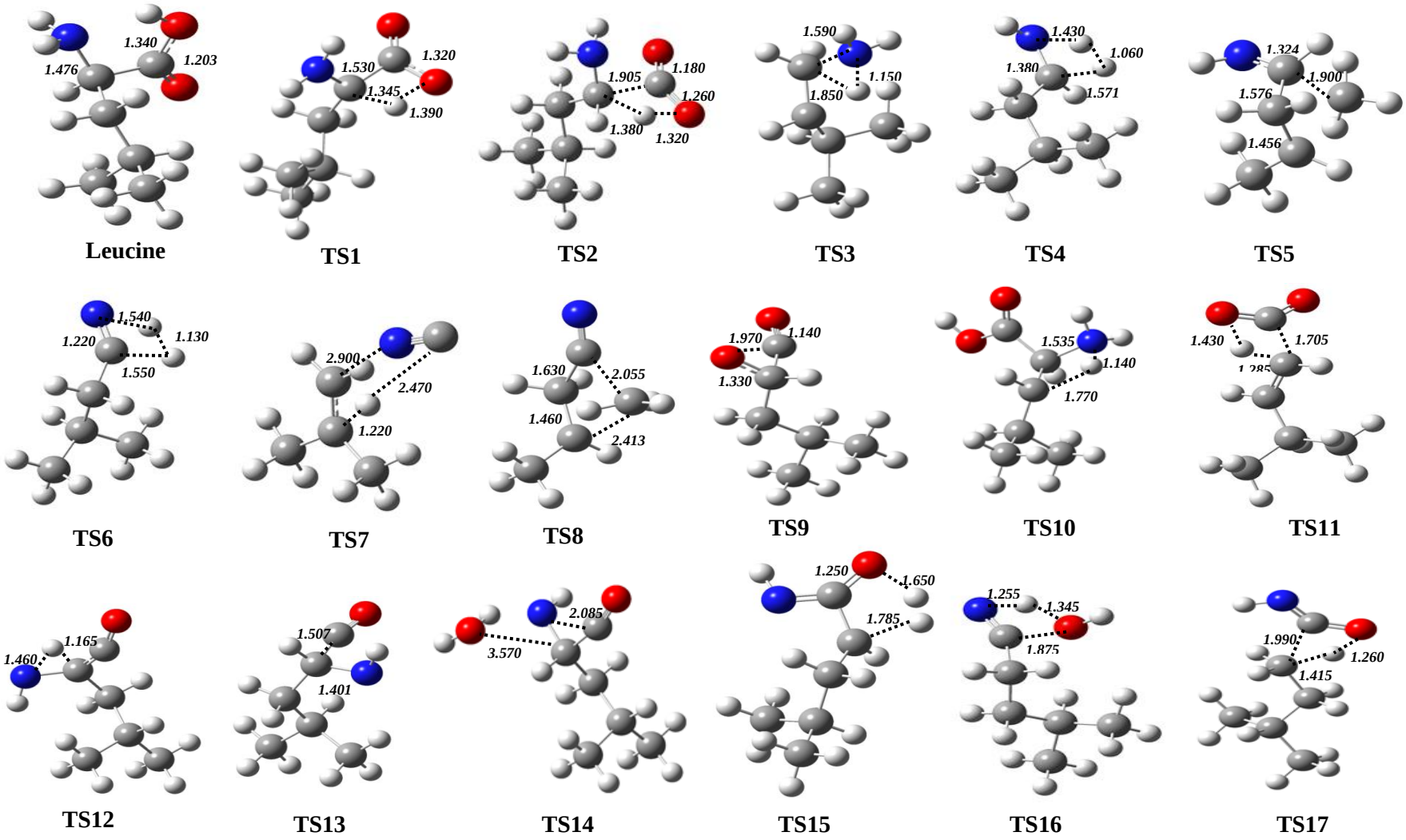

Figure 5-3: Optimised geometries for transition states involved in the unimolecular decomposition of Leucine molecule. Interatomic distances are in Å

Decarboxylation to produce amines and CO_2 constitutes the primary exit channel for amino acids as **Figure 5-2a** depicts. This reaction occurs either in a closed-shell (R → CO_2 + P1) or in an open-shell (R → H + M6 → CO_2 + I1). The formation of M6 (via loss of the α-H) moiety initiates the radical pathway for the decarboxylation followed by 1,3-H shift and CO_2 ejection passing through an enthalpic barrier of 189.5 kJ/mol (TS1) and entailing the reaction endothermicity of 43.4 kJ/mol. This reaction yields 1-amino-3-methylbutyl radical (I1) as an intermediate that could abstract an H atom from another species to generate iso-amylamine (P1), experimentally detected by GC-MS[211] and TG-FTIR.[97] A direct decarboxylation of leucine ensues by eliminating CO_2 from –COOH group attached to the α-carbon followed by a subsequent transfer of H atom to α-carbon. This reaction is slightly exothermic and demands an activation enthalpy of 299.5 kJ/mol (TS2). As shown in **Figure 5-2a**, the elimination of a CO_2 molecule on the open-shell enthalpy surface requires a significantly lower activation enthalpy when contrasted with the corresponding value for the closed-shell enthalpy surface, i.e., 189.5 kJ/mol versus 299.5 kJ/mol.

Several pyrolysis products like olefins, aldimines, and nitriles emerge from the fragmentation reactions of P1. In this study, we calculate enthalpic barriers for unimolecular decomposition reactions of P1 considered in the model of Simmonds et al.[210] These reactions afford the experimental products, e.g., 3-methyl-1-butene (P2)[211], 3-methylbutan-1-imine (P3)[210], 3-methylbutanenitrile (P4)[210], 2-methyl-1-propene (C_4H_8)[210], propene (C_3H_6)[210], CH_3CN[218], HCN[218-219], NH_3 and H_2. Deamination and dehydrogenation represent the most likely exit channels for P1, to produce P2 and P3, respectively. Formation of P2 through a loss of an ammonia molecule passes via the activation enthalpy barrier of 284.0 kJ/mol, as characterised by the transition structure TS3. In a competing isomerisation reaction, P3 forms through a 1,2-H combination reaction via a noticeably higher enthalpic barrier of 417.5 kJ/mol (TS4). The reaction enthalpies for the formation of P2 and P3 from P1 amount to 45.8 and 87.3 kJ/mol, in that order. Species P3 is an important intermediate that can either undergo bimolecular reactions or decompose to yield lower chain hydrocarbons. Decomposition of P3 via ß-C-C scission generates C_3H_6 and ethanimine (C_2H_5N) passing through TS5 (397.5 kJ/mol). According to the model of Simmonds et al.[210], P3 dissociates into P4 by expelling an H_2 molecule

over a sizable enthalpic barrier of 389.5 kJ/mol (TS6). The very high barrier of TS6 may indicate the accumulation of P3 as a major product of the pyrolysis. In practice, the elevated barrier of TS4 that leads to P3 makes this species unlikely to form. Thus, P2 signifies the most likely product from the fragmentation of P1.

Simmonds et al.[210] did not consider the unimolecular pathways for the formation of HCN and CH_3CN. These products stem from the decomposition of DKP, as illustrated in the case of glycine.[210] If P4 forms, it decomposes to yield HCN and CH_3CN via two distinct channels. Note that, while the present calculations deal with reactions in the gas phase, the experiments available to us involve the pyrolysis of the solid phase. Hence, prudently, we do not discard the pathways involving P4 from further consideration. An intramolecular H transferred from the methyl group in the P4 molecule to the C atom in the -C≡N group can generate C_4H_8 and HCN via TS7. Likewise, the breakage of a -C-C bond in P4, mediated by H transfer from the CH_3 group, produces CH_3CN and C_3H_6. Endothermicity of the latter reaction stands at 92.6 kJ/mol. Given a noticeable difference in activation energies between TS7 (406.5 kJ/mol) and TS8 (464.4 kJ/mol), i.e. 57.9 kJ/mol, unimolecular decomposition of P4 most likely generates HCN and the C_4H_8 isomer of 2-methyl-1-propene.

The radical and molecular pathways for deamination of leucine are displayed in **Figure 5-2b**. As discussed earlier, a potential chain initiation step for deamination signifies the formation of M3 radical by eliminating NH_2, which further abstracts an H from the M3 product to make NH_3 and an intermediate compound of oxiranone (I2). This reaction occurs without encountering an activation barrier. The further fragmentation of I2 encounters a rather modest energy barrier of 118.7 kJ/mol (TS9) producing 3-methylbutanal (P5) and CO. These reactions display an exothermicity of -178.2 and -52.7 kJ/mol, correspondingly. Both P5 and CO are among the reported experimental products from the pyrolytic decomposition of leucine.[211]

The molecular channel for the direct elimination of ammonia from leucine involves a 1,3-hydrogen shift affording 4-methylpent-2-enoic acid (P6) with reaction energy of 46 kJ/mol. The enthalpic barrier for this reaction corresponds to 278.8 kJ/mol (TS10) that is comparable to 271.9 kJ/mol for the direct elimination of NH_3 from 2-(vinyloxy) ethanamine.[204] However, P6 was not detected in experiments[211, 219] and

the direct expulsion of ammonia from amino acids does not constitute a major pathway.[212-213] Therefore, we consider a consumption corridor of P6, that is, its fragmentation into P2 passing through a barrier of 278.0 kJ/mol (TS11). This reaction occurs via a 1,3-hydrogen shift along with a subsequent ejection of CO_2 with trivial reaction energy of 8.1 kJ/mol. Ammonia also arises from the deamination of P1, as shown in **Figure 5-2a**.

Dehydration represents the third most dominant mechanism encountered in the thermal decomposition of amino acids. **Figure 5-2c** illustrates the radical and molecular pathways. The cleavage of the C-O linkage to liberate OH radical contributes minimally to the dehydration channel because of its elevated bond dissociation enthalpy of 468.6 kJ/mol. As fission of the C-OH bond may indeed occur in condensed media or via surface-assisted reactions, we elect herein to present the subsequent steps. The hydroxyl radical abstracts an H atom from the α-carbon of the M4 moiety to generate H_2O and 2-amino-4-methylpent-1-en-1-one (I3), as an intermediate. This reaction takes place without a potential barrier and experiences a considerable exothermicity of -304.1 kJ/mol. Along this pathway, I3 undergoes an intermolecular H-transfer from $-NH_2$ to the double-bonded carbon atom to generate 3-(2-methylpropyl) aziridin-2-one (I4), as an intermediate. The enthalpic barrier for this reaction amounts to 295.0 kJ/mol (TS12) with the reaction energy of 21.2 kJ/mol. We further consider the fragmentation of I4 into P3 and CO via TS13 (136.2 kJ/mol). The formation of P3 is exothermic by -62.9 kJ/mol.

According to Simmonds et al.[210], a closed-shell dehydration pathway affords directly the I4 intermediate. We calculate the enthalpic barrier for this reaction to be 289.3 kJ/mol (TS14) and its reaction energy as 185.7 kJ/mol. The I4 intermediate reacts with H_2 molecule to produce 4-methylpentanimidic acid (I5) as another intermediate.[210] The calculated activation and reaction energies for I5 amount to 182.0 (TS15) and -201.7 kJ/mol, correspondingly. Two exit channels for I5 generate {4-methylpentanenitrile (P7) + H_2O} and {2-methylbutane (P8) + HNCO}, respectively. The favourable route for the decomposition of I5 leads to P7 with an enthalpic barrier of 253.4 kJ/mol (TS16). This value falls substantially below that of the parallel competing pathway into P8 via TS17 of 340.7 kJ/mol. The two fragmentation reactions of I5 display the endothermicity of 24.1 and 5.5 kJ/mol,

respectively. Both species, P7 and P8, signify experimental products.[210] Furthermore, Li et al.[97] identified HNCO as a significant N-containing product from the pyrolysis of leucine, as did Baisuk for the case of the decomposition of DKP.[220]

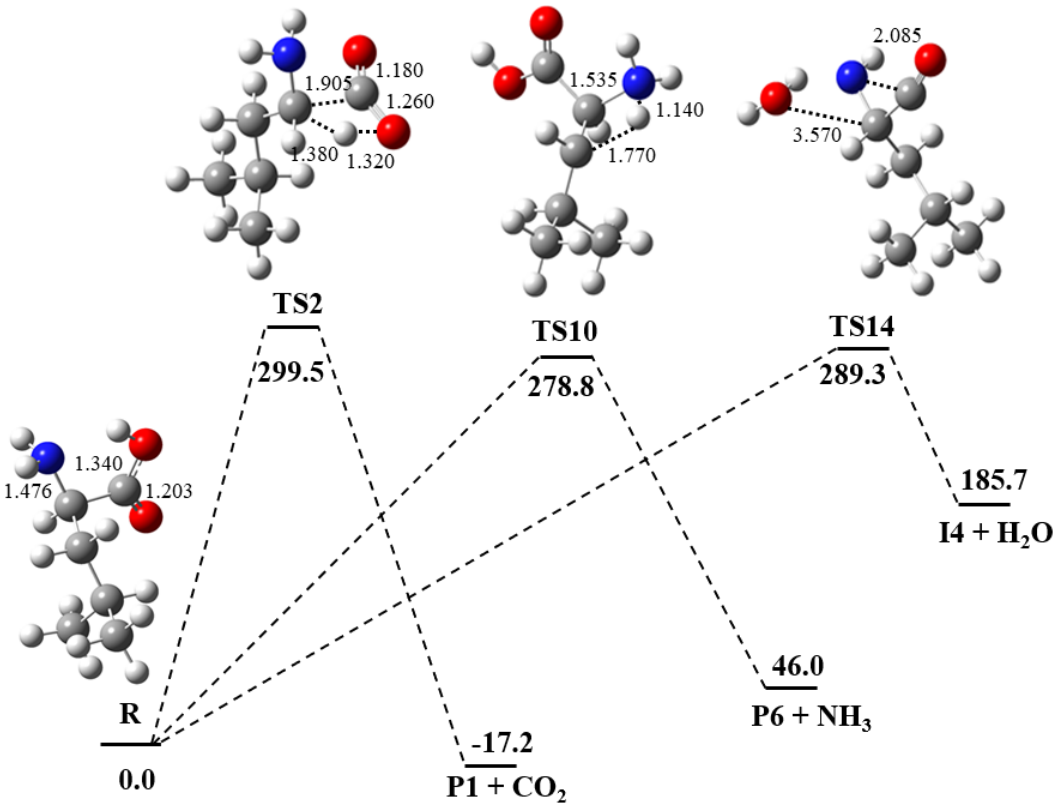

Figure 5-4: The potential energy surface for the most plausible unimolecular decomposition pathways of leucine. The activation and reaction enthalpies are in kJ/mol (at 298.15 K) and interatomic distances in Å.

Figure 5-4 presents the potential energy surface (PES) for the three most energetically favourable pathways in the unimolecular decomposition of leucine, leucine → P1 + CO_2, leucine → P6 + NH_3 and leucine → I4 + H_2O. These three pathways incur very comparable activation energies and are likely to proceed at the equivalent reaction rate constant. The formation of the I4 intermediate from leucine provides a direct precursor for the emergence of experimental products P2, P3, P7, P8 and HNCO as demonstrated earlier. **Figure 5-5** demonstrates that the I4 + H_2 reaction could account for the formation of P7 and P8 through the overall activation energy of 182.0 kJ/mol. However, a low concentration of hydrogen molecules at relatively low temperature may diminish the importance of this pathway for

removing I4. Alternatively, the reaction of I4 with a molecule of the parent leucine offers an energetically favourable pathway for the formation of P7, as illustrated at the lower half of **Figure 5-2c**. This reaction proceeds with a low-enthalpy barrier of 110.4 kJ/mol (TS18) affording intermediates I6 (1-hydroxy-4-methylpentylidene amino) and M6. Fragmentation of I6 presents an alternate route for the appearance of HNCO by cleaving the C–C bond as the molecule passing through the TS19 transition state, entailing a barrier of 52.9 kJ/mol. The resulting C_5H_{11} loses an H atom to form P2 via TS20 (149.0 kJ/mol). Products of this reaction reside 139.5 kJ/mol above the C_5H_{11} species. Another route for I4 consumption results in P7 by a two-step mechanism, initiated by the intermolecular H transfer to generate I7 (4-methyl-(1-hydroxyl) pentylidene) amino) via TS21 (178.8 kJ/mol). The reaction of I7 with H produces P7 and OH through an enthalpic barrier of 108.0 kJ/mol (TS22).

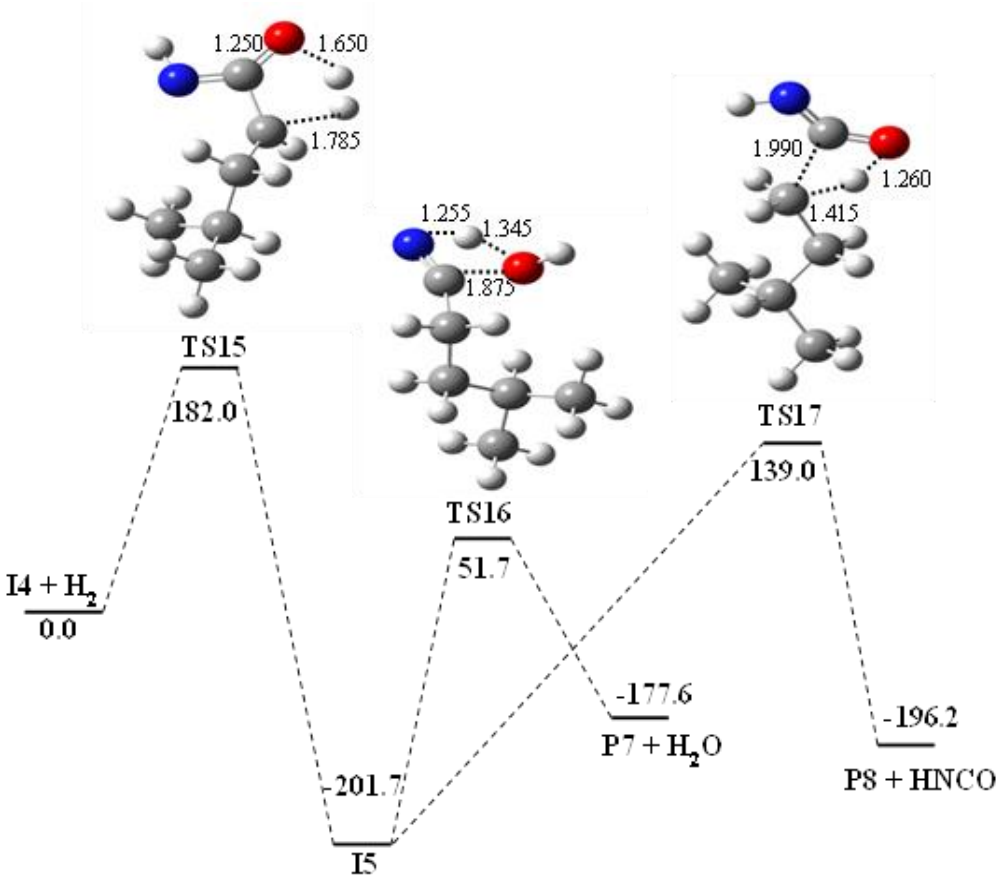

Figure 5-5: PES for the reaction I4 + H_2, mapped out at CBS-QB3 level of theory. The activation and reaction energies are in kJ/mol and interatomic distances are in Å.

The mechanistic model of Simmonds et al.[210] does not incorporate unimolecular pathways for the formation of HCN, CH_3CN, and HNCO. From the present work, fragmentation of P4 generates CH_3CN and HCN, and I4 decomposes into HNCO via two separate channels. However, high energy barriers for the synthesis of HCN (406.5 kJ/mol via TS7) could be responsible for the absence of this species in the experiments of Simmonds et al.[210] Experimental evidence for the appearance of CH_3CN presented by Simmond et al.[210], contrary to a sizable formation barrier (464.4 kJ/mol through TS8) in our calculations, suggest a possibility of an alternate route for its formation, perhaps, via the decomposition of DKP.[211]

5.4 Potential Energy Surface for the Bimolecular Decomposition of Leucine

N-isoamylidene-isoamylamine (P9) embodies one of the major experimental products either sourced from the bimolecular reactions between primary amine and aldimines or resultant from the decomposition of 2,5-DKP.[211] In the condensed-phase pyrolysis, the bimolecular reactions tend to govern the decomposition process in preference to unimolecular corridors that generally occur in the gas phase. In a previous study, we explained the importance of bimolecular reactions for expounding the experimentally observed products of the pyrolysis of acetamide.[221-222] Therefore, we put forward a mechanism to elucidate the biomolecular condensation pathways for the formation of P9. Three plausible channels serve this purpose. Two of them represent the self-condensation reactions of leucine featuring dehydration and deamination mechanisms. The third pathway signifies the reaction of P1 with a molecule of the parent leucine. **Figure 5-6** illustrates the optimised geometries of resultant compounds, [A], [B] and [C], for the reaction corridors postulated in **Figure 5-7**. **Figure 5-8** maps the PES of the biomolecular channels, and **Figure 5-9** presents the optimised structures of the transition states.

As displayed in **Figure 5-7a**, the hydroxyl group of one molecule of leucine abstracts an H atom from the hydroxyl group of the other to produce H_2O. An ether bridge forms between the two moieties, leading to the appearance of 2-amino-4-methylpentanoic anhydride [A]. This reaction passes through an activation barrier of 151.7 kJ/mol (TS23) and is associated with an endothermicity of 51.0 kJ/mol. The mechanism then proceeds by the dissociation of the ether linkage to produce the

radicals of 2-amino-4-methylpentanoyl (A1) and (2-amino-4-methylpentanoyl) oxidanyl (A2) that release CO and CO_2, respectively, to generate 1-amino-3-methylbutyl (A3) along both corridors. The formation of A3 from A1 occurs via an enthalpic barrier of 14.0 kJ/mol (TS24), while A2 liberates a CO_2 molecule without encountering a saddle point on the PES. The former reaction is endothermic by 8.0 kJ/mol, whereas the latter displays a considerable exothermicity of -117.6 kJ/mol. Further along the reaction corridor, A3 undergoes an intermolecular transfer of H atom from the NH_2 group to the α-carbon generating (3-methylbutyl) amino radical (A4) via an enthalpic barrier of 177.2 kJ/mol (TS25). Finally, the A3 and A4 radicals combine to form 3-methyl-N-(3-methylbutyl) butane-1,1-diamine (A5) through barrierless route. Deamination of A5 produces P9 via TS26 with an activation barrier of 225.8 kJ/mol. This reaction is endothermic by 41.1 kJ/mol.

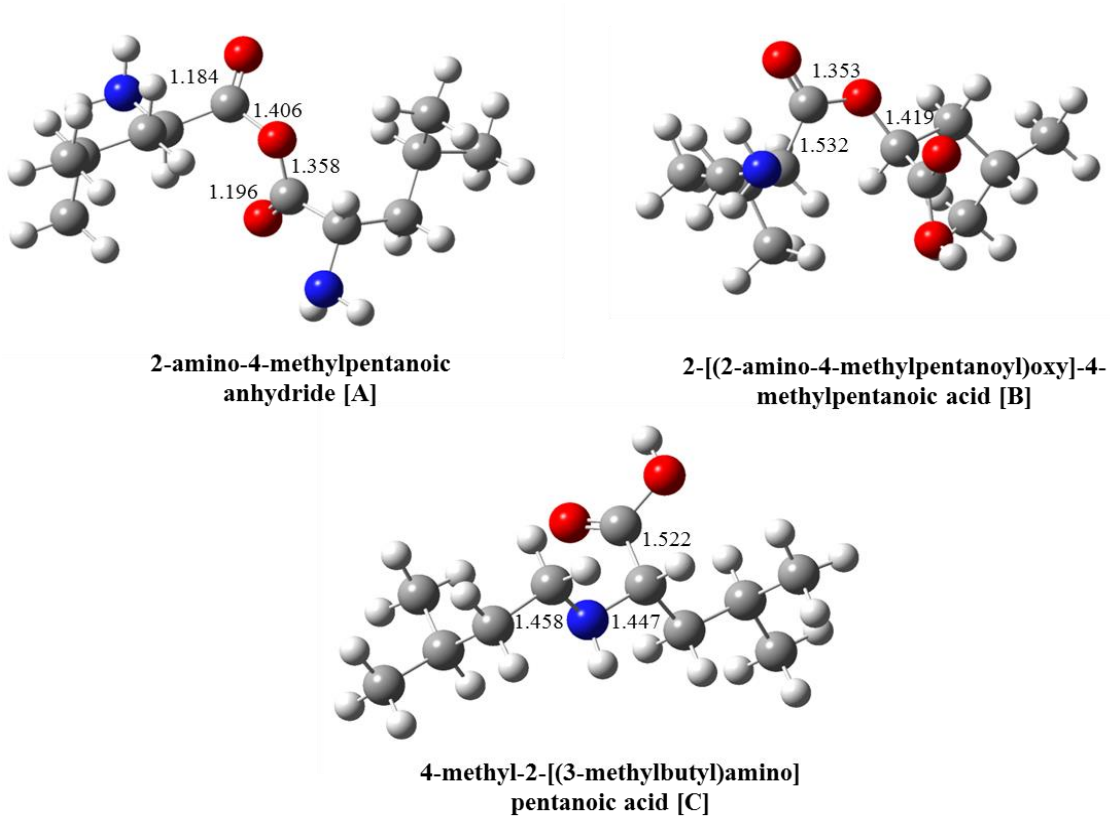

Figure 5-6: Optimised geometries of structures involved in the bimolecular decomposition of leucine. Interatomic distances are in Å.

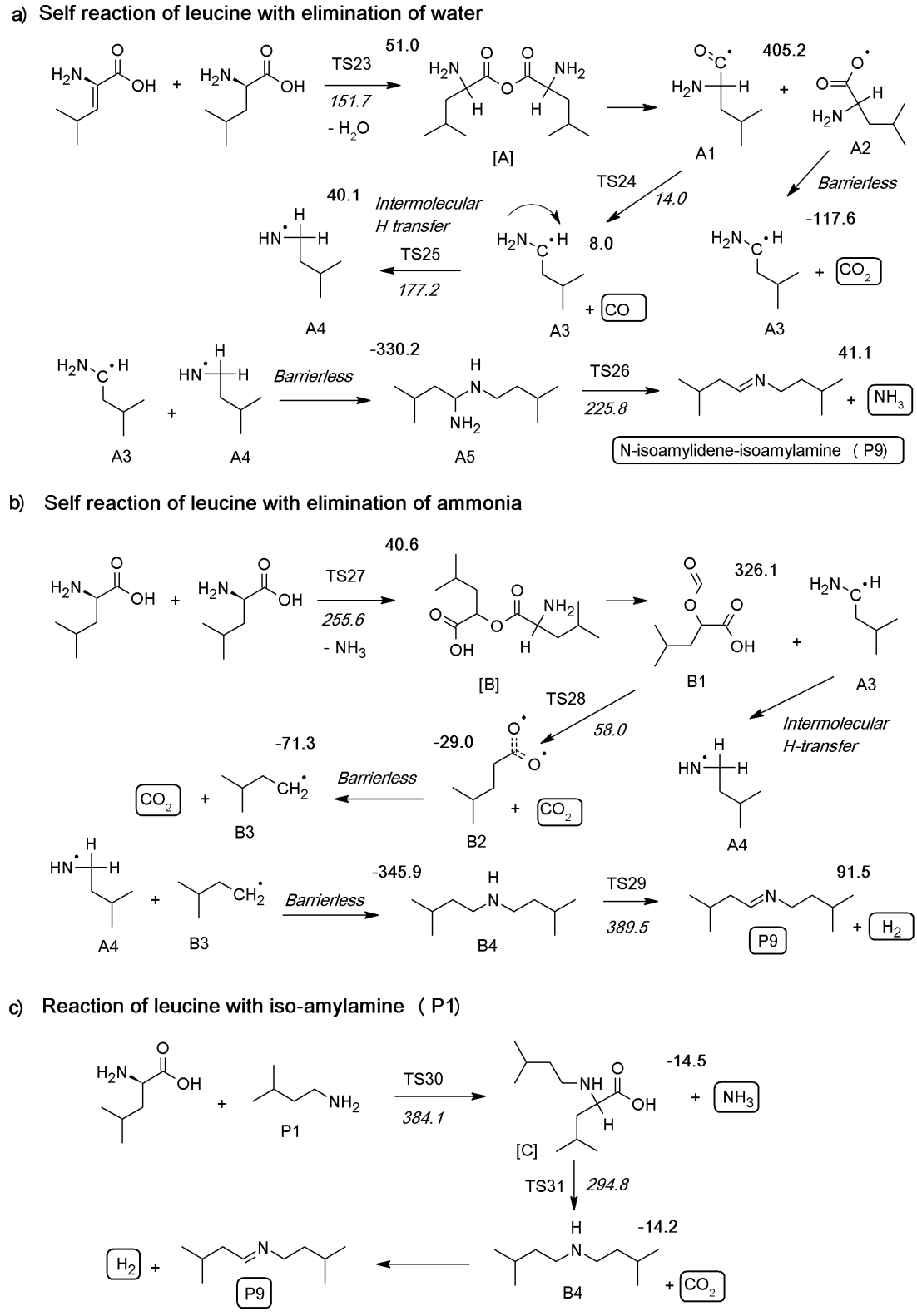

Figure 5-7: Self-reactions of leucine with (a) direct elimination of water, (b) direct elimination of ammonia, (c) reaction of leucine with P1. Values in bold are reaction enthalpies and values in italic stand for activation enthalpies. All values (in kJ/mol) are calculated at 298.15 K. Boxes enclose the products detected experimentally.

Figure 5-7b illuminates the second pathway for the formation of P9 in the self-condensation and deamination reaction of leucine. In more detail, this mechanism initiates by the elimination of an amino group from one leucine molecule and an H atom, from the -OH group, on the other, leading to the formation of ether-linked compound [B] (2-[(2-amino-4-methylpentanoyl) oxy]-4-methylpentanoic acid). This reaction exhibits the endothermicity of 40.6 kJ/mol and requires an activation enthalpy of 255.6 kJ/mol (TS27). The intermediates, 2-(formyl oxy)-4-methylpentanoic acid (B1) and 1-amino-3-methylbutyl (A3) result from ß-C-C scission of [B] with a sizable bond dissociation enthalpy of 326.1 kJ/mol. In the subsequent step, B1 undergoes a two-step decarboxylation reaction to generate 3-methylbutyl (B3). The first reaction is exothermic by -29.0 kJ/mol and passes through TS28 with an enthalpic barrier of 58.0 kJ/mol. The second reaction proceeds through a barrierless step with a noticeable reaction exothermicity of -71.3 kJ/mol. This mechanism concludes by a barrier-free and highly exothermic reaction (-345.9 kJ/mol) between A4 and B3 to generate 3-methyl-N-(3-methylbutyl) butan-1-amine (B4). Dehydrogenation of B4 produces P9 overcoming TS29 with an enthalpic barrier of 389.5 kJ/mol and endothermicity of 91.5 kJ/mol. The major products from this mechanism are NH_3, CO_2, H_2, and P9.

The third pathway to produce P9 constitutes a 3-step reaction of leucine with P1, as demonstrated in **Figure 5-7c**. Firstly, 4-methyl-2-[(3-methylbutyl) amino] pentanoic acid [C] arises from the reaction of R with P1 by passing through the activation barrier of 384.1 kJ/mol (TS30). The decarboxylation of the [C] moiety liberates CO_2 and B4. This reaction is exothermic by -14.2 kJ/mol and requires 294.8 kJ/mol (TS31) as an enthalpic barrier. Finally, P9 appears as a product of dehydrogenation of B4, as discussed in the preceding paragraph.

Figure 5-8 summarises the two most important self-condensation reactions of leucine. The most plausible channel for the formation of P9 is the self-condensation reaction of leucine with the elimination of water. Majority of bimolecular channels introduced in **Figure 5-7** require trivial barriers. Overall, the enthalpic barriers for bimolecular reactions fall below those of unimolecular reactions. Thus, it is anticipated that bimolecular reactions predominately occur in solid-state pyrolysis prior to evaporation of product species into the gas phase. Similar comportment

arises for the unimolecular and bimolecular decomposition reactions of acetamide[221-222], with the experimentally reported products from the decomposition of acetamide forming through complex bimolecular reactions rather than via unimolecular channels.

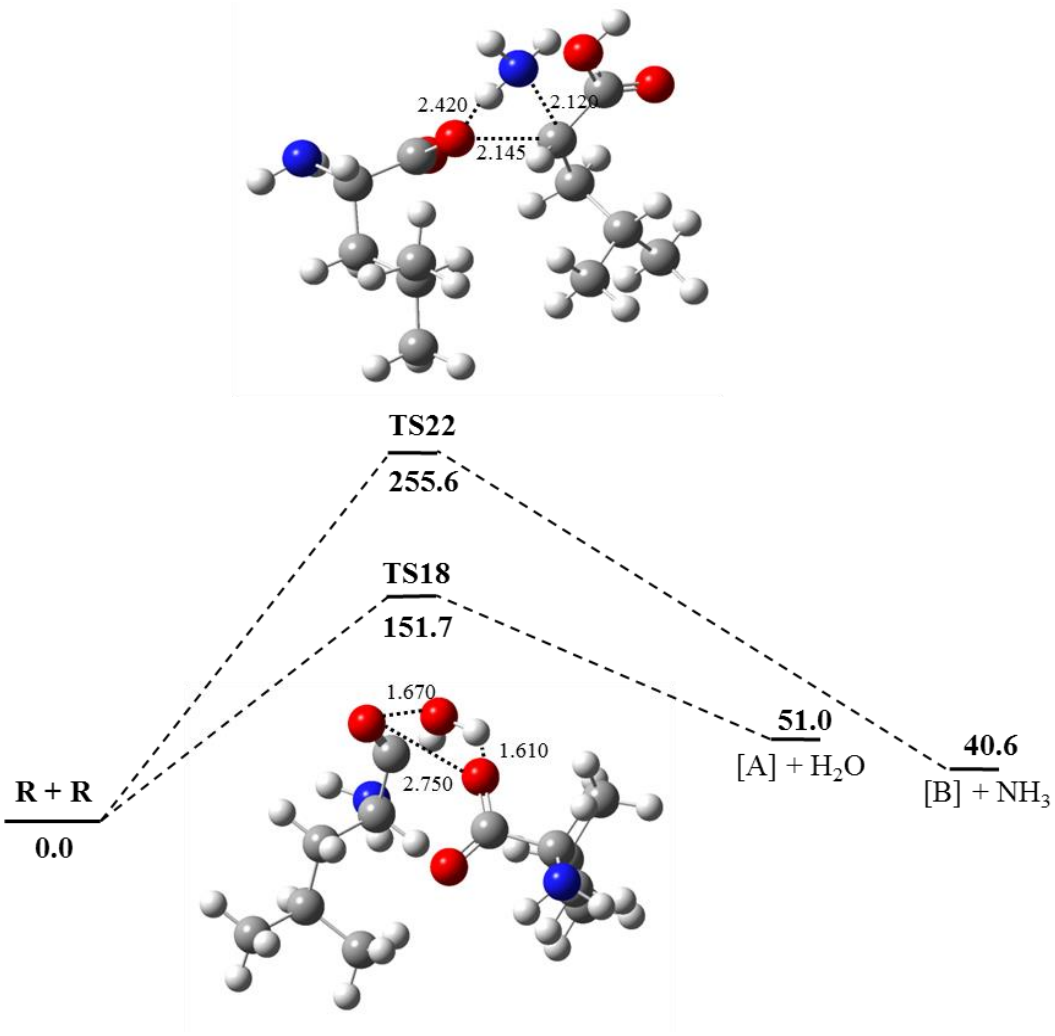

Figure 5- 8: PES for the bimolecular reactions, R + R → [A] + H2O and R + R → [B] + NH3 mapped out at CBS-QB3 theory. The activation and reaction energies are in kJ/mol and interatomic distances are in Å.

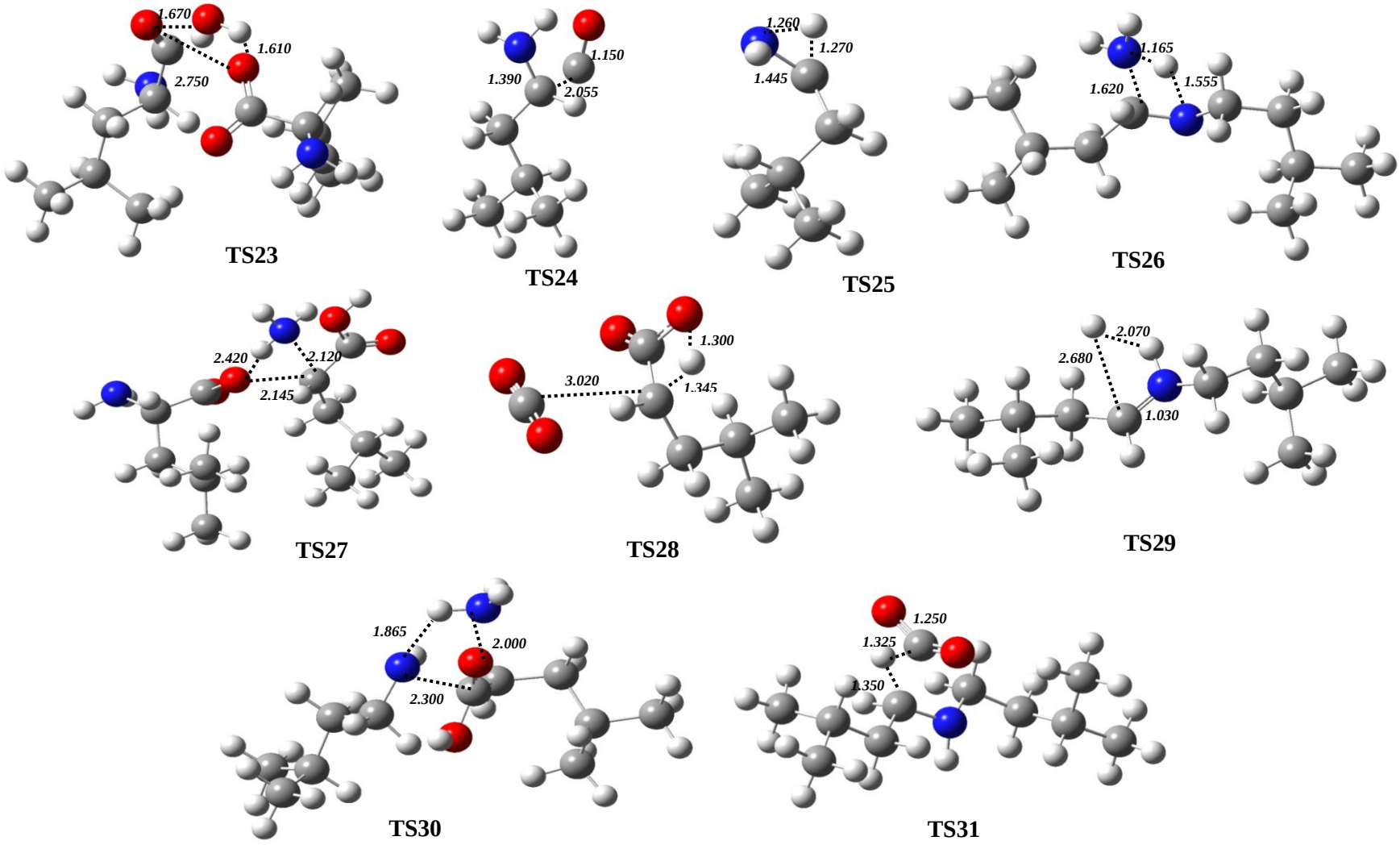

Figure 5-9: Optimised geometries for transition states involved in the bimolecular decomposition of Leucine molecule. Interatomic distances are in Å

5.5 Standard Enthalpies of Formation, Standard Entropies, and Heat Capacities

The standard enthalpy of formation ($\Delta_f H°_{298}$) of leucine is calculated using two isodesmic reactions R1 and R2:

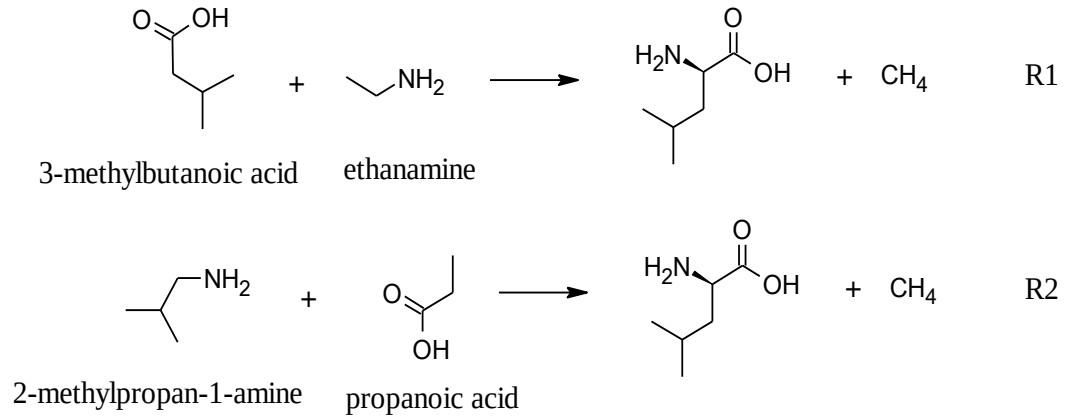

Scheme 2: Isodesmic reactions for leucine

Reaction R1 employs the experimental enthalpies of formation of methane (-74.85 ± 0.31 kJ/mol)[223], 2-methylbutane (-153.7 ± 0.59 kJ/mol)[224] and glycine (-393.7 ± 1.5 kJ/mol).[225] Reaction R2 applies the experimental enthalpies of formation of iso-butylamine (-98.62 ± 0.54 kJ/mol)[226] and propionic acid (-455.8 ± 2.0 kJ/mol).[227] The calculated reaction enthalpies at 298.15 K ($\Delta_r H°_{298}$) of Reactions R1 and R2, at the CBS-QB3 level, amount to 28.6 and -27.6 kJ/mol, respectively. The enthalpy of formation of leucine ($\Delta_f H°_{298}$) from Reaction R1 follows from the application of the Hess law as:

$$\Delta_f H°_{298\ \text{Leucine}} = \Delta_f H°_{298\ \text{2-methylbutane}} + \Delta_f H°_{298\ \text{glycine}} - \Delta_f H°_{298\ \text{methane}} - \Delta_r H°_{298}$$

The calculated $\Delta_f H°_{298}$ of leucine (x_j) from Reactions R1 and R2 correspond to -501.17 ± 1.64 and -507.14 ± 2.10 kJ/mol, respectively. The uncertainty limit (u_j) of each isodesmic reaction is estimated as $(\Sigma u_i^2)^{1/2}$, where u_i represents uncertainty linked to experimental heat of formation of the participating species in reactions R1 and R2. The overall uncertainty ($\bar{u}$) is obtained from $1/[\Sigma(1/u_j^2)]^{1/2,}$ and grand mean enthalpy ($\bar{x}$) is calculated as $\Sigma(x_j/u_j^2)/\Sigma(1/u_j^2)$ based on the approach of Simmie et al.[228] The overall enthalpy of formation of leucine stands at -503.44 kJ/mol with

uncertainty value of 1.30 kJ/mol (i.e. -503.44 ± 1.30 kJ/mol). This value concurs very well with the analogous experimental enthalpy of formation of leucine i.e. –497.6 ± 3.0.[225] **Table I** of Appendix assembles the values of $\Delta_f H°_{298}$ for leucine and reference compounds.

We calculate the standard enthalpy of formation ($\Delta_f H°_{298}$) of all products and intermediates based on the reaction enthalpies depicted in **Figures 5-2** and **Figure 5-7**, the computed $\Delta_f H°_{298}$ of leucine, and the experimental values of $\Delta_f H°_{298}$ of H atom (218.00 kJ/mol), CO_2 (-393.51 kJ/mol), NH_3 (-45.90 kJ/mol), H_2 (0.0 kJ/mol), HCN (135.14 kJ/mol), CH_3CN (74.04 kJ/mol), NH_2 (190.37 kJ/mol), CO (-110.53 kJ/mol), OH (39.00 kJ/mol), H_2O (-241.83 kJ/mol) and HNCO (-101.67 kJ/mol), as given in the NIST thermochemical data.[229] **Table 5-1** enlists the calculated $\Delta_f H°_{298}$ of all products and intermediates. To the best of our knowledge, $\Delta_f H°_{298}$ values of the product and intermediate species are not available in the literature. **Table 5-1** also assembles the standard entropies at 298.15 K ($S°_{298}$) and the heat capacities ($C_p°$ (T)) at specified temperatures for all the products and intermediates. These thermochemical parameters stem from the calculations based on the $\Delta_f H°_{298}$, vibrational frequencies, and rotational constants of the optimised geometries of the relevant species.

Table 5-1: Thermochemical Parameters, $\Delta_f H°_{298}$ Values (in kJ/mol), values of $S°_{298}$ and $C_p°$ *(T)* (in J/mol·K), and Temperature in K

	$\Delta_f H°_{298}$	$S°_{298}$	$C_p°$ *(T)*					
			300	500	800	1000	1200	1500
Leucine	-507.21	444.82	166.18	253.31	342.16	381.52	410.95	442.25
M3	-358.70	426.26	148.13	222.73	297.77	330.87	355.56	381.76
M4	-77.60	433.28	155.10	230.76	309.82	345.40	372.12	400.54
M6	-402.15	445.92	170.63	251.20	332.00	367.77	394.60	423.30
I1	34.81	390.60	129.73	197.50	269.44	302.33	327.28	354.10
I2	-300.57	414.78	137.54	208.70	281.50	313.56	337.28	362.18
I3	-100.92	425.60	150.50	221.40	295.33	328.70	353.77	380.45
I4	-79.70	415.20	143.00	219.00	295.73	329.62	354.83	381.46
I5	-281.35	430.70	152.10	235.70	321.70	360.00	388.70	419.26
I6	-92.20	465.88	160.50	243.90	328.51	363.55	388.44	413.75
I7	72.56	450.60	153.67	226.80	302.64	335.90	360.35	385.90
P1	-130.87	390.23	128.12	200.40	279.34	315.60	343.10	372.40
P2	-39.15	350.56	102.23	159.03	220.00	247.97	269.12	291.72
P3	-43.55	380.28	117.47	182.36	252.67	284.65	308.67	334.20
P4	-20.70	369.22	110.61	165.90	225.36	252.57	273.10	294.84
P5	-242.74	379.55	114.60	174.58	240.00	269.80	292.10	315.60
P6	-415.36	414.75	140.66	211.20	282.25	313.50	336.72	361.32
P7	-15.40	401.70	131.00	199.10	272.18	305.52	330.54	357.06
P8	-174.20	359.70	110.12	174.00	245.44	278.63	303.76	330.58
P9	-130.86	558.87	230.11	356.90	493.31	554.53	600.16	648.35
A	-721.60	693.10	329.54	492.85	659.73	733.10	787.54	845.20
A1	-82.40	446.18	162.05	237.46	315.51	350.13	375.95	403.35
A2	-234.00	476.25	175.74	255.78	337.48	373.16	399.56	427.44
A3	36.11	402.66	137.10	205.04	275.81	307.57	331.50	357.12
A4	76.20	404.46	133.71	201.87	274.81	307.53	332.00	357.96
A5	-217.83	581.04	258.20	402.70	555.10	623.31	674.42	728.80
B	-927.90	668.82	322.25	483.11	646.46	717.77	770.55	826.24
B1	-637.95	503.30	193.10	278.44	363.67	400.14	426.73	454.44
B2	-273.50	441.78	152.32	227.26	303.15	336.12	360.37	385.77
B3	48.72	379.30	121.31	180.22	243.00	271.47	292.94	315.85
B4	-220.97	555.67	237.16	372.95	519.41	585.30	634.53	686.70
C	-606.71	605.70	277.57	427.24	582.77	651.50	702.54	756.46

5.6 Reaction Rate Constants

To simulate the real pyrolysis conditions, we compute the reaction rate constants at a pressure of 101.3 kPa and fitted over a temperature range of 400 – 2000 K, for all channels encompassed in the unimolecular and bimolecular decomposition of leucine. **Table 5-2** records the reaction rate constants in terms of their Arrhenius parameters.

The leucine molecule branches into three competing channels via unimolecular reactions, namely leucine → P1 + CO_2, leucine → P6 + NH_3 and leucine → I4 + H_2O. **Figure 5-10** informs that the dehydration of leucine into I4 and H_2O and its decarboxylation into P1 and CO_2 assume very comparable importance across the considered temperature window. Deamination, to yield P6 and NH_3, is negligible at all temperatures. The Rice-Ramsperger-Kassel-Marcus (RRKM) kinetic analysis of the exit channels of I5 (P7 + H_2O and P8 + HNCO), displayed in **Figure 5-11a**, demonstrates the fate of I5 during pyrolysis. It indicates that I5 decomposes to yield P7 and H_2O over the entire temperature window. The rate of formation of P8 + HNCO seems negligible at all temperatures, and it accounts for only 0.1 % concentration of P8 in pyrolysate at 873 K.[210] Considering the branching of P3 into (P4 + H_2) and (C_2H_5N + C_3H_6) depicted in **Figure 5-11b**, it is evident that the disintegration of P3 leading to P4 and H_2 governs the decomposition process at all temperatures, however, with a noticeable contribution from the competing channel that forms C_2H_5N and C_3H_6, especially at temperatures lower than1000 K. This trend concurs with the detection of P4 among the major experimental products.[219]

By analysing the Arrhenius rate parameters for the self-condensation reactions shown in **Figure 5-7**, we observe that the value of E_a/R for the self-condensation/dehydration channel falls below the corridors of the self-condensation/de-amination and the reaction of leucine with P1. This means that bimolecular reactions favour the generation of [A] over [B] and [C], leading to the formation of P9. In summary, the experimental studies reveal P1, P4, P9, CO_2, NH_3, and H_2O as the major products.[23,24] The next section introduces the kinetic model that describes product profiles in the thermal decomposition of leucine and, through a sensitivity analysis, identifies the most critical reactions.

Table 5-2: Arrhenius rate parameters for the unimolecular and bimolecular decomposition of leucine in the temperature range of 300 – 2000 K. The pre-exponential constants, *A*, are expressed in 1/s or cm^3/ (molecule·s), depending on the reaction order, with E_a/R in K.

No.	Reactions	*A*	E_a/R
1	M6 → I1 + CO_2	4.17×10^{11}	22 650
2	R → P1 + CO_2	1.80×10^{16}	32 500
3	P1 → P2 + NH_3	4.18×10^{13}	31 100
4	P1 → P3 + H_2	5.10×10^{13}	46 200
5	P3 → C_2H_5N + C_3H_6	5.44×10^{12}	41 500
6	P3 → P4 + H_2	1.21×10^{18}	42 850
7	P4 → C_4H_8 + HCN	5.70×10^{15}	44 500
8	P4 → C_3H_6 + CH_3CN	1.20×10^{14}	55 600
9	I2 → P5 + CO	6.94×10^{13}	13 700
10	R → P6 + NH_3	5.80×10^{13}	30 250
11	P6 → P2 + CO_2	9.70×10^{13}	29 600
12	I3 → I4	2.35×10^{12}	34 300
13	I4 → P3 + CO	4.70×10^{13}	16 300
14	R → I4 + H_2O	1.97×10^{16}	32 500
15	I4 + H_2 → I5	8.20×10^{11}	30 000
16	I5 → P7 + H_2O	1.10×10^{14}	26 600
17	I5 → P8 + HNCO	2.10×10^{14}	36 000
18	I4 + R → I6 + M6	5.77×10^{8}	13 250
19	I6 → C_5H_{11} + HNCO	1.20×10^{14}	5 900
20	C_5H_{11} → P2 + H	3.02×10^{13}	16 250
21	I4 → I7	9.67×10^{12}	20 400
22	I7 + H → P7 + OH	2.62×10^{11}	12 250
23	R + R → A + H_2O	9.76×10^{09}	19 200
24	A1 → A3 + CO	2.30×10^{14}	1 200
25	A3 → A4	1.37×10^{13}	19 500
26	A5 → P9 + NH_3	4.10×10^{13}	25 000
27	R + R → B + H_2O	5.78×10^{09}	31 450
28	B1 → B2 + CO_2	2.70×10^{15}	4 500
29	B4 → P9 + H_2	2.30×10^{14}	44 500
30	R + P1 → C + NH_3	4.05×10^{10}	46 500
31	C → B4 + CO_2	9.20×10^{13}	32 750

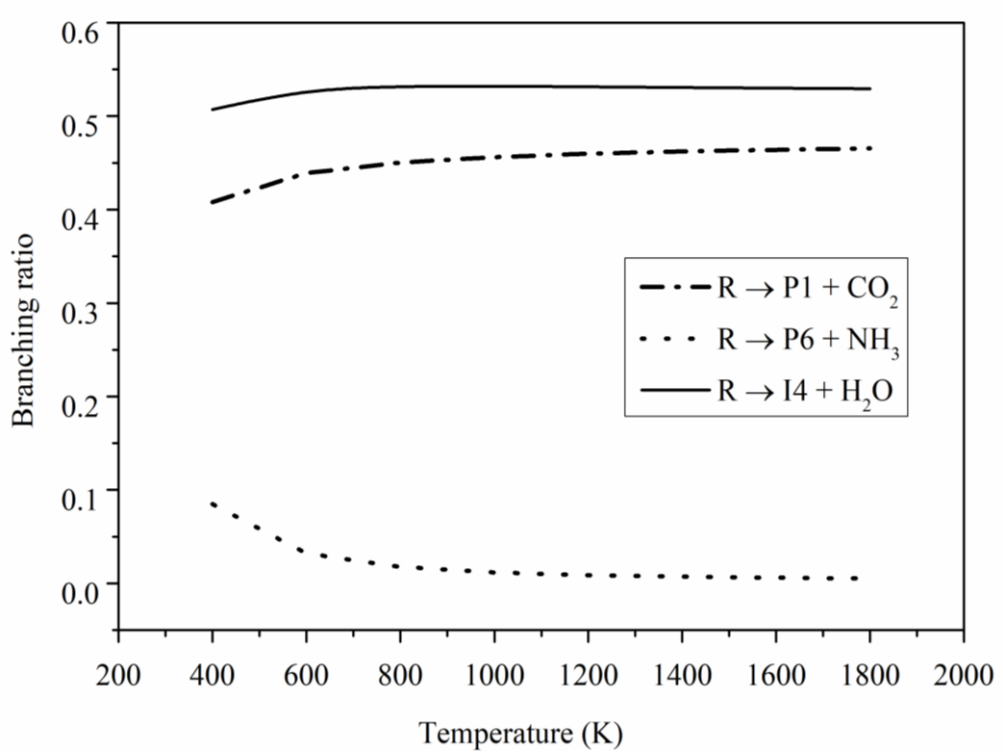

Figure 5-10: Branching ratios for the reactions (R → P1 + CO_2, R → P6 + NH_3 and R → I4 + H_2O) as a function of temperature in the range of 400 – 2000 K

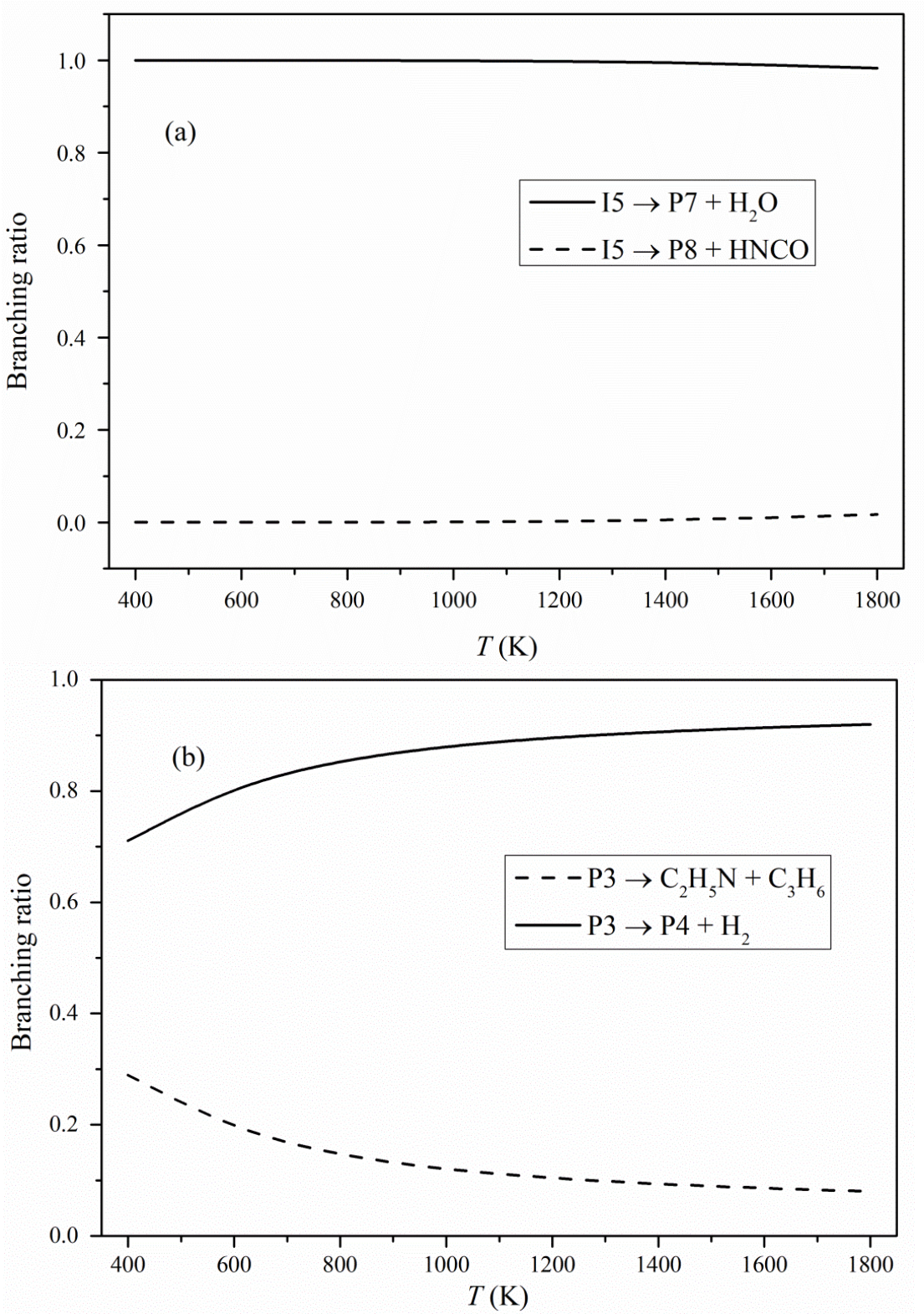

Figure 5-11: Branching ratios as a function of temperature in the range of 400 – 2000 K for the reactions a) (I5 → P7 + H_2O, I8 → P8 + HNCO) and b) (P3 → C_2H_5N + C_3H_6, P3 → P4 + H_2).

5.7 Kinetic Modeling

We constructed a kinetic model that consists of a network of 44 reactions and 49 species, and their calculated NASA polynomials (quoted in Appendix, Section 2). The model applies to the pyrolysis of leucine in the gas phase and can only yield qualitative insights into the fragmentation of leucine in the condensed phase. For this reason, a direct comparison between experimental (condensed phase) and modelling (gas phase) results is impossible. **Figure 5-12** plots the distribution of the major products and the fate of the N-containing species, as predicted from the kinetic model.

For 1000 ppm of leucine in a plug-flow reactor with a residence time at 10.0 s, the model predicts the reaction-initiation temperature of 700 K with 100 % decomposition achieved at 950 K. **Figure 5-13** shows two pathways for the formation of P3 that operate in our system. The dehydration route through intermediate I4 dominates the consumption of leucine, followed by its decarboxylation into P1. The onset temperature for the decomposition of P3 and P6 amounts to ≈ 900 K. Species P1 first accumulates and then dissociates at 950 K. The accumulation of P4 that occurs at temperatures higher than 950 K, concurs with a significant content (13.4%) of P4 in pyrolysate gases obtained from the solid-phase pyrolysis of leucine at 873 K.[23] Our model predicts negligible concentrations of P2 and P5 – P9, in accordance with the experimental findings of Simmonds et al. [210]

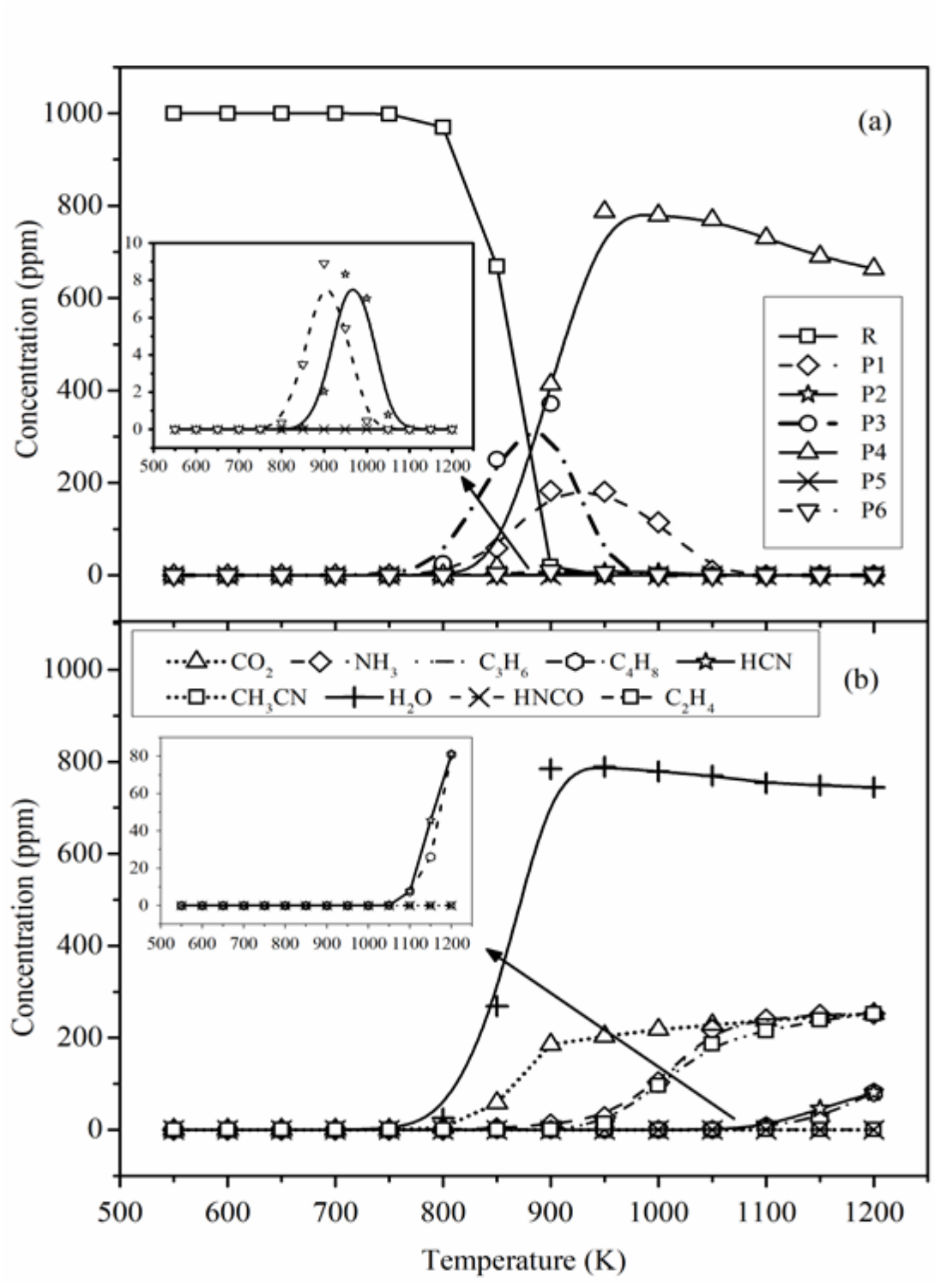

Figure 5-12: Kinetic model predictions for (a) major hydrocarbons, P1 – P6 (b) Light gases from thermal decomposition of leucine in the gas phase

Dissociation of leucine and the transition species produces H_2O, CO_2, NH_3, C_3H_6 and C_2H_4 in the temperature range 750 – 1200 K. Among N-containing species, the yield of NH_3 exceeds significantly that of HCN. This is primarily due to the direct

formation of ammonia from the initial decomposition of leucine at 800 K whereas formation of HCN originates from the secondary reaction of P4 at 1050 K. Ren et al.[96] observed similar patterns in the formation of NH_3 and HCN from the solid-phase pyrolysis of leucine at 1073 K, in a fixed bed tubular reactor. Conversely, Hansson et al.[219] found that 58 % of the nitrogen contents of leucine that pyrolysed at 973 K in a fluidised-bed reactor converted into HCN as compared to NH_3. We suggest that contradictions in experimental evidence regarding the yields of NH_3 and HCN stem from the fundamental differences in reactor configurations used in these two studies.[96, 219] A fluidised bed reactor promotes a better mixing of reactants, which may lead to self-condensation reactions of leucine to produce DKP, and hence HCN formation as discussed in Section 5.3. Our reactor model resembles the experimental setup of Ren et al.[96] and the present predictions show good agreement with the experimental measurements. The appearance of minor species of HNCO and CH_3CN, in model predictions, is probably because of the prevailing unimolecular pathways as opposed to the self-condensation channels of leucine that dominate the pyrolysis of the condensed phase. This is evident from the species profiles of complexes [A], [B] and [C] shown in **Figure 5-14**. The product [A] of self-condensation/dehydration path represents only a minor contribution to the overall reaction network. As P9 stems from [A], this accounts for negligible concentration of P9 in the predictions of our kinetic model.

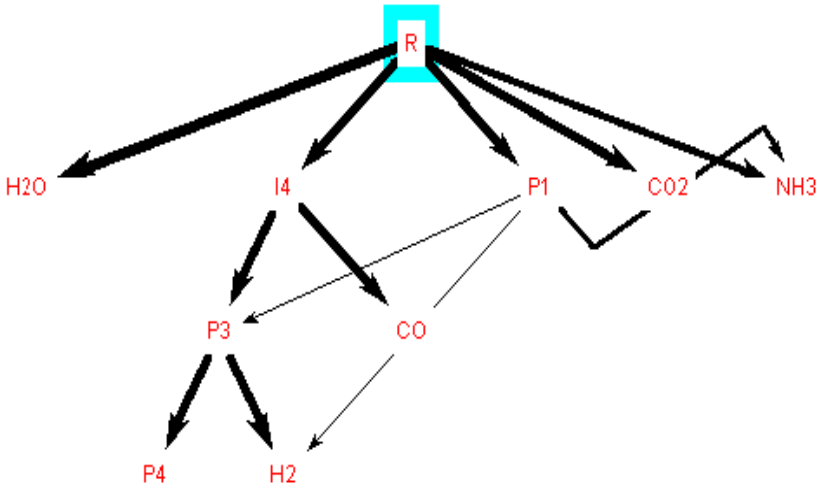

Figure 5-13: Important reaction pathways encountered in thermal decomposition of leucine determined by ChemKin Modelling

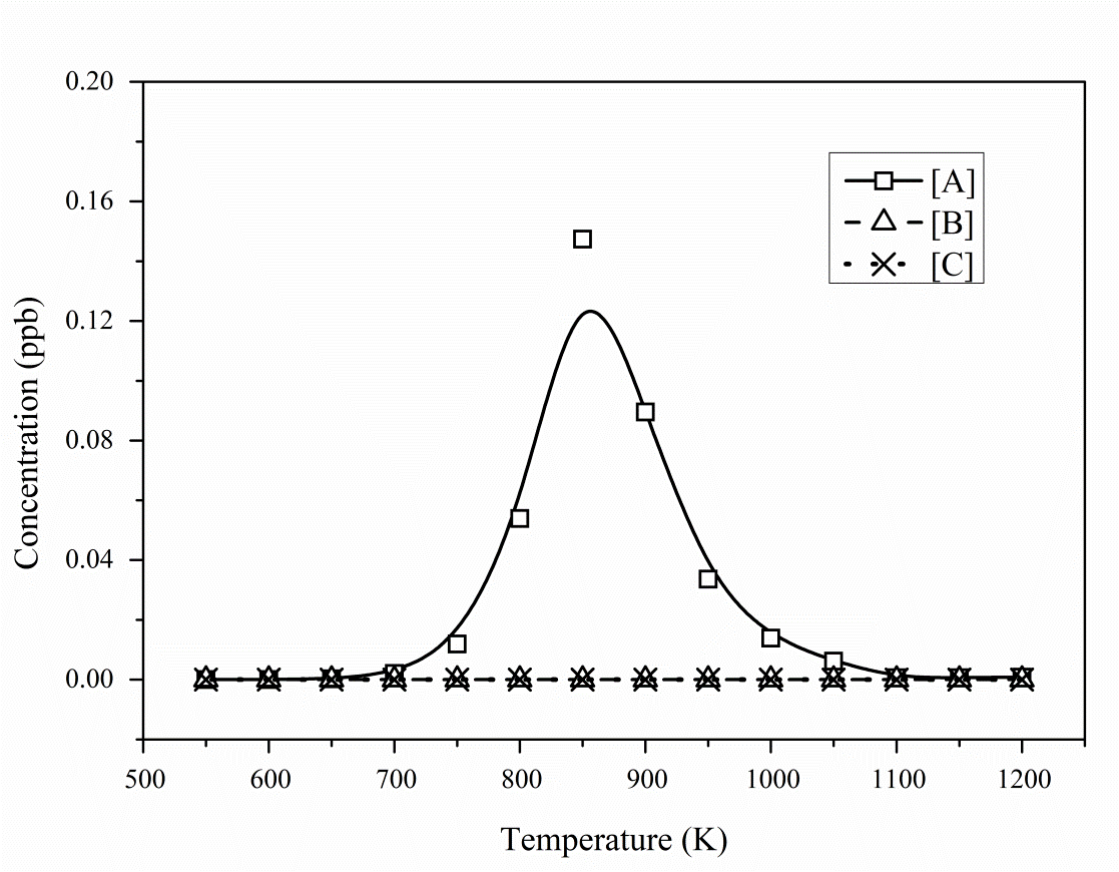

Figure 5- 14: Fate of biomolecular channels predicted by ChemKin modelling

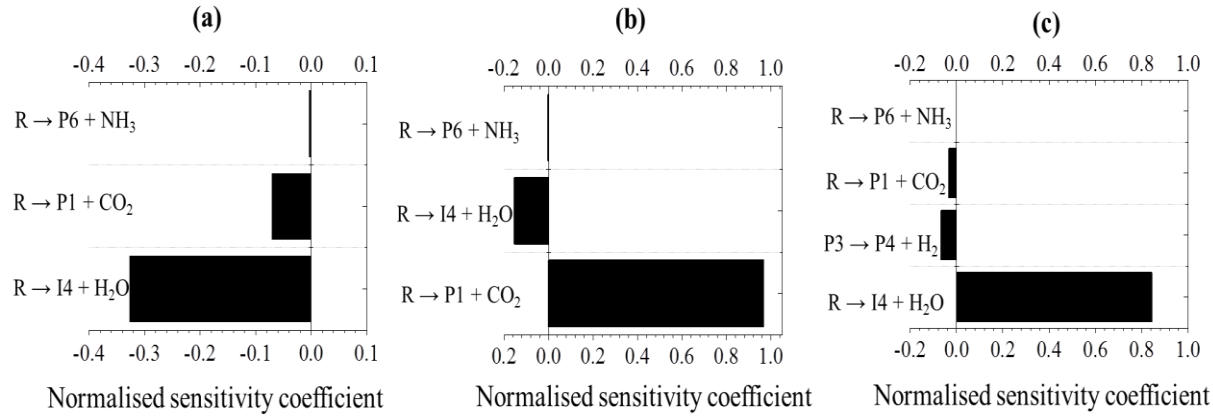

Figure 5-15: Normalised sensitivity coefficients for consumption of (a) leucine and products (b) P1 and (c) P3 at 850 K. The sensitivity coefficients follow from d([R])/d(A_i), where [R] represents mole fraction of leucine and A_i, the pre-exponential factor for the reaction *i*.

The normalised sensitivity coefficients calculated at the peak reaction temperature of 850 K for the consumption of R, P1, and P3 is illustrated in **Figure 5-15**. The sensitivity coefficients serve as a measure of the relative influence of reaction *i* on the overall consumption of leucine. The reaction R → I4 + H_2O displays sensitivity to the consumption of R and P3, while R → P6 + NH_3 represents the least responsive step.

We would like to stress that our plug flow reactor model presents profiles of gas-phase species, while experimental studies of the thermal decomposition of leucine focused on the solid phase. From this perspective, it suggests that, in the condensed phase, leucine undergoes self-condensation reactions, resulting in higher concentrations of diketopeprazine, P9, HNCO, CH_3CN, CH_4, and other dipeptides. Experimental studies on the gas phase decomposition of leucine and other protein model compounds could pinpoint salient mechanistic differences to those prevailing in the condensed media reported in the literature.

5.8 Conclusions

This Chapter presents the optimised geometries, Arrhenius rate parameters, and thermochemical properties for all intermediates, products, and transition states in the unimolecular and bimolecular reactions that operate during the pyrolysis of leucine. As a benchmark of accuracy, our calculated enthalpy of formation of leucine varies by only 1.2 % from its experimental value. Our computed reaction rate constants indicate comparable branching ratios for decarboxylation and dehydration channels with a minimal contribution from the deamination route. The calculated kinetic parameters serve to construct a plug-flow reactor model that demonstrates species profiles obtained from the thermal decomposition of leucine in the gas phase. The conversion of leucine attains 100 % in the temperature range 700 – 950 K. Our kinetics model predicts the formation of isoamylamine (P1), 3-methyl butane-1-imine (P3), 3-methylbutane nitrile (P4), CO_2, NH_3, H_2O, C_3H_6 and C_2H_4 as major products. Kinetic analysis of the plausible channels concludes that the dehydration constitutes the dominant pathway and self-condensation reactions contribute marginally to pyrolysis of leucine in the gas phase.

CHAPTER 6

Effects of Product Recovery Methods on the Yields and Properties of Hydrochars from Hydrothermal Carbonisation of Algal Biomass

6.1 Introduction

Following HTC, the hydrochar particles that retain the majority of lipids[40, 79, 81] are suspended in the mixture of biocrude and aqueous phase. In literature, there are mainly two methods used to recover hydrochar from the reaction products. One is to separate hydrochar directly from the aqueous phase by vacuum filtration, followed by water washing and subsequent drying.[27-28, 32, 83] Some other researchers modified this method by omitting water washing.[15, 29, 38, 55, 85] The other method involves dilution of sticky product mixture with an organic solvent such as dichloromethane (DCM), filtration of the diluted mixture to recover hydrochar, and subsequent phase separation to quantify the aqueous phase and biocrude.[15, 39, 43, 82]

The use of these different product recovery methods makes a comparison of the yields and properties of algal hydrochar from different studies difficult. Indeed, as shown in **Figure 6-1a**, under similar reaction severity, the yields of hydrochars collected with solvent washing/dilution are generally lower than those of hydrochars from direct filtration (i.e., without solvent washing/dilution). In particular, for the HTC of two *Chlorella* species (with comparable elemental composition, as shown in **Table 2-1**) under similar reaction severity, recovering hydrochar with solvent washing/dilution results in 65% of reduction in its yields, as compared to that from

direct filtration.[39, 55] The enhanced hydrochar yields from direct filtration are also accompanied by the increases in the contents of carbon in hydrochars and their higher heating values (HHVs), as illustrated in **Figures 6-1 (b & c)**.

Contradictory findings on the concentrations of key metallic species in hydrochars as a function of HTC temperature have also been reported in previous studies that employed different product recovery methods. For example, the concentration of sodium (Na) reduces from 0.10 to 0.05 wt %, db and that of potassium (K) from 0.16 to 0.07 wt %, db with an increase of HTC temperature from 200 to 250 °C, for the hydrochars obtained by direct filtration.[55] Oppositely, the solvent-aided recovery method leads to the increases in concentrations of Na (from 0.36 to 0.53 wt %, db) and K (from 0.02 to 0.17 wt %, db) in the hydrochars when the HTC temperatures increase from 170 to 250 °C.[39]

Although a literature survey suggests that hydrochar recovery methods significantly affect the yields and properties of algal hydrochar, their exact effects under various HTC conditions and the underlying mechanisms remain unclear due to the lack of studies that employ identical parent algal biomass and HTC conditions but different product recovery methods. Therefore, this chapter systematically investigates the impacts of product recovery methods i.e. direct filtration versus DCM-aided filtration (detailed in the **Figure 3-3)** on the yield and properties of hydrochars produced from HTC of *Chlorella* in a batch reactor (Section 3.2.2) under identical reaction conditions (solid loading: 10.0 wt %; temperature: 180 – 220 ºC; and holding time: 15 min and 60 min).

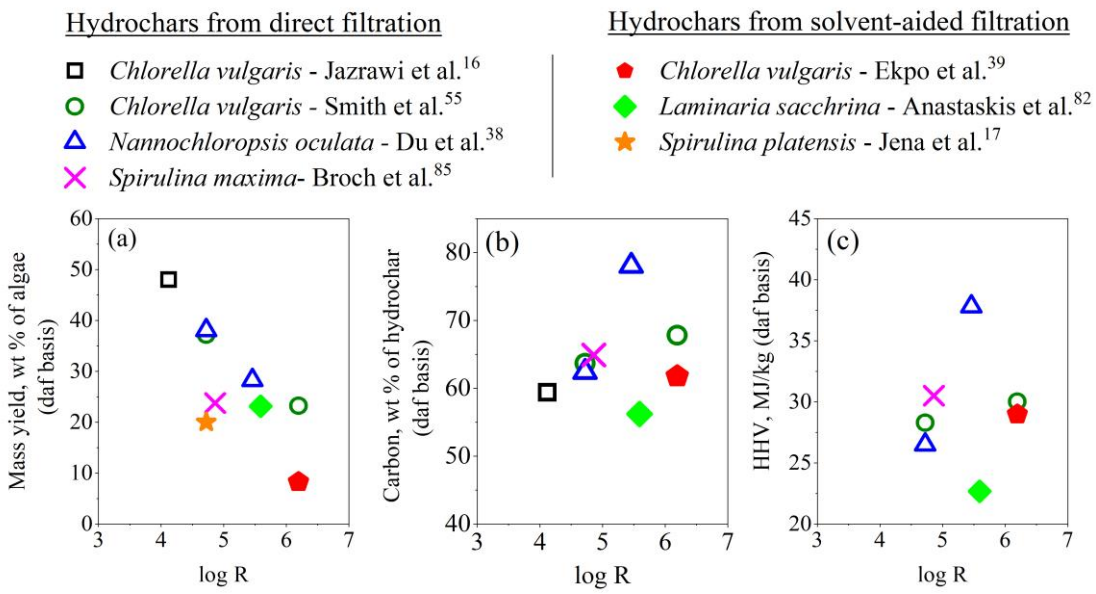

Figure 6-1: (a) Mass yield, (b) carbon content, and (c) HHV of hydrochars obtained by different recovery methods in the literature, plotted on dry and ash-free basis, as a function of Reaction Severity calculated as R = $\int_0^t e^{(T(t)\,°C - 100\,°C)/14.75\,°C}\,dt$; where '*T*' and '*t*' stands for reaction temperature and holding time, respectively.

6.2 Effect of Recovery Methods on Hydrochar Yields

Figure 6-2 presents the yields of hydrochar from HTC of *Chlorella* at 180 – 220 °C with holding times of 15 and 60 min, as recovered by direct filtration and DCM-aided filtration (Numeric form of the data is shown in Table II of the Appendix). With an increase of reaction temperature from 180 to 220 °C, hydrochar yield decreases by 30.6 % (from 60.1 to 41.6 wt %) and 55.2 % (from 54.4 to 24.4 wt %) for direct filtration and DCM-aided filtration, respectively, at the holding time of 15 min. Similar trends are observed at the holding time of 60 min. At identical reaction temperatures, holding for a longer time (from 15 to 60 min) also leads to reductions in hydrochar yield by 21.0, 25.2 and 34.5 %, for 180, 200, and 220 °C, respectively, recovered by DCM-aided filtration. Hydrochar recovery by direct filtration also results in similar reductions of mass yield with an increase in holding time. The reductions in hydrochar yields with the increase of reaction temperature and holding time are due to enhanced hydrolysis of algal macromolecules (carbohydrates, proteins, and lipids) to sugars, amino acids, and free fatty acids as the reaction

intermediate .[8-9, 50] Under the identical HTC conditions, direct filtration always gives higher hydrochar yield than DCM-aided filtration, the extent of which is intensified at a higher HTC temperature and longer holding time. For example, at 180 ºC and 15 min (**Figure 6-2a**), hydrochar yield from direct filtration is 10.4% higher than that from DCM-aided filtration. The differences are further increased to 26.2 and 70.9% with the elevation of temperature to 200 and 220 ºC, respectively. Similar discrepancies are also observed for the holding time of 60 min.

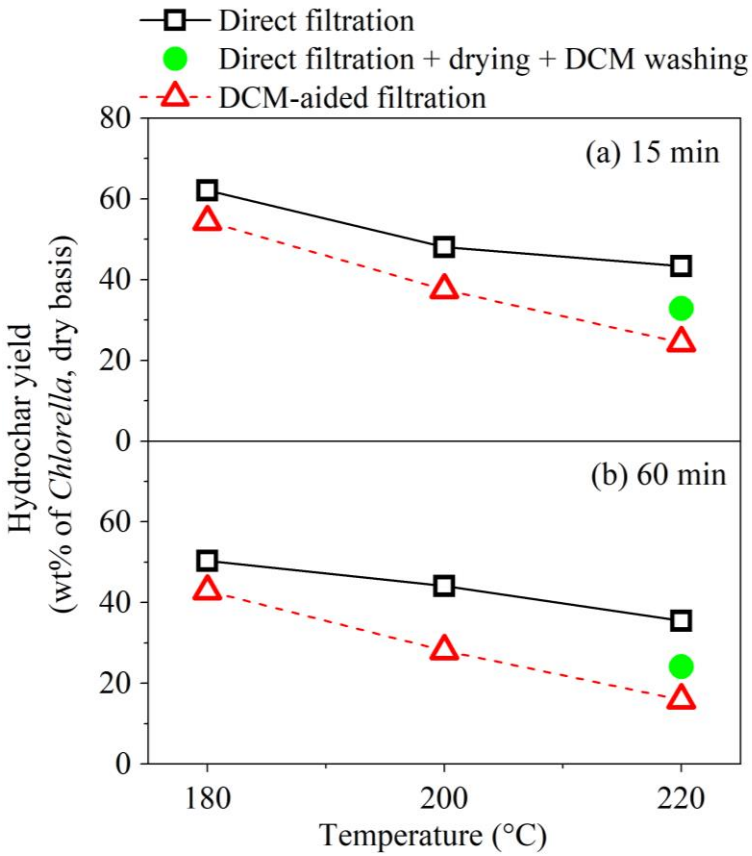

Figure 6-2: Mass yields of hydrochar from HTC of *Chlorella* at 180 – 220 °C with a holding time of (a) 15 and (b) 60 min, as collected from direct filtration, DCM-aided filtration and direct filtration + drying + DCM washing.

To understand the effects of product recovery methods on hydrochar yields, two efforts were made. In the first effort, we washed the pre-dried hydrochars collected from direct filtration with DCM to quantify the portion that is extractable by the solvent. Briefly, the dried hydrochar (~ 2 g) was dissolved in 20 mL of DCM and continuously stirred for 20 min, followed by the vacuum filtration. Excess DCM was used for the repeated washing of the hydrochar residue collected on the filter

paper after which the solid cake was dried at 65 °C for 24 hr. This method is termed as 'Direct filtration + drying + DCM washing', and the recovered biocrude is hereafter named as 'residual biocrude', which constitutes up to 24.2 % and 32.1 % of the total mass of hydrochar obtained by direct filtration at 220 ºC for 15 and 60 min, respectively. The hydrochar yield after direct filtration + drying + DCM washing was lowered to 32.9 wt % at 15 min and to 24.1 wt % at 60 min, based on the dry mass of *Chlorella*, for the reaction temperature of 220 ºC as presented (by green circles) in **Figure 6-2 (a & b)**. Additionally, the hydrochar yields for direct filtration + drying + DCM washing are still higher than that of DCM-aided filtration because of the incomplete removal of the biocrude by subsequent DCM washing of the pre-dried hydrochars.

Second is morphology observation of hydrochars produced at 220 ºC, under which the differences in the hydrochar yields from the two methods are the most significant. These images are shown in **Figure 6-3**. At 220 ºC for 15 min (**Figure 6-3a**), hydrochar recovered by direct filtration gives a smooth appearance due to the biocrude layer adsorbed on its surface. With the increase in residence time to 60 min (**Figure 6-3b**), the abundance of spherical deposits on the hydrochar surface is due to the enhanced condensation and polymerisation of organic compounds that were originally dissolved in the aqueous phase. Such spherical deposits are agglomerated with the hydrochar particles due to the sticky nature of the biocrude[230], and their linkages with the hydrochar surface cannot be eliminated during direct filtration of the product mixture. Contrarily, when DCM-aided filtration is applied, the adsorption of spherical deposits (or residual biocrude) on the hydrochar surface is effectively minimized due to the dissolution of biocrude with DCM as shown in **Figure 6-3 (c & d)**. Also, the hydrochars appear more fibrous due to the removal of the biocrude layer. Hence, the presence of biocrude or secondary char on the hydrochar (primary char) surface during direct filtration is the key reason for higher mass yields obtained. Further, the SEM analysis of the hydrochars from direct filtration + drying + DCM washing at 220 °C for 15 and 60 min is shown in **Figure 6-3e** & **6-3f** respectively. Apparently, the biocrude blocking the hydrochar pores is removed from the surface after DCM washing but the spherical deposits embedded inside the pores are retained by the hydrochar. These spherical deposits were

solidified and agglomerated with the hydrochar structure upon initial drying and became only partially solubilized in the solvent on subsequent DCM washing.

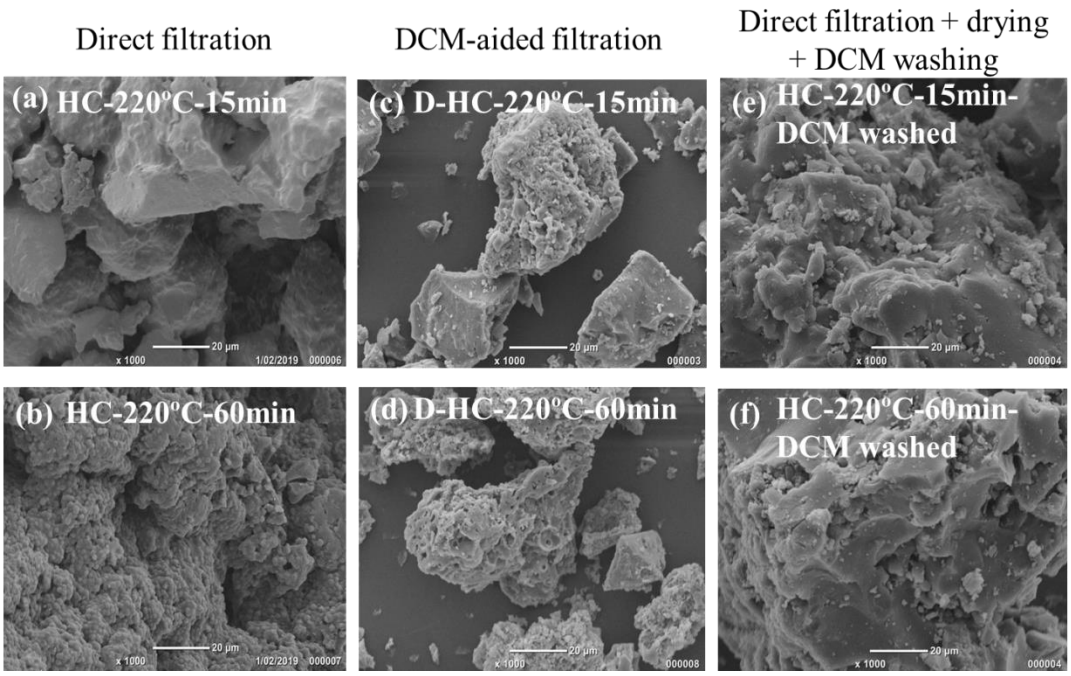

Figure 6-3. SEM analysis of the hydrochars at 220 º for 15 and 60 min from direct filtration (a & b), DCM-aided filtration (c & d) and direct filtration + drying + DCM washing (e & f)

Furthermore, the GPC analysis of the residual biocrude was compared with the biocrude recovered by DCM-aided filtration (referred to as 'bulk biocrude') at 220 °C for 15 and 60 min as depicted in **Figure 6-4**, which shows that the patterns of the molecular weight distribution for both bulk biocrude and residual biocrude are similar. However, the distribution of the heavier compounds in residual biocrude is shifted to a larger size as compared to that of the bulk biocrude, indicating that the heavy portion of biocrude produced during HTC is adsorbed on the hydrochar surface during direct filtration.

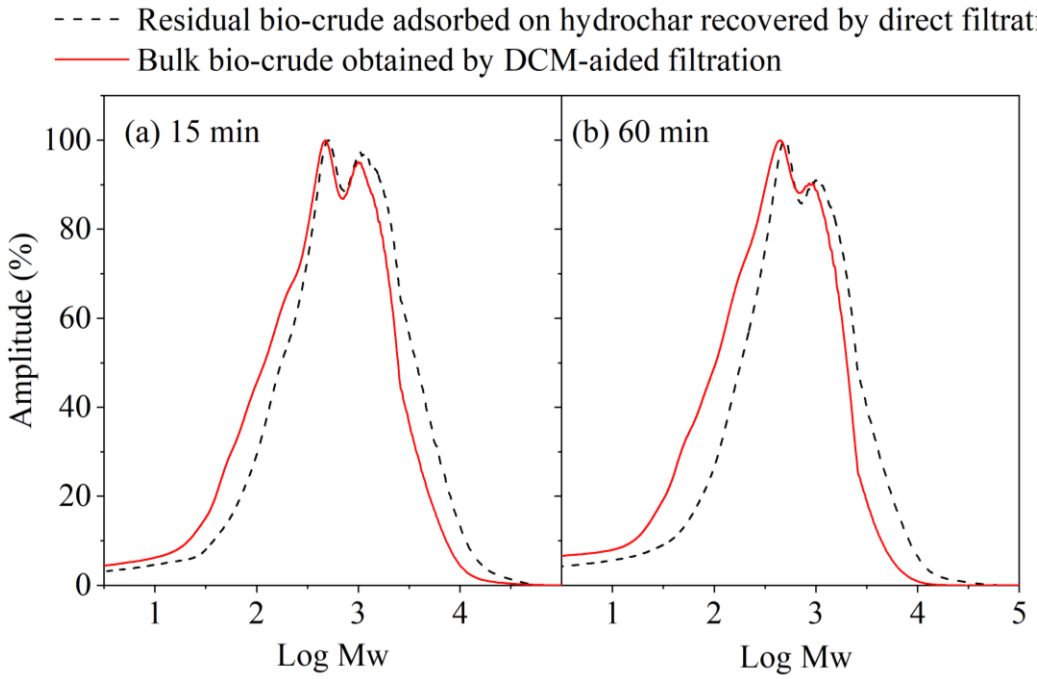

Figure 6-4: GPC analysis of residual biocrude obtained by direct filtration + drying + DCM washing compared with the bulk biocrude by DCM-aided filtration at 220 ºC for holding time of (a) 15 min and (b) 60 min

In summary, heavy biocrude formed during HTC is adsorbed on the hydrochar surface during direct filtration, which is further solidified and agglomerated with the hydrochar particles upon drying at 65 °C. The heavy biocrude cannot be completely removed by solvent washing of the pre-dried hydrochar and it is practically difficult to separate heavy biocrude from the solvent-soluble fraction of directly filtered hydrochar. Following this, the higher hydrochar yields from direct filtration are completely understood. However, the adsorption of heavy biocrude on the hydrochar surface during direct filtration may cause considerable differences in the hydrochar properties, as compared to those from DCM-aided filtration, which will be discussed in the following section.

6.3 Effects of Recovery Methods on Hydrochar Properties

6.3.1 Proximate Analysis

Table 6-1 illustrates the proximate analysis of hydrochars obtained from the two product recovery methods. It is evident that the volatile matter of the hydrochars

gradually reduces by 4.2 % (from 81.5 to 78.1 wt %) at 15 min and by 6.4 % (from 81.4 to 76.2 wt %) at 60 min with an increase in temperature from 180 to 220 °C for direct filtration. A similar trend is observed for DCM-aided filtration. At a fixed temperature, the increase of holding time also leads to a lower VM for both recovery methods. The reduction in VM with increasing reaction severity led to more carbonized hydrochar as indicated by the increase of fixed carbon. The product recovery method greatly affects the VM and FC of the derived hydrochars as demonstrated by the higher VM and lower FC for direct filtration of the reaction products as compared to that of DCM-aided filtration. This is attributed to the presence of biocrude on the hydrochar surface (from direct filtration), which quickly devolatilizes during the thermal analysis.[230] Alternatively, the hydrochars separated via DCM-aided filtration possesses higher FC or reduced VM/FC ratio, which is an important parameter to determine the soil stability and combustion characteristics of hydrochars. Such as the hydrochar produced at 220 °C and 60 min by DCM-aided filtration has the lowest VM/FC ratio i.e. 3.04 close that of Victorian brown coal[231] and Collie coal[232] and can be efficiently utilized for co-firing with aforementioned coals.[233] The lower VM/FC ratio of the hydrochar also relates to the higher proportion of stable carbon and hence greater stability in soil applications.[234]

Hydrochars are generally low in ash content as compared to that of raw algae (5.3 wt %, db) because of the solubilisation of the inorganics into the aqueous phase. This is consistent with the ash contents of raw algae and derived hydrochars for the case of *Laminaria Hyperborea*[55], *Nannochloropsis oculata*[38], *Spirulina maxima*[85], *Sargassum horneri*[84] and *Chlorella vulgaris*[15]. Ash content of hydrochar gradually increases with an increase in reaction temperature from 180 to 220 °C and this effect is magnified at a longer holding time of 60 min. For example, the ash content of hydrochars at 220 °C and 60 min are 3.7 wt %, db for direct filtration and 11.6 wt %, db for DCM-aided filtration. These findings are consistent with the drastically higher ash content (i.e. 50.3 wt %, db) of hydrochar obtained by DCM dilution[39] as compared to that of (i.e. 8.4 wt % db) direct filtration of reaction mixture[55] from HTC of *Chlorella* at the similar reaction conditions. Moreover, the retention of ash in the hydrochar obtained by two methods is plotted in **Figure 6-5 (a-b)**, which shows that direct filtration retains more inorganics in the hydrochar at 15 min, however the difference of ash retention between the recovery methods gradually

reduces with increase of temperature. As the holding time is increased, there is an abrupt rise in ash retention (i.e. 17.5 % at 200 to 34.0 % at 220 °C) for DCM-aided filtration. Such a drastic elevation in ash content and inorganic retention of DCM washed hydrochar as compared to that of unwashed hydrochar with increase of reaction temperature and holding time is explained below.

Firstly, the dilution of hydrochars by an adsorbed layer of heavy biocrude might be considered as one reason for lower ash content by direct filtration. To explain this, we evaluated the ash contents of hydrochars obtained by direct filtration + drying + DCM washing at 220 °C for 15 and 60 min, which comes out to be 3.6 and 3.9 wt % on a dry basis, respectively. These values were slightly higher than the ash content of raw hydrochars (i.e. 2.9 and 3.7 wt %, db) from direct filtration showing the dilution effect of heavy biocrude, the removal of which has lowered the hydrochar mass resulting in a higher yield of inorganic matter. Besides, the reasonably high ash content (i.e. 4.4 and 11.6 wt. % at 220 °C for 15 and 60 min respectively) of the counterpart hydrochars clearly shows that the dilution effect is not the only phenomenon responsible for high retention of inorganics by DCM-aided filtration. Instead, the experimental procedures of the recovery methods bring the drastic change in ash retention at 220 °C and 60 min. Hydrochar particles recovered by direct filtration were lumped together because of adsorbing heavy biocrude on the surface (see **Figure 6-3**), which prevented the adsorption of inorganics from the aqueous phase into the hydrochar. But for DCM-aided filtration, the hydrochar particles were well suspended in solvent diluted reaction mixture reabsorbing inorganics from the aqueous phase, hence yielding higher inorganic matter. This effect is prominent at a higher temperature and longer holding time because of the highest yield of heavy oil (i.e. 32 %) obtained. Therefore, the product recovery methods could result in wide differences between the typical hydrochar properties, and thus should be considered when comparing hydrochar from different studies.

Table 6-1. Proximate analysis of hydrochars obtained by direct filtration and DCM-aided filtration at 180 – 220 °C for retention times of 15 and 60 min, and VM / FC ratios of hydrochars compared with that of coal

Temperature	Time	M[a]	Ash	VM[b]	FC[c]	VM/FC
°C	min	% ar[d]		% db[e]		
Direct filtration						
180		2.1	3.0	81.5	15.5	5.30
200	15	1.1	2.3	80.4	17.2	4.68
220		1.9	2.9	78.0	19.1	4.10
180		1.5	2.0	81.4	16.5	4.92
200	60	1.9	2.8	79.2	17.9	4.41
220		1.7	3.7	76.2	20.1	3.78
DCM-aided filtration						
180		0.9	2.5	79.4	18.4	4.40
200	15	0.9	2.3	78.0	19.6	3.95
220		0.5	4.4	73.5	22.1	3.33
180		1.8	2.2	78.9	18.8	4.20
200	60	0.6	3.3	75.2	21.5	3.50
220		1.3	11.6	66.5	21.9	3.04
Victorian brown coal[231]		-	0.9	49.7	49.4	1.02
Collie coal[232]		-	5.6	37.8	56.6	0.67

[a] Moisture, [b] Volatile matter, [c] Fixed carbon, [d] as-received, and [e] dry basis

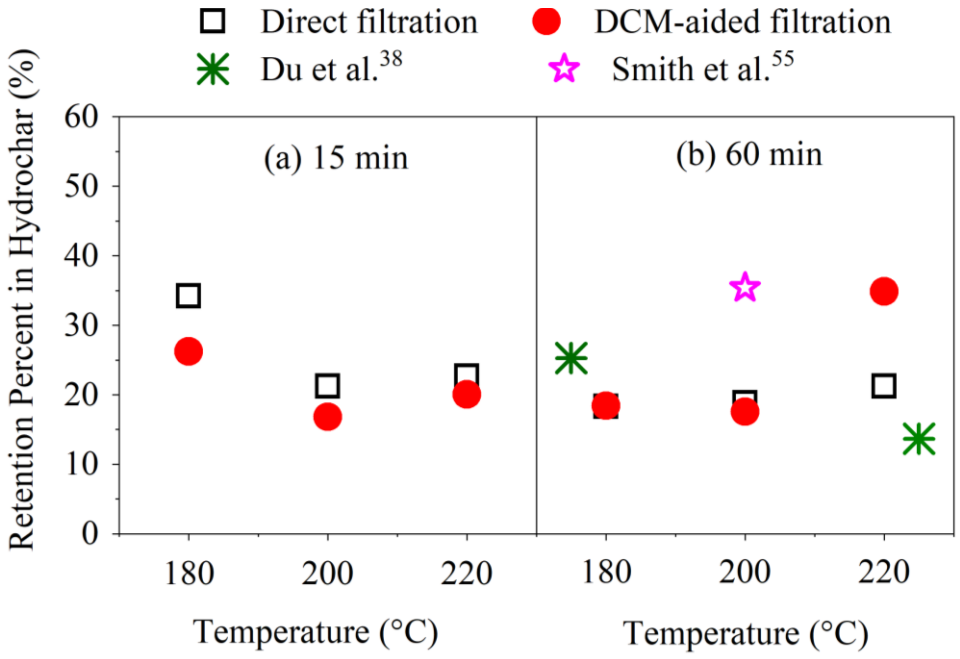

Figure 6-5: Ash retention in hydrochars obtained by direct filtration and DCM-aided filtration at 180 – 220 °C for retention times of (a) 15 min and (b) 60 min

6.3.2 Ultimate Analysis and Higher Heating Values

Figure 6-6 shows the effect of product recovery methods on the ultimate analysis of the hydrochars at 180 – 220 °C for holding time of 15 and 60 min. The numeric form of the data is presented in Table II of the Appendix. HTC treatment results in carbon enrichment of the hydrochars i.e. 58.9 – 73.4 % for direct filtration and 60.5 – 67.3 % for DCM-aided filtration, as compared to that of 52.1 % for raw *Chlorella* (all on the dry and ash-free basis). Carbon concentrations increase with increasing reaction severity because of both the greater decomposition of carbohydrates and the adsorption of heterocyclic Maillard reaction products on the hydrochar surface.[27] The oxygen levels of hydrochars are generally reduced with an increase in temperature and holding time because of dehydration and decarboxylation reactions responsible for removing oxygen mainly in the form of CO_2, CO and H_2O.[32, 39] Nitrogen concentrations in unwashed hydrochars (direct filtration) decrease linearly from 12.1 to 8.2 % at 15 min and from 12.7 to 7.7 % at 60 min, with an increase in temperature from 180 to 220 °C. Nitrogen decrease with an increase in reaction

severity due to the rapid hydrolysis of proteins and amino acids in acidic conditions of HTC that arises by decomposition of carbohydrates.[15, 107]

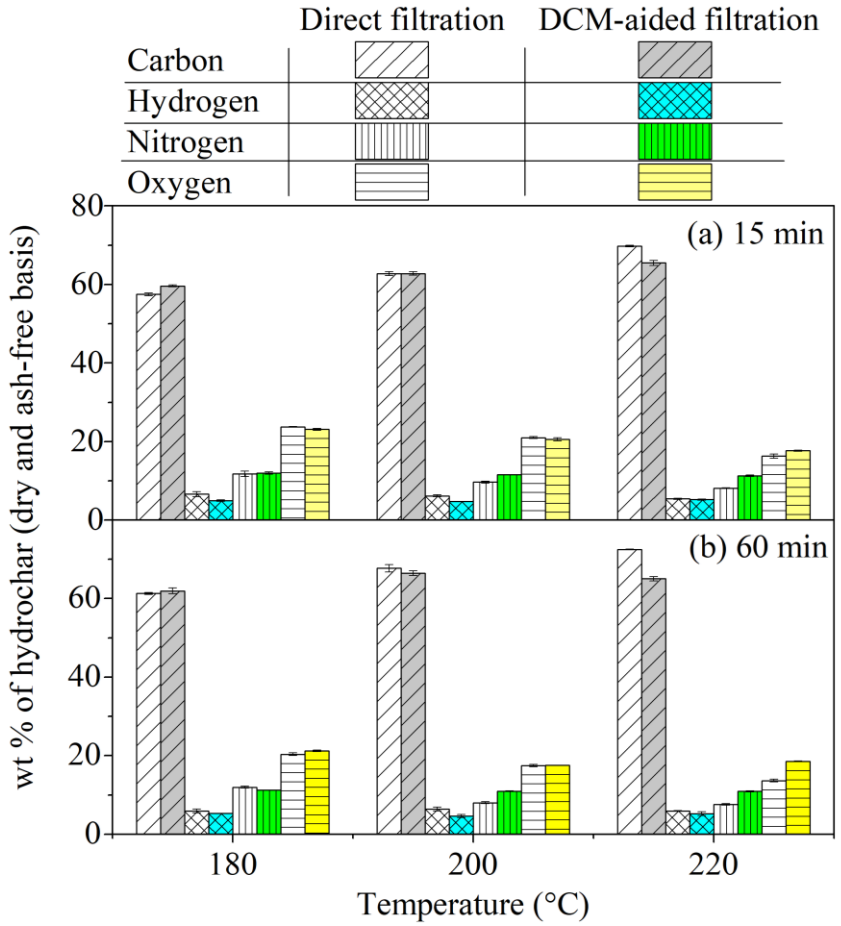

Figure 6-6: Ultimate analysis hydrochars obtained by direct filtration compared with DCM-aided filtration at 180 – 220 °C for retention times of 15 and 60 min

Considering the effect of the product recovery methods on the elemental composition of hydrochars, undiluted hydrochars (direct filtration) retain more C and H as compared to DCM diluted hydrochars, with a pronounced effect observed with an increase of reaction temperature and holding time. For example, carbon and hydrogen content of hydrochar at 220 ºC and 60 min by direct filtration is 72.5 and 6.0 %, respectively, which is reasonably higher than that of 65.0 and 5.2 % of C and H, respectively, for counterpart hydrochars. This is because of the high carbon and hydrogen contents of the residual biocrude that was adsorbed on the hydrochars recovered by direct filtration, as depicted in **Table 6-2**. The carbon content of the residual biocrude at 15 min (72.3 %) is slightly greater than that of 71.9 % at 60 min that is consistent with 73.2 and 70.6 % of carbon obtained in biocrudes after

hydrothermal processing for 5 and 60 min at 225 ºC.[43] The dilution of reaction media with DCM significantly impacts the nitrogen and oxygen concentrations of hydrochars predominantly at higher HTC temperature and holding time. For instance at 220 °C for 15 min, nitrogen and oxygen content is higher for DCM diluted hydrochars than the undiluted hydrochars (i.e. 11.3 % N & 17.6 % O for DCM-aided filtration versus 8.1% N & 16.3 % O for direct filtration). With the increase in holding time to 60 min, the nitrogen and oxygen concentrations for DCM-aided filtration are further increased by 30.2 % (from 7.6 to 10.9 %) and 26.2 % (from 13.6 to 18.5 %), respectively.

Table 6-2: Properties of residual biocrude adsorbed on hydrochars recovered by direct filtration at 220 °C for holding time of 15 and 60 min

Sample	C	H	N	O	S	Higher Heating Value
	wt. %, as-received basis					MJ/kg
*HBC-220-15	72.3	5.4	3.63	18.1	0.53	29.8
HBC-220-60	71.9	6.2	4.27	17.0	0.56	31.0

* Heavy biocrude-XXX-YY, where XXX is the temperature in 'ºC' and YY is the reaction time in 'min'.

In overall, the HTC derived hydrochars lies close to the Bituminous coal on Van-krevelen diagram presented in **Figure 6-7**. An increase in reaction temperature and holding time reduces the H/C and O/C atomic ratios of hydrochars representing the loss of oxygenated compounds predominately by dehydration. This results in the gain of hydrophobicity, which is a favourable characteristic during combustion.[102] Hydrochars recovered by DCM-aided filtration demonstrate comparatively low H/C atomic ratios, and hence better energy efficiency, and higher stability during carbon sequestration. Direct filtration displays slightly lower O/C atomic ratios, which are favoured for soil applications of hydrochars. In general, algal hydrochars display lower H/C and O/C atomic ratios in comparison with those derived from *Municipal solid waste*[230] and *Willow*[55] under similar experimental conditions.

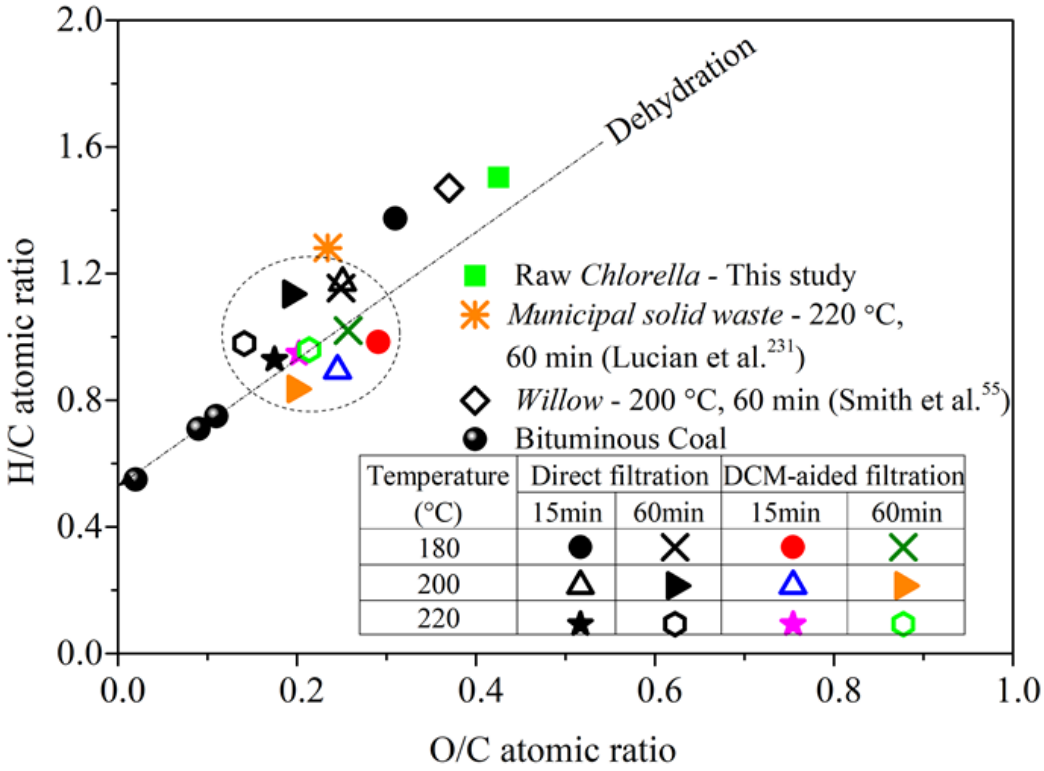

Figure 6-7: Van-Krevelen diagram for hydrochars from direct filtration and DCM-aided filtration at 180 – 220 °C for 15 and 60 min of holding time

The product recovery method not only affected the mass yield but also the energy yield of the hydrochars as shown in **Figure 6-8**. The energy yield is calculated by mass yield × (HHV of hydrochar/ HHV of raw *Chlorella*), all on a dry basis. At 15 min, HHVs of hydrochar increased from 26.5 to 30.5 MJ/kg for direct filtration and from 25.6 to 27.6 MJ/kg for DCM-aided filtration with the rise of temperature because of higher contents of carbon attained. A similar trend is obtained at 60 min, except for lowering of HHV value (27.8 to 24.9 MJ/kg) from 200 to 220 °C for DCM-aided filtration because of the high ash (11.6 wt %, db) and low carbon content (65.0 %, db) of the hydrochar. The energy yield decreased with an increase in reaction severity due to the reduction in mass yield. The highest energy yield of 70.1 % is obtained at 180 ºC and 15 min for direct filtration method, where analogous value for DCM-aided filtration recovery is 59.3 %. Moreover, the removal of the biocrude by DCM washing of pre-dried hydrochars (from direct filtration) led to a drop in HHV to 27.9 and 25.8 MJ/kg, and dip in energy yield to 38.4 and 26.5 % at 220 ºC for 15 and 60 min, respectively, as shown (by red

triangles) on **Figure 6-8**. Thus, heavy biocrude produced during HTC plays a vibrant role in advancing the fuel applications of hydrochar.

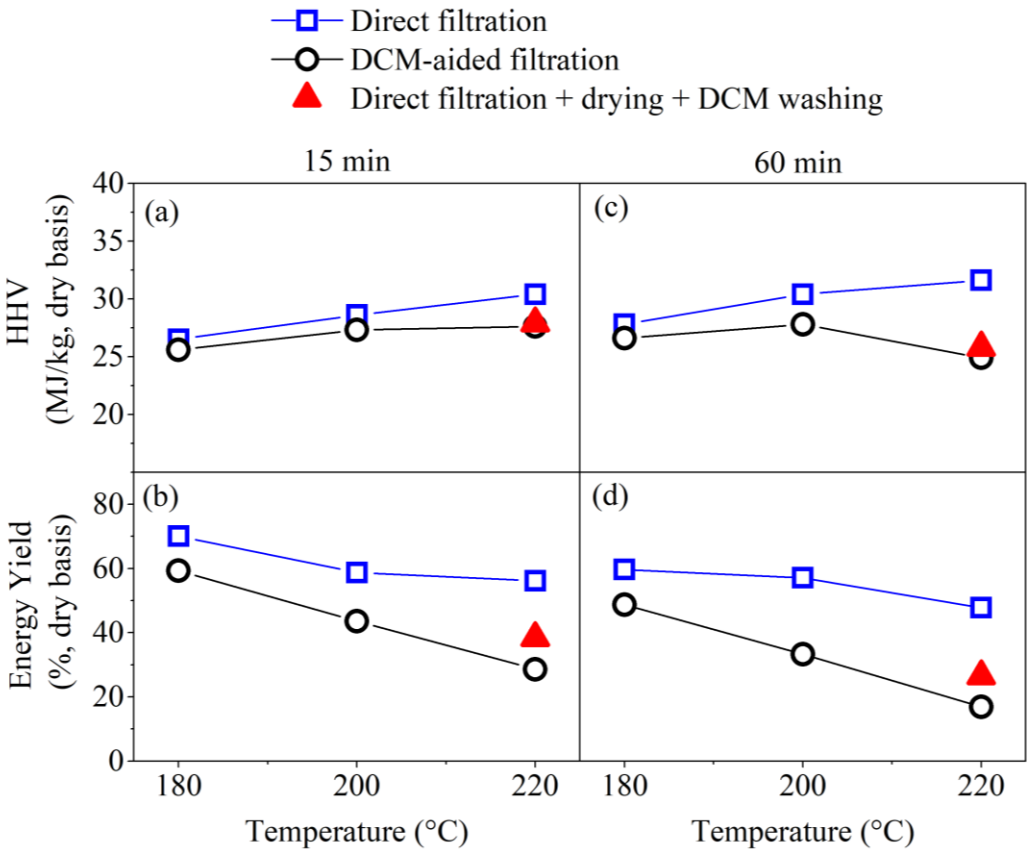

Figure 6-8: Effect of product recovery methods on HHV and Energy yield of hydrochars at 180 – 220 °C for holding time of 15 min (a & b) and 60 min (c & d). Red triangles depict the HHV and energy yield for the hydrochar obtained by direct filtration + drying + DCM washing.

6.3.3 Concentrations of Alkali and Alkaline Earth Metals and their Retentions in Hydrochars

To further explain the effect of product recovery methods on the extractions of alkali and alkaline earth metals in hydrochar, the concentration (wt %, db) of Na, K, Mg and Ca versus temperature are plotted at 15 and 60 min in **Figure 6-9**. With an increase in temperature, the concentration of K drops from 0.98 to 0.61 % at 15 min and from 0.65 to 0.22 % at 60 min for direct filtration, whereas an opposite trend is observed for DCM-aided filtration i.e. concentration of K rises from 0.34 to 0.45 % at 15 min and from 0.40 to 0.68 % at 60 min. A similar trend is observed for sodium

but with much smaller concentrations at all HTC conditions. Magnesium concentration slightly reduces from 0.20 (at 180 °C) to 0.15 % (at 200 °C) followed by a rise to 0.31 % at 220 °C for 15 min, while with the increase in holding time, a continuous increase in the concentration of Mg from 0.15 to 0.47 % with temperature is observed for direct filtration. For DCM-aided filtration, Mg increases in its concentration from 0.11 to 0.46 % at 15 min and from 0.13 to 2.1 % at 60 min, with an increase in temperature from 180 to 220 °C. Calcium follows exactly the similar trend as that of Mg for both recovery methods. It is worthwhile mentioning that highest concentrations of AAEM (Na = 0.03 %, K = 0.68 %, Mg = 2.1 %, and Ca = 0.31 %) is observed at 220 °C and 60 min for the case of DCM-aided filtration recovery corresponding the highest ash retention (**Figure 6-5**). In overall, the concentrations of Na and K reduce with temperature because of their existence as ionic salts in the biomass matrix that readily dissolve in the aqueous phase, while, that of Mg and Ca increase with reaction severity due to their association with organic matter that helps in cross-linking of oligomers during char formation reactions. The drop in the concentration of Ca and Mg at 200 ºC for 15 min (for direct filtration) can be explained by the solubilisation effect of their salts (e.g. chlorides and sulphate) in the aqueous phase.[39]

The product recovery method considerably affects the concentrations of AAEM in the hydrochars as indicated by the reasonably higher concentration of K by direct filtration (at 15 min) than that of DCM-aided filtration. With an increase in holding time, potassium concentration is reduced (at 220 °C) for direct filtration, where DCM-aided filtration surpassed at 0.68 % K versus 0.40 % K (for direct filtration). Moreover, the concentrations of Mg and Ca in the hydrochars are higher for DCM-aided filtration as compared to the direct filtration. Such differences in metal concentrations of hydrochars can be explained by the underlying chemistry of the recovery methods. For direct filtration, heavy biocrude adsorbed on the hydrochar surface serves as a layer of higher molecular weight compounds e.g. carboxylic acids, phenols, alcohols and ketones etc. Such compounds serve two functions. Firstly, the phenolic compounds due to their low hydrophobicity[235] may permeate into the char matrix, thereby increasing the assessability of the aqueous phase to hydrochar internal structure.[236-237] Secondly, the heavier compounds adsorbed on the hydrochar surface may limit the physical adsorption of the AAEM species in the

char structure.[238] For the case of DCM-aided filtration, the presence of a solvent may lead to two effects. One is the lowering of the dielectric constant of the reaction mixture, which increases the intermolecular forces between the ionic salts and the solvent and hinders the dissolution of metals salts in solvent-diluted aqueous media.[237] Other is the dilution of heavier compounds in reaction media or washing of the biocrude from the hydrochar surface, which exposes the pores / internal char structure as discussed in Section 6.2. Due to the combined effect of these factors, the AAEM species suspended in the aqueous phase is adsorbed into the hydrochar, which explains the higher concentrations of AAEM species at 220 °C and 60 min for DCM-aided filtration. However, this phenomenon is very sensitive to reaction temperature and holding time due to the increase of biocrude yield with reaction severity. Conversely, the higher concentrations of K by direct filtration can be explained either by blocking of the hydrochar pores by heavy biocrude hence preventing physical adsorption of K species in the char matrix or by bonding of the K species with heavy biocrude hence washing away with DCM.[237] Furthermore, the different behaviour of Na and K species from that of Mg and Ca species can be explained by stronger interactions of the later with phenolic compounds as compared to the former, which means the solubility of the Ca and Mg species in the aqueous media is least affected by the presence of phenols.[236-237]

To understand the dilution effect of heavy biocrude by direct filtration recovery, we evaluated the concentrations of AAEM species in hydrochars from direct filtration + drying + DCM washing, as depicted by green triangles on **Figure 6-9**, which shows that the metal concentrations are slightly higher than those of the raw hydrochars (from direct filtration). Further, the dilution effect of the biocrude can be omitted by presenting the retentions of AAEM species versus HTC reaction conditions, as shown in **Figure 6-10**. Retention of Na in the hydrochars reduces from 31.8 to 10.4 % for direct filtration and from 25.7 to 6.0 % for DCM-aided filtration when the temperature was raised from 180 to 220 ºC at 15 min. At the longer holding time, Na retention further reduces (from 20.3 at 180 ºC to 2.8 % at 220 ºC) for the former as opposed to the latter, (i.e. slightly rises from 8.0 to 12.4 %) with the increase in temperature. Likewise, potassium experiences higher retention in hydrochars recovered by direct filtration i.e. 24.0 % (at 180 ºC) to 10.4 % (at 220 ºC) as compared to hydrochars diluted by DCM (i.e. 7.3 at 180 ºC to 4.3 % at 220 ºC) at 15

min. A similar trend is observed for a longer holding time. For extractions of Ca and Mg in the hydrochar, reaction temperature and holding time has a significant impact as demonstrated by a rapid increase of retentions at 220 °C and 60 min i.e. 94 % Mg and 88 % Ca for DCM-aided filtration, and 48 % Mg, and 77 % Ca for the direct filtration. Overall, the higher retentions of AAEM species by direct filtration are explained by the permeation impact of phenolic compounds, which are more concentrated in the reaction mixture forming a layer on the hydrochar surface that aids the physical adsorption of AAEM species. However, the higher metal retention by DCM-aided filtration at 220 °C and 60 min are because of both the opening of the hydrochar pores and lowering of the dielectric constant of the DCM-diluted media, which significantly reduces the solubility of AAEM in the aqueous phase and increases their retention in hydrochar.

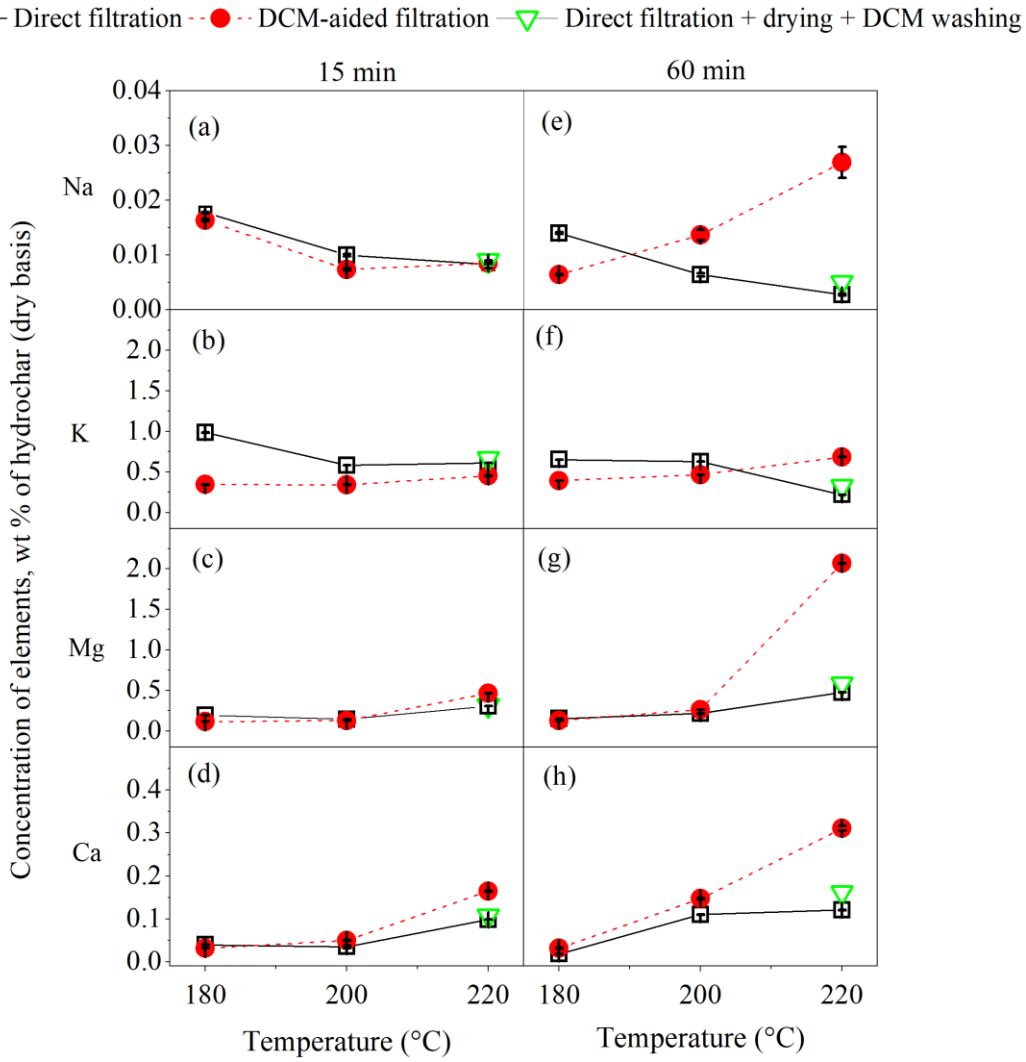

Figure 6-9: Concentrations of Na, K, Mg and Ca in hydrochars obtained by direct filtration, DCM-aided filtration, and direct filtration + drying + DCM washing for 15 min (a-d) and 60 min (e-h).

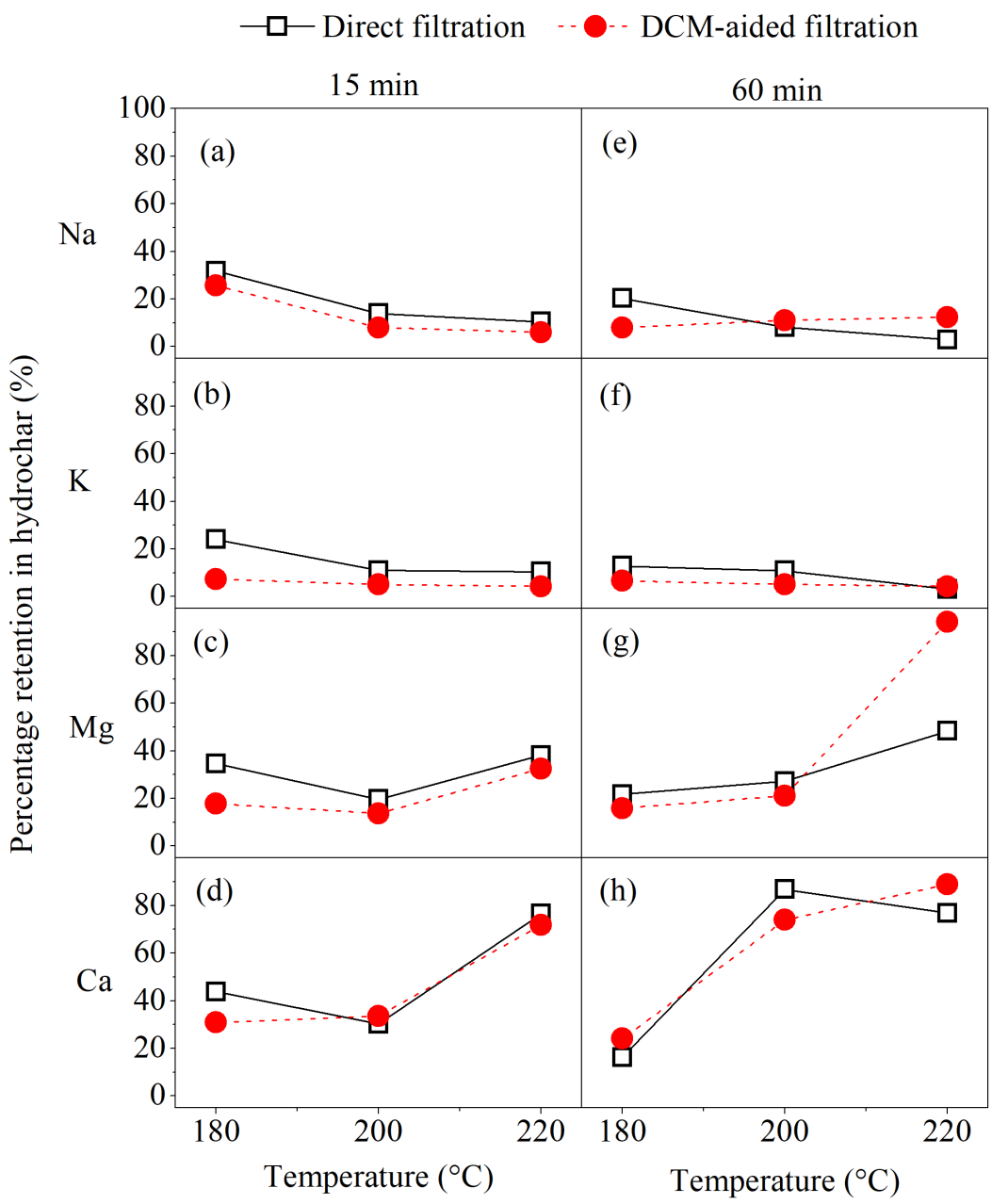

Figure 6-10: Retentions of Na, K, Mg and Ca in hydrochars obtained by direct filtration, and DCM-aided filtration for 15 min (a-d) and 60 min (e-h)

6.3.4 Specific Reactivity

The specific reactivity of hydrochars produced at the most severe conditions of 220 ºC for 15 and 60 min is displayed as **Figure 6-11**, which shows that reactivity increases with the conversion of hydrochars up to the maxima followed by an abrupt decline at higher conversions. At 15 min, hydrochars from direct filtration and DCM-aided filtration shows maxima of 0.046 min^{-1} at 76 % and of 0.06 min^{-1} at 70

% conversion, respectively. With an increase in holding time, the maxima for direct filtration (i.e. 0.065 min^{-1}) is achieved at 79 % conversion while that for DCM-aided filtration (i.e. 0.096 min^{-1}) at 55 % conversion. This shows that hydrochars produced at a longer holding time are more reactive for both recovery methods, however, higher conversion (up to 91 % at both 15 and 60 min) is achievable by direct filtration as compared to the DCM-aided filtration (90 % at 15 min and 85 % at 60 min). As the conversion of carbon increases, the concentration of inorganic matter in the residual mass also increases, which plays a catalytic role in increasing the specific reactivity.[239-241] Further, the drop in reactivity at higher conversions is due to the exposure of inert hydrochar surface to oxygen after the active reaction sites have been consumed.[240-241]

Considering the impact of the product recovery method, the overall lower conversion and higher reactivity for DCM-aided filtration is attributed to the low carbon content and high ash contents, respectively, of the hydrochars as compared to that of direct filtration. At low conversions, the huge difference between the reactivity of hydrochars from both recovery methods (particularly at 60 min) shows the incomplete devolatilisation of heavy biocrude (up to 400 °C) for the case of direct filtration, that has initially blocked the pores affecting penetration of reactive gas to the catalytic sites. However, this effect nullifies as conversion increases up to 80 %, where almost all the reactive carbon has been consumed. This is also obvious that the removal of heavy biocrude by direct filtration + drying + DCM washing has not only improved the specific reactivity but also reduced the overall conversion due to the decrease in carbon content. Therefore, the product recovery method has a drastic impact on hydrochar reactivity that influences its overall conversion rate during combustion in industrial reactors.

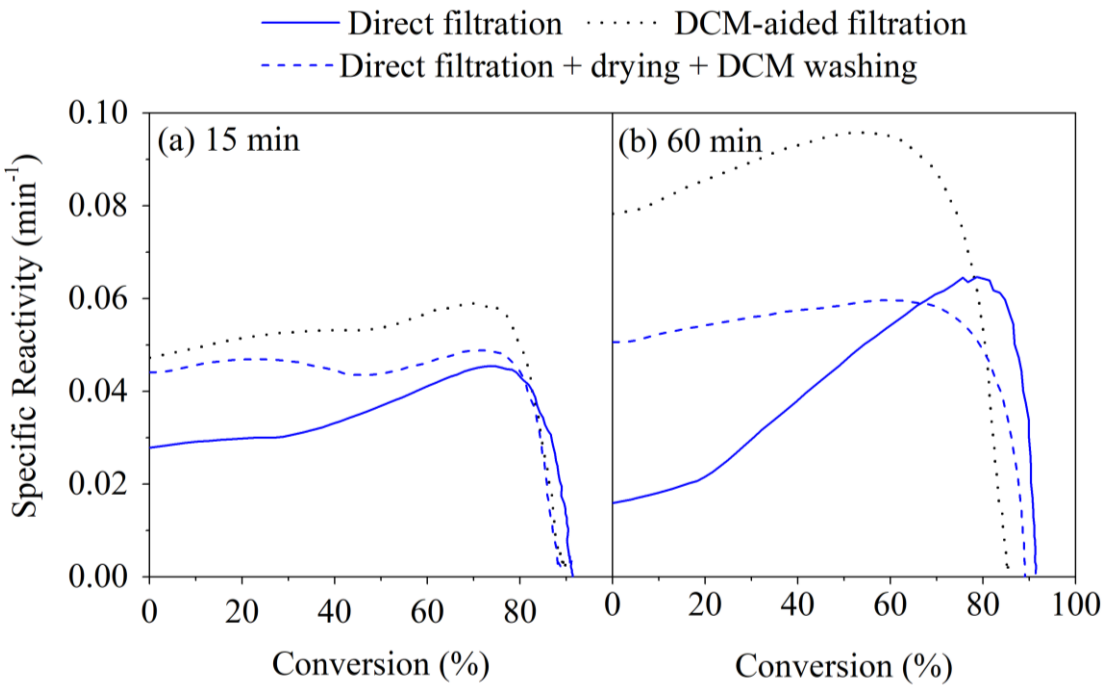

Figure 6-11: Reactivity measurements of hydrochars at 220 ºC for 15 and 60 min for the direct filtration, DCM-aided filtration, and direct filtration + drying + DCM washing

6.3.5 Functional Groups

The effect of the product recovery methods on the surface functionality of hydrochars and the FTIR spectra of the heavy biocrude at 220 ºC and 60 min is depicted in **Figure 6-12**. The broad spectra of O-H stretching vibrations (at 3264 cm^{-1}) and C-H stretching vibrations (at 2852 – 2922 cm^{-1}) indicate the presence of alcohol and phenols[242], and that of alkanes[243], respectively. Similarly, the bands at 1662 – 1704 cm^{-1} shows the existence of C=O stretching vibrations for aldehydes, carboxylic acids and ketones.[243] The other carbon linkages include C-H bending vibrations (1376 – 1456 cm^{-1}), C-O stretching vibrations (1174 cm^{-1}) and C-C skeleton (583 – 989 cm^{-1}). The hydrochar recovered by direct filtration has depicted strong intensities of all the bands showing the increased retention of phenols, alcohols, carboxylic acids and ketones. This is direct evidence of the presence of phenolic compounds on the hydrochars by direct filtration that has resulted in higher retentions of AAEM species as explained in Section 6.3.3. FTIR spectra of the residual biocrude (heavy biocrude) show the strongest band intensities, however, washing away of the biocrude from the hydrochar surface, either during the filtration

or after drying has significantly reduced the intensities of functional groups. Henceforth, the product recovery methods cause considerable differences between the properties of the hydrochars, which altogether effects their potential applications. So, attention must be paid while comparing the hydrochar properties from different studies.

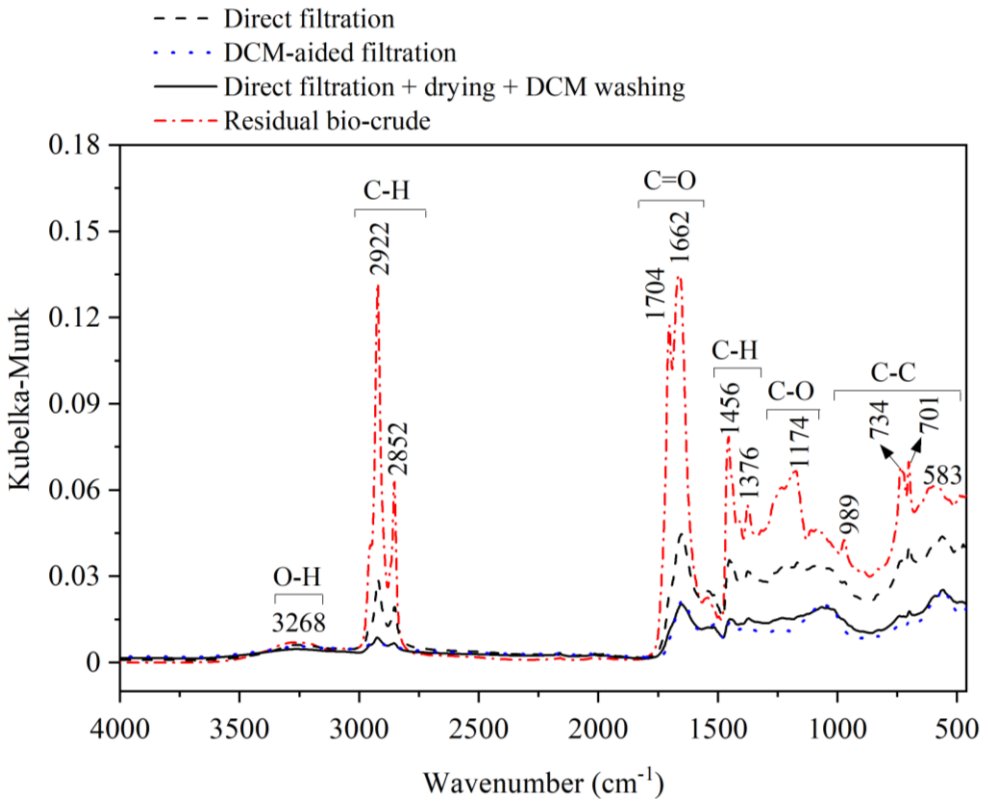

Figure 6-12: FTIR spectra for hydrochars at 220 ºC and 60 min from the direct filtration, DCM-aided filtration, and direct filtration + drying + DCM washing method

6.4 Conclusions

The impact of the product recovery methods (direct filtration versus DCM-aided filtration) on the yield and properties of hydrochar at identical HTC conditions using *Chlorella* as a feedstock is presented. Separation of hydrochar by direct filtration retains heavy biocrude on its surface, which results in higher mass yields. The heavy biocrude is agglomerated and cured into the hydrochar surface during drying and cannot be completely removed by subsequent washing with solvent. The properties

of the hydrochar are significantly impacted by the product recovery method adopted. The hydrochars recovered by direct filtration have a high volatile matter, low fixed carbon and low ash content as compared to that of DCM-aided filtration. More carbon and hydrogen while less nitrogen and oxygen is contained by the hydrochars from direct filtration that also increase their higher heating value and energy recovery. The concentrations of alkali and alkaline earth metals are a strong function of reaction temperature and holding time. Magnesium and calcium shows increase in concentration with increasing reaction severity, which is significant for DCM-aided filtration, whereas sodium and potassium exhibit the reverse trends i.e. concentration increases with reaction severity for DCM-aided filtration and decreases for direct filtration. Specific reactivity is higher and overall conversion is lower for DCM-aided filtration because of the high ash content and low carbon content of the hydrochar. Due to the adsorbed layer of biocrude, the intensities of functional groups (e.g. C-H, C=O and C-C) are much higher for direct filtration recovery. Hence, the recovery method greatly influences the hydrochar yields and properties and care must be taken when comparing the hydrochar recovered from different methods.

CHAPTER 7

Detailed Characterisation of Biocrude and Aqueous Phase from Hydrothermal Carbonisation of Algal Biomass

7.1 Introduction

Extensive characterisation of the HTC products has been conducted as summarised in **Table 7-1.** Most previous studies have focused on the hydrochar and aqueous phase, with very little attention being paid to biocrude. The properties of HTC biocrude are important for at least two reasons. First, when the HTC process is dedicated to the production of carbon materials or upgraded solid fuels, effective utilisation of HTC biocrude as a fuel or a source of value-added chemicals is required to improve the system/process's techno-economic performance. For example, biocrude from *Desmodesmus sp.* at 225 °C retains 40.7 % of carbon and 44.0 % of the energy of the raw algae[43], which is substantial to account for. Moreover, the knowledge of inorganic elements in the biocrude is crucial for their upgraded fuel applications. For instance, biocrude derived from *Nannochloropsis sp.* at 350 ºC contains 0.15 wt % Na and 0.25 wt % Fe, which may deposits as metal salts on reactor walls during their combustion causing the plugging and fouling problems.[244] For the HTC biocrude, the presence of such inorganic elements has not been studied so far. Second, the temperatures of HTC reactions have to be experienced by algal slurry even the process is designed for hydrothermal liquefaction (HTL). Therefore, addressing the quantitative and qualitative analysis of HTC biocrude is of fundamental importance to reveal the mechanisms that govern their transformation to HTL biocrude.

Table 7-1: Basic properties of hydrochar, biocrude and aqueous phase from hydrothermal carbonisation of various algal species used in the literature

Reference	Species	Ultimate Analysis				Metal Analysis						
		Wt%, dry & ash-free basis				Wt%, dry basis						
		C	H	N	O	Na	K	Mg	Ca	Fe	Al	Ni
Hydrochar												
Ekpo et al.[39]	*Chlorella* [a]	61.7	8.2	8.52	21.3	0.53	0.17	3.38	9.82	1.41	1.65	0.020
Smith et al.[55]	*Chlorella* [b]	53.3	7.9	8.60	29.8	0.10	0.16	0.70	1.53	0.06	-	-
Smith et al.[55]	*L.Hyperborea* [b]	53.6	5.2	2.53	38.4	1.06	1.91	0.48	0.96	0.03	-	-
Smith et al.[83]	*Alaria Esculenta* [b]	63.8	5.8	3.74	26.2	0.20	0.10	0.45	2.5	-	-	-
Smith et al.[83]	*Laminaria Digitata* [b]	63.7	6.7	3.04	25.5	0.05	0.04	1.12	5.60	-	-	-
Loes et al.[240]	*Saccharina Latissima* [c]	57.4	-	3.88	-	-	2.52	0.63	4.91	0.19	0.25	0.002
Bio-crude												
Alba et al.[43]	*Desmodesmus sp.* [d]	70.6	9.2	4.8	15.4	-	-	-	-	-	-	-
Jazrawi et al.[16]	*Chlorella* [e]	70.3	4.8	2.60	21.9	-	-	-	-	-	-	-
Jena et al.[17]	*Spirulina* [f]	55.5	8.5	5.48	28.8	-	-	-	-	-	-	-
Anastasakis et al.[82]	*L.Saccharina* [g]	76.6	7.6	5.2	10.3	-	-	-	-	-	-	-

Aqueous Phase

Reference	Species	Parameters			Macronutrients						Micronutrients		
		TOC[l]	TN[m]	pH	Na^+	K^+	Mg^{+2}	Ca^{+2}	NH_4^+	NO_3^-	Fe	Mn	Cr
		Wt%			Wt%						ppm		
		-	-	-	-	-	-	-	0.40	0.14	-	-	-
Smith et al.[83]	*A.Esculenta* [b]	14.8	-	-	3.27	2.97	0.56	0.49	0.22	0.23	-	-	-
Smith et al.[83]	*L.Digitata* [b]	17.7	-	-	3.71	4.08	0.65	0.59	-	0.23	-	-	-
Broch et al.[85]	*Spirulina* [i]	27.6	-	5.9	-	-	-	-	-	-	-	-	-
Levine et al.[29]	*Nannochloropsis* [j]	22.3	3.9	5-6	-	-	-	-	-	-	-	-	-
Du et al.[52]	*Nannochloropsis* [k]	4.5	0.9	-	0.89	0.07	-	-	0.13	0.02	3.08	0.01	0.11

Reaction conditions for [a] 250 °C, 60 min, 10 % solid loading; [b] 200 °C, 60 min & 9.8 % solid loading; [c] 200 °C, 60 min & 20 % solid loading; [d] 225 °C, 60 min, 7.8 % solid loading; [e] 250 °C, 3 min & 1 % solid loading; [f] 200 °C, 60 min & 20 % solid loading; [g] 250 °C, reaction time & solid loading unknown ; [h] 200 °C, 120 min & 10 % solid loading; [i] 215 °C, 30 min & 10 % solid loading; [j] 200 °C, 15 min & 15 % solid loading; [k] 200 °C, 40 min & 20 % solid loading; [l] Total Organic Carbon; [l] Total Nitrogen

From **Table 7-1**, the properties of aqueous phase that have been characterised mainly include total organic carbon (TOC), total nitrogen (TN), pH, and macronutrients (Na^+, K^+, Mg^{+2}, Ca^{+2}, NH_4^+, NO_3^-) to present the potential of recycling aqueous phase for the cultivation of algal biomass[29, 52, 57-58] and energy recovery via anaerobic digestion.[53-54] The presence of heavy metals in the HTC aqueous phase has enjoyed

a rather very limited focus in the literature. For the cultivation of algal biomass, the heavy metals (Fe, Mn, Zn, and Cu) act as micronutrients[108-109] and their presence in the aqueous phase along with macronutrients is desirable. Conversely, heavy metals solubilised in the aqueous phase exert detrimental effects on microbial activity during anaerobic digestion.[110-111] Although their concentrations in the aqueous phase are lower than the inhibitory limits, they are non-biodegradable and their accumulation in the digester over time may impact the overall energy recovery of anaerobic digestion. Considering the recycling of the aqueous phase into anaerobic digester or cultivation media, the knowledge on the recovery rate of the heavy metals is crucial towards the practical implications of the HTC process.

In this chapter, we performed a detailed characterisation of biocrude and aqueous phase obtained from HTC of *Chlorella* in a batch reactor (Section 3.2.2) using the DCM-aided filtration (see **Figure 3-3**) as a recovery method, corresponding to the research objective 4 as outlined in Section 2.7. We further investigated the impact of reaction temperature (180 – 220 °C) and holding time (15 and 60 min) on the properties and metal recoveries of the aqueous phase and biocrude. The energy recovery, GC-MS and GPC analysis, and metal retentions for biocrude, and, the TOC, TN, pH, and concentrations of macro- and micronutrients for the aqueous phase are reported in the following sections.

7.2 Yields of Biocrude and Aqueous Phase

Figure 7-1 shows the yield of biocrude and aqueous phase versus the reaction temperature and holding time in panel (a), and the reaction severity in panel (b). Reaction severity is defined as the logarithm of the reaction conditions (log R), and used as a measure of the intensity of hydrothermal treatment.[80] As expected, the yields of biocrude increase with increasing temperature, from 4.9 wt % at 180 °C to 26.0 wt % at 220 °C for a holding time of 15 min. Extending the holding time to 60 min results in increases of biocrude yields by 81 % (from 4.9 to 8.8 wt %), 43 % (from 13.4 to 19.2 wt %), and 33 % (from 26.0 to 34.6 wt %) at 180, 200 and 220 °C, respectively. The reason for increased biocrude yield with increasing reaction temperature and holding time is the rapid hydrolysis of algal macromolecules to form the biocrude in addition to the water-soluble organics that are further degraded

to contribute the biocrude.[43, 245] The highest yield of biocrude i.e. 34.6 wt % is obtained at the most severe reaction conditions of 220 °C and 60 min represented as log R = 5.3 in **Figure 7-1b**, and it can be explained by the additional effect of decomposition of water-soluble organics into biocrude.[246-247] Such high yield of biocrude is relevant to those reported in the literature i.e. 41.7 wt % (at log R = 5.1)[248] and 27.6 wt % (at log R = 5.4)[43] from hydrothermal processing of microalgae.

Compared to biocrude, the change of aqueous phase yield as a function of reaction temperature and holding time follows a different trend. At 15 min, the aqueous phase yield increases from 39.4 to 45.4 wt % when raising the temperature from 180 to 200 °C and then levels off with further increasing the temperature to 220 °C. On increasing the holding time, the yields remain unchanged from 180 to 200 °C (i.e. ~ 46 wt %), and then slightly decrease to 42.1 wt % at 220 °C. The increased aqueous phase yield at 180 °C for 60 min, as compared to that at 15 min, indicates enhanced hydrolysis of water-soluble disaccharides and oligomers of algal macromolecules at a longer reaction time.[245] The slight reduction of the aqueous phase yield at a higher temperature and longer holding time implies the conversion of water-soluble organics to biocrude and gaseous products via condensation, cyclization and polymerization reactions.[43, 90] The variation of the yield of aqueous phase versus reaction severity in **Figure 7-1b** is in quantitative agreement with the previous studies on HTC of microalgae.[39, 43] Therefore, under the considered conditions, the major contribution to biocrude is from DCM-soluble hydrolysis products of lipids, proteins and carbohydrates rather than the decomposition products of water-soluble organics.

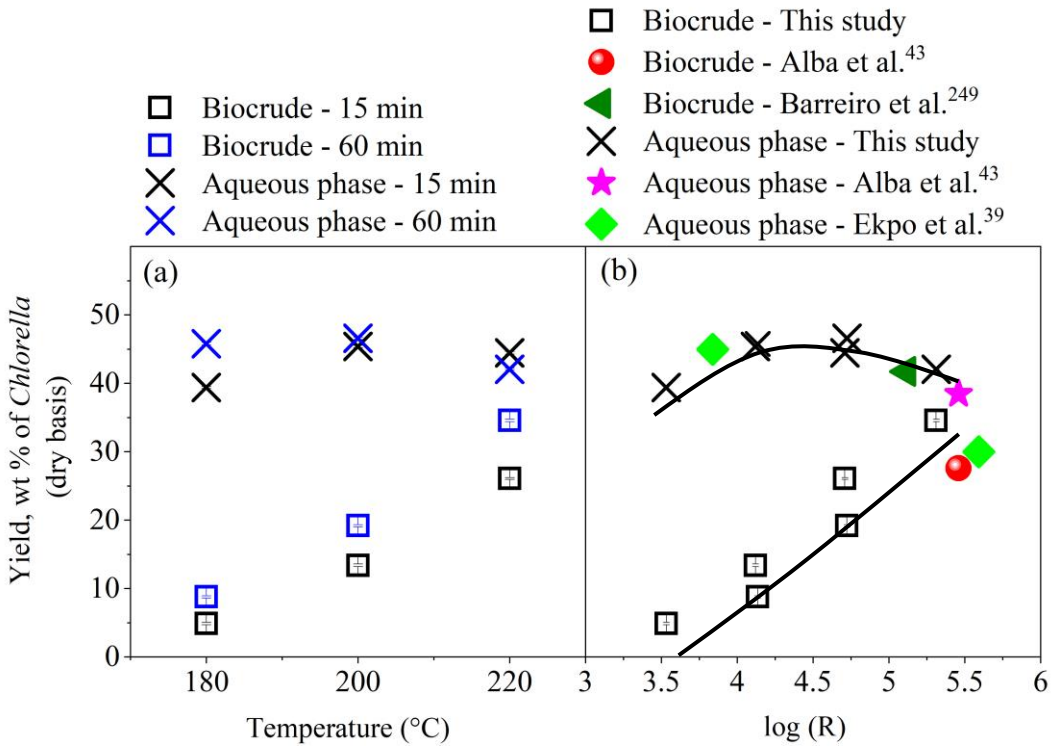

Figure 7-1: Yield of biocrude and aqueous phase from HTC of *Chlorella* versus (a) reaction temperature and holding time, and (b) Reaction Severity computed as R = $\int_0^t e^{(T(t)\,°C - 100\,°C)/14.75\,°C}\,dt$[80]; where '*T*' and '*t*' stands for reaction temperature and holding time, respectively.

7.3 Properties of Biocrude

7.3.1 Ultimate Analysis

The ultimate analysis, HHV and energy recovery of the biocrude obtained after HTC of *Chlorella* is enlisted in **Table 7-2**. The carbon content of the biocrude increases from 70.4 to 75.2 wt % by increasing temperature from 180 to 220 °C at 15 min. The similar trend is obtained at a longer holding time. The hydrogen concentrations of biocrude are elevated with the rise of reaction temperature and the effect is more pronounced at 60 min. Conversely, the oxygen content of biocrude is significantly lowered from 19.9 to 12.1 wt % at 15 min and from 17.0 to 10.4 wt % at 60 min, with an increase of temperature from 180 to 220 °C. The rise of carbon and hydrogen and the decline of oxygen of the biocrude by increasing reaction severity corresponds well with the previous studies.[32, 39, 43] This can be explained by the

decarboxylation, deoxygenation and dehydration reactions occurring concurrently in hydrothermal media that mainly release gaseous carbon dioxide and water, in addition to smaller hydrocarbons. As the oxygen is significantly reduced from the hydrothermal media in the form of CO_2 and H_2O, the concentrations of carbon and hydrogen in the biocrude are elevated, and this effect is prominent for carbon due to its high initial concentration in raw microalgae as compared to that of hydrogen. Furthermore, a remarkable increase in nitrogen content of the biocrude is observed i.e. from 2.51 wt % at 180 °C to 5.12 wt % at 220 °C for 15 min and from 2.77 wt % at 180 °C to 6.50 wt % at 220 °C for 60 min. This is because of the formation of a large number of DCM-soluble nitrogenous compounds in the hydrothermal media via the Maillard reactions and deamination pathways with an increase of reaction severity.[249] Due to the high nitrogen and oxygen content of the biocrude, it requires upgradation before being applied as a transportation fuel. The sulphur contents vary slightly over the studied HTC conditions. The elevation of carbon and hydrogen contents of the biocrude also results in increments of the HHV and the energy recovery, with an increase of reaction temperature and holding time. The highest energy recovery of 49.8 % is obtained at 220 ºC and 60 min with HHV of biocrude as 34.0 MJ/kg.

Table 7-2: Ultimate analysis, HHV and energy recovery of the biocrude at 180 – 220 °C for holding time of 15 and 60 min

Holding time (min)	Temperature (ºC)	Ultimate analysis (wt %, daf)					HHV	Energy recovery
		C	H	N	S	O	MJ/kg	%
15	180	70.4	6.8	2.51	0.44	19.9	30.4	6.3
	200	73.3	7.0	3.32	0.55	15.8	32.0	18.3
	220	75.2	7.0	5.12	0.53	12.1	33.0	36.5
60	180	72.6	7.1	2.80	0.54	17.0	31.7	11.9
	200	74.6	7.6	4.74	0.58	12.5	33.5	27.4
	220	75.0	7.7	6.30	0.57	10.4	34.0	49.8

The changes of O/C and H/C molar ratios as a function of HTC temperature and holding time (plotted on a dry and ash-free basis) are presented in **Figure 7-2**. The O/C and H/C ratio of biocrude is much smaller than that of raw *Chlorella* showing energy densification of the HTC process. The increase of temperature and holding time always led to a reduction of the O/C ratio because of the oxygen removal by a decarboxylation reaction. The H/C atomic ratio of the biocrude mostly falls in the narrow range of 1.11 to 1.23 and is substantially impacted by the holding time. At a fixed temperature, longer holding time enhances the H/C ratio due to removal of oxygen from the biocrude predominantly via decarboxylation[250], while smaller holding time reduces the H/C ratio through dehydration pathway. The O/C ratio of the biocrude at 220 °C and 60 min (i.e. 0.11) approaches that of the Bituminous coal (i.e. 0.10) and is lower than that of the biodiesel (i.e. 0.18)[18], while the H/C values are intermediate between the both. Also, the HTC biocrudes are comparable in their O/C values to those derived from HTL of *Chlorella*.[16, 18] The increment of H/C ratio with holding time implies that longer retention time under HTC conditions may produce a biocrude with energy densification adjacent to that of HTL biocrude.

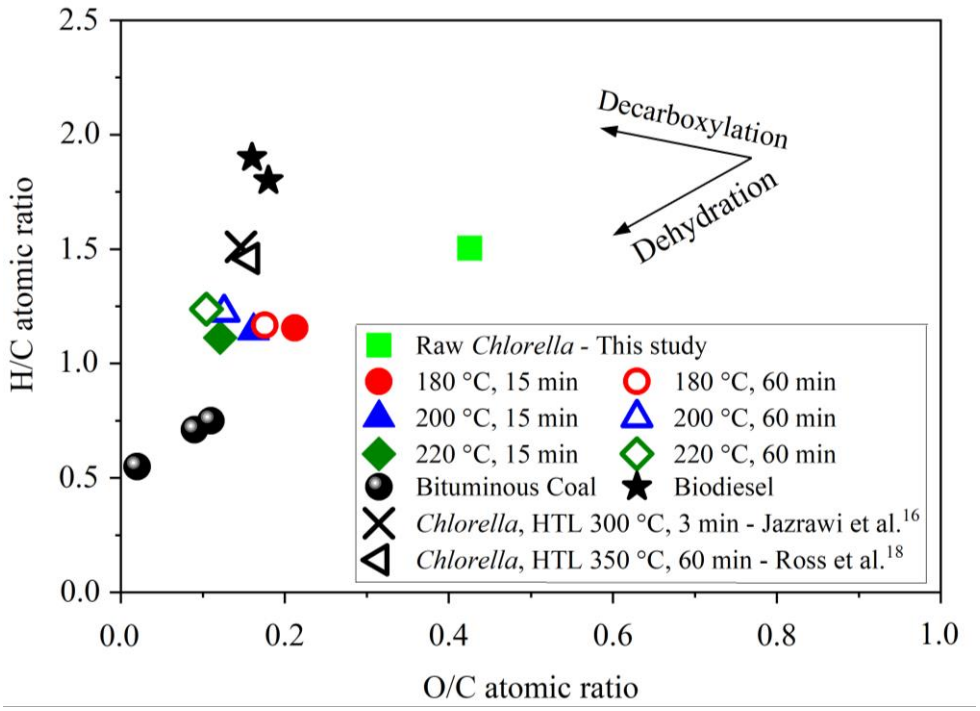

Figure 7-2: Van-krevelen diagram for biocrude from HTC of *Chlorella* at 180 – 220 °C for holding time of 15 and 60 min. H/C and O/C molar ratios are reported on a dry and ash-free basis.

To determine the element recovery of the HTC process, it is important to study the retentions of elements evaluated as the ratio of the concentration of an element in biocrude to the concentration of an element in raw *Chlorella* multiplied by the biocrude yield. The recovery of carbon and nitrogen in the biocrude as a function reaction temperature and holding time is shown in panel (a) and (b) of **Figure 7-3,** respectively. The retention of carbon and nitrogen always increases at higher reaction temperature and longer holding time. This is because of the rapid hydrolysis of carbohydrates, lipids and proteins to yield sugars, fatty acids and amino acids that undergo self-reactions or decomposing pathways to generate more DCM-soluble heterocyclic compounds e.g. fatty acids, long-chain hydrocarbons, pyrazines and cyclic dipeptides.[42] Biocrude at 220 °C and 60 min withdraws 50.6 % of starting carbon which is equivalent to 42.0 – 50.0 % of carbon extraction in biocrude from hydrothermal processing of microalgae.[82, 90] Moreover, nitrogen recovery of 24.1 % at 220 °C and 60 min is significantly lower than that of 40.0 % of nitrogen ending up in HTL biocrude.[82]

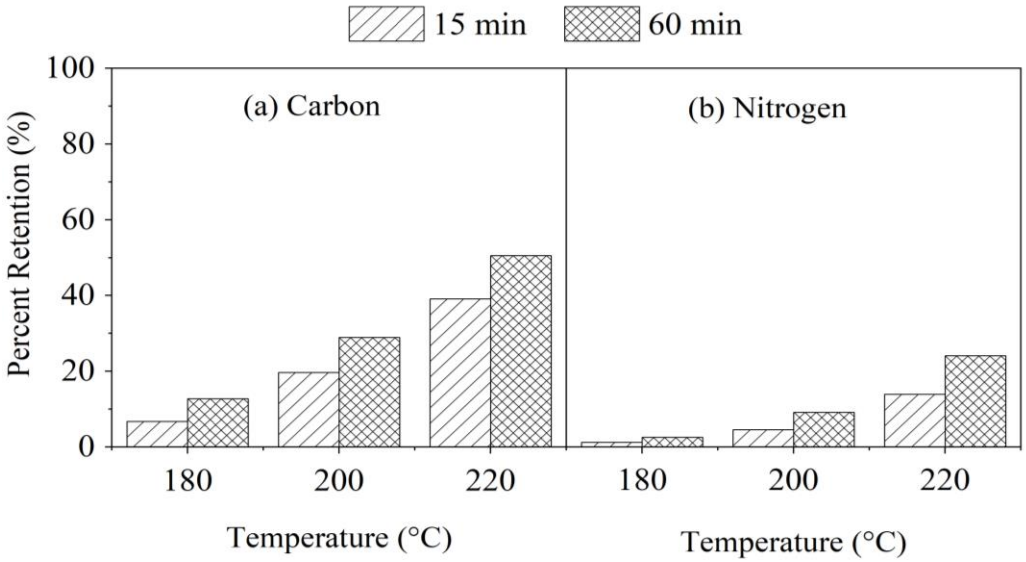

Figure 7-3: Recovery of (a) Carbon and (b) Nitrogen in the biocrude from HTC of *Chlorella* at 180 – 220 °C for holding time of 15 and 60 min

7.3.2 Inorganic Species

The concentrations of the inorganic species in biocrude at 180 – 220 °C for holding time of 15 and 60 min are enlisted in **Table 7-3**, which shows the abundant elements in the biocrude are Na, K, Mg, Ca, Fe and Zn. The concentrations of these metals

generally reduce with an increase in reaction temperature and holding time because of the greater yield of biocrude obtained. The decline in concentrations of Ca and Mg is more abrupt as compared to that of Na and K, which is because of their cross-linking with hydrochar structure at higher reaction severity, where, Na and K are mostly carried by the aqueous phase.[55] Iron decreases from 800.2 to 564.4 mg/kg with an increase of temperature at 15 min and a substantial reduction (from 1111.8 to 238.7 mg/kg) is observed at 60 min. It is because of the existence of iron as chelated complexes and porphyrins in microalgae that become more solubilized in the aqueous phase at high reaction severity. The high concentrations of iron in the biocrude can cause potential difficulties during its upgradation such as catalyst deactivation and large pressure drops.[244] Zinc also shows a reduction in its concentrations at higher reaction severity, as opposed to nickel that always increases, because of leaching of Ni from reactor walls.[39] The concentrations of Mn, Cr and Co are less than 5 mg/kg at all conditions. Besides, the concentrations of different metals in the biocrude also depends on the type of solvent used and whether the biocrude and aqueous phase were contacted during the product recovery procedure.[251] Dichloromethane tends to capture more metals in the biocrude because of its ability to extract less polar compounds from the aqueous phase to which the heteroatoms are attached. Over the studied HTC conditions, 220 °C and 60 min are believed to be optimized reaction conditions because of the lowest metal concentrations obtained along with the high yield of biocrude.

Table 7-3: Inorganic species in the biocrude from HTC of *Chlorella* at 180 – 220 °C for holding time of 15 min and 60 min

Holding time (min)	Temperature	Na	K	Mg	Ca	Fe	Cr	Mn	Co	Ni	Zn
	ºC	mg/kg, as-received mass of biocrude									
15	180	368.6	1351.1	370.9	103.1	800.23	0.20	4.14	0.50	1.95	115.92
	200	269.0	787.3	145.0	91.2	592.41	0.18	2.24	0.53	6.00	56.30
	220	93.1	123.3	14.5	10.5	564.45	0.30	0.61	0.16	9.33	23.10
60	180	202.1	474.0	97.7	62.1	1111.87	0.80	2.95	0.21	3.25	48.76
	200	97.2	52.4	5.5	5.3	483.33	0.44	3.57	0.02	5.66	21.23
	220	88.5	68.4	3.8	3.8	238.71	0.77	0.00	0.04	5.54	10.22

To understand the potential of HTC process for recovering inorganic species in the biocrude, we investigated the impact of reaction temperature and holding time on retentions of major inorganic elements (Na, K, Mg, Ca, Fe and Zn) presented as **Figure 7-4 (a – f)**. There is sizeable retention of sodium in the biocrude i.e. 5.1 to 10.3 % at 15 min and 5.1 – 8.7 % at 60 min as compared to potassium (less than 1.0 %), with an increase of reaction temperature. The overall rise of sodium retention with temperature is attributed to a higher yield of Na-containing salts of fatty acids that are extracted by DCM.[252] Sodium in the biocrude leads to the deposition of alkali salts on combustor walls that cause fouling and plugging problems. Lesser recovery of Ca and Mg in the biocrude, at all experimental conditions, is due to their retentions primarily in the hydrochar during HTC.[55, 83] The retention of iron and zinc in the biocrude is a strong function of reaction temperature and holding time. For example, iron increases substantially from 18.2 to 68.3 % by increasing temperature at 15 min. Extending the holding time results in the gradual reduction of Fe from 45.5 % at 180 °C to 38.4 % at 220 °C, which could be because of thermal degradation of iron porphyrins present in the biocrude at severe reaction conditions and their dissolution in the aqueous phase and hydrochar. Likewise, zinc depicts low retentions in the biocrude at longer holding time. This draws attention towards the careful selection of HTC conditions to get biocrude with low metal content. Although the relative retentions of Fe and Zn in the biocrude are higher than that of alkali and alkaline earth metals, their absolute concentrations in biocrude are still low (especially for Zn).

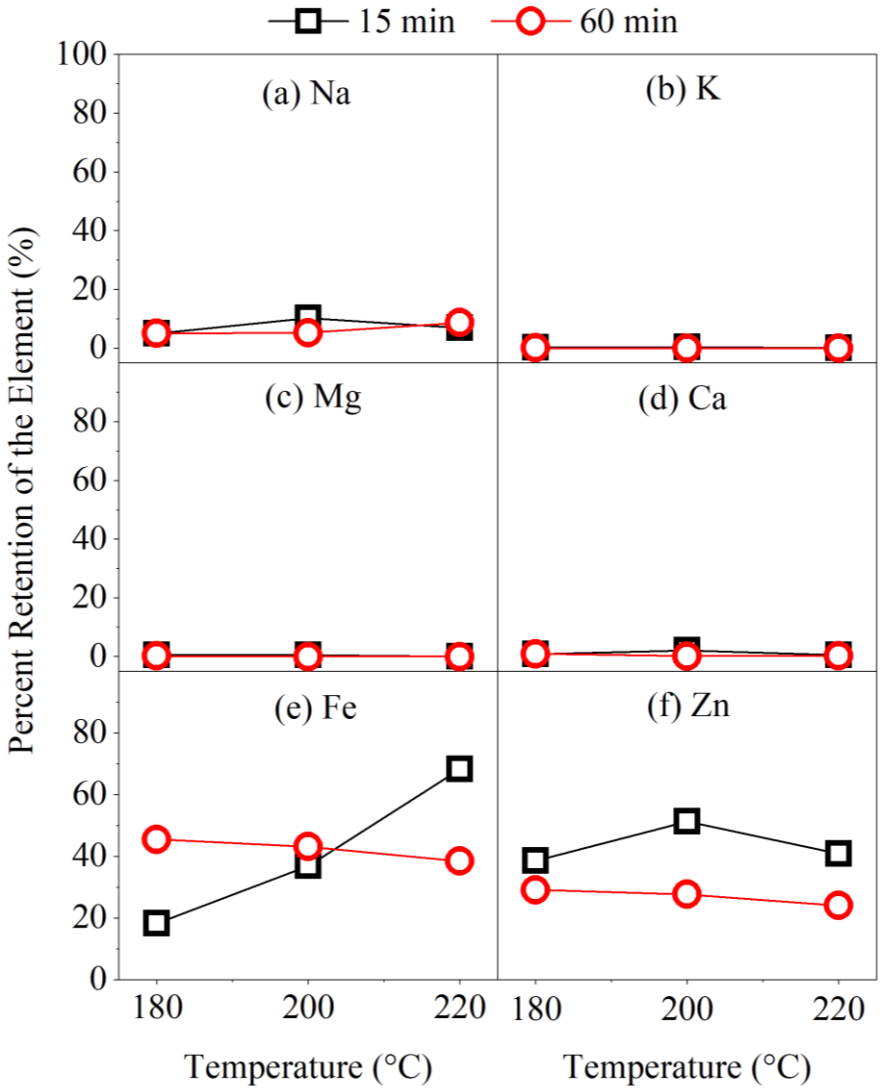

Figure 7-4: Retention of metals: (a) Na, (b) K, (c) Mg, (d) Ca, (e) Fe and (f) Zn in the biocrude from HTC of *Chlorella* versus reaction temperature for holding time of 15 and 60 min

We further compared the retentions of above-mentioned elements at our experimental conditions with those reported by Jiang et al.[244], plotted as a function of reaction severity in **Figure 7-5 (a – f)**. The HTC conditions of 180 – 220 °C with holding time of 15 and 60 min corresponds to the log R values in the range between 3.53 and 5.31 (represented by green symbols) and Jiang et al.[244] experimental conditions of 350 – 400 °C for 1 – 30 min of holding time represents the broader log R range of 2.59 to 8.84 (shown as blue symbols). The data shows that retentions of sodium in biocrude at 180 – 220 °C are 5 – 10 times higher than those obtained at 350 – 400 °C, showing that Na-containing salts of fatty acids might have dissociated

into water-soluble Na compounds at intense hydrothermal conditions. On the other hand, the recovery of K, Mg and Ca in the biocrude at the two experimental conditions is quite comparable. Moreover, the linkages of Fe and Zn with biocrude are not only limited to low temperatures but also prevails over higher temperatures as shown in **Figure 7-5 (e & f)**. Therefore, it seems practically impossible to produce an algal biocrude with low metal content.

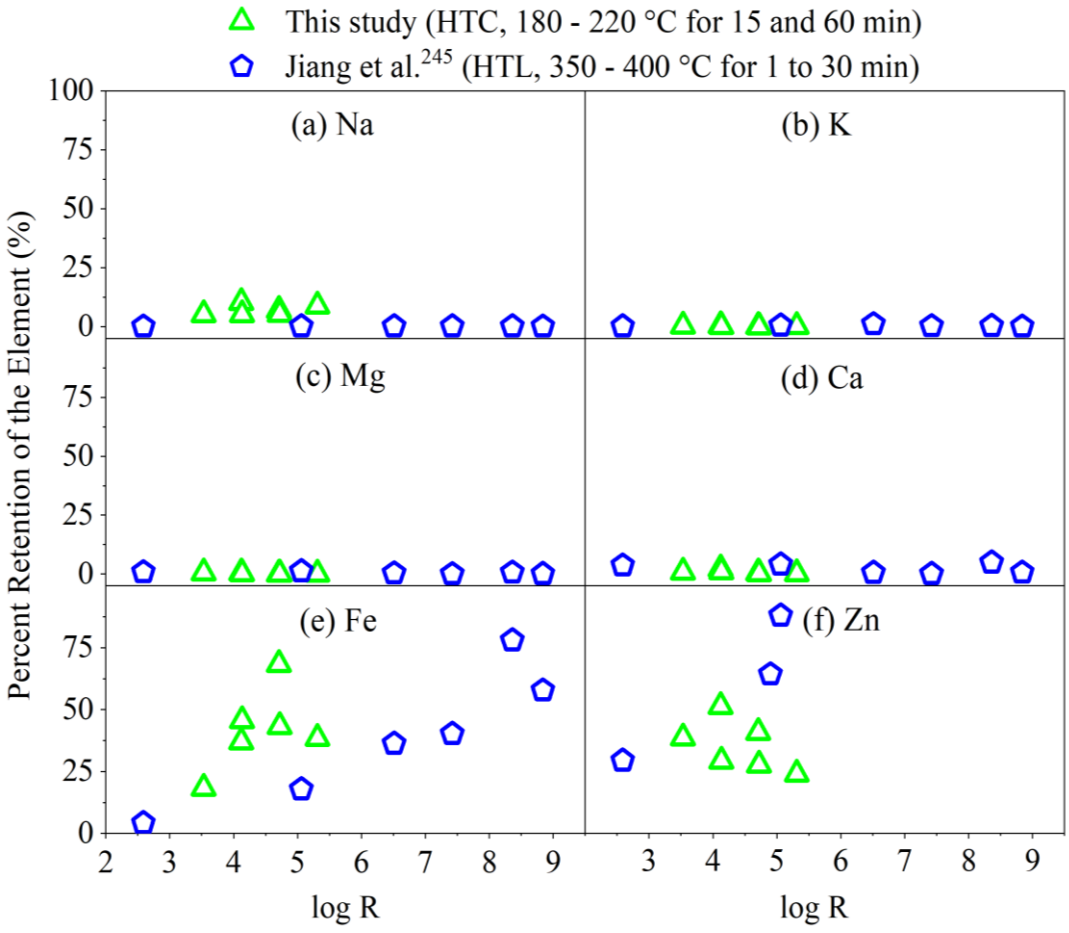

Figure 7-5: Percent retention of the elements: (a) Na, (b) K, (c) Mg, (d) Ca, (e) Fe and (f) Zn in biocrude from HTC of *Chlorella* compared with retention of the elements in biocrude from HTL of *Nannochloropsis sp.* versus the reaction severity

7.3.3 GC/MS-detectable Organic Compounds and GPC Analysis

The GC-MS analysis of the biocrude obtained at 180 – 220 ºC for holding time of 60 min is carried out with a total of 46 compounds detected that form roughly 96 % of the total area of chromatogram. They are categorised into several groups: cyclic hydrocarbons, hydrocarbons (straight or branched chain saturated and unsaturated),

N & O-containing compounds (pyrazines, pyrroles, pyrrolidine, and nitriles), amides, cyclic dipeptides, phenols, ketones, alcohols, fatty acids and its derivatives. **Figure 7-6** shows the relative trend observed by different classes of compounds, and **Table 7-4** displays the list of compounds detected.

At 180 °C, the major constituents of biocrude are hydrocarbons, N & O-containing compounds, phenols, ketones, alcohols and fatty acids, produced from the hydrolysis of carbohydrates, proteins and lipids. Alcohols (mainly 1-Hexadecen-3-ol, 3,7,11,15-tetramethyl) contribute nearly 50 % of all the compounds at 180 °C, which drastically diminishes to 13 % with an increase of temperature to 200 °C. Moreover, the relative abundances of ketones, phenols, and N & O-containing compounds are reduced, while that of fatty acids, cyclic dipeptides, amides and hydrocarbons (both straight-chain and cyclic) are increased by increasing the temperature to 200 °C. Further increasing the temperature to 220 °C intensifies this trend. It should be noticed that a drop in the relative abundance of O-containing compounds and rise in that of N-containing compounds in the biocrude is consistent with the trends of oxygen and nitrogen as discussed in **Table 7-2**. A considerable increase in peak areas of free fatty acids (e.g. n-hexadecanoic acid, tetradecanoic acid and 9,12,15-octadecanoic acid) is observed on increasing the temperature from 180 to 200 or 220 °C, due to their thermal stability in subcritical water.[89] Such compounds are also present in liquefaction biocrude at temperatures 300 ºC and above[82, 106, 143, 253-254], and contributes to the high viscosity of the biocrude.[89]

During hydrothermal processing, the macromolecules of microalgae are hydrolysed to yield a variety of compounds such as long-chain hydrocarbons, oxygenates (alcohols, phenols, ketones), amino acids and fatty acids. With an increase of reaction severity, such compounds concurrently undergo the complex network of reactions including decarboxylation, dehydration, deamination, condensation and polymerization.[255] Maillard reactions between carbohydrates and amino acids take place and produce cyclic dipeptides, the most common nitrogen-containing compounds in the biocrude.[28, 50, 89] A range of cyclic dipeptides are evidenced at 200 °C (**Table 7-4**) and their relative abundance increases with reaction temperature and holding time. The existence of Piperazin-2,5-dione in biocrude from hydrothermal processing of *Desmodesmus* at 200 ºC[42] and *Enteromorpha prolifera* at 300 ºC[87] is

reported in the literature. The identification of a large number of N-containing heterocyclic compounds in biocrude draws attention towards the extraction of valuable compounds e.g. Piperazin-2,5-dione, that are well-known for their biological activity and applications in medicine.[114]

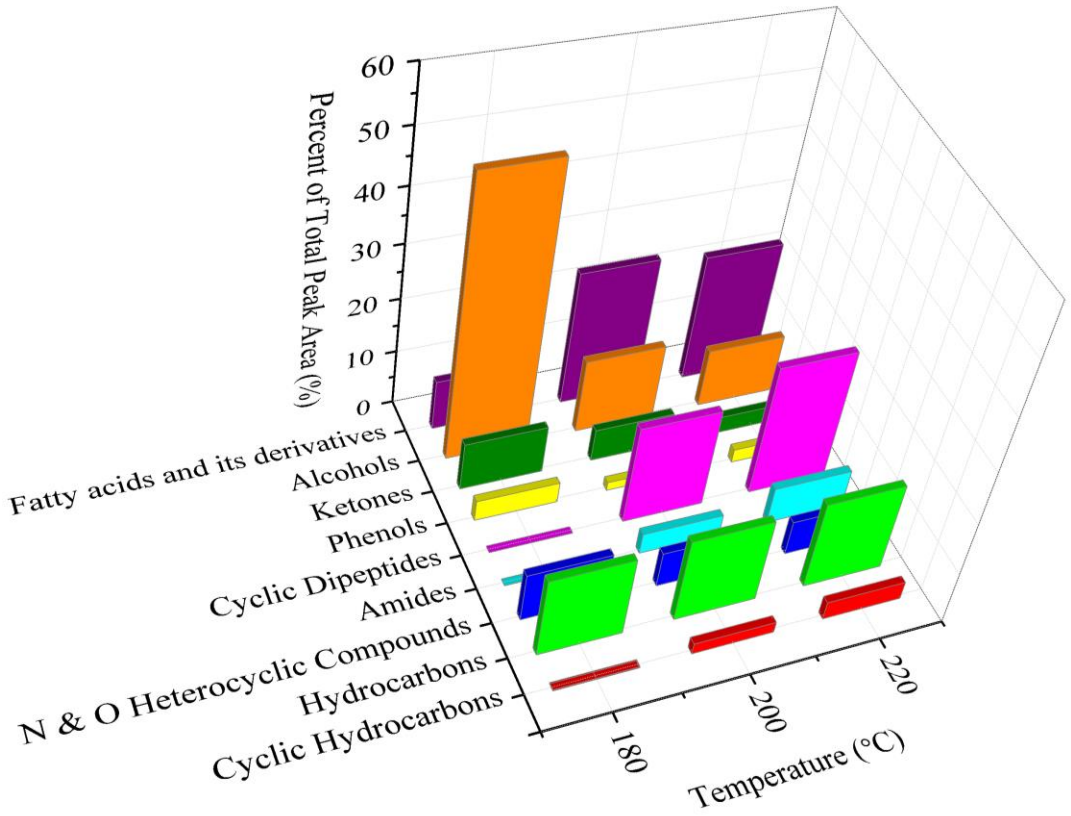

Figure 7-6: The classes of compounds detected in the biocrude from HTC of *Chlorella* at 180 – 220 ºC for holding time of 60 min, as determined by the GC-MS analysis

Table 7-4: Peak percent of the total peak area (%) of the compounds detected in GC-MS analysis of the biocrudes produced at 180 – 220 °C for 60 min of holding time

Compound name	Temperature (°C)		
	180	200	220
	Peak area (%)		
Cyclic Hydrocarbons			
Benzene,1,2,3,5-tetramethyl	-	1.05	1.8
Cyclohexane,1,2-diethyle-1-methyl	0.2	0.53	0.8
Cyclohexane,1,2,3,4-tetramethyl	-	0.46	0.8
Straight & Branched-chain Hydrocarbons			
Hexadecane	3.6	1.52	0.5
2-Undecane,3-methyl	-	1.78	2.8
Pentadecene	4	2.15	3.1
2-Hexadecene,3,7,11,15-tetramethyl	5.2	2.1	2.5
1-Tetradecyne	-	1.52	-
2-Tridecyne	-	1.41	2.9
Heptadecane	1.9	2.78	3.1
Nonane, 3-methylene	-	1.56	0.9
1,9-Dodecadiene	-	0.87	1
N & O Heterocyclic compounds			
Pyrazine, 2,6-dimethyl	-	1.56	1.1
2,5-Pyrrolidinedione,1-methyl	-	1.22	0.4
Pyrrole-2,5-dione,3-ethyle-4-methyl	1	0.35	-
2,5-dimethyl pyrrole	0.3	0.29	0.3
3-Pyrrolidin-2-yl-propionic acid	-	0.27	0.5
3-Phenylpropionitrile	-	1.34	2
Leucyl-l-leucine	3.4	-	-
1-(tert-butyl)-3-methyl piperidine	1.3	-	-
2,3,5-trimethyl indole	0.8	-	-
1-indole,2-methyl	2.1	1.54	1.2
Amides			
Hexadecanamide	-	3.24	4.7
9-Octadecenamide	-	0.61	2.2
Cyclic Dipeptides			
3,6-Diisopropylpiperazin-2,5-dione	-	2.4	4.5
2,5-Piperazinedione,3-(phenylmethyl)	-	2.5	4
2,5-Piperazinedione, 3,6-bis(2-methylpropyl)	-	5.6	5.3
2,5-Piperazinedione,3-benzyl-6-isopropyl	-	2.2	3.6
2,5-Piperazinedione,3,6-bis (phenyl methyl)	-	1.5	1.8
Piperazine-3,5-dione,1-tetradecanoyl	-	4.2	5.5

Phenols			
Phenol	3.8	0.28	0.2
Phenol, 4-methoxy	-	1.31	2.3
Ketones			
2-Pentadecanone,6,8,10-trimethyl	5.1	0.93	0.6
3,6-Nonadecadione	2.7	3.76	1.5
2-Cyclopenten-1-one, 3-methyl	1	0.45	0.1
2-Octanone,1-phenyl	-	0.89	0.9
Alcohols			
Pentadecadien-1-ol	2.9	4.6	3.8
2-Octadecen-1-ol	-	1.74	5.0
1-Hexadecen-3-ol, 3,7,11,15-tetramethyl	49	5.98	0.9
2-phenyl alcohol	-	1.47	1.2
Fatty acids and its derivatives			
n-Hexadecanoic acid	6.9	5.14	8.4
Tetradecanoic acid	0	8.85	5.7
9,12,15-Octadecanoic acid	-	7.81	6.6
Palmitic acid methyl ester	1	1.52	2.6
Dibutyl itaconate	1.3	1.78	0.5

Since compounds with high molecular weight (high boiling points) cannot elute from the GC-MS columns.[254] For a comprehensive study of the molecular weight distribution in the HTC biocrude, we did the GPC analysis of the samples produced at 180 – 220 °C for holding time of 60 min, presented in **Figure 7-7**. At 180 °C, the molecular weight of biocrude demonstrates a wider distribution, from 45 to 37001, with two peaks observed at 440 and 2238. Increasing HTC temperature from 180 to 220 ºC shifts molecular weight distribution curves to a smaller size, as demonstrated by increased amplitude for the peaks at ~ 440 and the shift of heavier peaks from 2238 to 1000. This is the direct evidence of the thermal degradation of the heavier compounds to the lighter ones with an increase of reaction temperature and holding time. Some lighter compounds with molecular weights even up to 7 appear at 200 ºC and above. This agrees well with a higher intensity of low molecular weight compounds in the biocrude at 225 ºC compared to that at 175 ºC during hydrothermal processing of *Desmodesmus*.[43]

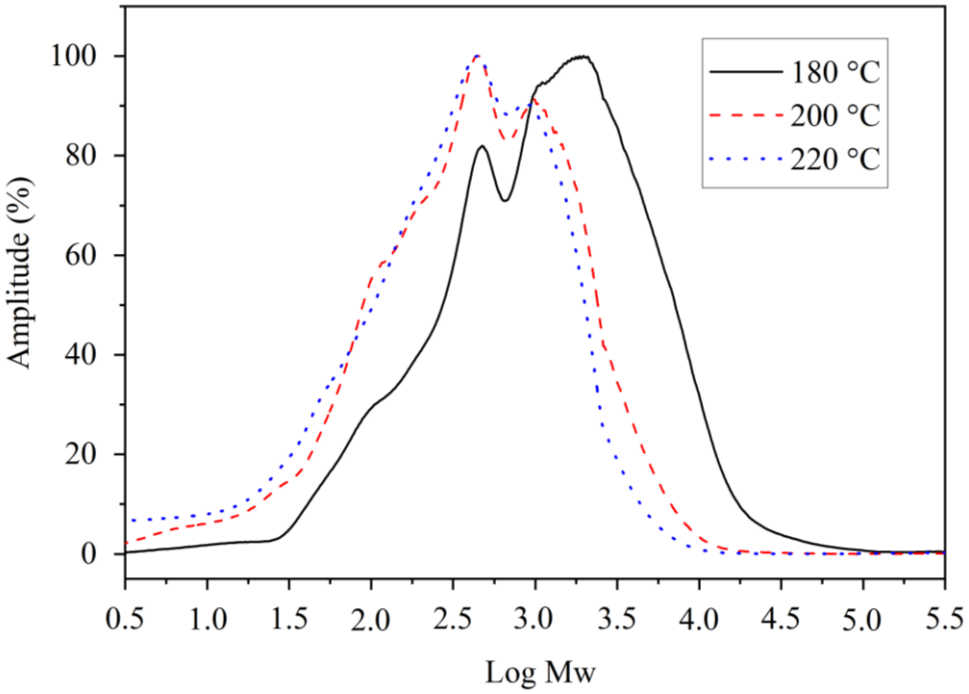

Figure 7-7: Molecular weight distribution of biocrude from HTC of *Chlorella* at 180 – 220 °C for holding times of 60 min as determined by GPC analysis

7.4 Properties of Aqueous Phase

7.4.1 Total Organic Carbon and pH

Table 7-5 shows the TOC, carbon retention and pH of the aqueous phase at 180 – 220 ºC for holding time of 15 and 60 min. Total organic carbon of the aqueous phase is beneficial for its use as a cultivation media in terms of supporting the mixotrophic growth of algae[57, 90] however; it is a more important parameter for anaerobic digestion of aqueous phase to produce methane gas.[53-54] Total organic carbon first increases (from 2.1 to 2.3 wt %) on raising the temperature from 180 to 200 °C, and then decreases (from 2.3 to 2.1 wt %) on a further increase of temperature to 220 °C at 15 min due to the fluctuations of the mass of organics dissolved in the aqueous phase. The effect of temperature is more pronounced at 60 min, where TOC shows a reduction of 13.6 % (from 2.2 to 1.9 wt %) with an increase of temperature. The decline in organic content of the aqueous phase stems from its re-polymerization to biocrude and gases with the increase of reaction temperature and holding time.[20] Our finding is in accordance with hydrothermal

processing of *Chlorella* showing a drop in TOC of the aqueous phase by 8.6 % with a rise of temperature at 60 min.[39] Moreover, carbon retention of the aqueous phase follows a trend similar to that of TOC i.e. it fluctuates between 35.6 and 45.2 % at 15 min, and decreases from 44.2 to 38.6 % at 60 min, with an increase of temperature. The recovery of carbon in aqueous phase under the studied conditions is higher than the carbon recovery of 28.0 % in aqueous phase from *Chlorella* at 350 °C[90], hence making the former more suitable for anaerobic digestion process.

The aqueous phase is acidic (pH ranging between 5.5 and 5.8) at 180 – 200 °C and 15 min, and gradually turns basic with an increase of reaction temperature and holding time (pH of 7.2 at 220 ºC and 60 min). The increasing trend of pH with reaction severity is attributed to the release of NH_4^+ ions in the aqueous phase. The pH of the aqueous phase in our study falls within the range of pH 5.0 and 7.1 for hydrothermal processing of *Chlorella*.[39] In addition, it resembles well with a pH value of 7.5 for the standard growth media BG 11 used for cultivation of *Chlorella* with high growth rates attained.[57]

Table 7-5: Total organic carbon, carbon retention, and pH of the aqueous phase from HTC of *Chlorella* at 180 – 220 °C for holding time of 15 min and 60 min

Reaction time (min)	Temperature (ºC)	TOC wt %	Carbon Retention %	pH
15	180	2.1	35.6	5.7
	200	2.3	45.2	5.5
	220	2.1	39.8	6.0
60	180	2.2	44.2	5.5
	200	2.0	40.5	5.8
	220	1.9	38.6	7.2
BG 11 growth media[58]		-	-	7.5

7.4.2 Distribution and Occurrence of Nitrogen

Nitrogen in the aqueous phase is primarily important for its application as a cultivation media for the growth of algal biomass. Nitrogen existing in biomass is

either organic or inorganic. Organic nitrogen is bonded to the organic compounds such as amino acids, peptides and other products arising from hydrolysis of proteins. While inorganic nitrogen is present in the form of salts such as compounds of ammonium, nitrate and nitrite with alkali or alkaline metals. In this study, we determined the concentrations of ammonium (NH_4^+) and nitrate (NO_3^-) in the aqueous phase, collectively considered as inorganic nitrogen. Then organic nitrogen is computed as a difference between the total nitrogen and inorganic nitrogen. **Figure 7-8a and 7-8b** represent the occurrence forms of nitrogen versus reaction temperature for holding time of 15 and 60 min, respectively.

The concentration of NH_4^+ in the aqueous phase gradually elevates from 0.032 wt % at 180 °C to 0.057 wt % at 220 °C for 15 min, and this trend is intensified at a longer holding time. On the other hand, the concentration of nitrogen as NO_3^- is too small (less than 0.006 wt %) and shows no dependence on the reaction temperature and holding time. This trend is consistent with the literature.[43, 107] Concentration of ammonium increases due to increased hydrolysis of proteins with reaction severity.[39] The higher concentration of ammonium as compared to that of nitrate in the aqueous phase is linked to the source of nitrogen originally present in the raw microalgae. Ammonium generates from hydrolysis of proteins that are the major constituent of *Chlorella* (around 60 %)[16], as opposed to nitrate liberating from a smaller fraction of inorganics present in microalgae. For a similar reason, the concentration of organic nitrogen in the aqueous phase is much higher than inorganic nitrogen at all HTC conditions (**Figure 7-8**). Also, organic nitrogen is mostly present in the form of heterocycles such as piperazine, pyrrole, peptides, and indole in the aqueous phase[58], and it forms over 85 % of the total nitrogen (at the studied conditions). Considering the effect of reaction conditions on organic nitrogen, it gradually increases with a rise in temperature from 180 to 200 °C and then levels off at 220 °C for 15 min. It is because of slower hydrolysis rates of proteins at the beginning of reaction causing a steady rise of organic nitrogen, which eventually becomes fully dissolved in the aqueous phase at high temperature. Also, longer holding time reduces the overall amount of total nitrogen and organic nitrogen in the aqueous phase and a slightly downward trend (of organic nitrogen) with increase of temperature is observed (**Figure 7-8b**). This can be explained by the dissolution of some of the cyclic dipeptides in the biocrude at higher reaction severity as discussed in Section 7.3.3.

Nevertheless, the total nitrogen of the aqueous phase stays fairly constant at around 0.58 wt % over the whole temperature range at holding time of 60 min.

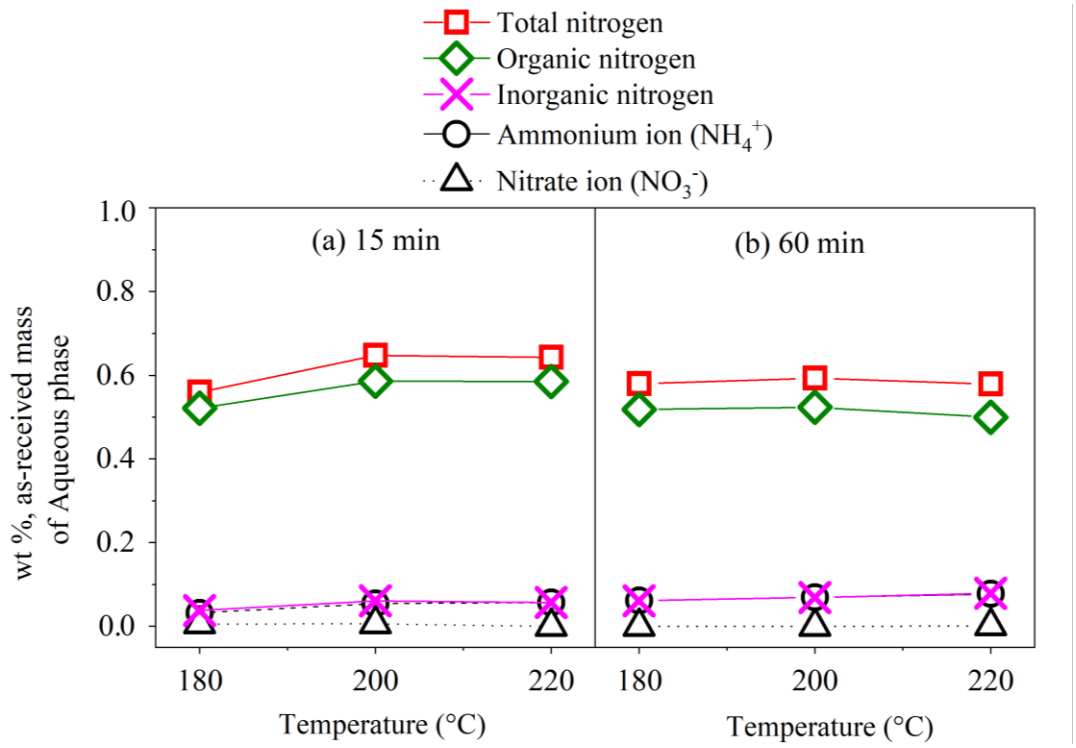

Figure 7-8: Occurrence forms of nitrogen in the aqueous phase from HTC of *Chlorella* at 180 – 220 °C for (a) 15 min and (b) 60 min

7.4.3 Anions and Alkali and Alkaline Earth Metals

Figure 7-9 (a-d) presents the anions and AAEM species found in the aqueous phase from HTC of *Chlorella* as a function of reaction temperature and holding time. The most prevalent species detected in the aqueous phase are dihydrogen phosphate ($H_2PO_4^-$), acetate (CH_3COO^-), formate ($HCOO^-$), potassium (K^+) and magnesium (Mg^{2+}) at all HTC conditions.

The concentration of $H_2PO_4^-$ is continuously declining from 0.401 to 0.362 wt % at 15 min and from 0.440 to 0.288 wt % at 60 min with increase of temperature (**Figure 7-9a** & **7-9b**). The decrease of $H_2PO_4^-$ in the aqueous phase originates from immobilization of phosphate with divalent Ca and Mg ions and hence their recovery in the hydrochar.[39, 43] Dihydrogen phosphate has been detected in the aqueous phase from HTC of *C. reinhardtii* at 200 ºC.[28] Acetate and formate are detected in the aqueous phase because to their tendency to form less volatile and stable salts with

basic elements.[87] Acetate is particularly important for the mixotrophic growth of algae to retain high carbon levels.[57] With an increase of reaction temperature from 180 to 220 °C, the concentration of acetate ions in the aqueous phase increases at 15 min (**Figure 7-9a**) and it stays fairly constant at 60 min (**Figure 7-9b**). Whereas, formate first tends to elevate when the temperature was raised from 180 to 200 ºC (at both 15 and 60 min), and then, it declines with a further increase of temperature to 220 ºC (at 60 min only). Both the acetate and formate are produced via dehydration of sugars and subsequent fragmentation of ring compounds into short-chain compounds, which tends to increase with reaction severity.[256] However at longer holding time, acetate remains stable because of its lesser tendency to decompose in the subcritical water[18], whereas formate readily degrades to CO_2 under hydrothermal conditions.[164] The concentrations of chloride (Cl^-) and sulphate (SO_4^{-2}) in the aqueous phase are negligibly small. Such nutrients exist in the form of hydrated metal salts e.g. $CaCl_2.2H_2O$, $CuSO_4.5H_2O$, and $ZnSO_4.7H_2O$ in standard growth media BG 11.[109]

The concentration of K^+ and Mg^{2+} in the aqueous phase generally decreases with the increase of temperature at both 15 and 60 min as shown in **Figure 7-9c & 7-9d**, respectively. So does the content of Na^+ and Ca^{2+}, but they are less obvious due to low concentrations of these species in the parent *Chlorella*. Therefore, we focus only on K^+ and Mg^{2+}. The overall decline in the concentration of K with increasing reaction severity is attributed to its increase in the hydrochar (see **Figure 6.9b** and **6.9f**). Potassium is normally present as ionic salts in biomass that readily dissolve in the aqueous phase but the presence of organic solvent (DCM used for biocrude recovery here) lowers the dielectric constant of the reaction mixture and increases the intermolecular forces between the ionic salts and aqueous media that hinder the dissolution of ionic salts in the aqueous phase at increased reaction severity.[237] The occurrence of $H_2PO_4^-$ along with high levels of potassium dictates the possible presence of water-soluble KH_2PO_4 salt in the aqueous phase[165], which is the major ingredient required for the cultivation of algal biomass.[109] The reduction for Mg^{2+} in the aqueous phase by increasing temperature and holding time is because of its higher recovery in the hydrochar at high temperature.[55] Magnesium is generally bonded with organic components of microalgae and promotes the cross-linking of oligomers during hydrochar formation reactions. Since higher HTC temperature

breaks more of the polymeric compounds into oligomers that incorporate more magnesium in the char structure and reduce it in the aqueous phase. The high concentrations of K^+, Mg^{2+}, CH_3COO^-, and $H_2PO_4^-$ as detected in our study are among the essential nutrients required for optimum growth of microalgae.[57]

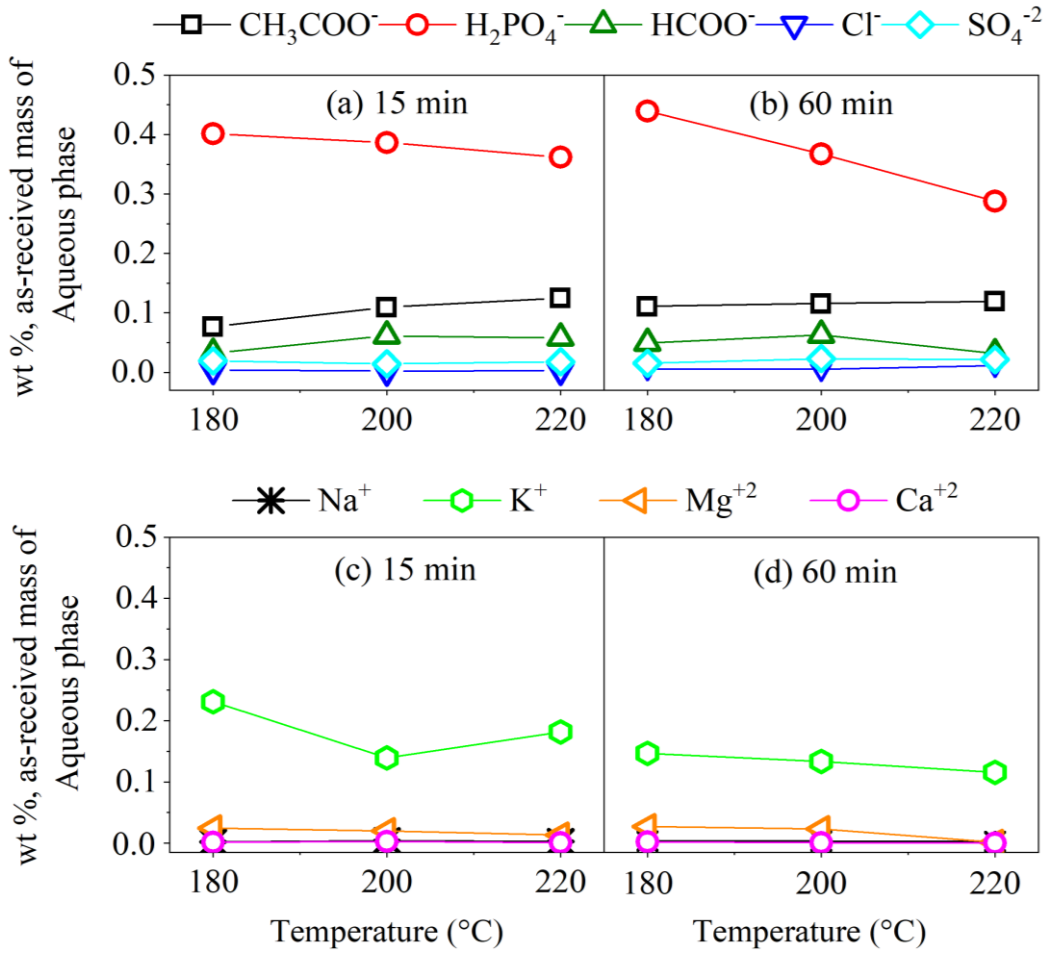

Figure 7-9: Anions (a & b) and AAEM species (c & d) in the aqueous phase from HTC of *Chlorella* at 180 – 220 °C for holding time of 15 and 60 min

We further studied the impact of HTC temperature and holding time on accumulations of K and Mg in the aqueous phase, presented as **Figure 7-10a** and **7-10b**, respectively. The retention of potassium first reduces from 67 to 45 % with an increase of temperature from 180 to 200 °C and then rises to 65 % at 220 °C for 15 min. With an increase of holding time to 60 min, the retention of K gradually reduces from around 50 % at 180 or 200 °C to 44 % at 220 °C. The exceptionally low retention of K at 200 °C (15 min) might be because of the loss of potassium during washing of the reactor; otherwise, the effect of temperature on K retention is

insignificant. However, the reduction of potassium retention in the aqueous phase at longer holding time as consistent with findings of Jiang et al.[244] can be explained by interfering effect of organic solvent introduced in the hydrothermal reaction media. Magnesium shows a reduction in its recovery in the aqueous phase with an increase of temperature. Also, longer holding time recovers more magnesium in the aqueous phase at 180 and 200 °C (around 67 % as opposed to ~ 50 % at 15 min), which than drastically reduces (to 3 %) with an increase of temperature to 220 °C. Magnesium also exists in the form of ionic salts in biomass, which at the beginning of reaction are dissolved in the aqueous phase and are attracted towards hydrochar matrix with an increase of reaction severity.[55] Hence, reaction temperature and holding time strongly impact the metal recoveries of the HTC aqueous phase and should be cautiously monitored to better utilize the resulting product.

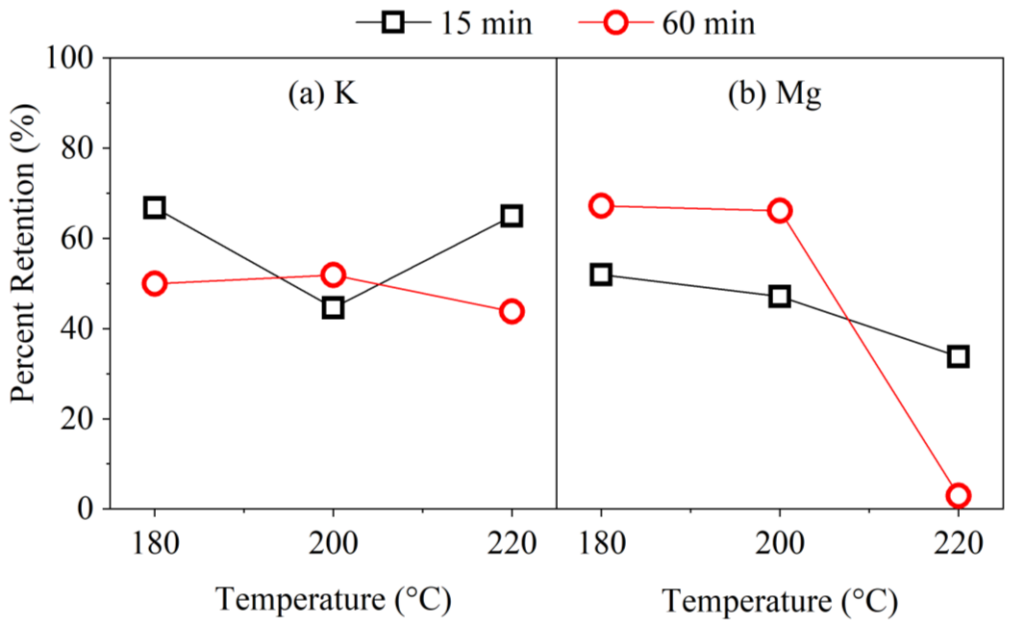

Figure 7-10: Retention of (a) K and (b) Mg in aqueous phase from HTC of *Chlorella* at 180 – 220 °C for holding time of 15 and 60 min

7.4.4 Heavy Metals

Table 7-6 enlists the heavy metal analysis of the aqueous phase from HTC of *Chlorella* at 180 – 220 °C for holding time of 15 and 60 min. Among Fe, Zn, Mn, Ni, Cr and Co, iron is relatively abundant that decreases from 8.91 mg/kg at 180 °C to 2.66 mg/kg at 220 °C for 15 min while at 60 min, its concentration fluctuates

between 3.55 and 5.60 mg/kg. The concentrations of all other elements are extremely low, i.e. less than 2 mg/kg at all conditions. Heavy metals (e.g. Fe, Zn, and Mn) act as micronutrients to aid the algal growth and are present in the form of ferric ammonium citrate, zinc sulphate and manganese chloride salts in various growth media.[108-109] Nickel inhibits the cell division of algal biomass as shown by low growth rates of microalgae grown in cultivation media with 1 – 10 mg/kg of Ni concentrations.[57, 257] Though the concentrations of heavy metals in the aqueous phase observed in our study are within the safe limits for the growth of algal biomass, but they may affect the microbial activity during anaerobic digestion.[110-111]

Table 7-6: Heavy metals in the aqueous phase from HTC of *Chlorella* at 180 – 220 °C for holding time of 15 min and 60 min

Holding time (min)	Temperature (°C)	Fe	Cr	Mn	Co	Ni	Zn
		mg/kg, as-received mass of aqueous phase					
15	180	8.91	0.15	1.52	0.04	0.13	1.10
	200	5.42	0.12	1.47	0.00	0.14	0.80
	220	2.66	0.13	0.46	0.00	0.15	0.57
60	180	4.50	0.08	1.44	0.01	0.13	1.13
	200	3.55	0.16	1.20	0.01	0.20	0.88
	220	5.60	0.14	0.13	0.00	0.20	0.40

We further investigated the recovery of iron in the aqueous phase as a function of reaction temperature and holding time presented as **Figure 7-11**. The accumulation of iron in the aqueous phase is always less than 32 % as opposed to the highest of 68 % of its recovery observed in the biocrude (**Figure 7-4**). The changes in iron retention in the aqueous phase as a function of reaction temperature and holding time is exactly opposite to that observed in the biocrude. The retention of iron decreases from 31 to 11 % at 15 min, and it increases from 18 to 25 % at 60 min with an increase of reaction temperature. This shows that iron porphyrins that initially migrated to biocrude (at 15 min) are degraded at longer holding time and hence, dissolved in the aqueous phase. Iron retentions in the aqueous phase under the studied HTC retentions are far greater than the iron recovery (around 3 %) observed

in the aqueous phase from HTL of *Nannochloropsis sp.*[244], where retention of iron in biocrude is equivalent (64 %) to that of our findings.

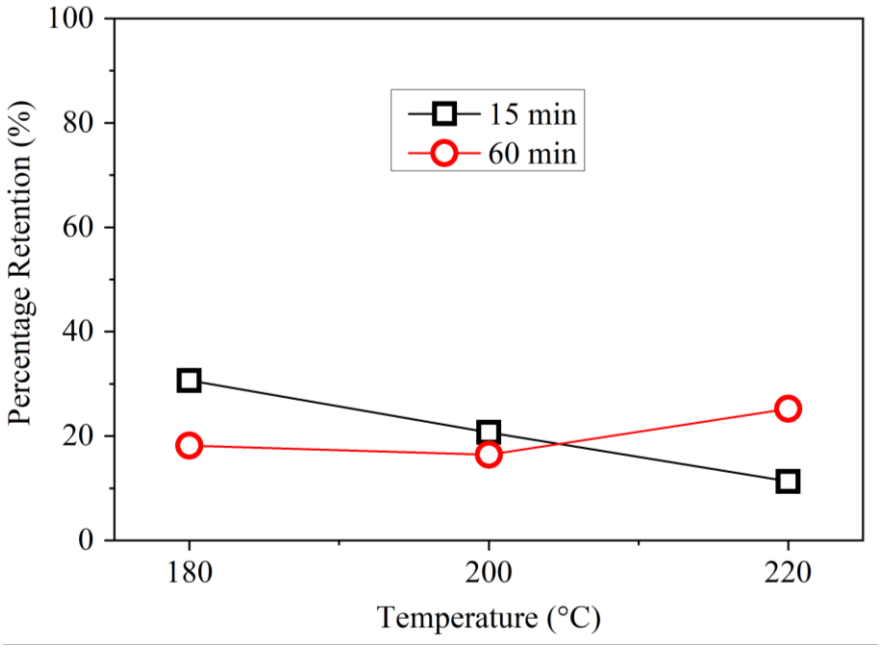

Figure 7-11: Retention of iron in aqueous phase from HTC of *Chlorella* at 180 – 220 °C for holding time of 15 min and 60 min

7.5 Conclusions

As the reaction proceeds from mild to severe HTC conditions, mass yield and energy recovery of biocrude increase, with the highest yield obtained as 34.6 wt %, on a dry basis of *Chlorella* and energy recovery as 49.8 % at 220 °C and 60 min. Aqueous phase affords the highest yield of 46.2 wt % at 200 ºC holding for 60 min, after which it is reduced, showing decomposition to biocrude and gaseous products. Carbon, hydrogen and nitrogen content of the biocrude increases while that of oxygen content decreases with the increase of reaction temperature and holding time. The abundant elements in the biocrude are Na, K, Mg, Ca, Fe and Zn, whose concentrations generally reduce with increase of reaction severity. The relative abundances of fatty acids and cyclic dipeptides in the biocrude increase and that of oxygenate (alcohols, phenols and ketones) decrease as the HTC reaction proceeds towards severity. Aqueous phase turns from acidic to basic with an increase of reaction temperature and holding time because of the liberation of ammonium from

hydrolysis of proteins. The concentration of organic nitrogen in the aqueous phase is much higher than that of inorganic nitrogen (NH_4^+ and NO_3^-) at all HTC conditions. The most dominant nutrient species detected in the aqueous phase are dihydrogen phosphate ($H_2PO_4^-$), acetate (CH_3COO^-), formate ($HCOO^-$), potassium (K^+) and magnesium (Mg^{2+}). Iron initially migrated to biocrude (at 15 min), and then dissolved in the aqueous phase at longer holding time (60 min).

CHAPTER 8

Conclusions and Recommendations

8.1 Introduction

The major research outcomes of this PhD study are summarised in this chapter. Overall, we are successful in delivering the key knowledge of the research objectives mentioned in Section 2.7. Firstly, this research was foremost to investigate the validity of conventional proximate analysis methods employed for the algal biomass and propose a three-step analytical procedure for proximate analysis of algal biomass. Secondly, a plug flow reactor model for thermal decomposition of leucine as an algal biomass surrogate compound was designed that principally accounts for the evolution of nitrogen-containing species from algal biomass. Thirdly, a thorough comparison of the hydrochar yield and properties from two different recovery methods under identical reaction conditions was presented that provides direct evidence on the key features that should be considered while comparing the hydrochar from different studies with dissimilar recovery methods. Finally, we carried out the detailed characterisation and elemental compositions of HTC aqueous phase and biocrude. This chapter outlines the major conclusions drawn throughout this study and recommends future work based on our findings and the data available in the literature.

8.2 Conclusions

8.2.1 Analytical Procedure for Proximate Analysis of Algal Biomass: Case Study for *Spirulina* and *Chlorella*

- The commonly used TGA-ASTM E870-82 method developed for proximate analysis of woody biomass is not valid to the algal biomass.
- The TGA-ASTM E870-82 overestimates the ash content of *Chlorella* and *Spirulina* because of the presence of unburnt carbon in ash residues, which arise due to incomplete oxidation of the quaternary nitrogenous compounds present in char at 950 °C. However, the volatile matter of the two species was accurately determined.
- *Spirulina* was completely ashed by direct heating in TGA at 600 °C in presence of air for 2h, while *Chlorella* stays entirely unoxidised under these conditions.
- For *Chlorella*, a novel ashing method was developed, which used hydrogen peroxide at 600 °C in a tubular reactor for holding time of 4 h. The method when used for *Chlorella* reduced the unburnt carbon in ash to as low as 1.0 wt % of dry ash residue, hence revealing the decomposition of quaternary nitrogenous compounds.
- A three-step analytical procedure is proposed for the proximate analysis of algal biomass that includes: (1) application of TGA-ASTM E870-82 to algal biomass; (2) direct oxidation of algal biomass in TGA at 600 °C in air for 2 h; and (3) oxidation of algal biomass in a tubular reactor at 600 °C in air/H_2O_2 atmosphere for holding time of 4 h, the number of which depends upon the properties of algal biomass.

8.2.2 Thermal Decomposition of Model Compound of Algal Biomass

- A wide array of molecular and radical pathways for the unimolecular and self-condensation bimolecular reactions of Leucine as a model compound of algal biomass during its thermal decomposition are investigated.

- The decarboxylation, deamination, and dehydration pathways, via radical-prompted pathways, systematically require lower energy barriers, in reference to closed-shell reaction corridors.
- The activation energies for direct elimination of CO_2, NH_3, and H_2O from leucine molecule lie within proximity of 20.7 kJ/mol. However, kinetic analysis shows the ruling of dehydration route over decarboxylation and deamination pathways.
- Kinetic analysis of gas-phase reactions, within the context of a plug-flow reactor model, accounts qualitatively for the formation of major products observed experimentally in the thermal degradation of the condensed-phase leucine. Among notable nitrogen-containing species, the model predicts the prevailing of NH_3 over HCN and HNCO, in addition to corresponding appreciable concentrations of amines, imines, and nitriles.

8.2.3 Effects of Product Recovery Methods on the Yields and Properties of Hydrochars from Hydrothermal Carbonisation of Algal Biomass

- Separation of hydrochar by direct filtration retains heavy biocrude on its surface, which results in higher mass and energy yields of hydrochar as compared to that of DCM-aided filtration.
- The hydrochars from direct filtration have high carbon content, low nitrogen, low ash content and improved higher heating value (HHV) as compared to their counterparts.
- The adsorption of viscous biocrude during direct filtration leads to blockage of pores and higher intensities of functional groups (oxygenated and carbonyl) on the hydrochar surface, both of which strongly influence the retentions of inorganic elements in the hydrochar.
- The DCM-aided filtration results in reduced carbon content, higher nitrogen, and oxygen level, increased ash content, lower HHV values, and higher reactivity of the produced hydrochar, all of which affects their application for energy production.
- The concentrations of Mg and Ca in hydrochars always increase at higher HTC temperature and longer holding time, irrespective of the recovery method. However, Na and K reduce in their concentrations with a rise in

reaction temperature and holding time for direct filtration, whereas the reverse trend is observed for DCM-aided filtration.

8.2.4 Detailed Characterisation of Biocrude and Aqueous Phase from Hydrothermal Carbonisation of Algal Biomass

- The mass yield and energy recovery of the biocrude increases with the increase of reaction temperature and holding time. The highest yield of biocrude is 34.6 wt %, on a dry basis of *Chlorella*, at 220 ºC and 60 min with the corresponding heating value of 34.0 MJ/kg.
- Aqueous phase affords the highest yield of 46.2 wt % at 200 ºC holding for 60 min, after which it is reduced, showing decomposition to biocrude and gaseous products.
- The relative abundance of N-containing heterocyclic compounds in the biocrude increase and that of oxygenates (alcohols, phenols & ketones) decrease with an increase of reaction temperature and holding time.
- The molecular weight distribution of the biocrude shifts to the smaller size range with an increase of reaction severity showing the degradation of heavier compounds into lighter ones.
- The recovery of different metals (Na, K, Mg, Ca, Fe and Zn) in biocrude is a strong function of reaction temperature and holding time. Biocrude accumulates reasonable levels of Na, Fe, and Zn based on the starting algae, which may affect its application for energy production.
- The pH of aqueous phase changes from acidic to basic with an increase of reaction temperature and holding time because of the liberation of ammonium ions from the decomposition of proteins and amino acids. Due to the similar reason, the aqueous phase is much higher in organic nitrogen than the inorganic nitrogen.
- The aqueous phase contains reasonable concentrations of dihydrogen phosphate, acetate, formate, potassium and magnesium ions. Among heavy metals, iron is more retained in the aqueous phase at longer holding time.

8.3 Recommendations

Based on the findings of this research, future work is recommended in the following areas:

1. The inapplicability of the conventional proximate analysis methods for algal biomass has been demonstrated in this study. Likewise, the validity of generalised expressions of higher heating values used for high-nitrogen containing algal biomass and derived fuels needs to be investigated yet.

2. The impact of solid loading of algal biomass on hydrochar yield and properties from HTC remains unclear. It is therefore suggested to carry out systematic research on the effects of different solid loading levels of high and low-ash containing algal species on yield and properties of HTC products.

3. Additional research is required on the influence of HTC reaction conditions on the surface porosity of hydrochar with a focus to improve the carbon sequestration and soil conditioning capacity of algal hydrochar.

4. In this thesis, the appreciable recoveries of potassium, magnesium and iron in the aqueous phase from HTC are shown. However, their impact on anaerobic digestion of the aqueous phase needs further study.

5. The identification of the toxic compounds such as polychlorinated dibenzo-p-dioxins (PCDD) and polycyclic aromatic hydrocarbons (PAHs) in the algal hydrochars and their effects on potential applications of hydrochar should be considered as another future work.

APPENDIX

This Appendix contains 3 Sections:

Section 1: Validation of the CBS-QB3 Method

Section 2: Kinetic and Thermodynamic data input for ChemKin Modelling

Section 3: Numeric form of the data plotted in Figure 6-2, Figure 6-6 and Figure 6-8

Section 1: Validation of the CBS-QB3 Method

To validate the CBS-QB3 Method, we calculated the standard enthalpy of formation ($\Delta_f H°_{298}$) of acetamide, glycine, alanine, proline and morpholine using the isodesmic reactions R1.1 – R1.2, R2.1 – R2.2, R3.1 – R3.2, R4.1 – R4.2 and R5.1 – R5, respectively, and compared the calculated values with experimental ones in **Table I**. The isodesmic reactions of standard compounds are shown as:

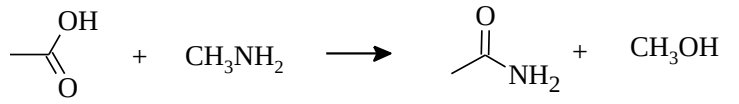
R1.1

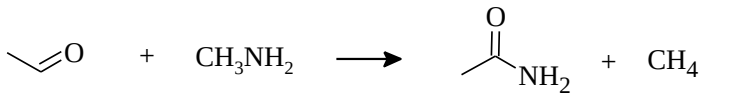
R1.2

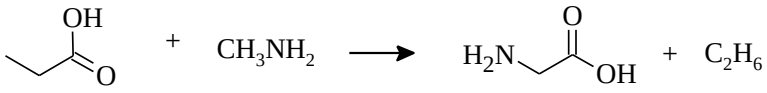
R2.1

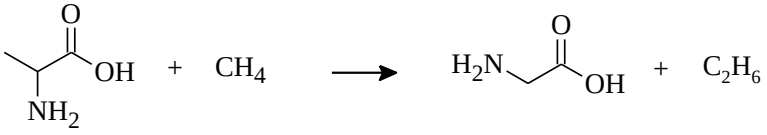
R2.2

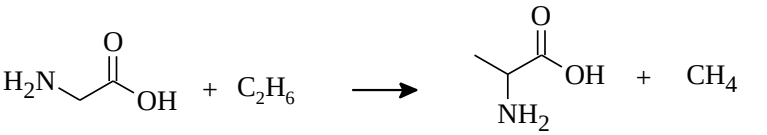
R3.1

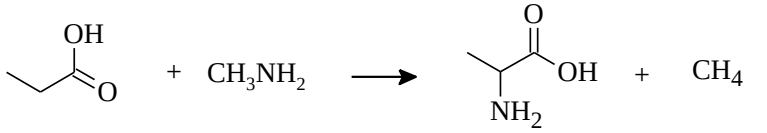
R3.2

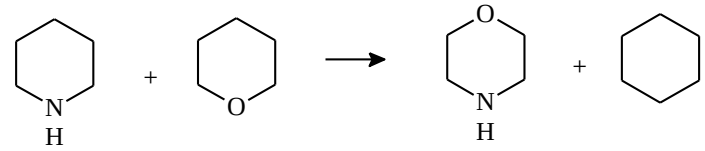
R4.1

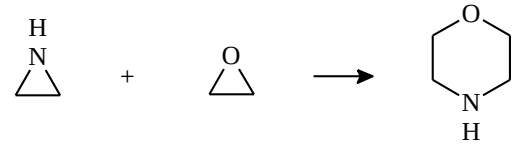
R4.2

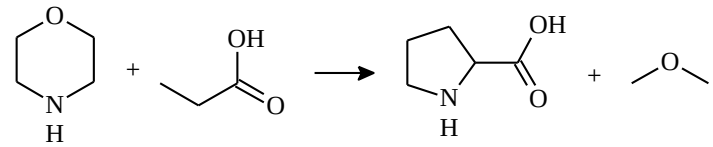
R5.1

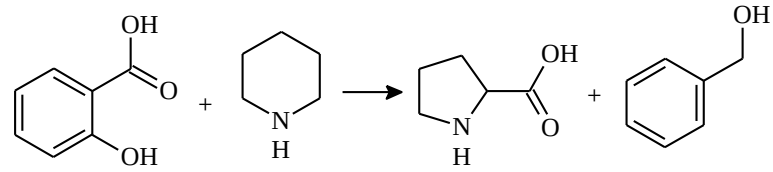
R5.2

The $\Delta_f H°_{298}$ is calculated based on standard enthalpy of reactions ($\Delta_r H°_{298)}$ and experimental $\Delta_f H°_{298}$ of CH_3COOH (-432.6 ± 1.67 kJ/mol) [258], CH_3NH_2 (-12.2 kJ/mol) [259], CH_4 (-74.85 ± 0.31 kJ/mol)[223], CH_3OH (-205.0 ± 10 kJ/mol) [260], CH_3CHO (-170.7 ± 1.5) [261], CH_3CH_2COOH (-455.8 ± 2.0 kJ/mol) [262], C_2H_6 (-83.8 ± 0.3 kJ/mol) [263], $CH_3CH_2NH_2$ (-57.7 kJ/mol) [264], CH_3OCH_3 (-218.5 ± 0.59 kJ/mol) [261], glycine (-393.7 ± 1.5 kJ/mol)[225], salicylic acid (-489.0 kJ/mol) [265], piperidine (-47.2 ± 0.62 kJ/mol) [266], benzyl alcohol (-94.6 ± 3.0 kJ/mol) [267], morpholine (-143.5) [268], tetrahydropyran (-223.8 ± 0.62 kJ/mol) [269], cyclohexane (-124.6 ± 0.83 kJ/mol) [270], aziridine (126.4 ± 0.83 kJ/mol) [271] and oxirane (-52.6 ± 0.62 kJ/mol) [269]. **Table I** enlists the $\Delta_f H°_{298}$ values obtained from individual isodesmic reactions and in overall along with the associated uncertainty limits, and their comparison with the analogous experimental $\Delta_f H°_{298.}$

Table I: $\Delta_f H°_{298}$ of Leucine and reference compounds [a]. All values are in kJ/mol.

Compound		Calculated $\Delta_f H°_{298}$		Calculated uncertainty		Experimental $\Delta_f H°_{298}$	Ref.
		x_j	$\bar{x}$	u_j	$\bar{u}$		
Leucine	R1	-501.2	-503.4	1.6	1.3	-497.6 ± 3.0	225
	R2	-507.1		2.1			
Acetamide	R1.1	-234.0	-235.3	10.1	1.2	-238.3 ± 0.8	272
	R1.2	-236.7		1.2			
Glycine	R2.1	-398.1	-395.0	2.0	1.4	-393.7 ± 1.5	225
	R2.2	-392.0		2.1			
Alanine	R3.1	-425.7	-429.0	1.6	1.2	-424.8 ± 2.0	225
	R3.2	-432.4		2.0			
Proline	R4.1	-373.5	-373.0	0.6	0.6	-366.2 ± 4.0	203
	R4.2	-372.6		2.1			
Morpholine	R5.1	-141.3	-144.8	1.2	0.8	-143.50	268
	R5.2	-148.4		1.2			

[a] x_j = enthalpy of each isodesmic reaction, $\bar{x}$ = grand mean enthalpy, u_j = uncertainty limit of each isodesmic reaction and $\bar{u}$ = overall uncertainty limit

Section 2: Kinetic and Thermodynamic data input for ChemKin Modelling

Kinetics Data

```
ELEMENTS
C  H  N  O
END

SPECIES
R M6 H I1 CO2 P1 P2 NH3 P3 H2 C2H5N C3H6 P4 C4H8 HCN CH3CN M3 NH2 I2 P5
CO P6 M4 H2O OH I3 I4 I5 P7 P8 HNCO A A1 A2 A3 A4 A5 P9 B B1 B2 B3 B4 C N2 I6
I7 C5H11 C2H4
END

REACTIONS                CAL/MOL
R=M6+H                    1.0E13   0.0    77212 ! R1 ESTIMATION Rx, estimated A

M6=I1+CO2                 4.17E11  0.0    45293 ! R2/TS1

I1+H=P1                   1.0E13   0.0    0.0 ! R3 ESTIMATION, estimated A

R=P1+CO2                  1.80E16  0.0    71580 ! R4/TS2

P1=P2+NH3                 4.18E13  0.0    67883 ! R5/TS3

P1=P3+H2                  5.10E13  0.0    99779 ! R6/TS4

P3=C2H5N+C3H6             5.44E12  0.0    95037 ! R7/TS5

P3=P4+H2                  1.21E18  0.0    93098 ! R8/TS6

P4=C4H8+HCN               5.70E15  0.0    97148 ! R9/TS7

P4=C3H6+CH3CN             1.20E14  0.0    110983 ! R10/TS8

R=M3+NH2                  1.0E13   0.0    81005 ! R11 ESTIMATION Rx, estimated A

M3+NH2=I2+NH3             1.0E13   0.0    0.0 ! R12 BARRIERLESS , estimated A

I2=P5+CO                  6.94E13  0.0    28377 ! R13/TS9

R=P6+NH3                  5.81E13  0.0    66645 ! R14/TS10

P6=P2+CO2                 9.70E13  0.0    66448 ! R15/TS11

R=M4+OH                   1.0E13   0.0    11200 ! R16 ESTIMATION Rx, estimated A

M4+OH=I3+H2O              1.0E13   0.0    0.0 ! R17 BARRIERLESS, estimated A

I3=I4                     2.35E12  0.0    70501 ! R18/TS12 H TRANSFER

I4=P3+CO                  4.70E13  0.0    32559 ! R19/TS13
```

```
R=I4+H2O                1.97E16    0.0     69156 ! R20/TS14
I4+H2=I5                8.20E11    0.0     43503 ! R21/TS15
I5=P7+H2O               1.10E14    0.0     60560 ! R22/TS16
I5=P8+HNCO              2.10E14    0.0     81429 ! R23/TS17
I4+R=I6+M6              9.52E13    0.0     26374 ! R24/TS18
I6=C5H11+HNCO           1.20E14    0.0     12634 ! R25/TS19
C5H11=P2+H              3.02E13    0.0     35630 ! R26/TS20
P2=C3H6+C2H4            3.16E12    0.0     57040 ! R27/LITERATURE
I4=I7                   9.67E12    0.0     42730 ! R28/TS21
I7+H=P7+OH              2.62E11    0.0     25790 ! R29/TS22
R+R=A+H2O               9.76E09    0.0     38171 ! R30/TS23
A=A1+A2                 1.0E13     0.0     96842 ! R31 ESTIMATION bde, estimated A
A1=A3+CO                2.29E14    0.0     2349 ! R32/TS24
A3=A4                   1.37E13    0.0     38861 ! R33/TS25
A2=A3+CO2               1.0E14     0.0     0.0 ! R34 BARRIERLESS, estimated A
A3+A4=A5                1.0E14     0.0     0.0 ! R35 BARRIERLESS, estimated A
A5=P9+NH3               4.10E13    0.0     49593 ! R36/TS26
R+R=B+NH3               5.77E9     0.0     62467 ! R37/TS27
B=B1+A3                 1.0E13     0.0     77932 ! R38 ESTIMATION bde, estimated A
B1=B2+CO2               2.70E15    0.0     8673  ! R39/TS28
B2=B3+CO2               1.0E14     0.0     0.0 ! R40 BARRIERLESS, estimated A
B3+A4=B4                1.0E14     0.0     0.0 ! R41 BARRIERLESS, estimated A
B4=P9+H2                2.27E14    0.0     88117 ! R42/TS29
R+P1=C+NH3              4.10E10    0.0     92428 ! R43/TS30
C=B4+CO2                9.20E13    0.0     65056 ! R44/TS31
END
```

Thermodynamics Data (NASA Polynomials)

```
THERMO
   300.000  1000.000  5000.000

R                 H  13C   6N   1O   2g    300.00   5000.00 1000.00                1
 1.63145331E+01 4.37734385E-02-1.69026165E-05 3.00044089E-09-2.00729918E-13       2
-6.95275804E+04-5.59932809E+01 1.80915366E-01 7.05100390E-02-4.94495875E-06       3
-4.03428327E-08 2.04990147E-11-6.40800706E+04 3.19779247E+01                      4
M6                H  12C   6N   1O   2g    300.00   5000.00 1000.00                1
 1.73317963E+01 3.97308392E-02-1.52634400E-05 2.70030423E-09-1.80231206E-13       2
-5.68563334E+04-6.01409474E+01 9.76642482E-01 7.38985396E-02-2.50691255E-05       3
-1.79055917E-08 1.23432286E-11-5.16941297E+04 2.72800726E+01                      4
M3                H  11C   6O   2    0g    300.00   5000.00 1000.00                1
 1.49763745E+01 3.67686999E-02-1.42253938E-05 2.52862533E-09-1.69329657E-13       2
-5.07131664E+04-4.80446002E+01 1.44702080E-01 6.53351149E-02-1.56588207E-05       3
-2.40822276E-08 1.40686057E-11-4.59054002E+04 3.18417508E+01                      4
M4                H  12C   6N   1O   1g    300.00   5000.00 1000.00                1
 1.46693173E+01 3.97901091E-02-1.53751706E-05 2.73021043E-09-1.82679853E-13       2
-1.69185760E+04-4.62288157E+01 2.03417867E+00 5.75856037E-02 2.69653167E-06       3
-3.95639411E-08 1.88034255E-11-1.24537643E+04 2.35418903E+01                      4
P1                H  13C   5N   1    0g    300.00   5000.00 1000.00                1
 1.03400593E+01 4.08225947E-02-1.57159878E-05 2.78312371E-09-1.85841413E-13       2
-2.19512433E+04-2.67245950E+01 1.53080720E+00 4.12823382E-02 3.35202764E-05       3
-6.52952361E-08 2.69329179E-11-1.82128216E+04 2.49332706E+01                      4
P2 (C5H10)        H  10C   5    0    0g    300.00   5000.00 1000.00                1
 8.50982882E+00 3.15389136E-02-1.21703387E-05 2.15849209E-09-1.44278886E-13       2
-9.67377749E+03-1.77432911E+01 6.06464512E-01 3.79061045E-02 1.36875342E-05       3
-3.96509856E-08 1.72856512E-11-6.62612220E+03 2.71111456E+01                      4
P3                H  11C   5N   1    0g    300.00   5000.00 1000.00                1
 1.00309821E+01 3.58728551E-02-1.38929935E-05 2.47051712E-09-1.65456645E-13       2
-1.10590940E+04-2.45549689E+01 1.49858027E+00 3.81624278E-02 2.78753829E-05       3
-5.69579329E-08 2.36702941E-11-7.52705532E+03 2.50343675E+01                      4
P4                H   9C   5N   1    0g    300.00   5000.00 1000.00                1
 9.69948635E+00 3.06687891E-02-1.18967295E-05 2.11766962E-09-1.41919026E-13       2
-7.76682224E+03-2.20123322E+01 1.69500926E+00 3.86826453E-02 8.57221391E-06       3
-3.33447428E-08 1.47822308E-11-4.73083624E+03 2.30989149E+01                      4
P5                H  10C   5O   1    0g    300.00   5000.00 1000.00                1
 9.98276583E+00 3.33716536E-02-1.29900581E-05 2.31800063E-09-1.55623914E-13       2
-3.48225158E+04-2.34819496E+01 2.14895512E+00 3.51451499E-02 2.54856295E-05       3
-5.15559793E-08 2.12372486E-11-3.15326241E+04 2.22043754E+01                      4
P6                H  10C   6O   2    0g    300.00   5000.00 1000.00                1
 1.43543879E+01 3.46096867E-02-1.34058462E-05 2.38504465E-09-1.59820469E-13       2
-5.71966842E+04-4.51327137E+01 4.03189863E-01 6.03854734E-02-1.14681916E-05       3
-2.59988169E-08 1.43938505E-11-5.26166078E+04 3.02899567E+01                      4
P7                H  11C   6N   1    0g    300.00   5000.00 1000.00                1
 1.15037856E+01 3.74557093E-02-1.45459622E-05 2.59137520E-09-1.73770336E-13       2
-8.23266379E+03-3.09395700E+01 1.70216449E+00 4.58217179E-02 1.51892751E-05       3
-4.59303396E-08 1.99751725E-11-4.44912951E+03 2.46419827E+01                      4
P8                H  12C   5    0    0g    300.00   5000.00 1000.00                1
 8.16220688E+00 3.75421859E-02-1.45149379E-05 2.57759717E-09-1.72442183E-13       2
-2.61976434E+04-1.66442736E+01 1.62587494E+00 3.23129393E-02 3.80636144E-05       3
-6.39170303E-08 2.54401387E-11-2.30947969E+04 2.31812575E+01                      4
P9                H  21C  10N   1    0g    300.00   5000.00 1000.00                1
 2.07094838E+01 6.82815098E-02-2.65555140E-05 4.73637673E-09-3.17898536E-13       2
-2.74939862E+04-7.62239434E+01 3.14577783E+00 7.31765964E-02 5.89726043E-05       3
-1.17056946E-07 4.84842665E-11-2.02444423E+04 2.57859282E+01                      4
```

```
I1                H  12C   5N   1    0g    300.00   5000.00 1000.00                                1
 1.12703452E+01 3.70523038E-02-1.42290558E-05 2.51550504E-09-1.67768855E-13                       2
-2.03159947E+03-3.06798879E+01 1.16459101E+00 4.85931366E-02 8.80717342E-06                       3
-4.07235220E-08 1.85334736E-11 1.67253531E+03 2.57806838E+01                                      4
I2                H  10C   6O   2    0g    300.00   5000.00 1000.00                                1
 1.38053623E+01 3.55629583E-02-1.38864812E-05 2.48380046E-09-1.67051775E-13                       2
-4.33157650E+04-4.23665277E+01 5.23824753E-01 5.65442560E-02-1.84238178E-06                       3
-3.46286218E-08 1.71286473E-11-3.87448715E+04 3.03935491E+01                                      4
I3                H  11C   6N   1O   1g    300.00   5000.00 1000.00                                1
 1.43096780E+01 3.73522296E-02-1.44366113E-05 2.56392355E-09-1.71569510E-13                       2
-1.94055857E+04-4.41651898E+01 2.14616063E+00 5.67400056E-02-4.37404297E-06                       3
-3.00704650E-08 1.51034384E-11-1.52099398E+04 2.24697203E+01                                      4
I4                H  11C   6N   1O   1g    300.00   5000.00 1000.00                                1
 1.42676609E+01 3.76614072E-02-1.46293866E-05 2.60738690E-09-1.74925296E-13                       2
-1.70337837E+04-4.56893157E+01-5.18428785E-01 6.46027190E-02-1.15781620E-05                       3
-2.84406997E-08 1.55920261E-11-1.21515571E+04 3.43604092E+01                                      4
I5                H  13C   6N   1O   1g    300.00   5000.00 1000.00                                1
 1.44594257E+01 4.26777844E-02-1.64697824E-05 2.92231377E-09-1.95438052E-13                       2
-4.16736308E+04-4.66029204E+01-2.46630460E-01 6.44996707E-02 2.29179945E-06                       3
-4.49212972E-08 2.16910599E-11-3.65756839E+04 3.42242871E+01                                      4
A                 H  24C  12N   2O   3g    300.00   5000.00 1000.00                                1
 3.34215607E+01 8.11554605E-02-3.14419635E-05 5.59483106E-09-3.74957036E-13                       2
-1.03697441E+05-1.38080092E+02 3.34157562E+00 1.26162421E-01 5.34760195E-06                       3
-8.99567968E-08 4.33028505E-11-9.32851038E+04 2.71705713E+01                                      4
A1                H  12C   6N   1O   1g    300.00   5000.00 1000.00                                1
 1.61574338E+01 3.84464398E-02-1.48714107E-05 2.64314665E-09-1.76986335E-13                       2
-1.79435243E+04-5.29155243E+01 3.02578723E+00 5.64009141E-02 6.04774439E-06                       3
-4.38896407E-08 2.05399987E-11-1.32971671E+04 1.96826152E+01                                      4
A2                H  12C   6N   1O   2g    300.00   5000.00 1000.00                                1
 1.83496480E+01 3.93523862E-02-1.52663256E-05 2.71916008E-09-1.82366490E-13                       2
-3.70362070E+04-6.24319906E+01 3.58562759E+00 6.00354733E-02 7.30418528E-06                       3
-4.90573650E-08 2.30280440E-11-3.18614859E+04 1.90106481E+01                                      4
A3                H  12C   5N   1    0g    300.00   5000.00 1000.00                                1
 1.29637415E+01 3.54877927E-02-1.36329817E-05 2.41127848E-09-1.60893537E-13                       2
-2.38402502E+03-3.86004107E+01 1.75656699E+00 5.01306828E-02 6.85619955E-06                       3
-4.06449809E-08 1.89064490E-11 1.60097267E+03 2.34879479E+01                                      4
A4                H  12C   5N   1    0g    300.00   5000.00 1000.00                                1
 1.23481590E+01 3.65273561E-02-1.41542286E-05 2.51821833E-09-1.68721660E-13                       2
 2.51081554E+03-3.52984200E+01 2.86402844E+00 3.94150386E-02 3.20377230E-05                       3
-6.39731333E-08 2.66594244E-11 6.38739411E+03 1.96605106E+01                                      4
A5                H  24C  10N   2    0g    300.00   5000.00 1000.00                                1
 2.35602835E+01 7.61170253E-02-2.94127240E-05 5.22317589E-09-3.49506801E-13                       2
-3.94320545E+04-9.27288560E+01 1.37242341E+00 9.51386608E-02 4.11851274E-05                       3
-1.11065291E-07 4.83664140E-11-3.10070330E+04 3.27449304E+01                                      4
B                 H  23C  12N   1O   4g    300.00   5000.00 1000.00                                1
 3.32908473E+01 7.86892244E-02-3.05448625E-05 5.44271399E-09-3.65132099E-13                       2
-1.28376907E+05-1.39580451E+02 2.72538430E+00 1.26041964E-01 1.93386830E-06                       3
-8.64979964E-08 4.21546927E-11-1.17885537E+05 2.79200067E+01                                      4
B1                H  11C   7O   4    0g    300.00   5000.00 1000.00                                1
 2.13981680E+01 3.97979970E-02-1.55747073E-05 2.79131958E-09-1.88046558E-13                       2
-8.67770165E+04-7.71957754E+01 3.59410995E+00 7.02712411E-02-6.15502893E-06                       3
-4.00711446E-08 2.05009896E-11-8.08002966E+04 1.96880938E+01                                      4
B2                H  11C   6O   2    0g    300.00   5000.00 1000.00                                1
 1.60012639E+01 3.63420158E-02-1.41997194E-05 2.54128315E-09-1.70999964E-13                       2
-4.08785370E+04-5.21592682E+01 1.52041540E+00 5.87680694E-02 9.39864039E-07                       3
-4.05211874E-08 1.97323438E-11-3.58975772E+04 2.72230684E+01                                      4
B3                H  11C   5    0    0g    300.00   5000.00 1000.00                                1
 1.10292837E+01 3.20011464E-02-1.23553326E-05 2.19233816E-09-1.46598849E-13                       2
 4.81455364E+01-2.89471995E+01 2.49190365E+00 3.89617268E-02 1.56598516E-05                       3
-4.33017361E-08 1.88503406E-11 3.32117506E+03 1.94505563E+01                                      4
```

```
B4                H  23C  10N   1    0g    300.00   5000.00 1000.00                        1
 2.07971933E+01 7.35665810E-02-2.85428482E-05 5.08250451E-09-3.40735175E-13               2
-3.87373048E+04-7.89657391E+01 2.57043033E+00 7.61113096E-02 6.85557466E-05               3
-1.30622160E-07 5.38089336E-11-3.11007310E+04 2.74865038E+01                              4
C                 H  23C  11N   1O   2g    300.00   5000.00 1000.00                        1
 2.70136195E+01 7.61739105E-02-2.95686142E-05 5.26807365E-09-3.53357658E-13               2
-8.74750469E+04-1.09999979E+02 1.67836005E+00 1.04957457E-01 2.88949171E-05               3
-1.03647026E-07 4.65022096E-11-7.82122487E+04 3.15251622E+01                              4
C2H5N             H   5C   2N   1    0g    300.00   5000.00 1000.00                        1
 5.28761345E+00 1.48226236E-02-5.66005610E-06 9.96335737E-10-6.62336111E-14               2
 2.53052942E+02 6.51063350E-01 2.54089838E+00 1.51891857E-02 9.07441893E-06               3
-1.97171480E-08 8.26822114E-12 1.40831290E+03 1.67020563E+01                              4
C3H6              H   6C   3    0    0g    300.00   5000.00 1000.00                        1
 6.34146052E+00 1.69668174E-02-6.58097786E-06 1.17159642E-09-7.85323245E-14               2
-3.52288693E+03-6.27661731E+00 1.77354012E+00 1.94382137E-02 1.22255437E-05               3
-2.71309142E-08 1.14820581E-11-1.70697423E+03 1.99337068E+01                              4
C4H8              H   8C   4    0    0g    300.00   5000.00 1000.00                        1
 6.62860624E+00 2.48657533E-02-9.57587304E-06 1.69580847E-09-1.13225515E-13               2
-9.00854167E+03-7.86662803E+00 8.01712834E-01 2.99600875E-02 7.87711638E-06               3
-2.71196471E-08 1.19362244E-11-6.76723027E+03 2.51384884E+01                              4
HNCO              H   1C   1N   1O   1g    300.00   5000.00 1000.00                        1
 4.83354137E+00 4.06199080E-03-1.49879265E-06 2.57533712E-10-1.68250985E-14               2
-1.39462728E+04 3.74390484E+00 3.06463833E+00 1.06092251E-02-1.14040436E-05               3
 7.36675369E-09-2.00563159E-12-1.35301836E+04 1.24943949E+01                              4
H               L 6/94H   1    0    0    0G   200.000  6000.000 1000.                     1
 0.25000000E+01 0.00000000E+00 0.00000000E+00 0.00000000E+00 0.00000000E+00               2
 0.25473660E+05-0.44668285E+00 0.25000000E+01 0.00000000E+00 0.00000000E+00               3
 0.00000000E+00 0.00000000E+00 0.25473660E+05-0.44668285E+00 0.26219035E+05               4
CO2               L 7/88C   1O   2    0    0G   200.000  6000.000 1000.                     1
 0.46365111E+01 0.27414569E-02-0.99589759E-06 0.16038666E-09-0.91619857E-14               2
-0.49024904E+05-0.19348955E+01 0.23568130E+01 0.89841299E-02-0.71220632E-05               3
 0.24573008E-08-0.14288548E-12-0.48371971E+05 0.99009035E+01-0.47328105E+05               4
NH3  RRHO         A12/04H  3.N  1.   0.   0.G   200.000  6000.000 1000.                     1
 2.09566674E+00 6.14750045E-03-2.00328925E-06 3.01334626E-10-1.71227204E-14               2
-6.30945436E+03 9.59574081E+00 4.46075151E+00-5.68781763E-03 2.11411484E-05               3
-2.02849980E-08 6.89500555E-12-6.70753514E+03-1.34450793E+00-5.48041917E+03               4
H2 REF ELEMENT    tpis78H  2.   0.   0.   0.G   200.000  6000.000 1000.                     1
 2.93286575E+00 8.26608026E-04-1.46402364E-07 1.54100414E-11-6.88804800E-16               2
-8.13065581E+02-1.02432865E+00 2.34433112E+00 7.98052075E-03-1.94781510E-05               3
 2.01572094E-08-7.37611761E-12-9.17935173E+02 6.83010238E-01 0.00000000E+00               4
HCN               ATcT/AH  1.C  1.N  1.   0.G   200.000  6000.000 1000.                     1
 3.80231648E+00 3.14630087E-03-1.06315727E-06 1.66185438E-10-9.79891962E-15               2
 1.42849502E+04 1.57501632E+00 2.25901199E+00 1.00510475E-02-1.33514567E-05               3
 1.00920479E-08-3.00880408E-12 1.45903166E+04 8.91631960E+00 1.56111424E+04               4
CO                RUS 79C   1O   1    0    0G   200.000  6000.000 1000.                     1
 0.30484859E+01 0.13517281E-02-0.48579405E-06 0.78853644E-10-0.46980746E-14               2
-0.14266117E+05 0.60170977E+01 0.35795335E+01-0.61035369E-03 0.10168143E-05               3
 0.90700586E-09-0.90442449E-12-0.14344086E+05 0.35084093E+01-0.13293628E+05               4
H2O               L 5/89H   2O   1    0    0G   200.000  6000.000 1000.                     1
 0.26770389E+01 0.29731816E-02-0.77376889E-06 0.94433514E-10-0.42689991E-14               2
-0.29885894E+05 0.68825500E+01 0.41986352E+01-0.20364017E-02 0.65203416E-05               3
-0.54879269E-08 0.17719680E-11-0.30293726E+05-0.84900901E+00-0.29084817E+05               4
OH HYDROXYL RADI  IU3/03O  1.H  1.   0.   0.G   200.000  6000.000 1000.                     1
 2.83853033E+00 1.10741289E-03-2.94000209E-07 4.20698729E-11-2.42289890E-15               2
 3.69780808E+03 5.84494652E+00 3.99198424E+00-2.40106655E-03 4.61664033E-06               3
-3.87916306E-09 1.36319502E-12 3.36889836E+03-1.03998477E-01 4.48613328E+03               4
NH2  AMIDOGEN RAD IU3/03N  1.H  2.   0.   0.G   200.000  3000.000 1000.                     1
 2.59263049E+00 3.47683597E-03-1.08271624E-06 1.49342558E-10-5.75241187E-15               2
 2.15737320E+04 7.90565351E+00 4.19198016E+00-2.04602827E-03 6.67756134E-06               3
-5.24907235E-09 1.55589948E-12 2.11863286E+04-9.04785244E-02 2.23945849E+04               4
```

```
CH3CN Methyl-Cya  T01/03C  2.H  3.N  1.   0.G   200.000  6000.000 1000.                1
 5.09921882E+00 9.69585649E-03-3.48051966E-06 5.61420173E-10-3.35835856E-14             2
 6.60967324E+03-3.36087178E+00 3.82392803E+00 4.08201943E-03 2.16209537E-05             3
-2.89807789E-08 1.12962700E-11 7.44430382E+03 5.52656156E+00 8.90492212E+03             4
N2 REF ELEMENT    G 8/02N  2.   0.   0.   0.G   200.000  6000.000 1000.                1
 2.95257637E+00 1.39690040E-03-4.92631603E-07 7.86010195E-11-4.60755204E-15             2
-9.23948688E+02 5.87188762E+00 3.53100528E+00-1.23660988E-04-5.02999433E-07             3
 2.43530612E-09-1.40881235E-12-1.04697628E+03 2.96747038E+00 0.00000000E+00             4
I6                H  12C   6N   1O   1g    300.00   5000.00 1000.00                    1
 1.86819525E+01 3.75530095E-02-1.49262922E-05 2.70379214E-09-1.83529539E-13             2
-2.04334044E+04-6.60162002E+01 2.55164995E+00 5.11078941E-02 3.67487935E-05             3
-8.12114038E-08 3.45471651E-11-1.43036612E+04 2.52677186E+01                           4
I7                H  11C   6N   1O   1g    300.00   5000.00 1000.00                    1
 1.57497632E+01 3.67146386E-02-1.43791430E-05 2.57738920E-09-1.73613507E-13             2
 8.35627487E+02-4.96768475E+01 2.89482848E+00 5.19927228E-02 1.23378662E-05             3
-4.87419022E-08 2.19290687E-11 5.52932757E+03 2.20351386E+01                           4
C2H4            g 1/00C  2.H  4.   0.   0.G   200.000  6000.000 1000.                1
 3.99182724E+00 1.04833908E-02-3.71721342E-06 5.94628366E-10-3.53630386E-14             2
 4.26865851E+03-2.69081762E-01 3.95920063E+00-7.57051373E-03 5.70989993E-05             3
-6.91588352E-08 2.69884190E-11 5.08977598E+03 4.09730213E+00 6.31426266E+03             4
C5H11           T 6/13C  5.H 11.   0.   0.G   200.000  6000.000 1000.                1
 1.03957478E+01 2.93753720E-02-1.04269815E-05 1.66933976E-09-9.93401866E-14             2
-2.82049806E+02-2.71065333E+01 4.98546164E+00 1.25990543E-02 7.99239513E-05             3
-1.11788241E-07 4.51939112E-11 2.70516240E+03 8.36313138E+00 5.25811094E+03             4
End
```

Section 3: Numeric form of the data plotted in Figure 6-2, Figure 6-6 and Figure 6-8

Table II: Mass yield, ultimate analysis, HHV and energy yield of hydrochar obtained via direct filtration, DCM-aided filtration and direct filtration + drying + DCM washing from HTC of *Chlorella* at 180 – 220 °C for 15 and 60 min

Holding time (min)	Temperature (°C)	Yield	Ultimate analysis (wt %, daf)					HHV	Energy Yield
		wt %, db	C	H	N	O	S	MJ/kg	%
Direct Filtration									
	180	60.1	57.5	6.6	11.78	23.75	0.4	26.5	70.1
15	200	47.4	62.8	6.1	9.66	21.00	0.4	28.6	58.7
	220 [a]	41.6	69.8	5.4	8.13	16.28	0.4	30.4	56.2
	180	48.4	61.3	5.9	11.97	20.35	0.5	27.8	59.7
60	200	42.7	67.7	6.4	8.01	17.46	0.4	30.4	57.1
	220 [b]	33.9	72.5	5.9	7.60	13.65	0.4	31.6	47.8
DCM-aided Filtration									
	180	54.4	59.6	4.9	11.98	23.11	0.4	25.6	59.3
15	200	37.5	62.8	4.7	11.55	20.53	0.5	27.3	43.6
	220	24.4	65.5	5.2	11.28	17.66	0.4	27.6	28.6
	180	43.0	61.9	5.3	11.20	21.23	0.5	26.6	48.7
60	200	28.1	66.4	4.6	10.93	17.57	0.4	27.8	33.3
	220	16.0	65.0	5.2	10.89	18.52	0.4	24.9	16.9

[a] For direct filtration + drying + DCM washing, Mass yield =32.4 wt %, db, HHV = 27.9 MJ/kg and energy yield = 38.4 %; [b] For direct filtration + drying + DCM washing, Mass yield = 25.2 wt %, db, HHV = 25.8 MJ/kg and energy yield = 26.5 %

REFERENCES

1. Riedy, C.; Diesendorf, M., Financial subsidies to the Australian fossil fuel industry. *Energy Policy* **2003,** *31* (2), 125-137.

2. Review of Climate Change Policies. *Commonwealth of Australia December 2017, Retrieved 15 December 2018*.

3. Stucley, C., Schuck, S., Sims, R., Bland, J., Marino, B., Borowitzka, M., Abadi, A., Bartle, J., Giles, R. and Thomas, Q, Bioenergy in Australia: Status and opportunities. *Bioenergy Australia* **2012**.

4. Burns, A.; Ryder, D. S., Potential for biofilms as biological indicators in Australian riverine systems. *Ecological Management & Restoration* **2001,** *2* (1), 53-64.

5. Ganf, G. G.; Rea, N., Potential for algal blooms in tropical rivers of the Northern Territory, Australia. *Marine and Freshwater Research* **2007,** *58* (4), 315-326.

6. Kent, M.; Welladsen, H. M.; Mangott, A.; Li, Y., Nutritional Evaluation of Australian Microalgae as Potential Human Health Supplements. *PLOS ONE* **2015,** *10* (2), e0118985.

7. Li, Y.; Moheimani, N. R.; Schenk, P. M., Current research and perspectives of microalgal biofuels in Australia. *Biofuels* **2012,** *3* (4), 427-439.

8. Biller, P.; Ross, A. B., Hydrothermal processing of algal biomass for the production of biofuels and chemicals. *Biofuels* **2012,** *3* (5), 603-623.

9. Tian, C.; Li, B.; Liu, Z.; Zhang, Y.; Lu, H., Hydrothermal liquefaction for algal biorefinery: A critical review. *Renewable and Sustainable Energy Reviews* **2014,** *38*, 933-950.

10. Subhadra, B.; Grinson-George, Algal biorefinery-based industry: an approach to address fuel and food insecurity for a carbon-smart world. *Journal of the Science of Food and Agriculture* **2011,** *91* (1), 2-13.

11. Subhadra, B. G., Sustainability of algal biofuel production using integrated renewable energy park (IREP) and algal biorefinery approach. *Energy Policy* **2010,** *38* (10), 5892-5901.

12. Neveux, N.; Magnusson, M.; Maschmeyer, T.; de Nys, R.; Paul, N. A., Comparing the potential production and value of high-energy liquid fuels and protein from marine and freshwater macroalgae. *GCB Bioenergy* **2015,** *7* (4), 673-689.

13. Neveux, N.; Yuen, A. K. L.; Jazrawi, C.; Magnusson, M.; Haynes, B. S.; Masters, A. F.; Montoya, A.; Paul, N. A.; Maschmeyer, T.; de Nys, R., Biocrude yield and productivity from the hydrothermal liquefaction of marine and freshwater green macroalgae. *Bioresource Technology* **2014,** *155*, 334-341.

14. Huang, Y.; Chen, Y.; Xie, J.; Liu, H.; Yin, X.; Wu, C., Bio-oil production from hydrothermal liquefaction of high-protein high-ash microalgae including wild Cyanobacteria sp. and cultivated Bacillariophyta sp. *Fuel* **2016,** *183*, 9-19.

15. Jazrawi, C.; Biller, P.; He, Y.; Montoya, A.; Ross, A. B.; Maschmeyer, T.; Haynes, B. S., Two-stage hydrothermal liquefaction of a high-protein microalga. *Algal Research* **2015,** *8*, 15-22.

16. Jazrawi, C.; Biller, P.; Ross, A. B.; Montoya, A.; Maschmeyer, T.; Haynes, B. S., Pilot plant testing of continuous hydrothermal liquefaction of microalgae. *Algal Research* **2013,** *2* (3), 268-277.

17. Jena, U.; Das, K. C.; Kastner, J. R., Effect of operating conditions of thermochemical liquefaction on biocrude production from Spirulina platensis. *Bioresour Technol* **2011,** *102* (10), 6221-9.

18. Ross, A. B.; Biller, P.; Kubacki, M. L.; Li, H.; Lea-Langton, A.; Jones, J. M., Hydrothermal processing of microalgae using alkali and organic acids. *Fuel* **2010,** *89* (9), 2234-2243.

19. Valdez, P. J.; Nelson, M. C.; Wang, H. Y.; Lin, X. N.; Savage, P. E., Hydrothermal liquefaction of Nannochloropsis sp.: Systematic study of process variables and analysis of the product fractions. *Biomass and Bioenergy* **2012,** *46*, 317-331.

20. Valdez, P. J.; Savage, P. E., A reaction network for the hydrothermal liquefaction of Nannochloropsis sp. *Algal Research* **2013,** *2* (4), 416-425.

21. Bagnoud-Velásquez, M.; Brandenberger, M.; Vogel, F.; Ludwig, C., Continuous catalytic hydrothermal gasification of algal biomass and case study on the toxicity of aluminium as a step toward effluents recycling. *Catalysis Today* **2014,** *223*, 35-43.

22. Duman, G.; Uddin, M. A.; Yanik, J., Hydrogen production from algal biomass via steam gasification. *Bioresource technology* **2014,** *166*, 24-30.

23. Norouzi, O.; Safari, F.; Jafarian, S.; Tavasoli, A.; Karimi, A., Hydrothermal gasification performance of Enteromorpha intestinalis as an algal biomass for hydrogen-rich gas production using Ru promoted Fe–Ni/γ-Al2O3 nanocatalysts. *Energy Conversion and Management* **2017,** *141*, 63-71.

24. Stucki, S.; Vogel, F.; Ludwig, C.; Haiduc, A. G.; Brandenberger, M., Catalytic gasification of algae in supercritical water for biofuel production and carbon capture. *Energy & Environmental Science* **2009,** *2* (5), 535-541.

25. Brown, T. M.; Duan, P.; Savage, P. E., Hydrothermal liquefaction and gasification of Nannochloropsis sp. *Energy & Fuels* **2010,** *24* (6), 3639-3646.

26. Guan, Q.; Savage, P. E.; Wei, C., Gasification of alga Nannochloropsis sp. in supercritical water. *The Journal of Supercritical Fluids* **2012,** *61*, 139-145.

27. Heilmann, S. M.; Davis, H. T.; Jader, L. R.; Lefebvre, P. A.; Sadowsky, M. J.; Schendel, F. J.; von Keitz, M. G.; Valentas, K. J., Hydrothermal carbonization of microalgae. *Biomass and Bioenergy* **2010,** *34* (6), 875-882.

28. Heilmann, S. M.; Jader, L. R.; Harned, L. A.; Sadowsky, M. J.; Schendel, F. J.; Lefebvre, P. A.; von Keitz, M. G.; Valentas, K. J., Hydrothermal carbonization of microalgae II. Fatty acid, char, and algal nutrient products. *Applied Energy* **2011,** *88* (10), 3286-3290.

29. Levine, R. B.; Sierra, C. O. S.; Hockstad, R.; Obeid, W.; Hatcher, P. G.; Savage, P. E., The use of hydrothermal carbonization to recycle nutrients in algal biofuel production. *Environmental Progress & Sustainable Energy* **2013,** *32* (4), 962-975.

30. Lee, J.; Sohn, D.; Lee, K.; Park, K. Y., Solid fuel production through hydrothermal carbonization of sewage sludge and microalgae Chlorella sp. from wastewater treatment plant. *Chemosphere* **2019,** *230*, 157-163.

31. Park, K. Y.; Lee, K.; Kim, D., Characterized hydrochar of algal biomass for producing solid fuel through hydrothermal carbonization. *Bioresource Technology* **2018,** *258*, 119-124.

32. Falco, C.; Sevilla, M.; White, R. J.; Rothe, R.; Titirici, M. M., Renewable nitrogen-doped hydrothermal carbons derived from microalgae. *ChemSusChem* **2012,** *5* (9), 1834-40.

33. Sevilla, M.; Gu, W.; Falco, C.; Titirici, M. M.; Fuertes, A. B.; Yushin, G., Hydrothermal synthesis of microalgae-derived microporous carbons for electrochemical capacitors. *Journal of Power Sources* **2014,** *267*, 26-32.

34. Fan, Y.; Yang, X.; Zhu, B.; Liu, P.-F.; Lu, H.-T., Micro-mesoporous carbon spheres derived from carrageenan as electrode material for supercapacitors. *Journal of Power Sources* **2014,** *268*, 584-590.

35. Fu, X.; Li, D.; Chen, J.; Zhang, Y.; Huang, W.; Zhu, Y.; Yang, J.; Zhang, C., A microalgae residue based carbon solid acid catalyst for biodiesel production. *Bioresour Technol* **2013,** *146*, 767-770.

36. Safari, F.; Javani, N.; Yumurtaci, Z., Hydrogen production via supercritical water gasification of almond shell over algal and agricultural hydrochars as catalysts. *International Journal of Hydrogen Energy* **2018,** *43* (2), 1071-1080.

37. Jiménez Toro, M. J.; Dou, X.; Ajewole, I.; Wang, J.; Chong, K.; Ai, N.; Zeng, G.; Chen, T., Preparation and Optimization of Macroalgae-Derived Solid Acid Catalysts. *Waste and Biomass Valorization* **2017,** *10* (4), 805-816.

38. Du, Z.; Mohr, M.; Ma, X.; Cheng, Y.; Lin, X.; Liu, Y.; Zhou, W.; Chen, P.; Ruan, R., Hydrothermal pretreatment of microalgae for production of pyrolytic bio-oil with a low nitrogen content. *Bioresour Technol* **2012,** *120*, 13-8.

39. Ekpo, U.; Ross, A. B.; Camargo-Valero, M. A.; Williams, P. T., A comparison of product yields and inorganic content in process streams following thermal hydrolysis and hydrothermal processing of microalgae, manure and digestate. *Bioresour Technol* **2016,** *200*, 951-60.

40. Levine, R. B.; Bollas, A.; Savage, P. E., Process improvements for the supercritical in situ transesterification of carbonized algal biomass. *Bioresour Technol* **2013,** *136*, 556-64.

41. Liu, H.; Chen, Y.; Yang, H.; Gentili, F. G.; Söderlind, U.; Wang, X.; Zhang, W.; Chen, H., Hydrothermal carbonization of natural microalgae containing a high ash content. *Fuel* **2019,** *249*, 441-448.

42. Torri, C.; Garcia Alba, L.; Samorì, C.; Fabbri, D.; Brilman, D. W. F., Hydrothermal Treatment (HTT) of Microalgae: Detailed Molecular Characterization of HTT Oil in View of HTT Mechanism Elucidation. *Energy & Fuels* **2012,** *26* (1), 658-671.

43. Garcia Alba, L.; Torri, C.; Samorì, C.; van der Spek, J.; Fabbri, D.; Kersten, S. R. A.; Brilman, D. W. F., Hydrothermal Treatment (HTT) of Microalgae: Evaluation of the Process As Conversion Method in an Algae Biorefinery Concept. *Energy & Fuels* **2011,** *26* (1), 642-657.

44. Mohr, A.; Raman, S., Lessons from first generation biofuels and implications for the sustainability appraisal of second generation biofuels. *Energy Policy* **2013,** *63*, 114-122.

45. Naik, S. N.; Goud, V. V.; Rout, P. K.; Dalai, A. K., Production of first and second generation biofuels: A comprehensive review. *Renewable and Sustainable Energy Reviews* **2010,** *14* (2), 578-597.

46. Demirbas, M. F., Biofuels from algae for sustainable development. *Applied Energy* **2011,** *88* (10), 3473-3480.

47. Kumar, M.; Olajire Oyedun, A.; Kumar, A., A review on the current status of various hydrothermal technologies on biomass feedstock. *Renewable and Sustainable Energy Reviews* **2018,** *81*, 1742-1770.

48. O'Connell, D.; Savelski, M.; Slater, C. S., Life cycle assessment of dewatering routes for algae derived biodiesel processes. *Clean Technologies and Environmental Policy* **2013,** *15* (4), 567-577.

49. Lardon, L.; Hélias, A.; Sialve, B.; Steyer, J.-P.; Bernard, O., Life-cycle assessment of biodiesel production from microalgae. ACS Publications: **2009**.

50. López Barreiro, D.; Prins, W.; Ronsse, F.; Brilman, W., Hydrothermal liquefaction (HTL) of microalgae for biofuel production: State of the art review and future prospects. *Biomass and Bioenergy* **2013,** *53*, 113-127.

51. Peterson, A. A.; Vogel, F.; Lachance, R. P.; Fröling, M.; Antal Jr, M. J.; Tester, J. W., Thermochemical biofuel production in hydrothermal media: a review of sub-and supercritical water technologies. *Energy & Environmental Science* **2008,** *1* (1), 32-65.

52. Du, Z.; Hu, B.; Shi, A.; Ma, X.; Cheng, Y.; Chen, P.; Liu, Y.; Lin, X.; Ruan, R., Cultivation of a microalga Chlorella vulgaris using recycled aqueous phase nutrients from hydrothermal carbonization process. *Bioresource Technology* **2012,** *126*, 354-357.

53. Marin-Batista, J. D.; Villamil, J. A.; Rodriguez, J. J.; Mohedano, A. F.; de la Rubia, M. A., Valorization of microalgal biomass by hydrothermal carbonization and anaerobic digestion. *Bioresource Technology* **2019,** *274*, 395-402.

54. Bampalioutas, K.; Vlysidis, A.; Lyberatos, G.; Vlyssides, A., Detoxification and methane production kinetics from three-phase olive mill wastewater using Fenton's reagent followed by anaerobic digestion. *Journal of Chemical Technology & Biotechnology* **2019,** *94* (1), 265-275.

55. Smith, A. M.; Singh, S.; Ross, A. B., Fate of inorganic material during hydrothermal carbonisation of biomass: Influence of feedstock on combustion behaviour of hydrochar. *Fuel* **2016,** *169*, 135-145.

56. Faeth, J. L.; Valdez, P. J.; Savage, P. E., Fast Hydrothermal Liquefaction of Nannochloropsis sp. To Produce Biocrude. *Energy & Fuels* **2013,** *27* (3), 1391-1398.

57. Biller, P.; Ross, A. B.; Skill, S. C.; Lea-Langton, A.; Balasundaram, B.; Hall, C.; Riley, R.; Llewellyn, C. A., Nutrient recycling of aqueous phase for microalgae cultivation from the hydrothermal liquefaction process. *Algal Research* **2012,** *1* (1), 70-76.

58. Jena, U.; Vaidyanathan, N.; Chinnasamy, S.; Das, K. C., Evaluation of microalgae cultivation using recovered aqueous co-product from thermochemical liquefaction of algal biomass. *Bioresour Technol* **2011,** *102* (3), 3380-7.

59. Nuchdang, S.; Frigon, J. C.; Roy, C.; Pilon, G.; Phalakornkule, C.; Guiot, S. R., Hydrothermal post-treatment of digestate to maximize the methane yield from the anaerobic digestion of microalgae. *Waste Manag* **2018,** *71*, 683-688.

60. Oshio, Y.; Hase, E., Studies on nucleic acids in chloroplasts isolated from Chlorella protothecoides. *Plant Cell Physiol* **1968,** *9* (1), 69-85.

61. Yang, H.; Yan, R.; Chen, H.; Lee, D. H.; Zheng, C., Characteristics of hemicellulose, cellulose and lignin pyrolysis. *Fuel* **2007,** *86* (12), 1781-1788.

62. Skreiberg, A.; Skreiberg, Ø.; Sandquist, J.; Sørum, L., TGA and macro-TGA characterisation of biomass fuels and fuel mixtures. *Fuel* **2011,** *90* (6), 2182-2197.

63. Piorreck, M.; Pohl, P., Formation of biomass, total protein, chlorophylls, lipids and fatty acids in green and blue-green algae during one growth phase. *Phytochemistry* **1984,** *23* (2), 217-223.

64. Neish, A. C., Studies on chloroplasts: their chemical composition and the distribution of certain metabolites between the chloroplasts and the remainder of the leaf1. *Biochem J* **1939,** *33* (3), 300.

65. Iwamura, T.; Kuwashima, S., Two DNA species in chloroplasts of Chlorella. *Biochim Biophys Acta, Nucleic Acid Protein Synth* **1969,** *174* (1), 330-339.

66. Laurens, L. M.; Dempster, T. A.; Jones, H. D.; Wolfrum, E. J.; Van Wychen, S.; McAllister, J. S.; Rencenberger, M.; Parchert, K. J.; Gloe, L. M., Algal biomass constituent analysis: method uncertainties and investigation of the underlying measuring chemistries. *Analytical chemistry* **2012,** *84* (4), 1879-1887.

67. Vassilev, S. V.; Vassileva, C. G., Composition, properties and challenges of algae biomass for biofuel application: An overview. *Fuel* **2016,** *181*, 1-33.

68. Chen, C.-Y.; Zhao, X.-Q.; Yen, H.-W.; Ho, S.-H.; Cheng, C.-L.; Lee, D.-J.; Bai, F.-W.; Chang, J.-S., Microalgae-based carbohydrates for biofuel production. *Biochemical Engineering Journal* **2013,** *78*, 1-10.

69. Safi, C.; Zebib, B.; Merah, O.; Pontalier, P.-Y.; Vaca-Garcia, C., Morphology, composition, production, processing and applications of Chlorella vulgaris: A review. *Renewable and Sustainable Energy Reviews* **2014,** *35*, 265-278.

70. Becker, E. W., Micro-algae as a source of protein. *Biotechnology Advances* **2007,** *25* (2), 207-210.

71. Liang, Y.; Sarkany, N.; Cui, Y., Biomass and lipid productivities of Chlorella vulgaris under autotrophic, heterotrophic and mixotrophic growth conditions. *Biotechnology letters* **2009,** *31* (7), 1043-9.

72. Williams, P. J. l. B.; Laurens, L. M. L., Microalgae as biodiesel & biomass feedstocks: Review & analysis of the biochemistry, energetics & economics. *Energy & Environmental Science* **2010,** *3* (5), 554.

73. Nigam, P. S.; Singh, A., Production of liquid biofuels from renewable resources. *Progress in Energy and Combustion Science* **2011,** *37* (1), 52-68.

74. Bi, Z., Characterization of Microalgae for Biofuel Production *American Society of Agricultural and Biological Engineers* **2013,** *56*.

75. Sanchez-Silva, L.; López-González, D.; Garcia-Minguillan, A. M.; Valverde, J. L., Pyrolysis, combustion and gasification characteristics of Nannochloropsis gaditana microalgae. *Bioresour Technol* **2013,** *130*, 321-331.

76. Garcia, R.; Pizarro, C.; Lavin, A. G.; Bueno, J. L., Biomass proximate analysis using thermogravimetry. *Bioresour Technol* **2013,** *139*, 1-4.

77. Bach, Q.-V.; Chen, W.-H.; Lin, S.-C.; Sheen, H.-K.; Chang, J.-S., Wet torrefaction of microalga Chlorella vulgaris ESP-31 with microwave-assisted heating. *Energy Conversion and Management* **2017,** *141*, 163-170.

78. Miao, C.; Chakraborty, M.; Chen, S., Impact of reaction conditions on the simultaneous production of polysaccharides and bio-oil from heterotrophically grown Chlorella sorokiniana by a unique sequential hydrothermal liquefaction process. *Bioresour Technol* **2012,** *110*, 617-27.

79. Levine, R. B.; Bollas, A. A.; Durham, M. D.; Savage, P. E., Triflate-catalyzed (trans)esterification of lipids within carbonized algal biomass. *Bioresour Technol* **2012,** *111*, 222-9.

80. Lu, Y.; Levine, R. B.; Savage, P. E., Fatty Acids for Nutraceuticals and Biofuels from Hydrothermal Carbonization of Microalgae. *Industrial & Engineering Chemistry Research* **2014,** *54* (16), 4066-4071.

81. Lu, Y.; Savage, P. E., Supercritical water gasification of lipid-extracted hydrochar to recover energy and nutrients. *The Journal of Supercritical Fluids* **2015,** *99*, 88-94.

82. Anastasakis, K.; Ross, A. B., Hydrothermal liquefaction of the brown macro-alga Laminaria saccharina: effect of reaction conditions on product distribution and composition. *Bioresour Technol* **2011,** *102* (7), 4876-83.

83. Smith, A. M.; Ross, A. B., Production of bio-coal, bio-methane and fertilizer from seaweed via hydrothermal carbonisation. *Algal Research* **2016,** *16*, 1-11.

84. Xu, Q.; Qian, Q.; Quek, A.; Ai, N.; Zeng, G.; Wang, J., Hydrothermal Carbonization of Macroalgae and the Effects of Experimental Parameters on the Properties of Hydrochars. *ACS Sustainable Chemistry & Engineering* **2013,** *1* (9), 1092-1101.

85. Broch, A.; Jena, U.; Hoekman, S.; Langford, J., Analysis of Solid and Aqueous Phase Products from Hydrothermal Carbonization of Whole and Lipid-Extracted Algae. *Energies* **2014,** *7* (1), 62-79.

86. Yao, C.; Wu, P.; Pan, Y.; Lu, H.; Chi, L.; Meng, Y.; Cao, X.; Xue, S.; Yang, X., Evaluation of the integrated hydrothermal carbonization-algal cultivation process for enhanced nitrogen utilization in Arthrospira platensis production. *Bioresour Technol* **2016,** *216*, 381-90.

87. Zhou, D.; Zhang, L.; Zhang, S.; Fu, H.; Chen, J., Hydrothermal Liquefaction of Macroalgae Enteromorpha prolifera to Bio-oil. *Energy & Fuels* **2010,** *24* (7), 4054-4061.

88. Jain, A.; Balasubramanian, R.; Srinivasan, M. P., Hydrothermal conversion of biomass waste to activated carbon with high porosity: A review. *Chemical Engineering Journal* **2016,** *283*, 789-805.

89. Guo, Y.; Yeh, T.; Song, W.; Xu, D.; Wang, S., A review of bio-oil production from hydrothermal liquefaction of algae. *Renewable and Sustainable Energy Reviews* **2015,** *48*, 776-790.

90. Biller, P.; Ross, A. B., Potential yields and properties of oil from the hydrothermal liquefaction of microalgae with different biochemical content. *Bioresour Technol* **2011,** *102* (1), 215-25.

91. Grierson S, S. V., Ellem G, McGregor R, Herbertson J, Thermal characterisation of microalgae under slow pyrolysis conditions. *J Anal Appl Pyrolysis* **2009,** *85* (1), 118-123.

92. Du Z, L. Y., Wang X, Wan Y, Chen Q, Wang C, Lin X, Liu Y, Chen P, Ruan R, Microwave-assisted pyrolysis of microalgae for biofuel production. *Bioresour Technol* **2011,** *102* (7), 4890-4896.

93. Wang K, B. R., Homsy S, Martinez L, Sidhu SS, Fast pyrolysis of microalgae remnants in a fluidized bed reactor for bio-oil and biochar production. *Bioresour Technol* **2013,** *127*, 494-499.

94. Chen WH, L. B., Huang MY, Chang JS, Thermochemical conversion of microalgal biomass into biofuels: A review. *Bioresour Technol* **2015,** *184*, 314-327.

95. Oluwoye I, D. B., Gore J, Oskierski HC, Altarawneh M, Atmospheric emission of NOx from mining explosives: A critical review. *Atmos Environ* **2017,** *167*, 81-96.

96. Ren Q, Z. C., Chen X, Duan L, Li Y, Ma C, NOx and N2O precursors (NH3 and HCN) from biomass pyrolysis: Co-pyrolysis of amino acids and cellulose, hemicellulose and lignin. *Proc Combust Inst* **2011,** *33* (2), 1715-1722.

97. Li, J.; Wang, Z.; Yang, X.; Hu, L.; Liu, Y.; Wang, C., Decomposing or subliming? An investigation of thermal behavior of L-leucine. *Thermochimica acta* **2006,** *447* (2), 147-153.

98. Li, J.; Wang, Z.; Yang, X.; Hu, L.; Liu, Y.; Wang, C., Evaluate the pyrolysis pathway of glycine and glycylglycine by TG–FTIR. *Journal of Analytical and Applied Pyrolysis* **2007,** *80* (1), 247-253.

99. Reza, M. T.; Andert, J.; Wirth, B.; Busch, D.; Pielert, J.; Lynam, J. G.; Mumme, J., Hydrothermal carbonization of biomass for energy and crop production. *Applied Bioenergy* **2014,** *1* (1), 11-29.

100. Tian, C.; Liu, Z.; Zhang, Y.; Li, B.; Cao, W.; Lu, H.; Duan, N.; Zhang, L.; Zhang, T., Hydrothermal liquefaction of harvested high-ash low-lipid algal biomass from Dianchi Lake: effects of operational parameters and relations of products. *Bioresour Technol* **2015,** *184*, 336-343.

101. Yu, K. L.; Lau, B. F.; Show, P. L.; Ong, H. C.; Ling, T. C.; Chen, W.-H.; Ng, E. P.; Chang, J.-S., Recent developments on algal biochar production and characterization. *Bioresource Technology* **2017,** *246*, 2-11.

102. Kambo, H. S.; Dutta, A., A comparative review of biochar and hydrochar in terms of production, physico-chemical properties and applications. *Renewable and Sustainable Energy Reviews* **2015,** *45*, 359-378.

103. Zhang, Z.; Wang, K.; Atkinson, J. D.; Yan, X.; Li, X.; Rood, M. J.; Yan, Z., Sustainable and hierarchical porous Enteromorpha prolifera based carbon for CO2 capture. *J Hazard Mater* **2012,** *229-230*, 183-91.

104. Inyang, M. I.; Gao, B.; Yao, Y.; Xue, Y.; Zimmerman, A.; Mosa, A.; Pullammanappallil, P.; Ok, Y. S.; Cao, X., A review of biochar as a low-cost adsorbent for aqueous heavy metal removal. *Critical Reviews in Environmental Science and Technology* **2016,** *46* (4), 406-433.

105. Abel, S.; Peters, A.; Trinks, S.; Schonsky, H.; Facklam, M.; Wessolek, G., Impact of biochar and hydrochar addition on water retention and water repellency of sandy soil. *Geoderma* **2013,** *202*, 183-191.

106. Jena, U.; Das, K. C., Comparative Evaluation of Thermochemical Liquefaction and Pyrolysis for Bio-Oil Production from Microalgae. *Energy & Fuels* **2011,** *25* (11), 5472-5482.

107. Kruse, A.; Koch, F.; Stelzl, K.; Wüst, D.; Zeller, M., Fate of Nitrogen during Hydrothermal Carbonization. *Energy & Fuels* **2016,** *30* (10), 8037-8042.

108. Dayananda, C.; Sarada, R.; Usha Rani, M.; Shamala, T. R.; Ravishankar, G. A., Autotrophic cultivation of Botryococcus braunii for the production of hydrocarbons and exopolysaccharides in various media. *Biomass and Bioenergy* **2007,** *31* (1), 87-93.

109. Gour, R. S.; Bairagi, M.; Garlapati, V. K.; Kant, A., Enhanced microalgal lipid production with media engineering of potassium nitrate as a nitrogen source. *Bioengineered* **2018,** *9* (1), 98-107.

110. Lee, J.; Park, K. Y.; Cho, J.; Kim, J. Y., Releasing characteristics and fate of heavy metals from phytoremediation crop residues during anaerobic digestion. *Chemosphere* **2018,** *191*, 520-526.

111. Mueller, R.; Steiner, A., Inhibition of anaerobic digestion caused by heavy metals. *Water Science and Technology* **1992,** *26* (3-4), 835-846.

112. Durán, I.; Rubiera, F.; Pevida, C., Microalgae: Potential precursors of CO2 adsorbents. *Journal of CO2 Utilization* **2018,** *26*, 454-464.

113. Ennis, C. J.; Clarke, J.; Neate, K.; Cerejeira, J.; Tull, L., Hydrothermal Extraction of Microalgae Fatty Acid Influences Hydrochar Phytotoxicity. *Frontiers in Environmental Science* **2017,** *5*.

114. Martins, M. B.; Carvalho, I., Diketopiperazines: biological activity and synthesis. *Tetrahedron* **2007,** *63* (40), 9923-9932.

115. Lubitz, J. A., The Protein Quality, Digestibility, and Composition of Algae, Chlorella 71105a. *J. Food Sci.* **1963,** *28* (2), 229-232.

116. Hempel N, P. I., Behrendt F, Biomass productivity and productivity of fatty acids and amino acids of microalgae strains as key characteristics of suitability for biodiesel production. *J Appl Phycol* **2012,** *24* (6), 1407-1418.

117. Williams AE, B. R., Nitrogen Fixation by Blue-Green Algae and Their Nitrogenous Composition. *Am J Bot* **1952,** *39* (5), 340-342.

118. Frisch, M.; Trucks, G.; Schlegel, H. B.; Scuseria, G.; Robb, M.; Cheeseman, J.; Scalmani, G.; Barone, V.; Mennucci, B.; Petersson, G., Gaussian 09, revision a. 02, gaussian. *Inc., Wallingford, CT* **2009,** *200*.

119. Sirjean, B.; Fournet, R.; Glaude, P.-A.; Ruiz-López, M. F., Extension of the composite CBS-QB3 method to singlet diradical calculations. *Chem Phys Lett* **2007,** *435* (1), 152-156.

120. Sirjean, B.; Glaude, P. A.; Ruiz-Lopez, M. F.; Fournet, R., Detailed Kinetic Study of the Ring Opening of Cycloalkanes by CBS-QB3 Calculations. *J Phys Chem A* **2006,** *110* (46), 12693-12704.

121. Ess, D. H.; Houk, K. N., Activation Energies of Pericyclic Reactions: Performance of DFT, MP2, and CBS-QB3 Methods for the Prediction of Activation Barriers and Reaction Energetics of 1,3-Dipolar Cycloadditions, and Revised Activation Enthalpies for a Standard Set of Hydrocarbon Pericyclic Reactions. *J Phys Chem A* **2005,** *109* (42), 9542-9553.

122. Casasnovas, R.; Frau, J.; Ortega-Castro, J.; Salvà, A.; Donoso, J.; Muñoz, F., Simplification of the CBS-QB3 method for predicting gas-phase deprotonation free energies. *International Journal of Quantum Chemistry* **2010,** *110* (2), 323-330.

123. Lily, M.; Mishra, B. K.; Chandra, A. K., Kinetics, mechanism and thermochemistry of the gas phase reactions of CF3CH2OCH2CF3 with OH radicals: A theoretical study. *J Fluor Chem* **2014,** *161* (Supplement C), 51-59.

124. Walker, M.; Harvey, A. J. A.; Sen, A.; Dessent, C. E. H., Performance of M06, M06-2X, and M06-HF Density Functionals for Conformationally Flexible Anionic Clusters: M06 Functionals Perform Better than B3LYP for a Model System with Dispersion and Ionic Hydrogen-Bonding Interactions. *J Phys Chem A* **2013,** *117* (47), 12590-12600.

125. Zhao, Y.; Truhlar, D. G., Applications and validations of the Minnesota density functionals. *Chem Phys Lett* **2011,** *502* (1), 1-13.

126. Mokrushin, V.; Bedanov, V.; Tsang, W.; Zachariah, M.; Knyazev, V., ChemRate. Version: **2006**.

127. Canneaux, S.; Bohr, F.; Henon, E., KiSThelP: a program to predict thermodynamic properties and rate constants from quantum chemistry results. *Journal of computational chemistry* **2014,** *35* (1), 82-93.

128. Altarawneh, M.; Dlugogorski, B. Z., Formation and Chlorination of Carbazole, Phenoxazine, and Phenazine. *Environ. Sci. Technol.* **2015,** *49* (4), 2215-2221.

129. Al-Nu'airat, J.; Altarawneh, M.; Gao, X.; Westmoreland, P. R.; Dlugogorski, B. Z., Reaction of Aniline with Singlet Oxygen (O2 1Δg). *J Phys Chem A* **2017,** *121* (17), 3199-3206.

130. Altarawneh, M.; Almatarneh, M. H.; Marashdeh, A.; Dlugogorski, B. Z., Decomposition of ethylamine through bimolecular reactions. *Combust Flame* **2016,** *163*, 532-539.

131. Siddique, K.; Altarawneh, M.; Gore, J.; Westmoreland, P. R.; Dlugogorski, B. Z., Hydrogen Abstraction from Hydrocarbons by NH2. *J Phys Chem A* **2017,** *121* (11), 2221-2231.

132. Vedaraman, N.; Gadkari, P.; Manohar, B.; Sandhya, K.; Brunner, G.; Sankar, K. U., Solubility Modeling of N-CBZ Derivatised Amino Acids in Supercritical Carbon Dioxide. *Int J Anal Mass Spectrom Cromatogr* **2014,** *2* (02), 52.

133. Design, R., Chemkin-pro release 15131. *Reaction Design, San Diego, CA* **2013**.

134. Daniell, A. E.; Peterson, W. R., Oxidation of carbon black. Google Patents: **1966**.

135. Channiwala, S. A.; Parikh, P. P., A unified correlation for estimating HHV of solid, liquid and gaseous fuels. *Fuel* **2002,** *81* (8), 1051-1063.

136. Komada, T.; Anderson, M. R.; Dorfmeier, C. L., Carbonate removal from coastal sediments for the determination of organic carbon and its isotopic signatures, δ13C and Δ14C: comparison of fumigation and direct acidification by hydrochloric acid. *Limnol Oceanogr Methods* **2008,** *6* (6), 254-262.

137. GB/T 212-2008 Proximate analysis of coal. Standardization Administration of China: **2008**.

138. Chen, C.; Ma, X.; Liu, K., Thermogravimetric analysis of microalgae combustion under different oxygen supply concentrations. *Appl Energ* **2011,** *88* (9), 3189-3196.

139. Qing, X.; Xiaoqian, M.; Zhaosheng, Y.; Zilin, C.; Changming, L., Decomposition Characteristics and Kinetics of Microalgae in N2 and CO2 Atmospheres by a Thermogravimetry. *J Comb* **2017,** *2017*, 1-7.

140. Zhang, J.; Jiang, B.; Wang, D., Thermogravimetric and kinetic analysis of bio-crude from hydrothermal liquefaction of Enteromorpha prolifera. *Algal Res* **2016,** *18*, 45-50.

141. Bhola, V.; Desikan, R.; Santosh, S. K.; Subburamu, K.; Sanniyasi, E.; Bux, F., Effects of parameters affecting biomass yield and thermal behaviour of Chlorella vulgaris. *J Biosci Bioeng* **2011,** *111* (3), 377-382.

142. López, R.; Fernández, C.; Gómez, X.; Martínez, O.; Sánchez, M. E., Thermogravimetric analysis of lignocellulosic and microalgae biomasses and their blends during combustion. *J Therm Anal Calorim* **2013,** *114* (1), 295-305.

143. Xu, D.; Savage, P. E., Characterization of biocrudes recovered with and without solvent after hydrothermal liquefaction of algae. *Algal Research* **2014,** *6*, 1-7.

144. Xu, Y.; Yu, H.; Hu, X.; Wei, X.; Cui, Z., Bio-oil Production from Algae via Thermochemical Catalytic Liquefaction. *Energy Sources, Part A: Recovery, Utilization, and Environmental Effects* **2013,** *36* (1), 38-44.

145. Yang, W.; Li, X.; Li, Z.; Tong, C.; Feng, L., Understanding low-lipid algae hydrothermal liquefaction characteristics and pathways through hydrothermal liquefaction of algal major components: crude polysaccharides, crude proteins and their binary mixtures. *Bioresour Technol* **2015,** *196*, 99-108.

146. Sait, H. H.; Hussain, A.; Salema, A. A.; Ani, F. N., Pyrolysis and combustion kinetics of date palm biomass using thermogravimetric analysis. *Bioresour Technol* **2012,** *118*, 382-389.

147. Mishra S, S. N., Sarma AK, Assessment of a Novel Algal Strain Chlamydomonas debaryana NIREMACC03 for Mass Cultivation, Biofuels Production and Kinetic Studies. *Appl Biochem Biotechnol* **2015,** *176* (8), 2253-2266.

148. Zhang, J.; Chen, W. T.; Zhang, P.; Luo, Z.; Zhang, Y., Hydrothermal liquefaction of Chlorella pyrenoidosa in sub- and supercritical ethanol with heterogeneous catalysts. *Bioresour Technol* **2013,** *133*, 389-97.

149. Zhang, J.; Zhang, Y., Hydrothermal Liquefaction of Microalgae in an Ethanol–Water Co-Solvent To Produce Biocrude Oil. *Energy & Fuels* **2014,** *28* (8), 5178-5183.

150. Zou, S.; Wu, Y.; Yang, M.; Li, C.; Tong, J., Bio-oil production from sub- and supercritical water liquefaction of microalgae Dunaliella tertiolecta and related properties. *Energy Environ. Sci.* **2010,** *3* (8), 1073-1078.

151. Agrawal, A.; Chakraborty, S., A kinetic study of pyrolysis and combustion of microalgae Chlorella vulgaris using thermo-gravimetric analysis. *Bioresour Technol* **2013,** *128*, 72-80.

152. Demirbas, A., Combustion characteristics of different biomass fuels. *Prog Energ Combust Sci* **2004,** *30* (2), 219-230.

153. Jenkins, B. M.; Baxter, L. L.; Miles, T. R.; Miles, T. R., Combustion properties of biomass. *Fuel Process Technol* **1998,** *54* (1), 17-46.

154. Li, D.; Chen, L.; Yi, X.; Zhang, X.; Ye, N., Pyrolytic characteristics and kinetics of two brown algae and sodium alginate. *Bioresour Technol* **2010,** *101* (18), 7131-7136.

155. Li, D.; Chen, L.; Zhang, X.; Ye, N.; Xing, F., Pyrolytic characteristics and kinetic studies of three kinds of red algae. *Biomass Bioenergy* **2011,** *35* (5), 1765-1772.

156. Sharara, M. A.; Holeman, N.; Sadaka, S. S.; Costello, T. A., Pyrolysis kinetics of algal consortia grown using swine manure wastewater. *Bioresour Technol* **2014,** *169* (Supplement C), 658-666.

157. ASTM E870-82(2019), Standard Test Methods for Analysis of Wood Fuels, ASTM International, West Conshohocken, PA, 2019, www.astm.org.

158. Seo, D. K.; Park, S. S.; Hwang, J.; Yu, T.-U., Study of the pyrolysis of biomass using thermo-gravimetric analysis (TGA) and concentration measurements of the evolved species. *J Anal Appl Pyrolysis* **2010,** *89* (1), 66-73.

159. Bui, H.-H.; Tran, K.-Q.; Chen, W.-H., Pyrolysis of microalgae residues – A kinetic study. *Bioresour Technol* **2016,** *199* (Supplement C), 362-366.

160. ISO 18134-1 Solid biofuels – Determination of moisture content – Oven dry method. British Standards Institution: **2015**.

161. ISO 18122 Solid biofuels - Determination of ash content. British Standards Institution: **2015**.

162. López-González, D.; Fernandez-Lopez, M.; Valverde, J. L.; Sanchez-Silva, L., Kinetic analysis and thermal characterization of the microalgae combustion process by thermal analysis coupled to mass spectrometry. *Appl Energ* **2014,** *114*, 227-237.

163. López-González, D.; Fernandez-Lopez, M.; Valverde, J. L.; Sanchez-Silva, L., Pyrolysis of three different types of microalgae: Kinetic and evolved gas analysis. *Energy* **2014,** *73*, 33-43.

164. Yu, J.; Savage, P. E., Decomposition of formic acid under hydrothermal conditions. *Industrial & Engineering Chemistry Research* **1998,** *37* (1), 2-10.

165. Werkelin, J.; Skrifvars, B.-J.; Zevenhoven, M.; Holmbom, B.; Hupa, M., Chemical forms of ash-forming elements in woody biomass fuels. *Fuel* **2010,** *89* (2), 481-493.

166. Kambo, H. S.; Dutta, A., Strength, storage, and combustion characteristics of densified lignocellulosic biomass produced via torrefaction and hydrothermal carbonization. *Applied Energy* **2014,** *135*, 182-191.

167. Conti, R.; Fabbri, D.; Vassura, I.; Ferroni, L., Comparison of chemical and physical indices of thermal stability of biochars from different biomass by analytical pyrolysis and thermogravimetry. *J Anal Appl Pyrolysis* **2016,** *122* (Supplement C), 160-168.

168. Liu, Y.-Q.; Lim, L. R.; Wang, J.; Yan, R.; Mahakhant, A., Investigation on Pyrolysis of Microalgae Botryococcus braunii and Hapalosiphon sp. *Ind Eng Chem Res* **2012,** *51* (31), 10320-10326.

169. Santillan-Jimenez, E.; Pace, R.; Marques, S.; Morgan, T.; McKelphin, C.; Mobley, J.; Crocker, M., Extraction, characterization, purification and catalytic upgrading of algae lipids to fuel-like hydrocarbons. *Fuel* **2016,** *180*, 668-678.

170. Francavilla, M.; Kamaterou, P.; Intini, S.; Monteleone, M.; Zabaniotou, A., Cascading microalgae biorefinery: Fast pyrolysis of Dunaliella tertiolecta lipid extracted-residue. *Algal Res* **2015,** *11* (Supplement C), 184-193.

171. Kebelmann, K.; Hornung, A.; Karsten, U.; Griffiths, G., Intermediate pyrolysis and product identification by TGA and Py-GC/MS of green microalgae and their extracted protein and lipid components. *Biomass Bioenergy* **2013,** *49*, 38-48.

172. Rizzo, A. M.; Prussi, M.; Bettucci, L.; Libelli, I. M.; Chiaramonti, D., Characterization of microalga Chlorella as a fuel and its thermogravimetric behavior. *Appl Energ* **2013,** *102*, 24-31.

173. Wang, K.; Brown, R. C., Catalytic pyrolysis of microalgae for production of aromatics and ammonia. *Green Chemistry* **2013,** *15* (3), 675.

174. Kim, S. W.; Koo, B. S.; Lee, D. H., A comparative study of bio-oils from pyrolysis of microalgae and oil seed waste in a fluidized bed. *Bioresour Technol* **2014,** *162*, 96-102.

175. Babich, I. V.; van der Hulst, M.; Lefferts, L.; Moulijn, J. A.; O'Connor, P.; Seshan, K., Catalytic pyrolysis of microalgae to high-quality liquid bio-fuels. *Biomass Bioenergy* **2011,** *35* (7), 3199-3207.

176. Ross, A. B.; Jones, J. M.; Kubacki, M. L.; Bridgeman, T., Classification of macroalgae as fuel and its thermochemical behaviour. *Bioresour Technol* **2008,** *99* (14), 6494-504.

177. Roberts, G. W.; Sturm, B. S. M.; Hamdeh, U.; Stanton, G. E.; Rocha, A.; Kinsella, T. L.; Fortier, M.-O. P.; Sazdar, S.; Detamore, M. S.; Stagg-Williams, S. M., Promoting catalysis and high-value product streams by in situ hydroxyapatite crystallization during hydrothermal liquefaction of microalgae cultivated with reclaimed nutrients. *Green Chem* **2015,** *17* (4), 2560-2569.

178. Anastasakis, K.; Ross, A. B.; Jones, J. M., Pyrolysis behaviour of the main carbohydrates of brown macro-algae. *Fuel* **2011,** *90* (2), 598-607.

179. Biller, P.; Ross, A. B., Pyrolysis GC–MS as a novel analysis technique to determine the biochemical composition of microalgae. *Algal Res* **2014,** *6*, 91-97.

180. Ceylan, S.; Kazan, D., Pyrolysis kinetics and thermal characteristics of microalgae Nannochloropsis oculata and Tetraselmis sp. *BioresourTechnol* **2015,** *187*, 1-5.

181. Zakariah, N. A.; Rahman, N. A.; Him, N. R. N., Effects of nitrogen supplementation in replete condition on the biomass yield and microalgae properties of Chlorella Sorokiniana. *ARPN J Eng Appl Sci* **2006,** *4* (10), 1.

182. Mwangi, J. K.; Lee, W.-J.; Whang, L.-M.; Wu, T. S.; Chen, W.-H.; Chang, J.-S.; Chen, C.-Y.; Chen, C.-L., Microalgae oil: Algae cultivation and harvest, algae residue torrefaction and diesel engine emissions tests. *Aerosol Air Qual Res* **2015,** *15*, 81-98.

183. Maddi, B.; Viamajala, S.; Varanasi, S., Comparative study of pyrolysis of algal biomass from natural lake blooms with lignocellulosic biomass. *Bioresour Technol* **2011,** *102* (23), 11018-11026.

184. Gai, C.; Zhang, Y.; Chen, W.-T.; Zhang, P.; Dong, Y., Thermogravimetric and kinetic analysis of thermal decomposition characteristics of low-lipid microalgae. *Bioresour Technol* **2013,** *150*, 139-148.

185. Bach, Q.-V.; Chen, W.-H., Pyrolysis characteristics and kinetics of microalgae via thermogravimetric analysis (TGA): A state-of-the-art review. *Bioresour Technol* **2017,** *246*, 88-100.

186. Latham, K. G.; Ferguson, A.; Donne, S. W., Influence of ammonium salts and temperature on the yield, morphology and chemical structure of hydrothermally carbonized saccharides. *Appl Sci* **2018,** *1* (1), 54.

187. Pels, J. R.; Kapteijn, F.; Moulijn, J. A.; Zhu, Q.; Thomas, K. M., Evolution of nitrogen functionalities in carbonaceous materials during pyrolysis. *Carbon* **1995,** *33* (11), 1641-1653.

188. Liu, J.; Pan, Y.; Yao, C.; Wang, H.; Cao, X.; Xue, S., Determination of ash content and concomitant acquisition of cell compositions in microalgae via thermogravimetric (TG) analysis. *Algal Res* **2015,** *12*, 149-155.

189. Xiao, R.; Chen, X.; Wang, F.; Yu, G., The physicochemical properties of different biomass ashes at different ashing temperature. *Renew Energ* **2011,** *36* (1), 244-249.

190. Arvelakis, S.; Jensen, P. A.; Dam-Johansen, K., Simultaneous Thermal Analysis (STA) on Ash from High-Alkali Biomass. *Energ Fuels* **2004,** *18* (4), 1066-1076.

191. Wang, S.; Jiang, X. M.; Han, X. X.; Wang, H., Fusion Characteristic Study on Seaweed Biomass Ash. *Energy Fuels* **2008,** *22* (4), 2229-2235.

192. Jansen, R. J. J.; van Bekkum, H., Amination and ammoxidation of activated carbons. *Carbon* **1994,** *32* (8), 1507-1516.

193. Westbrook, C. K.; Dryer, F. L., Chemical kinetic modeling of hydrocarbon combustion. *Prog Energy Combust Sci* **1984,** *10* (1), 1-57.

194. Gascoin, N.; Gillard, P.; Mangeot, A.; Navarro-Rodriguez, A., Detailed kinetic computations and experiments for the choice of a fuel–oxidiser couple for hybrid propulsion. *J Anal Appl Pyrolysis* **2012,** *94*, 33-40.

195. Sabourin, J.; Risha, G.; Yetter, R.; Son, S.; Tappan, B., Combustion characteristics of nanoaluminum, liquid water, and hydrogen peroxide mixtures. *Combust Flame* **2008,** *154* (3), 587-600.

196. Bauhn, L.; Hansson, N.; Ekberg, C.; Fors, P.; Spahiu, K., The fate of hydroxyl radicals produced during H2O2 decomposition on a SIMFUEL surface in the presence of dissolved hydrogen. *J Nucl Mater* **2018,** *507*, 38-43.

197. Giguère, P. A.; Liu, I., Kinetics of the thermal decomposition of hydrogen peroxide vapor. *Can J Chem* **1957,** *35* (4), 283-293.

198. Irabien, A.; Viguri, J. R.; Ortiz, I., Thermal dehydration of calcium hydroxide. 1. Kinetic model and parameters. *Ind Eng Chem Res* **1990,** *29* (8), 1599-1606.

199. Anderson, P.; Horlock, R., Thermal decomposition of magnesium hydroxide. *J Chem Soc Faraday Trans* **1962,** *58*, 1993-2004.

200. Di Blasi, C.; Galgano, A.; Branca, C., Effects of potassium hydroxide impregnation on wood pyrolysis. *Energy Fuel* **2009,** *23* (2), 1045-1054.

201. Yurkinskii, V.; Firsova, E.; Proskura, S., Thermal dissociation of sodium hydroxide upon evacuation. *Russ J Appl Chem* **2005,** *78* (3), 360-362.

202. EW, B., Micro-algae as a source of protein. *Biotechnol Adv* **2007,** *25* (2), 207-210.

203. Rawadieh, S.; Altarawneh, I.; Alateyat, H. B.; Altarawneh, M., Theoretical study on the unimolecular decomposition of proline. *Comput Theor Chem* **2013,** *1018*, 45-49.

204. Altarawneh M, D. B., A Mechanistic and Kinetic Study on the Decomposition of Morpholine. *J Phys Chem A* **2012,** *116* (29), 7703-7711.

205. Lucassen A, L. N., Westmoreland PR, Kohse-Höinghaus K Combustion chemistry and fuel-nitrogen conversion in a laminar premixed flame of morpholine as a model biofuel. *Combust Flame* **2011,** *158* (9), 1647-1666.

206. Tian Z, L. Y., Zhang T, Zhu A, Cui Z, Qi F, An experimental study of low-pressure premixed pyrrole/oxygen/argon flames with tunable synchrotron photoionization. *Combust Flame* **2007,** *151* (1), 347-365.

207. Tian Z, L. Y., Zhang T, Zhu A, Qi F, Identification of Combustion Intermediates in Low-Pressure Premixed Pyridine/Oxygen/Argon Flames. *J Phys Chem A* **2008,** *112* (51), 13549-13555.

208. Zhang K, L. Y., Yuan T, Cai J, Glarborg , Qi F, An experimental and kinetic modeling study of premixed nitromethane flames at low pressure. *Proc Combust Inst* **2011,** *33* (1), 407-414.

209. JA, L., The Protein Quality, Digestibility, and Composition of Algae, Chlorella 71105a. *J Food Sci* **1963,** *28* (2), 229-232.

210. Simmonds, P.; Medley, E.; Ratcliff, M.; Shulman, G., Thermal decomposition of aliphatic monoaminomonocarboxylic acids. *Analytical chemistry* **1972,** *44* (12), 2060-2066.

211. Lien YC, N. W., Thermal decomposition of some amino acids. Valine, leucine and lsoleucine. *J Food Sci* **1974,** *39* (5), 911-913.

212. Ratcliff MA, M. E., Simmonds PG, Pyrolysis of amino acids. Mechanistic considerations. *J Org Chem* **1974,** *39* (11), 1481-1490.

213. Chiavari G, G. G., Pyrolysis—gas chromatography/mass spectrometry of amino acids. *J Anal Appl Pyrolysis* **1992,** *24* (2), 123-137.

214. Blanksby SJ, E. G., Bond Dissociation Energies of Organic Molecules. *Acc Chem Res* **2003,** *36* (4), 255-263.

215. Lalevee J, A. X., Fouassier JP, N-H and alpha(C-H) bond dissociation enthalpies of aliphatic amines. *Journal of the American Chemical Society* **2002,** *124* (32), 9613-21.

216. Hadad CM, R. P., Wiberg KB, C−O and C−S Bonds: Stability, Bond Dissociation Energies, and Resonance Stabilization. *J Org Chem* **1998,** *63* (24), 8668-8681.

217. Rai AK, X. X., Lin Z, Rai DK, Conformational search for zwitterionic leucine and hydrated conformers of both the canonical and zwitterionic leucine using the DFT-CPCM model. *Vib Spectrosc* **2011,** *56* (1), 74-81.

218. Sacks GL, B. J., High-Precision Position-Specific Isotope Analysis of 13C/12C in Leucine and Methionine Analogues. *Anal Chem* **2003,** *75* (20), 5495-5503.

219. Hansson KM, Å. L., Habermann A, Winter F, Pyrolysis of poly-l-leucine under combustion-like conditions☆. *Fuel* **2003,** *82* (6), 653-660.

220. VA, B., Pyrolysis of valine and leucine at 500°C: identification of less-volatile products using gas chromatography-Fourier transform infrared spectroscopy-mass spectrometry. *J Anal Appl Pyrolysis* **1998,** *47* (2), 127-143.

221. Altarawneh M, A.-M. A., Almatarneh MH, Poirier RA, Assaf NW, Altarawneh K, Theoretical Investigation into Competing Unimolecular Reactions Encountered in the Pyrolysis of Acetamide. *J Phys Chem A* **2011,** *115* (48), 14092-14099.

222. Altarawneh M, A. K., A theoretical study on the bimolecular reactions encountered in the pyrolysis of acetamide. *J Phys Org Chem* **2012,** *25* (5), 431-436.

223. Prosen EJ, R. F., Heats of combustion and formation of the paraffin hydrocarbons at 25° C. *J Res NBS* **1945,** *34* (3), 263-257.

224. WD, G., The enthalpies of combustion and formation of the isomeric pentanes. *J Chem Thermodyn* **1970,** *2* (2), 237-244.

225. Dorofeeva OV, R. O., Gas-phase enthalpies of formation and enthalpies of sublimation of amino acids based on isodesmic reaction calculations. *J Phys Chem A* **2014,** *118* (19), 3490-502.

226. Good WD, M. R., Enthalpies of formation of ethylenediamine, 1,2,-propanediamine, 1,2,-butanediamine, 2-methyl-1,2-propanediamine, and isobutylamine C-N and N-F Thermochemical bond energies. *J Chem Eng Data* **1970,** *15*, 150-154.

227. ND, L., Heats of combustion of monocarboxylic acids. *Russ J Phys Chem* **1964,** *38*, 1435-143.

228. Simmie JM, B. G., Curran HJ, Hinde JP, Enthalpies of formation and bond dissociation energies of lower alkyl hydroperoxides and related hydroperoxy and alkoxy radicals. *J Phys Chem A* **2008,** *112* (22), 5010-5016.

229. Linstrom PJ, M. W., The NIST Chemistry WebBook: A Chemical Data Resource on the Internet. *J Chem Eng Data* **2001,** *46* (5), 1059-1063.

230. Lucian, M.; Volpe, M.; Gao, L.; Piro, G.; Goldfarb, J. L.; Fiori, L., Impact of hydrothermal carbonization conditions on the formation of hydrochars and secondary chars from the organic fraction of municipal solid waste. *Fuel* **2018,** *233*, 257-268.

231. Gao, X.; Rahim, M. U.; Chen, X.; Wu, H., Significant contribution of organically-bound Mg, Ca, and Fe to inorganic PM10 emission during the combustion of pulverized Victorian brown coal. *Fuel* **2014,** *117*, 825-832.

232. Gao, X.; Li, Y.; Garcia-Perez, M.; Wu, H., Roles of Inherent Fine Included Mineral Particles in the Emission of PM10 during Pulverized Coal Combustion. *Energy & Fuels* **2012,** *26* (11), 6783-6791.

233. Sami, M.; Annamalai, K.; Wooldridge, M., Co-firing of coal and biomass fuel blends. *Progress in Energy and Combustion Science* **2001,** *27* (2), 171-214.

234. Leng, L.; Huang, H.; Li, H.; Li, J.; Zhou, W., Biochar stability assessment methods: A review. *Science of The Total Environment* **2019,** *647*, 210-222.

235. Froehner, S.; Martins, R. F.; Furukawa, W.; Errera, M. R., Water Remediation by Adsorption of Phenol onto Hydrophobic Modified Clay. *Water, Air, and Soil Pollution* **2009,** *199* (1), 107-113.

236. Karnowo; Zahara, Z. F.; Kudo, S.; Norinaga, K.; Hayashi, J.-i., Leaching of Alkali and Alkaline Earth Metallic Species from Rice Husk with Bio-oil from Its Pyrolysis. *Energy & Fuels* **2014,** *28* (10), 6459-6466.

237. Zhang, M.; Wu, H., Bioslurry as a Fuel. 6. Leaching Characteristics of Alkali and Alkaline Earth Metallic Species from Biochar by Bio-oil Model Compounds. *Energy & Fuels* **2015,** *29* (4), 2535-2541.

238. Reza, M. T.; Lynam, J. G.; Uddin, M. H.; Coronella, C. J., Hydrothermal carbonization: Fate of inorganics. *Biomass and Bioenergy* **2013,** *49*, 86-94.

239. Halim, N.; Tajima, A.; Asano, S.; Kudo, S.; Hayashi, J.-i., Change in Catalytic Activity of Potassium during CO2 Gasification of Char. *Energy & Fuels* **2020,** *34* (1), 225-234.

240. Wu, H.; Gauthier, D.; Yu, Y.; Gao, X.; Flamant, G., Solar-Thermal Pyrolysis of Mallee Wood at High Temperatures. *Energy & Fuels* **2018,** *32* (4), 4350-4356.

241. Wu, H.; Li, X.; Hayashi, J.-i.; Chiba, T.; Li, C.-Z., Effects of volatile–char interactions on the reactivity of chars from NaCl-loaded Loy Yang brown coal. *Fuel* **2005,** *84* (10), 1221-1228.

242. Zhu, X.; Liu, Y.; Qian, F.; Zhang, S.; Chen, J., Investigation on the Physical and Chemical Properties of Hydrochar and Its Derived Pyrolysis Char for Their Potential Application: Influence of Hydrothermal Carbonization Conditions. *Energy & Fuels* **2015,** *29* (8), 5222-5230.

243. Keiller, B. G.; Muhlack, R.; Burton, R. A.; van Eyk, P. J., Biochemical Compositional Analysis and Kinetic Modeling of Hydrothermal Carbonization of Australian Saltbush. *Energy & Fuels* **2019,** *33* (12), 12469-12479.

244. Jiang, J.; Savage, P. E., Metals and Other Elements in Biocrude from Fast and Isothermal Hydrothermal Liquefaction of Microalgae. *Energy & Fuels* **2017,** *32* (4), 4118-4126.

245. Funke, A.; Ziegler, F., Hydrothermal carbonization of biomass: A summary and discussion of chemical mechanisms for process engineering. *Biofuels, Bioproducts and Biorefining* **2010,** *4* (2), 160-177.

246. Heilmann, S. M.; Jader, L. R.; Sadowsky, M. J.; Schendel, F. J.; von Keitz, M. G.; Valentas, K. J., Hydrothermal carbonization of distiller's grains. *Biomass and Bioenergy* **2011,** *35* (7), 2526-2533.

247. Aveldano, M. I.; Horrocks, L. A., Quantitative release of fatty acids from lipids by a simple hydrolysis procedure. *Journal of lipid research* **1983,** *24* (8), 1101-1105.

248. Lopez Barreiro, D.; Zamalloa, C.; Boon, N.; Vyverman, W.; Ronsse, F.; Brilman, W.; Prins, W., Influence of strain-specific parameters on hydrothermal liquefaction of microalgae. *Bioresour Technol* **2013,** *146*, 463-471.

249. Yu, G.; Zhang, Y.; Schideman, L.; Funk, T.; Wang, Z., Distributions of carbon and nitrogen in the products from hydrothermal liquefaction of low-lipid microalgae. *Energy & Environmental Science* **2011,** *4* (11).

250. Yoo, G.; Park, M. S.; Yang, J.-W.; Choi, M., Lipid content in microalgae determines the quality of biocrude and Energy Return On Investment of hydrothermal liquefaction. *Applied Energy* **2015,** *156*, 354-361.

251. Jiang, J.; Savage, P. E., Using Solvents To Reduce the Metal Content in Crude Bio-oil from Hydrothermal Liquefaction of Microalgae. *Industrial & Engineering Chemistry Research* **2019,** *58* (50), 22488-22496.

252. Jiang, J.; Savage, P. E., Influence of process conditions and interventions on metals content in biocrude from hydrothermal liquefaction of microalgae. *Algal Research* **2017,** *26*, 131-134.

253. Li, H.; Liu, Z.; Zhang, Y.; Li, B.; Lu, H.; Duan, N.; Liu, M.; Zhu, Z.; Si, B., Conversion efficiency and oil quality of low-lipid high-protein and high-lipid low-protein microalgae via hydrothermal liquefaction. *Bioresour Technol* **2014,** *154*, 322-9.

254. Valdez, P. J.; Dickinson, J. G.; Savage, P. E., Characterization of Product Fractions from Hydrothermal Liquefaction of Nannochloropsis sp. and the Influence of Solvents. *Energy & Fuels* **2011,** *25* (7), 3235-3243.

255. Meetani, M. A.; Zahid, O. K.; Michael Conlon, J., Investigation of the pyrolysis products of methionine-enkephalin-Arg-Gly-Leu using liquid chromatography–tandem mass spectrometry. *Journal of Mass Spectrometry* **2010,** *45* (11), 1320-1331.

256. Zhu, Z.; Rosendahl, L.; Toor, S. S.; Yu, D.; Chen, G., Hydrothermal liquefaction of barley straw to bio-crude oil: Effects of reaction temperature and aqueous phase recirculation. *Applied Energy* **2015,** *137*, 183-192.

257. Haiduc, A. G.; Brandenberger, M.; Suquet, S.; Vogel, F.; Bernier-Latmani, R.; Ludwig, C., SunCHem: an integrated process for the hydrothermal production of methane from microalgae and CO2 mitigation. *Journal of Applied Phycology* **2009,** *21* (5), 529-541.

258. Curtiss, L. A.; Raghavachari, K.; Redfern, P. C.; Pople, J. A., Assessment of Gaussian-2 and density functional theories for the computation of enthalpies of formation. *The Journal of Chemical Physics* **1997,** *106* (3), 1063-1079.

259. Aston, J.; Siller, C.; Messerly, G., Heat capacities and entropies of organic compounds. III. Methylamine from 11.5 K. to the boiling point. Heat of vaporization and vapor pressure. The entropy from molecular data. *Journal of the American Chemical Society* **1937,** *59* (9), 1743-1751.

260. Ruscic, B.; Berkowitz, J., Heat of formation of hydroxymethyl and methanol D0 (H-CH2OH). *The Journal of Physical Chemistry* **1993,** *97* (44), 11451-11455.

261. Wiberg, K. B.; Crocker, L. S.; Morgan, K. M., Thermochemical studies of carbonyl compounds. 5. Enthalpies of reduction of carbonyl groups. *Journal of the American Chemical Society* **1991,** *113* (9), 3447-3450.

262. Lebedeva, N., Heats of combustion of monocarboxylic acids. *Russ. J. Phys. Chem.* **1964,** *38*, 1435-143.

263. Pittam, D.; Pilcher, G., Measurements of heats of combustion by flame calorimetry. Part 8.—Methane, ethane, propane, n-butane and 2-methylpropane. *Journal of the Chemical Society, Faraday Transactions 1: Physical Chemistry in Condensed Phases* **1972,** *68*, 2224-2229.

264. Lemoult, M. P., Research theoretical and experimental on the heats of combustion and formation of organic compounds. *Ann. Chim. Phys* **1907,** *12*, 395-432.

265. Colomina, M.; Jimenez, P.; Roux, M.; Turrion, C., Thermochemical properties of o-, m-and p-hydroxybenzoic acids. *J Calorim Anal Therm* **1980,** *11*, 1-6.

266. Good, W. D., Enthalpies of combustion of nine organic nitrogen compounds related to petroleum. *Journal of Chemical and Engineering Data* **1972,** *17* (1), 28-31.

267. Papina, T.; Pimenova, S.; Luk'yanova, V.; Kolesov, V., Standard enthalpies of formation of benzyl alcohol and alpha, alpha, alpha-trichlorotoluene. *Russian journal of physical chemistry* **1995,** *69* (12), 1951-1953.

268. Verevkin, S. P., Thermochemistry of amines: strain in six-membered rings from experimental standard molar enthalpies of formation of morpholines and piperazines. *The Journal of Chemical Thermodynamics* **1998,** *30* (9), 1069-1079.

269. Pell, A.; Pilcher, G., Measurements of heats of combustion by flame calorimetry. Part 3.—Ethylene oxide, trimethylene oxide, tetrahydrofuran and tetrahydropy. *Transactions of the Faraday Society* **1965,** *61*, 71-77.

270. Spitzer, R.; Huffman, H. M., The heats of combustion of cyclopentane, cyclohexane, cycloheptane and cyclooctane. *Journal of the American Chemical Society* **1947,** *69* (2), 211-213.

271. Pedley, J.; Naylor, R.; Kirby, S.; Francis, P., Thermochemical data of organic compounds, 2nd edn: Chapman and Hall, London, 1986 (ISBN 0-412-27100-1). xi+ 791 pp. Price£ 55.00. *Analytica Chimica Acta* **1987,** *194*, 330-331.

272. Barnes, D.; Pilcher, G., Enthalpies of combustion of ethanamide, propanamide, and butanamide. *The Journal of Chemical Thermodynamics* **1975,** *7* (4), 377-382.

Learning and teaching should not stand on opposite banks and just watch the river flow by; instead, they should embark together on a journey down the water. Through an active, reciprocal exchange, teaching can strengthen learning how to learn.

- Loris Malaguzzi